OPTIMAL AND ROBUST
CONTROL AND ESTIMATION
OF TRANSITION, CONVECTION, AND TURBULENCE

A DISSERTATION
SUBMITTED TO THE DEPARTMENT OF MECHANICAL ENGINEERING
AND THE COMMITTEE ON GRADUATE STUDIES
OF STANFORD UNIVERSITY
IN PARTIAL FULFILLMENT OF THE REQUIREMENTS
FOR THE DEGREE OF
DOCTOR OF PHILOSOPHY

Thomas R. Bewley
August 1999

I certify that I have read this dissertation and that in my opinion it is fully adequate, in scope and quality, as a dissertation for the degree of Doctor of Philosophy.

Parviz Moin
(Principal Adviser)

I certify that I have read this dissertation and that in my opinion it is fully adequate, in scope and quality, as a dissertation for the degree of Doctor of Philosophy.

William C. Reynolds

I certify that I have read this dissertation and that in my opinion it is fully adequate, in scope and quality, as a dissertation for the degree of Doctor of Philosophy.

Stephen P. Boyd

I certify that I have read this dissertation and that in my opinion it is fully adequate, in scope and quality, as a dissertation for the degree of Doctor of Philosophy.

Roger Temam
(Indiana University and Université de Paris-Sud)

Approved for the University Committee on Graduate Studies:

Preface

"In order to know the true science of the flight of birds,
one must first know the science of the winds."

Man has been at the same time fascinated and stymied by the enigma of fluid turbulence for hundreds of years. In the above quote and several of his drawings (see figure 1), Leonardo da Vinci eloquently expressed man's yearning to understand chaotic fluid motion. Turbulent flow phenomena are ubiquitous and consequential, both in nature and in flows around and through man-made devices. Particular flows of interest in engineering include those of air, water, blood, molten metal, combustion reactants, and hot combustion products. The large increases in drag, cyclic structural loading, internal stresses, mixing, noise, and heat transfer caused by turbulence in such flows have motivated engineers to study turbulence and attempt to alter its effects. However, turbulence is inherently a multi-scale phenomenon, in which fluid motion at the large spatial scales is inherently coupled with fluid motion at the small spatial scales by the complex, chaotic physical process of vortex stretching. This makes turbulence difficult to characterize in simple terms and difficult to predict with low-dimensional simulations. To properly understand, simulate, and, ultimately, control a turbulent flow, this multi-scale nature of turbulence must be accounted for properly.

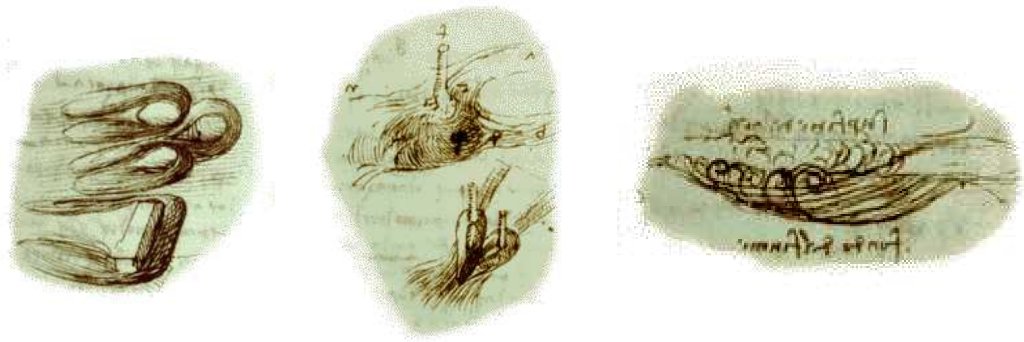

Figure 1: Sketches of turbulent flows from Leonardo da Vinci's *Codex Leicester*, circa 1508.

Turbulent flows are often quite sensitive to both active control and control/optimization by passive techniques, and have a complex, sometimes large, and (in certain respects) predictable response to system disturbances. Unfortunately, our knowledge of how best to determine, suppress, and/or exploit the sensitivities of turbulent flows for particular engineering objectives is, in most cases, quite limited. These sensitivities must be understood and harnessed before current approaches to the design of multi-scale flow systems can be advanced. Such is the topic of distributed control.

The current state-of-the-art in many arenas of control and design optimization for complex flow systems, such as the prevention of combustion instabilities in jet engines, is to conservatively probe the system, trying what seems plausible based almost on the intuition of the engineer alone. For a low-dimensional problem dominated by simple behaviour in the hands of an experienced engineer, such approaches are usually effective. However, as we move to the design of multi-scale, coupled, inherently nonlinear problems, such as the coordination of large arrays of turbulence control devices, intuition can fail us, and a mathematical approach to the design problem is preferred. The purpose of the present work is to establish and demonstrate such an approach for the problem of control of wall-bounded turbulence.

The nonlinear partial differential equation believed to govern turbulent flows, now known as the Navier-Stokes equation, was derived well over a century ago. The mathematical properties of solutions to this seemingly innocuous equation are extremely difficult to characterize, and constitute the primary topic of dozens of books and literally thousands of research papers. Topics of interest include the determination of when chaotic, bounded solutions to the Navier-Stokes equation even exist, when such solutions are unique, and how optimized controls for flows governed by the Navier-Stokes equation might be found. The mathematical approach to answering these questions is very involved and leads to (among other things) the rigorous foundation for the present work; however, this analysis also leads to some insights which are askew with the physical picture. Reconciliation of two viewpoints, drawing both from our *mathematical understanding* of the Navier-Stokes equation and from our *physical understanding* of turbulent flows, is an important part of making turbulence control an engineering reality.

The ability to simulate turbulent flows in simple geometries, integrating the delicate governing equation in time, was mastered well over a decade ago. With the benefit of such simulations, the fundamental physics of certain classes of turbulent flows is now well understood. For example, the driving instability of near-wall turbulence is now known to be closely linked to the chaotic interaction of the vortical regions of near-wall fluid, which are created by the mean shear of the viscous flow near the wall. The regions of the flow with high vorticity near the wall, commonly referred to as the coherent structures, have a characteristic behaviour that has been carefully studied. These vortical regions often appear as “hairpins” and longitudinal “tubes”, as shown in figure 2, that tangle, interact, and evolve in a complex, intermittent fashion.

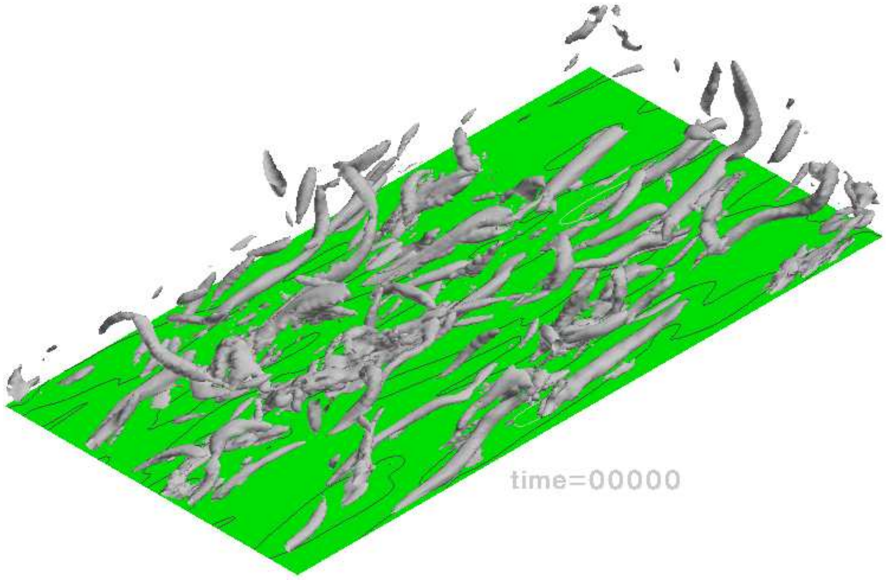

Figure 2: The coherent structures of near-wall turbulence.

With the abundance of computational power currently available, and the relatively mature numerical techniques to leverage this power, many complex flows of interest may now be modeled accurately by simulation of the Navier-Stokes equation or filtered versions thereof. Further, a significant expansion of this capability might be projected over the next several years, resulting from both increases in computational power (via parallel computers currently being developed) and improvements in numerical techniques. We must ask ourselves, however, what we plan to do with all of this simulation capability.

Leveraging these two advances—a mathematical understanding of the equation governing turbulence and the computational ability to simulate turbulence accurately—the time is ripe to make the next major advance: the control and optimization of flow systems dominated by the effects of turbulence for desired engineering objectives. Such a goal is now feasible because it is possible to utilize the equation governing turbulence in a computational setting to optimize and control a turbulent flow in an efficient manner. The objective of this work is to study and demonstrate how this may be done. This report has been organized as four self-contained articles. These articles lay out a progression over the following four topics:

I linear feedback for a linear flow system (transition),

II linear feedback for a nonlinear flow system (convection),

III predictive optimization of controls for a nonlinear flow system (turbulence), and

IV a framework for the optimization of robust controls for nonlinear flow systems.

These four articles are now summarized briefly.

Part I - Optimal and robust control and estimation
of linear paths to transition

It is generally inappropriate to treat multi-scale systems governed by nonlinear PDEs with classical control techniques (such as PID approaches and techniques based on Bode and root-locus analyses) or even "modern" control techniques (such as linear optimal control with Kalman filtering—designs based on analysis of transfer function norms and solved with Riccati-based approaches). Such techniques generally have been developed with low-order systems in mind, where the order of the state $N \lesssim O(100)$, whereas accurate simulations of turbulence routinely require $N \gtrsim O(10^6)$. Further, some of these techniques, such as approaches based on root-locus (eigenvalue) analysis, are not appropriate for systems with highly nonorthogonal eigenvectors, as often encountered in fluid mechanics. However, some specific PDE systems (under linear approximation) do decouple into several low-order systems amenable to analysis by the usual control strategies. Transition in a plane channel flow is just such a problem. This model problem, in addition to being a physically relevant problem in its own right, provides a very good starting point with which to introduce the topics of control and estimation in a fluid-mechanical setting. This problem also introduces the important concept of the noncooperative game framework, referred to as robust control, which is extended to the nonlinear Navier-Stokes equation in Part IV.

Part II - Linear control and estimation of nonlinear chaotic convection:
harnessing the butterfly effect

A control engineer's first instinct after solving the linear transition control problem of Part I might be to attempt to apply the linear control feedback so determined directly to the fully nonlinear problem of turbulence. This section examines the hazards of such a procedure (applying linear feedback to nonlinear systems) by examining a very low-order nonlinear convection problem which is easily amenable to analysis. The approach of applying linear feedback to both the controller and the estimator is ultimately made to work for this nonlinear convection problem, but only after the appropriate safeguards are taken. Further, the problem of turbulence is distinctly different from the convection problem studied here, as discussed in detail in this article. These differences appear to indicate that control of turbulence by simple linear feedback is a dubious proposition at best, and more appropriate feedback strategies need to be developed.

Part III - DNS-based predictive control of turbulence:
an optimal benchmark for feedback algorithms

For a mathematically rigorous framework for the control of nonlinear systems governed by the Navier-Stokes equation, we turn to the versatile yet cumbersome framework of predictive control. In this setting, a fully nonlinear flow problem (turbulent channel flow) is optimized over a receding finite horizon with the adjoint-based tools of optimal control theory. The results obtained (relaminarization of the turbulent flow with small amounts of blowing and suction) far surpass the results obtained with every other control algorithm tested in this flow to date.

The control strategy used is akin to that used to play a game of chess, in that future possible evolutions of the system are explored iteratively. The key feature that makes such an optimization tractable for the high-dimensional problem of turbulence, for which random or "brute-force" search algorithms are far too expensive even to consider, is that gradient information based on an adjoint analysis may be determined to update the controls efficiently for the desired purpose at each iteration. The adjoint field central to this approach is based on a mathematical statement of the engineering problem at hand and a nonlinear PDE representation of the equation governing the system of interest, obviating the need for *ad hoc* assumptions about the turbulence dynamics. Techniques proposed to extend the approach implemented here to a practical setting are discussed in detail.

Part IV - A general framework for robust control in fluid mechanics

For the application of control feedback in practical situations for which only limited, noisy measurements of the turbulent flow will be available, a degree of "robustness" will be very important in the control algorithm. The topic of robust control is a natural extension to that of optimal control. The analogy used to motivate this noncooperative-game approach is Murphy's law: *If a worst case disturbance can disrupt a controlled closed-loop system, it will.* Thus, in the robust framework, the controls are optimized in the presence of a finite component of that disturbance which is maximally detrimental to the control objective. Controls which are effective even in the presence of such a disturbance are also effective in the presence of a broad class of other disturbances.

Rather than a simple minimization problem, as encountered in optimal control, the robust control problem is an infinite-dimensional extrapolation of a saddle-point problem for the "best" control in the presence of the "worst" disturbance. The mathematical character of this saddle point problem is explored in detail in this article.

It is well known, even in the linear setting, that the performance of optimal control strategies is significantly degraded in noisy environments. For example, in the optimal linear setting (see Part I), disturbances are accounted for only in the estimator, not in the computation of the control feedback. This leads to the possibility for inappropriate control feedback arising from those modes of the system which can not be estimated accurately. Similar difficulties may be expected in the nonlinear setting. The robust framework naturally couples the control and estimation problems, accounting for the possible effects of disturbances when computing the control. For this reason, robust control of the nonlinear Navier-Stokes equation has been introduced and analyzed as a viable new tool for the optimization of practical, disturbed turbulent flow systems in which only limited, noisy measurement information is available. This robust approach is likely to be a key component of much of our future work in this area.

Literature surveys

The field of flow control is a very active field of research, and very significant contributions have been made by many different research groups. In order to review this field thoroughly, multiple comprehensive literature surveys have been completed in the course of this work. The first, published in June of 1994, is included as the appendix to this report. This review encapsulates the broad field of flow control at its state-of-the-art in 1994, citing scores of relevant references ranging from experimental, computational, and theoretical approaches to related flow control problems. It also summarizes our motivation for developing mathematically-based control algorithms for flow control problems, identifying a general taxonomy of schemes commonly used to attack flow control problems and describing how mathematically-based approaches fit with this big picture. In short, four general catagories of schemes are identified by examining the extent to which they are based on the governing flow equations. These catagories are:

- adaptive schemes,
- schemes based on understanding of dominant physics,
- schemes based on reduced-order systems, such as dynamical systems theory, and
- schemes based on optimal control theory.

It is noted that simple flow systems which behave approximately linearly may be controlled effectively by simple "black-box" strategies or by control strategies inspired by a general understanding of the flow physics. However, for distributed, multi-scale, chaotic flow systems such as turbulence, the effectiveness of such approaches is limited, and we are thus motivated to base our control algorithms on the Navier-Stokes equation known to govern the phenomena of interest.

In addition to this dedicated review paper, the literature was again carefully reviewed when composing each of the four main parts in the body of this report, and references which appeared in the last few years were paid particularly close attention. In this regard, note especially

a. the introduction and conclusions of Part II, which discuss feedback approaches for the control of low-dimensional nonlinear systems and their possible connection with the problem of control of turbulence, and

b. the introduction of Part III, which essentially re-reviews recent approaches taken to the turbulence control problem and discusses where optimal control theory fits into the larger picture.

Future work

Given current trends in simulation capability, it is clear that control and optimization of distributed systems by mathematically-based approaches will be commonplace in 20 years. The foundation for this design paradigm is being set today. The present collection of articles represents four new steps in this direction. Much work remains to be done. Several projects have been initiated which follow up on the present work and are currently under active investigation.

Acknowledgments

“When I heard the learn’d astronomer,
When the proofs, the figures, were ranged in columns
before me,
When I was shown the charts and diagrams, to add, divide,
and measure them,
When I sitting heard the astronomer where he lectured with
much applause in the lecture-room,
How soon unaccountable I became tired and sick,
Till rising and gliding out I wandered off by myself,
In the mystical moist night-air, and from time to time
Looked up in perfect silence at the stars.”

- Walt Whitman (1865)

This thesis is dedicated to my parents, who taught me to keep looking up.

Contents

Part I

Optimal and robust control and estimation of linear paths to transition

Part I has been published as

Bewley, T.R., & Liu, S. 1998 Optimal and robust control and estimation of linear paths to transition. *J. Fluid Mech.* **365**, 305-349.

Abstract

Optimal and robust control theories are used to determine effective, estimator-based feedback control rules for laminar plane channel flows that effectively stabilize linearly unstable flow perturbations at $Re = 10,000$ and linearly stable flow perturbations, characterized by mechanisms for very large disturbance amplification, at $Re = 5,000$. Wall transpiration (unsteady blowing/suction) with zero net mass flux is used as the control, and the flow measurement is derived from the wall skin-friction. The control objective, beyond simply stabilizing any unstable eigenvalues (which is relatively easy to accomplish), is to minimize the energy of the flow perturbations created by external disturbance forcing. This is important because, when mechanisms for large disturbance amplification are present, small amplitude external disturbance forcing may excite flow perturbations with sufficiently large amplitude to induce nonlinear flow instability.

The control algorithms used in the present work account for system disturbances and measurement noise in a rigorous fashion by application of modern linear control techniques to the discretized linear stability problem. The disturbances are accounted for both as uncorrelated white Gaussian processes ($\mathcal{H}_2$ or "optimal" control) and as finite "worst case" inputs which are maximally detrimental to the control objective ($\mathcal{H}_\infty$ or "robust" control). Root loci and transient energy growth analyses are shown to be inadequate measures to characterize overall system performance. Instead, appropriately-defined transfer function norms are used to characterize all systems considered in a consistent and relevant manner. In order to make a parametric study tractable in this high-dimensional system, a convenient new scaling to the estimation problem is introduced such that three scalar parameters $\{\gamma, \alpha, \ell\}$ may be individually adjusted to achieve desired closed-loop characteristics of the resulting systems. These scalar parameters may be intuitively explained, and are defined such that the resulting control equations retain the natural dual structure between the control parameter, ℓ, and the estimation parameter, α. The performance of the present systems with respect to these parameters is thoroughly investigated, and comparisons are made to simple proportional schemes where appropriate.

Chapter 1

Introduction

The behaviour of small flow perturbations in simple laminar shear flows is an important and well-understood problem (Drazin & Reid 1981). As the Reynolds number is increased, laminar flows often become unstable and transition to turbulence occurs. The effects of the turbulence produced are very significant and often undesirable, resulting in increased drag and heat transfer at flow boundaries. Thus, a natural engineering problem is to develop methods of flow control which can delay or eliminate transition to turbulence.

A firm theoretical basis for the control of small perturbations in viscous shear flows is only beginning to emerge. Some important steps in this direction, for the consideration of two-component (2C) disturbances, are provided by Hu & Bau (1994), Joshi, Speyer, & Kim (1995, 1997), and Joslin *et al.* (1997). In these works, the eigenvalues of the linearized transition problem are successfully stabilized in a closed-loop framework such that the dynamics of the vertical velocity component of the flow acting in concert with the controller is considered. Hu & Bau (1994) examines a restricted class of multiple-input/multiple-output (MIMO) proportional controllers with a single controller gain, with skin friction as the measurement and wall temperature as the actuation. Joshi, Speyer, & Kim (1997) examines a single-input/single-output (SISO) proportional-integral (PI) controller (i.e., a controller with both proportional and integral terms), with a single-point skin friction measurements used to determine each sine-wave component of the distributed wall velocity actuation. Joshi, Speyer, & Kim (1995) consider the $\mathcal{H}_2$ control of a problem related to the supercritical case presented here, reducing the problem to the 9 least-stable modes in a Matlab implementation of an $\mathcal{H}_2$ controller, and make several interesting theoretical observations about the effects of the distributed nature of the problem at hand. A formal treatment of the distributed nature of the present problem is given by Bamieh (1997). Joslin *et al.* (1997) also apply $\mathcal{H}_2$ control theory to a problem related to the supercritical case presented here; in their approach, the control is determined through an adjoint formulation requiring full flowfield information.

Root loci, which partially characterize system behaviour by tracking the movement of closed-loop system *eigenvalues* as a function of control parameters (Joshi, Speyer, & Kim 1995, 1997), are inadequate to quantify the performance of the present closed-loop systems, as they do not address the nonorthogonality of system *eigenvectors* (Trefethen *et al.* 1993). It is possible to characterize the nonorthogonality of a set of eigenvectors by determining the maximum transient energy growth of a stable system from a deleterious set of initial conditions by a variational formulation (Butler & Farrell 1992). However, such an approach is, at best, a dubious approximation of the method by which external disturbance forcing actually excites flow perturbations.

To adequately characterize the behaviour of a nonorthogonal linear system and its excitation by external disturbances, taking into account any known structure by which external disturbances force the state equation, *transfer function norms* are the appropriate measure (Skogestad & Postlethwaite 1996). In the present work, norms of the disturbance to state ($\mathbf{w} \to \mathbf{x}$) transfer function and the disturbance to control ($\mathbf{w} \to \mathbf{u}$) transfer function are introduced to quantify separately the response of the state and the response of the control to Gaussian and worst-case disturbances. For both of the cases considered, it is shown that the state response is significantly reduced in the closed-loop systems by application of modern control theory. Further, the rms of the control applied to achieve this reduced state response is bounded and may be kept small. On the other hand, the rms of controllers which contain a proportional component, such as that of Joshi, Speyer, & Kim (1997), in response to Gaussian disturbances is shown to be unbounded.

The present work improves upon previous analyses of flow transition by rigorously accounting for state disturbances and measurement noise in both a Gaussian and a worst-case sense. The controllers and estimators used are determined by application of $\mathcal{H}_2$ ("optimal") and $\mathcal{H}_\infty$ ("robust") approaches for linear problems. These techniques have recently been put in a compact form by Doyle *et al.* (1989), and are shown to be well suited to the current problem.

A two-step control approach is used. First, a state estimate is developed from a (potentially inaccurate) model of the flow equations, with corrections to this state estimate provided by (noisy) flow measurements fed back through an estimator feedback matrix L. This state estimate is then multiplied by a controller feedback matrix K to determine the control. Control theory is used simply to compute the matrices K and L.

Potentially, this approach can yield better results than a proportional controller. In comparison to the SISO proportional approach, the present estimator-based approach has many more parameters in the control law (specifically, the elements of the matrices K and L), which are rigorously optimized for a clearly defined objective. In this manner, large multiple-input/multiple-output (MIMO) systems are handled naturally and the controller is coupled with an estimator which models the known dynamics of the system itself.

Classical control approaches, such as the PI controller of Joshi, Speyer, & Kim (1997), are sufficient to stabilize any unstable eigenvalues in the present problems. However, modern (i.e., optimal and robust) control approaches produce closed-loop systems which are *far* less sensitive to external disturbances (as quantified in §6.1), and thus are far less likely to exhibit nonlinear instabilities when said external disturbance forcing is of finite magnitude. Many problems in fluid mechanics, including the later stages of transition and turbulence, are dominated by nonlinear behaviour. In such problems, the linear analysis performed in this article is not valid. Iterative optimal control approaches over finite time intervals, which make use of full state information, may still be formulated (Abergel & Temam 1990) and performed (Moin & Bewley 1995) with impressive results. In order to make such schemes practical, one must understand how to account for disturbances in a rigorous fashion and how to estimate accurately the necessary components of the state (for instance, the location and strength of the near-wall coherent structures) based on limited flow measurements. The present article makes these concepts clear in a fluid-mechanical sense, albeit for a linear problem, and thus provides a step in this development. Techniques to extend the robust control concept, introduced for problems in fluid mechanics in the present work, to nonlinear problems (such as turbulence) are discussed in Bewley, Moin, & Temam (1997) and Bewley, Temam, & Ziane (1998).

1.1 Outline of article

The structure of the remainder of the article is:

§2. The governing equations for the flow stability problem are put in a standard notation which makes subsequent application of control theory straightforward. Two specific cases are identified to be examined in detail: one supercritical and one subcritical.

§3. The control approach and numerical method used are briefly summarized.

§4. The methods used to analyze the open-loop and closed-loop systems are reviewed.

§5. The uncontrolled ("open-loop") systems are studied in detail.

§6. The controlled ("closed-loop") systems are studied in detail. Root loci, which demonstrate the movement of the closed-loop system eigenvalues with respect to control parameters, are shown to illuminate some general trends, but fail to provide a quantitative measure of system performance. Maximum transient energy growth, which indicates nonorthogonality of closed-loop system eigenvectors, also fails to provide a quantitative measure of system performance. The rms response of the state and the control to white Gaussian disturbances and "worst-case" disturbances is ultimately quantified using the 2-norm and the ∞-norm of the appropriate transfer functions, and the system behaviour as a function of the control parameters $\{\gamma, \alpha, \ell\}$ is thoroughly investigated.

§7. Important results are summarized and concluding remarks are made.

Chapter 2

Governing equations

In this chapter, the equations governing small flow perturbations in a laminar channel flow (Poiseuille flow) are succinctly summarized in a form to which standard control techniques may be applied. This familiar discussion is presented to precisely define the problem under consideration, and to demonstrate that the simpler and more intuitive "classical" derivation of the flow stability problem may be used easily in a controls setting, bypassing the involved stream function derivation of Joshi, Speyer, & Kim (1995, 1997) which leads to a state-space formulation for two-component (2C) perturbations only. Readers interested only in how the control techniques are applied to the flow stability problem derived here are advised to proceed directly to §3.

In the present development, it is assumed that an array of sensors, which measure streamwise and spanwise skin-friction, and actuators, which provide wall-normal blowing and suction with zero net mass flux, are mounted on the walls of a laminar channel flow. It is also assumed that a sufficient number of sensors and actuators is installed in both the streamwise and spanwise directions so that, in these directions, individual Fourier components of wall skin-friction and wall transpiration may be approximated. The control analyses in the present work are then carried through for particular wavenumber pairs. The next natural step after the present work is to compute an array of controllers at an array of wavenumber pairs with the methods developed herein, then to inverse transform the resulting set of controllers back to the physical domain. Recent theoretical work by Bamieh (1997) indicates that such a procedure should result in spatial convolution kernels with compact support such that the weights on sensor measurements eventually decay exponentially as a function of distance from the actuator. This property will allow the convolution kernels to be truncated with a prescribed degree of accuracy at a finite distance from each actuator, resulting in implementable schemes in the physical domain. The present work sets the stage for this development.

2.1 Continuous form of flow equations

Consider a steady plane channel flow with maximum velocity U_0 and channel half-width δ. Non-dimensionalizing all velocities by U_0 and lengths by δ, the mean velocity profile in the streamwise direction (x) may be written $U(y) = 1 - y^2$ on the domain $y \in [-1, 1]$. The equations governing small, incompressible, three-dimensional perturbations $\{u, v, w, p\}$ to the mean flow U are given by the linearized Navier-Stokes and continuity

$$\dot{u} + U\frac{\partial}{\partial x}u + U'v = -\frac{\partial p}{\partial x} + \frac{1}{Re}\Delta u \tag{2.1a}$$
$$\dot{v} + U\frac{\partial}{\partial x}v = -\frac{\partial p}{\partial y} + \frac{1}{Re}\Delta v \tag{2.1b}$$
$$\dot{w} + U\frac{\partial}{\partial x}w = -\frac{\partial p}{\partial z} + \frac{1}{Re}\Delta w \tag{2.1c}$$

$$\frac{\partial u}{\partial x} + \frac{\partial v}{\partial y} + \frac{\partial w}{\partial z} = 0, \tag{2.2}$$

where $\Delta \triangleq \partial^2/\partial x^2 + \partial^2/\partial y^2 + \partial^2/\partial z^2$ is the Laplacian, $Re \triangleq U_0\delta/\nu$ is the Reynolds number, ν is the kinematic viscosity, dot ($\dot{}$) denotes $\partial/\partial t$, and prime ($'$) denotes d/dy. A single equation for the normal component of velocity v, found by taking the Laplacian of (2.1b), substituting for Δp from the divergence of (2.1), and applying (2.2), is

$$\Delta\dot{v} = \Big\{ -U\frac{\partial}{\partial x}\Delta + U''\frac{\partial}{\partial x} + \Delta(\Delta/Re)\Big\}\ v. \tag{2.3a}$$

The equation for the normal component of vorticity $\omega \triangleq \partial u/\partial z - \partial w/\partial x$, found by subtracting $\partial/\partial x$ of (2.1c) from $\partial/\partial z$ of (2.1a), is

$$\dot{\omega} = \Big\{ -U'\frac{\partial}{\partial z}\Big\}\ v + \Big\{ -U\frac{\partial}{\partial x} + \Delta/Re\Big\}\ \omega. \tag{2.3b}$$

The flow perturbation problem in $\{u, v, w, p\}$ with second-order partial derivatives in (2.1)-(2.2) has been reduced to a problem in $\{v, \omega\}$ with fourth-order partial derivatives in (2.3) with no loss of generality; essentially, the three-component velocity field has been projected onto a two-component divergence-free manifold by eliminating the pressure from the equations and applying continuity. Such a manipulation is standard practice for both the present derivation (Gustavsson & Hultgren 1980) and the fully nonlinear Navier-Stokes equation (Kim, Moin, & Moser 1987).

As the domain is homogeneous in the x and z directions, we may Fourier transform the solution such that

$$v(x,y,z,t) = \sum_{k_x,k_z} \hat{v}(k_x,y,k_z,t)\exp[i(k_x\,x + k_z\,z)]$$
$$\omega(x,y,z,t) = \sum_{k_x,k_z} \hat{\omega}(k_x,y,k_z,t)\exp[i(k_x\,x + k_z\,z)].$$

As the various Fourier modes are orthogonal and equations (2.3a) and (2.3b) are linear, the solution for each wavenumber pair (k_x, k_z) is decoupled and obeys the equations

$$\Delta\,\dot{v} = \{-i\,k_x\,U\,\Delta + i\,k_x\,U'' + \Delta(\Delta/Re)\}\;v \tag{2.4a}$$
$$\dot{\omega} \;= \{-i\,k_z\,U'\}\;v + \;\{-i\,k_x\,U + \Delta/Re\}\;\omega, \tag{2.4b}$$

where the hat accents ($\hat{}$) have been dropped for notational convenience and the Laplacian now takes the form $\Delta \triangleq \partial^2/\partial y^2 - k_x^2 - k_z^2$. Equation (2.4a) is the well-known (fourth order) Orr-Sommerfeld equation for the wall-normal velocity modes, and (2.4b) is the (second order) equation for the wall-normal vorticity modes. Note the one-way coupling between these two equations. Also note that, from any solution $\{v, \omega\}$, the values of u and w may be extracted by manipulation of the above equations into the forms

$$u = \frac{i}{k_x^2 + k_z^2}\left(k_x\,\frac{\partial v}{\partial y} - k_z\,\omega\right) \qquad \text{and} \qquad w = \frac{-i}{k_x^2 + k_z^2}\left(k_z\,\frac{\partial v}{\partial y} - k_x\,\omega\right), \tag{2.5}$$

and p may be found by solution of the equation $\Delta p = -2i\,k_x\,U'\,v$. Control is applied at the wall as a boundary condition on the wall-normal component of velocity v. The boundary conditions on u and w are no-slip ($u = w = 0$), which implies that, at the wall, $\omega = 0$ and (by continuity) $\partial v/\partial y = 0$.

2.2 Discrete form of flow equations

The continuous equations for the $\{v, \omega\}$ perturbations in (2.4) are now discretized on a grid of $N+1$ Chebyshev-Gauss-Lobatto points in the wall-normal direction such that

$$y_\kappa = \cos(\pi\kappa/N) \qquad \text{for } 0 \le \kappa \le N.$$

An $(N+1)\times(N+1)$ matrix $\mathscr{D}$ may be expressed (Canuto *et al.* 1988, eqn. 2.4.31) such that the derivative of $\boldsymbol{\omega}$ with respect to y on the discrete set of $N+1$ points is given by

$$\boldsymbol{\omega}' = \mathscr{D}\,\boldsymbol{\omega} \qquad \text{and} \qquad \boldsymbol{\omega}'' = \mathscr{D}\,\boldsymbol{\omega}',$$

where the prime ($'$) indicates the derivative of the vector $\boldsymbol{\omega}$ with respect to y. The homogeneous Neumann boundary condition on $\mathbf{v}$ is accomplished by modifying the first derivative matrix such that

$$\tilde{\mathscr{D}}_{\iota\kappa} = \begin{cases} 0 & \iota = 0, N \\ \mathscr{D}_{\iota\kappa} & 1 \leq \iota \leq N-1. \end{cases}$$

Differentiation of $\mathbf{v}$ with respect to y is then given by

$$\mathbf{v}' = \tilde{\mathscr{D}}\,\mathbf{v}, \qquad \mathbf{v}'' = \mathscr{D}\,\mathbf{v}', \qquad \mathbf{v}''' = \mathscr{D}\,\mathbf{v}'', \qquad \text{and} \qquad \mathbf{v}'''' = \mathscr{D}\,\mathbf{v}'''.$$

With these derivative matrices, it is straightforward to write (2.4) in matrix form. This is accomplished by first expressing the matrix form of (2.4) on all $N+1$ collocation points such that[1]

$$\dot{\mathbf{v}} = \mathscr{L}\,\mathbf{v} \tag{2.6a}$$

$$\dot{\boldsymbol{\omega}} = \mathscr{C}\,\mathbf{v} + \mathscr{S}\,\boldsymbol{\omega}, \tag{2.6b}$$

where the $(N+1)\times(N+1)$ matrices $\mathscr{L}$, $\mathscr{C}$, and $\mathscr{S}$ represent the spatial discretization of the bracketed operations in (2.4). The Dirichlet boundary conditions are explicitly prescribed as separate "forcing" terms. To accomplish this, decompose $\mathscr{L}$, $\mathscr{C}$, and $\mathscr{S}$ according to

$$\mathscr{L} = \begin{pmatrix} * & * & * \\ \mathbf{b}_{11} & \mathscr{L}_c & \mathbf{b}_{12} \\ * & * & * \end{pmatrix} \qquad \mathscr{C} = \begin{pmatrix} * & * & * \\ \mathbf{b}_{21} & \mathscr{C}_c & \mathbf{b}_{22} \\ * & * & * \end{pmatrix} \qquad \mathscr{S} = \begin{pmatrix} * & * & * \\ * & \mathscr{S}_c & * \\ * & * & * \end{pmatrix}$$

where $\mathscr{L}_c$, $\mathscr{C}_c$, and $\mathscr{S}_c$ are $(N-1)\times(N-1)$ and $\mathbf{b}_{11}$, $\mathbf{b}_{12}$, $\mathbf{b}_{21}$, and $\mathbf{b}_{22}$ are $(N-1)\times 1$. Noting that $\omega_0 = \omega_N = 0$ by the no-slip condition, and defining

$$\mathbf{x} \triangleq \begin{pmatrix} v_1 \\ \vdots \\ v_{N-1} \\ \omega_1 \\ \vdots \\ \omega_{N-1} \end{pmatrix} \qquad A \triangleq \begin{pmatrix} \mathscr{L}_c & 0 \\ \mathscr{C}_c & \mathscr{S}_c \end{pmatrix} \qquad B \triangleq \begin{pmatrix} -\mathbf{b}_{11} & \mathbf{b}_{12} \\ -\mathbf{b}_{21} & \mathbf{b}_{22} \end{pmatrix} \qquad \mathbf{u} \triangleq \begin{pmatrix} -v_0 \\ v_N \end{pmatrix},$$

[1]Note that, for $k_x^2 + k_z^2 \neq 0$, the matrix form of the LHS of (2.4a) is invertible, so the form (2.6a) is easily determined.

where $\mathbf{x}$ is $2(N-1)\times 1$, A is $2(N-1)\times 2(N-1)$, B is $2(N-1)\times 2$, and $\mathbf{u}$ is 2×1, we may express (2.6) in the form

$$\boxed{\dot{\mathbf{x}} = A\mathbf{x} + B\mathbf{u}.} \tag{2.7}$$

The vector $\mathbf{x}$, which contains the normal velocity fluctuations v_i and normal vorticity fluctuations ω_i at the grid points on the interior of the channel, is referred to as the "state". The vector $\mathbf{u}$, which contains the blowing/suction velocity at the top and bottom walls, is referred to as the "control".

2.3 Wall measurements

We will consider control algorithms using both full flowfield information and wall information only. For the latter case, we will assume that measurements made at the wall provide information about the streamwise and spanwise skin-friction, from which (subtracting out the known influence of $\partial v/\partial x$ and $\partial v/\partial z$ from the stress tensor at the wall) we may determine the following four quantities:

$$\begin{aligned} y_{m1} &= -\frac{1}{Re}\frac{\partial u}{\partial y}\Big|_{\text{upper wall}} & \qquad y_{m2} &= \frac{1}{Re}\frac{\partial u}{\partial y}\Big|_{\text{lower wall}} \\ y_{m3} &= -\frac{1}{Re}\frac{\partial w}{\partial y}\Big|_{\text{upper wall}} & \qquad y_{m4} &= \frac{1}{Re}\frac{\partial w}{\partial y}\Big|_{\text{lower wall}}. \end{aligned} \tag{2.8}$$

With (2.5), we may express these measurements as linear combinations of v and ω. Defining $a \triangleq i\,k_x/(k_x^2+k_z^2)/Re$ and $b \triangleq -i\,k_z/(k_x^2+k_z^2)/Re$, the measurements are expressed in terms of the discrete vectors $\mathbf{v}$ and $\boldsymbol{\omega}$ as

$$\begin{aligned} y_{m1} &= \Big(-a\,\mathscr{D}\,\tilde{\mathscr{D}}\,\mathbf{v} - b\,\mathscr{D}\,\boldsymbol{\omega}\Big)\Big|_{\text{upper wall}} & \qquad y_{m2} &= \Big(a\,\mathscr{D}\,\tilde{\mathscr{D}}\,\mathbf{v} + b\,\mathscr{D}\,\boldsymbol{\omega}\Big)\Big|_{\text{lower wall}} \\ y_{m3} &= \Big(-b\,\mathscr{D}\,\tilde{\mathscr{D}}\,\mathbf{v} - a\,\mathscr{D}\,\boldsymbol{\omega}\Big)\Big|_{\text{upper wall}} & \qquad y_{m4} &= \Big(b\,\mathscr{D}\,\tilde{\mathscr{D}}\,\mathbf{v} + a\,\mathscr{D}\,\boldsymbol{\omega}\Big)\Big|_{\text{lower wall}}. \end{aligned}$$

Decompose $\mathscr{D}$, $\tilde{\mathscr{D}}$, and $(\mathscr{D}\,\tilde{\mathscr{D}})$ according to

$$\mathscr{D} = \begin{pmatrix} * & \mathbf{c}_3 & * \\ * & * & * \\ * & \mathbf{c}_4 & * \end{pmatrix} \qquad \tilde{\mathscr{D}} = \begin{pmatrix} * & * & * \\ * & \tilde{\mathscr{D}}_c & * \\ * & * & * \end{pmatrix} \qquad (\mathscr{D}\,\tilde{\mathscr{D}}) = \begin{pmatrix} d_1 & \mathbf{c}_1 & d_3 \\ * & * & * \\ d_2 & \mathbf{c}_2 & d_4 \end{pmatrix},$$

where $\tilde{\mathscr{D}}_c$ (to be used in the following section) is $(N-1)\times(N-1)$, $\mathbf{c}_1$, $\mathbf{c}_2$, $\mathbf{c}_3$, and $\mathbf{c}_4$ are $1\times(N-1)$, and d_1, d_2, d_3, and d_4 are 1×1. Finally, defining

$$\mathbf{y}_m \triangleq \begin{pmatrix} y_{m1} \\ y_{m2} \\ y_{m3} \\ y_{m4} \end{pmatrix} \qquad C \triangleq \begin{pmatrix} -a\,\mathbf{c}_1 & -b\,\mathbf{c}_3 \\ a\,\mathbf{c}_2 & b\,\mathbf{c}_4 \\ -b\,\mathbf{c}_1 & -a\,\mathbf{c}_3 \\ b\,\mathbf{c}_2 & a\,\mathbf{c}_4 \end{pmatrix} \qquad D \triangleq \begin{pmatrix} a\,d_1 & -a\,d_3 \\ -a\,d_2 & a\,d_4 \\ b\,d_1 & -b\,d_3 \\ -b\,d_2 & b\,d_4 \end{pmatrix},$$

where $\mathbf{y}_m$ is 4×1, C is $4\times 2(N-1)$, and D is 4×2, allows us to express $\mathbf{y}_m$ in the form of a linear combination of the state $\mathbf{x}$ and the control $\mathbf{u}$

$$\boxed{\mathbf{y}_m = C\mathbf{x} + D\mathbf{u}.} \tag{2.9}$$

The vector $\mathbf{y}_m$ is referred to as the "measurement".

2.4 Inner product, vector 2-norm, and energy density

Define the inner product for two discrete vectors $\mathbf{u}$ and $\mathbf{v}$ discretized on the collocation points $y_\kappa = \cos(\pi\kappa/N)$ by

$$(\mathbf{u},\,\mathbf{v}) \triangleq \sum_{\kappa=0}^{N} u_\kappa^*\, v_\kappa\, \zeta_\kappa, \qquad \text{where} \qquad \zeta_\kappa \triangleq \begin{cases} \dfrac{\pi}{2N} & \kappa = 0, N \\ \dfrac{\pi}{N} & 1 \le \kappa \le N-1. \end{cases}$$

Orthogonality of two vectors implies that their inner product is zero, $(\mathbf{u},\mathbf{v}) = 0$. The 2-norm of a vector $\mathbf{u}$, denoted $||\mathbf{u}||$, is defined as the square root of $(\mathbf{u},\mathbf{u})$. Note that, for two vectors of the same dimension as the state vector $\mathbf{x}$, which is defined only on the interior grid points, the inner product is given simply by

$$(\mathbf{u},\,\mathbf{v}) = \frac{\pi}{N}\,\mathbf{u}^*\,\mathbf{v}, \tag{2.10}$$

where star $(^*)$ applied to a vector denotes conjugate transpose. The corresponding inner product for two continuous complex functions u, v on the domain $y \in [-1,1]$ is given by

$$(u,\,v) \triangleq \int_{-1}^{1} u^*\, v\,\eta\, dy, \qquad \text{where} \qquad \eta(y) \triangleq (1-y^2)^{-1/2}$$

and the star $(^*)$ denotes the complex conjugate. For sufficiently smooth functions u, v on a sufficiently large number N of Chebyshev-Gauss-Lobatto grid points (Canuto *et al.* 1988), this inner product of the continuous functions approximates the inner product of the discrete vectors, $(u,\,v) \approx (\mathbf{u},\,\mathbf{v})$.

The implication of using a discretization dependent weighting factor, such as $\eta(y)$, to develop a control rule is discussed in §6.2.

For the purpose of developing control rules, the kinetic energy density is a more physically relevant quantity than measures derived from a (discretization dependent) 2-norm of the discretized vector, such as that given by $\eta(y)$ above. The kinetic energy density of a flow perturbation in the physical domain is

$$\mathscr{E} = \frac{1}{V} \int_{-1}^{1} \int_{0}^{2\pi/k_x} \int_{0}^{2\pi/k_z} \frac{u^2 + v^2 + w^2}{2} \, dz \, dx \, dy,$$

where $V = 8\pi/(k_x k_z)$ is the volume of the domain under consideration. Considering a single Fourier mode (k_x, k_z) and (again) dropping the hat accents $(\hat{\ })$ for notational convenience, the kinetic energy density is expressed in terms of $\{\hat{v}, \hat{\omega}\}$ as

$$\mathscr{E} = \frac{1}{8} \int_{-1}^{1} \left[v^* v + \frac{1}{k_x^2 + k_z^2} \left(\frac{\partial v^*}{\partial y} \frac{\partial v}{\partial y} + \omega^* \omega \right) \right] dy.$$

For the discrete state vector $\mathbf{x}$, this integration corresponds to

$$\boxed{\mathscr{E} = \mathbf{x}^* \, Q \, \mathbf{x},} \qquad \text{where} \qquad Q = \frac{1}{8} \begin{pmatrix} \Omega + \dfrac{1}{k_x^2 + k_z^2} \tilde{\mathscr{D}}_c^* \, \Omega \, \tilde{\mathscr{D}}_c & 0 \\ 0 & \dfrac{1}{k_x^2 + k_z^2} \Omega \end{pmatrix}$$

and Ω is an $(N-1) \times (N-1)$ diagonal matrix with nonzero entries $\Omega_{\kappa\kappa} = \zeta_\kappa / \eta(y_\kappa)$, where $1 \leq \kappa \leq N-1$, to properly account for the integrations on the stretched mesh.

2.5 Cases studied

It is well known that, for supercritical $Re > 5772$, the uncontrolled problem is linearly unstable, with the most unstable modes occurring for flow perturbations with $k_z \approx 0$, and that, for subcritical $Re \leq 5772$, the uncontrolled problem is linearly stable. However, transition often occurs at a Reynolds number well below that required for linear instability of the laminar flow. Butler & Farrell (1992) show that the non-orthogonality of the eigenmodes of subcritical flows, especially for flow perturbations with $k_x \approx 0$, implies that flow perturbations of a particular initial structure will experience large, $O(Re)$ amplification of energy before their eventual decay. They suggest that such transient linear amplification can sometimes lead to flow perturbations large enough for nonlinear instability to be triggered, if such initial conditions ever happen to be encountered. This article will explore control techniques which simultaneously a) stabilize any unstable system eigenvalues, and b) greatly reduce the maximum transient energy growth of small flow perturbations due to nonorthogonal system eigenvectors. The quantitative comparison of the various controlled closed-loop systems, however, will finally be obtained by the transfer function analysis to be described in §4.4.

To simplify our discussion, we will restrict our attention in the remainder of this work to one supercritical case and one subcritical case:

CASE (i): $Re = 10,000$, $k_x = 1$, $k_z = 0$;
CASE (ii): $Re = \ \ 5,000$, $k_x = 0$, $k_z = 2.044$.

Case (i), which is supercritical, is the "classic" $Re = 10,000$ case benchmarked by Orszag (1971). It has been studied by several authors since, including Joshi, Speyer, & Kim (1997). Case (ii), which is subcritical, is the wavenumber pair that gives the maximum transient energy growth at $Re = 5,000$, as shown by Butler & Farrell (1992).

For case (i), $k_z = 0$ and thus $\mathscr{C} = 0$ in (2.6), entirely decoupling the $\boldsymbol{\omega}$ eigenmodes from both the $\mathbf{v}$ eigenmodes and from the control $\mathbf{u} = (v_0,\ v_N)^T$. The $\boldsymbol{\omega}$ eigenmodes are thus unaffected by the application of the control $\mathbf{u}$. Fortunately, it is also found that the $\boldsymbol{\omega}$ eigenmodes are stable. Thus, for the purpose of studying the effect of the control in case (i) (only), we may restrict our attention to the $\mathbf{v}$ eigenmodes according to a reduced system with

$$\mathbf{x} \triangleq \begin{pmatrix} v_1 \\ \vdots \\ v_{N-1} \end{pmatrix} \qquad A \triangleq \begin{pmatrix} & & \\ & \mathscr{L}_c & \\ & & \end{pmatrix} \qquad B \triangleq \begin{pmatrix} -\mathbf{b}_{11} & \mathbf{b}_{12} \end{pmatrix} \qquad \mathbf{u} \triangleq \begin{pmatrix} -v_0 \\ v_N \end{pmatrix},$$

where $\mathbf{x}$ is $(N-1)\times 1$, A is $(N-1)\times(N-1)$, B is $(N-1)\times 2$, and $\mathbf{u}$ is 2×1, and

$$\mathbf{y}_m \triangleq \begin{pmatrix} y_{m1} \\ y_{m2} \\ y_{m3} \\ y_{m4} \end{pmatrix} \qquad C \triangleq \begin{pmatrix} -a\,\mathbf{c}_1 \\ a\,\mathbf{c}_2 \\ -b\,\mathbf{c}_1 \\ b\,\mathbf{c}_2 \end{pmatrix} \qquad D \triangleq \begin{pmatrix} a\,d_1 & -a\,d_3 \\ -a\,d_2 & a\,d_4 \\ b\,d_1 & -b\,d_3 \\ -b\,d_2 & b\,d_4 \end{pmatrix},$$

where $\mathbf{y}_m$ is 4×1, C is $4\times(N-1)$, and D is 4×2. The full dynamics of the controlled system for case (i) is simply the dynamics of the controlled reduced system for $\mathbf{v}$ together with the decoupled, stable dynamics of the uncontrolled system for $\boldsymbol{\omega}$.

For case (ii), as $\mathscr{C} \neq 0$, we must use the full coupled system derived in §2.2 and §2.3. Note that case (ii), which consists of three-component $\{u, v, w\}$ perturbations, varies only in the y and z directions, and therefore is properly referred to (Reynolds & Kassinos 1995) as 2D, 3C (two-dimensional, three-component). Case (i), for which we consider only the two-component $\{u, v\}$ perturbations, varies only in the x and y directions, and therefore is referred to as 2D, 2C (two-dimensional, two-component).

2.6 State disturbances and measurement noise

State disturbances of some level are inevitable in any flow. They arise from sources such as acoustics, surface irregularities, vibrations of the wind-tunnel walls, etc. Measurement noise of some level is also inevitable. It arises from inaccuracies of the sensors and from the electronics processing their signals. These phenomena are now accounted for in a general form. The simple assumptions used to solve the problem here may be refined as more information is learned about particular flows of interest.

Define G_1 as the square root of the expected covariance of the state disturbances to be added to (2.7) and G_2 as the square root of the expected covariance of measurement noise to be added to (2.9). Note that G_1 and G_2 are time invariant, and it can be assumed that G_2 is nonsingular due to the inevitability of noise in measurements. In the present problem, as nothing yet is known about the state disturbances or measurement noise *a priori*, they are assumed to have the simple covariances

$$G_1 \triangleq I \qquad \text{and} \qquad G_2 \triangleq \alpha I \ \Rightarrow \ \alpha G_2^{-1} = I.$$

The parameter α^2 is defined as the ratio of the maximum singular value, $\sigma_{\max}$, of the covariance of the measurement noise to the maximum singular value of the covariance of the state disturbances,

$$\alpha^2 \triangleq \frac{\sigma_{\max}(G_2^2)}{\sigma_{\max}(G_1^2)},$$

and the problem is normalized such that $\sigma_{\max}(G_1^2) = 1$. Known structure of these covariances (for example, if one sensor is known to be noisier than another) is accounted for by replacing the identity matrices in the above expressions with appropriate matrices of unit maximum singular value, retaining the quantity α to reflect the balance between the magnitudes of the two types of disturbances[2].

The disturbed system under consideration may be written

$$\begin{aligned} \dot{\mathbf{x}} &= A\mathbf{x} + G_1\mathbf{w}_1 + B\mathbf{u} \\ \mathbf{y}_m &= C\mathbf{x} + G_2\mathbf{w}_2 + D\mathbf{u}. \end{aligned}$$

The controllers developed in this work will rigorously account for the state disturbances $G_1\mathbf{w}_1$ and the measurement noise $G_2\mathbf{w}_2$. These "disturbances", as they shall generically be referred to, are considered both in a Gaussian sense and in a worst-case sense; the present system definition is

[2]This scaling of the problem is used because it turns out to be quite convenient in the derivation of the $\mathcal{H}_\infty$ estimator in the development to follow. Note that the definition of α is based on the ratio of maximum singular values of the covariance matrices; the maximum singular value is also referred to as the induced matrix 2-norm, i.e., $||G_2^2||_2 \triangleq \sigma_{\max}(G_2^2)$.

convenient for the consideration of both types of disturbances.

When optimizing the system response to disturbances with a Gaussian structure, as any covariance of the disturbances known in advance is accounted for in G_1 and G_2, the external signals $\mathbf{w}_1$ and $\mathbf{w}_2$ are taken as uncorrelated, zero-mean, white Gaussian processes with covariance $E[\,\mathbf{w}_1\,\mathbf{w}_1^*\,] = I$, $E[\,\mathbf{w}_2\,\mathbf{w}_2^*\,] = I$. Note that, for the present system, the expectation value may be written

$$E[\cdot] = \lim_{T\to\infty} \frac{1}{T} \int_0^T [\cdot]\, dt.$$

When optimizing the system response to worst-case disturbances, as, again, any covariance of the disturbances known in advance is accounted for in G_1 and G_2, no disturbance structure is assumed at all. Instead, a finite "unstructured" disturbance is found which maximizes a cost function representing the control objective. Simultaneously, a controller is found which minimizes the same cost function in the presence of this disturbance. This is the essence of noncooperative game theory, and will be discussed further in §3.

To account for disturbances in a more tractable manner in the control theory, define a new "observation" vector $\mathbf{y}$ by a simple change of variables such that

$$\mathbf{y} \triangleq \alpha\, G_2^{-1}(\mathbf{y}_m - D\,\mathbf{u}).$$

The observation $\mathbf{y}$ is easily determined from the flow measurements. Also, define

$$B_1 \triangleq \begin{pmatrix} G_1 & 0 \end{pmatrix}, \qquad B_2 \triangleq B, \qquad C_2 \triangleq \alpha\, G_2^{-1} C, \qquad D_{21} \triangleq \begin{pmatrix} 0 & \alpha\, I \end{pmatrix}, \qquad \mathbf{w} \triangleq \begin{pmatrix} \mathbf{w}_1 \\ \mathbf{w}_2 \end{pmatrix}.$$

The system is then written in the standard form

$$\boxed{\begin{aligned} \dot{\mathbf{x}} &= A\,\mathbf{x} + B_1\,\mathbf{w} + B_2\,\mathbf{u} \\ \mathbf{y} &= C_2\mathbf{x} + D_{21}\mathbf{w}. \end{aligned}} \tag{2.11}$$

Chapter 3

Application of control theory and numerical method

3.1 Summary of control approach

In §2, it was shown that the equations governing small flow perturbations in a laminar channel flow may be expressed in the standard form

$$\dot{\mathbf{x}} = A\,\mathbf{x} + B_1\,\mathbf{w} + B_2\mathbf{u} \tag{3.1a}$$

$$\mathbf{y} = C_2\mathbf{x} + D_{21}\mathbf{w}. \tag{3.1b}$$

A simple method is sought to "close the loop" to stabilize the system; i.e., to determine a control $\mathbf{u}$ based on the observations $\mathbf{y}$ to force the state $\mathbf{x}$ towards zero in a manner which rigorously accounts for the disturbances $\mathbf{w}$. A system model with a structure similar to the system (3.1) itself, but without the influence of the unknown disturbances, is used for this purpose such that

$$\dot{\hat{\mathbf{x}}} = A\,\hat{\mathbf{x}} + B_2\mathbf{u} - \hat{\mathbf{u}} \tag{3.2a}$$

$$\hat{\mathbf{y}} = C_2\hat{\mathbf{x}}, \tag{3.2b}$$

with feedback $\hat{\mathbf{u}}$ based on the difference between the observations of the state $\mathbf{y}$ and the corresponding quantity in the model $\hat{\mathbf{y}}$ such that

$$\hat{\mathbf{u}} = L(\mathbf{y} - \hat{\mathbf{y}}). \tag{3.2c}$$

The control $\mathbf{u}$, in turn, is based on the state estimate $\hat{\mathbf{x}}$ such that

$$\mathbf{u} = K\hat{\mathbf{x}}. \tag{3.3}$$

Equation (3.1), is referred to as the "plant", (3.2) is referred to as the "estimator", and (3.3) is referred to as the "controller". The problem at hand is to compute linear time-invariant (LTI) matrices L and K such that i) the estimator feedback $\hat{\mathbf{u}}$ forces the state estimate $\hat{\mathbf{x}}$ in the estimator towards the state $\mathbf{x}$ in the plant, and ii) the controller feedback $\mathbf{u}$ forces the state $\mathbf{x}$ towards zero in the plant.

The flow of information is illustrated schematically in the following block diagram.

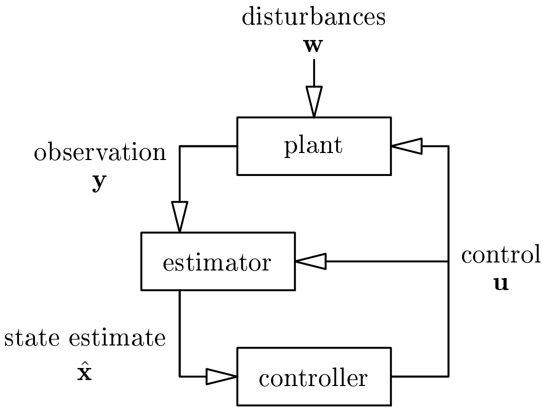

The plant, forced by external disturbances, has an internal state $\mathbf{x}$ which cannot be observed. Instead, a noisy observation $\mathbf{y}$ is made and an estimate of the state $\hat{\mathbf{x}}$ determined. This state estimate is then fed through the controller to determine the control $\mathbf{u}$ to be applied on the plant to regulate $\mathbf{x}$ to zero.

Several recent references describe in detail how $\mathcal{H}_2$ ("optimal") and $\mathcal{H}_\infty$ ("robust") techniques determine L and K for systems of the form (3.1)—(3.3) in the presence of structured and unstructured disturbances $\mathbf{w}$. The reader is referred in particular to Doyle *et al.* (1989), Dailey *et al.* (1990), Green & Limebeer (1995), and Zhou, Doyle, & Glover (1996) for further discussion of these control theories, and Bewley & Agarwal (1996) for a tutorial in the context of the current problem. To summarize briefly, a cost function $\mathcal{J}$ describing the control problem at hand is defined that weighs together the state $\mathbf{x}$, the control $\mathbf{u}$, and the disturbance $\mathbf{w}$ such that

$$\mathcal{J} \triangleq E\Big[\mathbf{x}^*\, Q\,\mathbf{x} + \ell^2\,\mathbf{u}^*\mathbf{u} - \gamma^2\,\mathbf{w}^*\mathbf{w}\Big] = E\Big[\mathbf{z}^*\,\mathbf{z} - \gamma^2\,\mathbf{w}^*\mathbf{w}\Big] \tag{3.4a}$$

where

$$\boxed{\mathbf{z} = C_1\mathbf{x} + D_{12}\mathbf{u}} \tag{3.4b}$$

with

$$C_1 \triangleq \begin{pmatrix} Q^{1/2} \\ 0 \end{pmatrix} \qquad D_{12} \triangleq \begin{pmatrix} 0 \\ \ell\, I \end{pmatrix}.$$

This cost function is minimized with respect to the control $\mathbf{u}$ and maximized with respect to the disturbance $\mathbf{w}$. For sufficiently large γ and a stabilizable, detectable system (as defined in §4.1), this results in finite values for both $\mathbf{u}$ and $\mathbf{w}$, the magnitudes of which are governed by the three scalars $\{\gamma, \alpha, \ell\}$. Recall that α^2, defined earlier, quantifies the relative level to which the observation $\mathbf{y}$ is corrupted by measurement noise.

The parameter ℓ^2 may be interpreted as the "price" of the control. The $\ell \to \infty$ limit, which corresponds to "expensive control", results in the smallest possible $\mathbf{u}$ which stabilizes the system, i.e., makes $E[\,\mathbf{x}^*\, Q\, \mathbf{x}\,]$ finite. Reduced values of ℓ penalize the cost function less upon the application of control, and thereby tend to result in a larger control magnitude $E[\,\mathbf{u}^*\, \mathbf{u}\,]$ and a smaller energy density of the state $E[\,\mathbf{x}^*\, Q\, \mathbf{x}\,]$.

Consider the min/max problem just described as a differential game between a fluid dynamicist seeking the "best" control $\mathbf{u}$ which stabilizes the flow perturbation with limited control effort and nature seeking the "maximally malevolent" small disturbance $\mathbf{w}$ which destabilizes the flow perturbation (Green & Limebeer 1995, pg 218). The parameter γ^2 factors into such a competition as a weighting on the magnitude of the disturbance which nature can afford to offer, in a manner analogous to the parameter ℓ^2, which is a weighting on the magnitude of the control which the fluid dynamicist can afford to offer. The negative sign on the term involving γ^2 is necessary because the cost function is maximized with respect to the disturbance $\mathbf{w}$, while it is minimized with respect to the control $\mathbf{u}$. The $\gamma \to \infty$ limit, referred to as the $\mathcal{H}_2$ solution, removes the disturbance "player" from the noncooperative game between $\mathbf{u}$ and $\mathbf{w}$ (i.e., $\mathbf{w} \to \mathbf{0}$ in the maximization). This limit may also be interpreted as assuming the disturbance $\mathbf{w}$ is white and uncorrelated with the control applied, i.e., $E[\,\mathbf{w}\,\mathbf{w}^*\,] = I$ and $E[\,\mathbf{w}\,\mathbf{u}^*\,] = 0$, which implies that the problems of control and estimation in the $\mathcal{H}_2$ limit are decoupled. Reduced values of γ introduce a "maximally malevolent" disturbance $\mathbf{w}$ of increased magnitude relative to the magnitude of the control $\mathbf{u}$.

Solving for the feedback which is effective even in the presence of such malevolent disturbances achieves system robustness. In the present systems, for $\gamma < \gamma_0$ for some critical value γ_0 (which may be found by trial and error), the noncooperative game does not have a finite solution; essentially, nature wins. The feedback corresponding to $\gamma = \gamma_0$ results in a stable system even when nature is on the brink of making the system unstable. This is sometimes referred to as the "optimal" $\mathcal{H}_\infty$ feedback, as it is the feedback which is "most robust". However, the "optimal" $\mathcal{H}_\infty$ feedback is generally not the most suitable choice overall, as discussed in §6.1.1 and §6.1.2.

The parameter γ in the min/max problem formulated above in the time domain is also, it turns out, an upper bound on the ∞-norm of the transfer function from the disturbance $\mathbf{w}$ to the performance measure $\mathbf{z}$ in the frequency domain, defined precisely in §4.4 and denoted $||T_{\mathbf{zw}}||_\infty$ (Zhou, Doyle, & Glover 1996). Thus, by reducing γ to the minimum values possible (γ_0) when computing the estimator feedback matrix L and the controller feedback matrix K, the most restrictive bounds on $||T_{\mathbf{zw}}||_\infty$ in the resulting closed-loop systems are attained.

An estimator/controller which minimizes $\mathcal{J}$ in the presence of that disturbance which simultaneously maximizes $\mathcal{J}$ is given by the estimator feedback

$$L = -\frac{1}{\alpha^2} Y C_2^*, \qquad \text{where} \qquad Y = \mathrm{Ric}\begin{pmatrix} A^* & \frac{1}{\gamma^2} C_1^* C_1 - \frac{1}{\alpha^2} C_2^* C_2 \\ -B_1 B_1^* & -A \end{pmatrix}, \tag{3.5}$$

and the controller feedback

$$K = -\frac{1}{\ell^2} B_2^* X \qquad \text{where,} \qquad X = \mathrm{Ric}\begin{pmatrix} A & \frac{1}{\gamma^2} B_1 B_1^* - \frac{1}{\ell^2} B_2 B_2^* \\ -C_1^* C_1 & -A^* \end{pmatrix}, \tag{3.6}$$

where $\mathrm{Ric}(\cdot)$ denotes the solution of the associated Riccati problem (Doyle *et al.* 1989). Standard numerical techniques to solve equations of this form are well developed (Laub 1991). Solutions to these Riccati problems exist only for sufficiently large γ at a given values of ℓ and α. As previously stated, the smallest $\gamma = \gamma_0$ for which solutions to these equations exist may be found by trial and error.

3.2 Comparison of optimal and robust control

Most of the robustness problems associated with $\mathcal{H}_2$ stem from the state estimation. Optimal controllers provided with full state information (i.e., without estimators) generally have excellent performance and robustness properties (Dailey *et al.* 1990). Note that the problems of control and state estimation in the $\mathcal{H}_2$ formulation ($\gamma \to \infty$) are *decoupled*. Other then the system matrix A, K depends only upon $\{\ell, B_2, C_1\}$, and L depends only upon $\{\alpha, B_1, C_2\}$. This is a result of the celebrated Separation Principle of the $\mathcal{H}_2$ formulation (Green & Limebeer 1995, Lewis & Syrmos 1995).

An important observation is that the problems of control and state estimation in the $\mathcal{H}_\infty$ formulation are coupled. Specifically, the computation of K in (3.6) depends on the expected covariance of the state disturbances, which are accounted for in B_1, and the computation of L in (3.5) depends on the weightings in the cost function, which are accounted for in C_1. This is one of the essential features of $\mathcal{H}_\infty$ control.

The $\mathcal{H}_\infty$ controller takes into account the expected covariance of the state disturbances, reflected in B_1, when determining the state feedback matrix K. By so doing, the components of $\mathbf{x}$ that are expected to have the largest excitation by external disturbances are forced with the largest feedback by the relationship $\mathbf{u} = K\,\hat{\mathbf{x}}$ in the equation for the controller.

Similarly, the $\mathcal{H}_\infty$ estimator takes into account the weightings in the cost function, reflected in C_1, when determining the estimator feedback matrix L. By so doing, the components of $\hat{\mathbf{x}}$ corresponding to the components of $\mathbf{x}$ that are most important in the computation of the cost function are forced with the largest feedback by the relationship $\hat{\mathbf{u}} = L(\mathbf{y} - \hat{\mathbf{y}})$ in the equation for the estimator.

By applying strong control only to those components of $\mathbf{x}$ significantly excited by external disturbances (by keeping ℓ large and reducing γ), and by applying strong estimator corrections only to those components of $\hat{\mathbf{x}}$ important in the computation of the cost function (by keeping α large and reducing γ), $\mathcal{H}_\infty$ feedback gains for components of the system not relevant to the control problem at hand may be kept at a minimum. With such feedback gains kept small, the stability properties of $\mathcal{H}_\infty$ estimator/controllers in the presence of system uncertainties may be dramatically improved over $\mathcal{H}_2$ counterparts which, for an equivalent worst-case response of the nominal plant, require reduced values of ℓ and α and, therefore, larger feedback gains. The reduced feedback applied in the $\mathcal{H}_\infty$ approach results in reduced opportunity for improper feedback to disrupt the closed-loop system.

3.3 Comparison with proportional control

A single-input, single-output (SISO) proportional controller for the present regulation problem is one which computes a single control variable simply by multiplying a single flow measurement by a complex scalar. In a slightly more general form, a multiple-input, multiple-output (MIMO) proportional controller computes each component of the control by a simple linear combination of multiple flow measurements, as shown in the following block diagram.

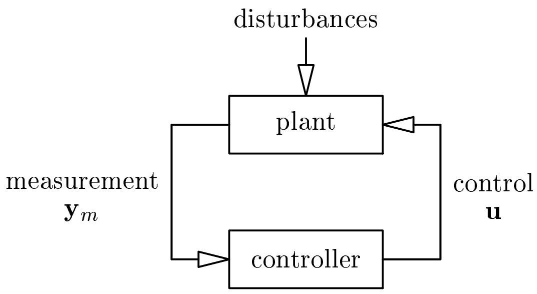

A proportional controller for the present problem takes the form $\mathbf{u} = K\mathbf{y}_m$, where the (complex) elements of K must be determined by parametric variation. It may be argued that the streamwise velocity fluctuations are more important than the spanwise velocity fluctuations in both case (i) and case (ii). Further, one can easily apply control at both walls based on local measurements of streamwise skin-friction only. Thus, it is reasonable to consider two SISO proportional controllers for the present problem put together in a restricted MIMO form

$$\mathbf{u} = \begin{pmatrix} k_1\, e^{i\phi_1} & 0 & 0 & 0 \\ 0 & k_2\, e^{i\phi_2} & 0 & 0 \end{pmatrix} \mathbf{y}_m \triangleq K \mathbf{y}_m \tag{3.7}$$

where the k_i and ϕ_i are chosen by parametric variation. It is found by such a parametric variation that $\phi_i = 0$ is most effective in this framework, and that the best performance is obtained near $k_1 = k_2 = 60$ for case (i) and $k_1 = k_2 = 10$ for case (ii). These restricted MIMO proportional controllers will be used as a basis for comparison in the analysis of the estimator/controllers based on modern control theory in §6.

More general forms for K in a proportional controller may be considered, but, as the dimension of the problem grows, searching parametrically for effective K_{ij} becomes intractable, and the benefit of an approach based on control theory to determine the feedback matrices becomes apparent. With the present theory, the feedback matrices for systems of arbitrary dimension are developed as a function of just three scalar parameters $\{\gamma, \alpha, \ell\}$, each of which may be intuitively understood and individually adjusted to achieve desired system characteristics.

3.4 Numerical method

Standard numerical techniques are now applied to the control problem posed in (3.1)—(3.6). The algebraic Riccati equations are solved using the method of Laub (1991), which involves a Schur factorization. This is found to be a stable numerical algorithm for all cases tested. The implementation of Laub's method is written in Fortran 90 and follows closely the algorithm used by the Matlab function `are.m` (Grace *et al.* 1992). A Lyapunov solver, modeled after the Matlab function `lyap.m`, is also used. Two LAPACK routines (Anderson *et al.* 1995), `zgeev.f` and `zgees.f`, are used to compute eigenvalues/eigenvectors and Schur factorizations.

All routines are compiled in quad precision (128 bits per real number) to ensure sufficient numerical precision in the eigenvalue computation. Computations are carried out with $N = 140$ for case (i) and $N = 70$ for case (ii) to ensure good resolution of all significant eigenmodes. The eigenvalues of A for case (i) in table 1 match those tabulated by Orszag (1971) to eight significant figures, and the maximum transient energy growth for case (ii) in figure 3b matches that obtained by Butler & Farrell (1992) to four significant figures, indicating that the present numerical method is sufficiently accurate.

3.4.1 Spurious eigenmodes

It is a well-known computational challenge that, in addition to all of the well-resolved eigenmodes of a particular continuous PDE, several poorly-resolved eigenmodes inevitably result from the solution of a discrete matrix eigenvalue problem. Such spurious eigenmodes are sometimes referred to as "two-delta waves" because their dominant wavelength is approximately twice the local grid spacing. Unfortunately, the (spurious) eigenvalues of these poorly-resolved eigenmodes may be near the (valid) eigenvalues of the well-resolved eigenmodes, even though the spurious modes are physically meaningless. For example, the first spurious eigenvalue computed for case (i) with $N = 140$ occurs at $\lambda = -0.0235 + 1.520\,i$. Spurious eigenmodes may be identified easily in two ways: i) the eigenvalue λ moves significantly when N is modified slightly, though the remaining eigenvalues remain converged to all significant figures, and ii) when plotted, spurious eigenvectors $\boldsymbol{\xi}$ are characterized by large oscillations from grid point to grid point across the domain, though converged eigenmodes are well resolved, as depicted in figure 1b in §5.

Inclusion of spurious eigenmodes in the system matrix A to be controlled may cause problems when applying control theory to modify the closed-loop characteristics of the entire system, as these modes may be uncontrollable and/or unobservable. In order to ensure problems related to these modes do not arise, the spurious eigenmodes of A are identified, the corresponding eigenvalues modified to a "benign", well-damped location, and the system matrix reconstructed according to

$$A_{\text{modified}} = \Xi\,\Lambda_{\text{modified}}\,\Psi^*. \tag{3.8}$$

Note that $\Lambda_{\text{modified}}$ is the matrix of eigenvalues with the eigenvalues corresponding to spurious modes moved to $\lambda_\kappa = -500$, and Ψ and Ξ are the corresponding left and right eigenvector matrices. This ensures that the dynamics of these spurious modes are damped sufficiently to be insignificant with respect to the rest of the system. The modified matrix A_{modified} is implied by the symbol A in the remainder of this work.

A minimal realization approach (Kailath 1980) is well suited to greatly reduce the dimension of the matrices and vectors involved, and thus the computer time needed, in the present computations. With this approach, uncontrollable, unobservable, spurious, and highly damped modes may be removed altogether from the representation of the system to be controlled. This idea will be explored in future work. The purpose of the present work, however, is to study the effects of control and estimation on the entire locus of eigenvalues in a well-resolved implementation. Thus, the matrix A is considered with no modifications beyond the damping of the spurious modes as described above. Note that, though controllers may be *designed* based on reduced systems, they must always be *analyzed* based on the complete system to accurately characterize system behaviour.

Chapter 4

Methods of analysis

This chapter reviews four methods to analyze various properties of a generic system

$$\dot{\tilde{\mathbf{x}}} = \tilde{A}\,\tilde{\mathbf{x}} + \tilde{B}_1\,\tilde{\mathbf{w}} + \tilde{B}_2\,\tilde{\mathbf{u}} \tag{4.1a}$$

$$\tilde{\mathbf{z}} = \tilde{C}_1\tilde{\mathbf{x}} + \tilde{D}_{12}\tilde{\mathbf{u}} \tag{4.1b}$$

$$\tilde{\mathbf{y}} = \tilde{C}_2\tilde{\mathbf{x}} + \tilde{D}_{21}\tilde{\mathbf{w}}. \tag{4.1c}$$

The methods of analysis presented in this chapter are applied to the present flow transition problem for the open-loop systems in §5 and the closed-loop systems in §6 by appropriate definition of the above tilde (˜) variables in the respective sections. It is therefore instructive to first review the analysis techniques from a generic perspective.

In §4.1, the controllability and observability system Gramians are reviewed as a means to characterize the system as a whole. However, this approach alone does not characterize the stabilizability of uncontrollable systems or the detectability of unobservable systems. As shown in §4.2, it is useful to analyze the individual eigenmodes of the system under consideration separately, and to identify the degree to which each of these modes may be modified by the control and the sensitivity with which each may be detected by the observations. Nonorthogonality of the eigenmodes is reviewed in §4.3 as a method by which transient energy growth is possible in stable systems, and a method is discussed by which the maximum possible transient energy growth may be quantified. In §4.4, quantitative measures of the effects of both Gaussian and worst-case disturbances $\tilde{\mathbf{w}}$ on a relevant performance measure $\tilde{\mathbf{z}}$ are described. In §4.5, it is shown that all four methods of analysis presented in this chapter are immediately applicable to open-loop systems, closed-loop controllers with full state information, closed-loop estimators with no control, and composite closed-loop estimator/controller systems by appropriate definition of the tilde (˜) variables in (4.1).

4.1 System Gramians

We first address whether or not *all* of a given system's eigenmodes may be altered by the control $\tilde{\mathbf{u}}$, and whether or not *all* of these eigenmodes may be discerned with the observations $\tilde{\mathbf{y}}$. To accomplish this, it is standard practice (Lewis & Syrmos 1995) to consider two matrices which characterize the controllability and observability of the system (4.1) as a whole, assuming for the moment that $\tilde{\mathbf{w}} = \mathbf{0}$. These are the system controllability Gramian L_c of $(\tilde{A}, \tilde{B}_2)$ and the system observability Gramian L_o of $(\tilde{C}_2, \tilde{A})$, which may be found by solution of

$$\begin{aligned} \tilde{A}\, L_c + L_c\, \tilde{A}^* + \tilde{B}_2\, \tilde{B}_2^* &= 0 \\ \tilde{A}^*\, L_o + L_o\, \tilde{A} + \tilde{C}_2^*\, \tilde{C}_2 &= 0. \end{aligned}$$

Stable numerical techniques to solve equations of this form, referred to as Lyapunov equations, are well developed (Bartels & Stewart 1972).

If L_c is (nearly) singular, there is at least one eigenmode of the system which is (nearly) unaffected by any choice of control $\tilde{\mathbf{u}}$, and the system is called "uncontrollable". If all uncontrollable eigenmodes are stable, and the dynamics of the system may be made stable by the application of controller feedback, the system is called "stabilizable".

Similarly, if L_o is (nearly) singular, there is at least one eigenmode of the system which is (nearly) indiscernible by the observations $\tilde{\mathbf{y}}$, and the system is called "unobservable". If all unobservable eigenmodes are stable, and the dynamics of the error of the estimate may be made stable by the application of estimator feedback, the system is called "detectable".

System Gramians alone do not identify *which* of the eigenmodes are unaffected by $\tilde{\mathbf{u}}$ or indiscernible by $\tilde{\mathbf{y}}$. Thus, determination of whether or not an uncontrollable system is stabilizable or an unobservable system is detectable requires further analysis.

4.2 Eigenmode analysis

Modal canonical form (Kailath 1980) will now be used to quantify the sensitivity of each individual eigenmode of a system matrix $\tilde{A}$ to both control and observation. Though this is common practice in linear systems theory (Skogestad & Postlethwaite 1996, p. 122 and 126) a brief review helps establish two scalars, denoted here f_κ and g_κ, which indicate the controllability and observability of each individual eigenmode of the system.

Define the eigenvalues λ_κ and the left and right eigenvectors, $\boldsymbol{\psi}_\kappa$ and $\boldsymbol{\xi}_\kappa$, and the corresponding eigenvalue and eigenvector matrices[1], such that

$$\begin{array}{llll} \text{left eigenvectors:} & \boldsymbol{\psi}_\kappa^* \tilde{A} = \lambda_\kappa \boldsymbol{\psi}_\kappa^* & \Rightarrow & \Psi^* \tilde{A} = \Lambda \Psi^* \\ \text{right eigenvectors:} & \tilde{A} \boldsymbol{\xi}_\kappa = \lambda_\kappa \boldsymbol{\xi}_\kappa & \Rightarrow & \tilde{A} \Xi = \Xi \Lambda, \end{array}$$

where

$$\Lambda = \begin{pmatrix} \lambda_1 & & \\ & \lambda_2 & \\ & & \ddots \end{pmatrix} \qquad \Psi^* = \sqrt{\frac{\pi}{N}} \begin{pmatrix} \boldsymbol{\psi}_1^* \\ \boldsymbol{\psi}_2^* \\ \vdots \end{pmatrix} \qquad \Xi = \sqrt{\frac{\pi}{N}} \begin{pmatrix} \boldsymbol{\xi}_1 & \boldsymbol{\xi}_2 & \cdots \end{pmatrix}.$$

The system $\dot{\tilde{\mathbf{x}}} = \tilde{A}\,\tilde{\mathbf{x}}$ is stable if $\Re(\lambda_\kappa) < 0$ for all κ. For systems (such as the present) with distinct eigenvalues, the (mutually orthogonal) left and right eigenvectors may be normalized such that

$$(\boldsymbol{\xi}_\kappa, \boldsymbol{\xi}_\kappa) = 1 \qquad \text{and} \qquad (\boldsymbol{\psi}_\iota, \boldsymbol{\xi}_\kappa) = \delta_{\iota\kappa} \qquad \Rightarrow \qquad \Psi^* \Xi = I. \tag{4.2}$$

Note that the right eigenvectors $\boldsymbol{\xi}_\kappa$ themselves are linearly independent but *not* orthogonal; i.e., $(\boldsymbol{\xi}_\iota, \boldsymbol{\xi}_\kappa) \neq 0$ for $\iota \neq \kappa$. Any $\tilde{\mathbf{x}}$ may be uniquely decomposed via a projection vector $\boldsymbol{\chi}$ as a linear combination of these nonorthogonal right eigenvectors such that

$$\tilde{\mathbf{x}} = \Xi\,\boldsymbol{\chi} = \sum_\kappa \chi_\kappa\,\boldsymbol{\xi}_\kappa \qquad \Rightarrow \qquad \dot{\tilde{\mathbf{x}}} = \Xi\,\dot{\boldsymbol{\chi}} = \sum_\kappa \dot{\chi}_\kappa\,\boldsymbol{\xi}_\kappa. \tag{4.3}$$

4.2.1 Definition of modal control residual

By (4.1a) and (4.3) and assuming, for the moment, that $\tilde{\mathbf{w}} = \mathbf{0}$, we have

$$\sum_\kappa \dot{\chi}_\kappa\,\boldsymbol{\xi}_\kappa = \tilde{A} \sum_\kappa \chi_\kappa\,\boldsymbol{\xi}_\kappa + \tilde{B}_2\,\tilde{\mathbf{u}} = \sum_\kappa \chi_\kappa\,\lambda_\kappa\,\boldsymbol{\xi}_\kappa + \tilde{B}_2\,\tilde{\mathbf{u}}.$$

Taking the inner product with $\boldsymbol{\psi}_\iota$

$$\left(\boldsymbol{\psi}_\iota, \sum_\kappa \dot{\chi}_\kappa\,\boldsymbol{\xi}_\kappa\right) = \left(\boldsymbol{\psi}_\iota, \sum_\kappa \chi_\kappa\,\lambda_\kappa\,\boldsymbol{\xi}_\kappa\right) + (\boldsymbol{\psi}_\iota, \tilde{B}_2\,\tilde{\mathbf{u}})$$

and noting (2.10) and (4.2) yields

$$\dot{\chi}_\kappa = \lambda_\kappa\,\chi_\kappa + \frac{\pi}{N}(\tilde{B}_2^*\,\boldsymbol{\psi}_\kappa)^*\,\tilde{\mathbf{u}}.$$

[1]The $\sqrt{\pi/N}$ term in the definition of Ξ and Ψ is required to maintain consistency with the definition of an inner product which converges upon refining N, as discussed in §2.4.

If the vector $(\pi/N)\tilde{B}_2^* \boldsymbol{\psi}_\kappa = \mathbf{0}$, then $\dot{\chi}_\kappa = \lambda_\kappa \chi_\kappa$ for any $\tilde{\mathbf{u}}$. In other words, the component of $\tilde{\mathbf{x}}$ parallel to $\boldsymbol{\xi}_\kappa$ is not affected by the control $\tilde{\mathbf{u}}$, and the eigenmode is said to be "uncontrollable". Further, the 2-norm of the vector $(\pi/N)\tilde{B}_2^* \boldsymbol{\psi}_\kappa$

$$f_\kappa = \frac{\pi}{N} \sqrt{\boldsymbol{\psi}_\kappa^* \, \tilde{B}_2 \, \tilde{B}_2^* \, \boldsymbol{\psi}_\kappa}\,, \tag{4.4}$$

termed here the "control residual" of mode κ, is a quantitative measure of the sensitivity of the eigenmode κ to the control $\tilde{\mathbf{u}}$. Note the dependence of this expression on the matrix $\tilde{B}_2 \, \tilde{B}_2^*$, which is the matrix which drives the Lyapunov equation for controllability Gramian L_c.

4.2.2 Definition of modal observation residual

By (4.1c) and (4.3) and assuming, for the moment, that $\tilde{\mathbf{w}} = \mathbf{0}$, we have

$$\tilde{\mathbf{y}} = \sum_\kappa \chi_\kappa \, \tilde{C}_2 \, \boldsymbol{\xi}_\kappa.$$

If the vector $\tilde{C}_2 \, \boldsymbol{\xi}_\kappa = 0$, then $\tilde{\mathbf{y}}$ will not be a function of χ_κ. In other words, the component of $\tilde{\mathbf{x}}$ parallel to $\boldsymbol{\xi}_\kappa$ does not contribute to the observations $\tilde{\mathbf{y}}$, and the eigenmode is said to be "unobservable". Further, the (scaled) 2-norm of the vector $\tilde{C}_2 \, \boldsymbol{\xi}_\kappa$

$$g_\kappa = Re \sqrt{\boldsymbol{\xi}_\kappa^* \, \tilde{C}_2^* \, \tilde{C}_2 \, \boldsymbol{\xi}_\kappa}\,, \tag{4.5}$$

similarly termed the "observation residual" of mode κ, is a quantitative measure of the sensitivity of the observation $\tilde{\mathbf{y}}$ to eigenmode κ. Note the dependence of this expression on the matrix $\tilde{C}_2^* \, \tilde{C}_2$, which is the matrix which drives the Lyapunov equation for observability Gramian L_o. Note also that the scaling Re is used simply for numerical convenience.

4.3 Transient energy growth

Consider an initial state $\tilde{\mathbf{x}}(0)$ of a stable system which may be decomposed into several constituent nonorthogonal eigenmodes which destructively interfere in such a way that the energy of the initial state $\mathscr{E}(0) = \tilde{\mathbf{x}}^*(0) \, Q \, \tilde{\mathbf{x}}(0)$ is small. Such destructive interference may reduce in time as some eigenmodes decay more quickly than others. This can result in a large transient growth in the kinetic energy density $\mathscr{E}(t)$ of the state before an eventual exponential decay of energy at the rate of the least-stable constituent eigenmode.

Over a particular time interval τ, the shape of the most amplified initial conditions $\tilde{\mathbf{x}}(0)$ may be found by a variational formulation (Butler and Farrell 1992). As introduced in (4.3), a state $\tilde{\mathbf{x}}(0)$ may be decomposed onto the eigenvector matrix Ξ via a projection vector $\boldsymbol{\chi}$. Solving the system of simple ODE's resulting from application of (4.3) to (4.1a), assuming for the moment that $\tilde{\mathbf{u}} = \tilde{\mathbf{w}} = \mathbf{0}$, $\tilde{\mathbf{x}}(t)$ may be written

$$\tilde{\mathbf{x}}(t) = \Xi\, e^{\Lambda t}\, \boldsymbol{\chi}.$$

where the projection $\boldsymbol{\chi}$ is independent of time. The initial state $\tilde{\mathbf{x}}(0)$ maximizing energy growth at $t = \tau$ may be found by considering the cost function

$$\begin{aligned}
\mathcal{J}_{\mathscr{E}} &= \mathscr{E}(\tau) - \theta\,[\mathscr{E}(0) - 1] \\
&= \tilde{\mathbf{x}}^*(\tau)\, Q\, \tilde{\mathbf{x}}(\tau) - \theta\,[\tilde{\mathbf{x}}^*(0)\, Q\, \tilde{\mathbf{x}}(0) - 1] \\
&= \boldsymbol{\chi}^*\,(e^{\Lambda^*\tau}\, \Xi^*\, Q\, \Xi\, e^{\Lambda\tau})\, \boldsymbol{\chi} - \theta\,[\boldsymbol{\chi}^*\,(\Xi^*\, Q\, \Xi)\, \boldsymbol{\chi} - 1],
\end{aligned}$$

setting the derivative with respect to the Lagrange multiplier θ equal to zero

$$\frac{\partial \mathcal{J}_{\mathscr{E}}}{\partial \theta} = 0 \qquad \Rightarrow \qquad \mathscr{E}(0) = 1$$

and the gradient with respect to the projection vector $\boldsymbol{\chi}$ equal to zero

$$\begin{aligned}
\frac{\partial \mathcal{J}_{\mathscr{E}}}{\partial \boldsymbol{\chi}} = 0 \qquad &\Rightarrow \qquad (e^{\Lambda^*\tau}\, \Xi^*\, Q\, \Xi\, e^{\Lambda\tau})\, \boldsymbol{\chi} = \theta\,(\Xi^*\, Q\, \Xi)\, \boldsymbol{\chi} \\
&\Rightarrow \qquad \theta = \frac{\mathscr{E}(\tau)}{\mathscr{E}(0)} = \frac{\boldsymbol{\chi}^*\,(e^{\Lambda^*\tau}\, \Xi^*\, Q\, \Xi\, e^{\Lambda\tau})\, \boldsymbol{\chi}}{\boldsymbol{\chi}^*\,(\Xi^*\, Q\, \Xi)\, \boldsymbol{\chi}}.
\end{aligned}$$

The first condition normalizes the energy of the initial state. The second condition results in a generalized eigenproblem of the form $R\,\boldsymbol{\chi} = \theta\, S\, \boldsymbol{\chi}$, whose maximum eigenvalue $\theta_{\max}$ corresponds to the maximum energy growth $\mathscr{E}(\tau)/\mathscr{E}(0)$ by the corresponding initial state $\tilde{\mathbf{x}}(0) = \Xi\, \boldsymbol{\chi}_{\max}$. A search routine may be used to find the time interval τ for which this approach leads to the greatest possible energy growth.

4.4 Transfer function norms

Quantitative measures of the effects of both Gaussian and worst-case disturbances $\tilde{\mathbf{w}}$ on relevant performance measures $\tilde{\mathbf{z}}$ are sought to characterize the various systems. The 2-norm and the ∞-norm of the transfer function from $\tilde{\mathbf{w}}$ to $\tilde{\mathbf{z}}$, which we shall call here $T_{\tilde{\mathbf{z}}\tilde{\mathbf{w}}}$, are commonly used for this purpose.

Taking the Laplace transform of the generic system (4.1), assuming for the moment that $\tilde{\mathbf{u}} = \mathbf{0}$, it is easy to determine the transfer function $T_{\tilde{\mathbf{z}}\tilde{\mathbf{w}}}(s)$ from $\tilde{\mathbf{w}}(s)$ to $\tilde{\mathbf{z}}(s)$ (the Laplace transforms of $\tilde{\mathbf{w}}$ and $\tilde{\mathbf{z}}$) such that

$$\tilde{\mathbf{z}}(s) = \tilde{C}_1\,(\,s\,I - \tilde{A}\,)^{-1}\,\tilde{B}_1\,\tilde{\mathbf{w}}(s) \;\triangleq\; T_{\tilde{\mathbf{z}}\tilde{\mathbf{w}}}(s)\,\tilde{\mathbf{w}}(s).$$

Norms the transfer function $T_{\tilde{\mathbf{z}}\tilde{\mathbf{w}}}(s)$, also referred to as system norms, quantify how relevant performance measures $\tilde{\mathbf{z}}$ respond to disturbances $\tilde{\mathbf{w}}$ in the present systems, as shown below. These norms turn out to be finite for all $\mathcal{H}_2$- and $\mathcal{H}_\infty$-controlled systems considered here, but not for the proportionally controlled systems, as explained in detail in §4.6.

4.4.1 Transfer function 2-norms

The 2-norm of a stable transfer function $T_{\tilde{\mathbf{z}}\tilde{\mathbf{w}}}(s)$ may be defined (Doyle *et al.* 1989) as

$$||T_{\tilde{\mathbf{z}}\tilde{\mathbf{w}}}||_2^2 \triangleq \frac{1}{2\pi}\int_{-\infty}^{\infty} \mathrm{trace}\Big[T_{\tilde{\mathbf{z}}\tilde{\mathbf{w}}}(j\omega)^* T_{\tilde{\mathbf{z}}\tilde{\mathbf{w}}}(j\omega)\Big]d\omega. \tag{4.6}$$

It is finite when $\tilde{A}$ is stable (i.e., all of the eigenvalues of $\tilde{A}$ have negative real part) and $T_{\tilde{\mathbf{z}}\tilde{\mathbf{w}}}(j\omega)$ is "strictly proper" (i.e., when $T_{\tilde{\mathbf{z}}\tilde{\mathbf{w}}}(j\omega) \to 0$ as $\omega \to \infty$).

The norm $||T_{\tilde{\mathbf{z}}\tilde{\mathbf{w}}}||_2$ is a very useful measure, as it is exactly the expected rms value of the output $\tilde{\mathbf{z}}$, i.e., $||T_{\tilde{\mathbf{z}}\tilde{\mathbf{w}}}||_2^2 = E[\,\tilde{\mathbf{z}}^*\,\tilde{\mathbf{z}}\,]$, when the input $\tilde{\mathbf{w}}$ is a unit variance white Gaussian process. The 2-norm of $T_{\tilde{\mathbf{z}}\tilde{\mathbf{w}}}$ may be found by solving a Lyapunov equation

$$\tilde{A}^*\,L_o + L_o\,\tilde{A} + \tilde{C}_1^*\,\tilde{C}_1 = 0 \qquad \Rightarrow \qquad ||T_{\tilde{\mathbf{z}}\tilde{\mathbf{w}}}||_2^2 = \mathrm{trace}(\tilde{B}_1^* L_o \tilde{B}_1).$$

As stated previously, stable numerical techniques to solve Lyapunov equations are well developed (Bartels & Stewart 1972).

4.4.2 Transfer function ∞-norms

The ∞-norm of a stable transfer function $T_{\tilde{\mathbf{z}}\tilde{\mathbf{w}}}$ may be defined (Doyle *et al.* 1989) as

$$||T_{\tilde{\mathbf{z}}\tilde{\mathbf{w}}}||_\infty \triangleq \sup_\omega \sigma_{\max}\Big[T_{\tilde{\mathbf{z}}\tilde{\mathbf{w}}}(j\omega)\Big] \quad \text{with} \quad \sigma_{\max} \triangleq \text{maximum singular value.} \tag{4.7}$$

It is finite when $\tilde{A}$ is stable (i.e., all of the eigenvalues of $\tilde{A}$ have negative real part) and $T_{\tilde{\mathbf{z}}\tilde{\mathbf{w}}}(j\omega)$ is "semi-proper" (i.e., when $T_{\tilde{\mathbf{z}}\tilde{\mathbf{w}}}(j\omega)$ is finite as $\omega \to \infty$).

The norm $||T_{\tilde{\mathbf{z}}\tilde{\mathbf{w}}}||_\infty$ is very useful, as it is a measure of the "worst case" amplification of the disturbance $\tilde{\mathbf{w}}$ by the system. Unfortunately, the ∞-norm of $T_{\tilde{\mathbf{z}}\tilde{\mathbf{w}}}$ must be sought by an iterative search. The approach used here, suggested by Doyle *et al.* (1989), is:

1. Guess a value of γ.
2. Compute the eigenvalues of the Hamiltonian $H = \begin{pmatrix} \tilde{A} & \frac{1}{\gamma^2}\tilde{B}_1\tilde{B}_1^* \\ -\tilde{C}_1^*\tilde{C}_1 & -\tilde{A}^* \end{pmatrix}$
3. $||T_{\tilde{\mathbf{z}}\tilde{\mathbf{w}}}||_\infty < \gamma$ iff H has no eigenvalues on the imaginary axis and $H \in \mathrm{dom(Ric)}$. (See Doyle *et al.* 1989 for definition of the latter property.) Thus, we may increase or decrease γ accordingly, using a golden section search, and repeat from (*b*) until bounds on $||T_{\tilde{\mathbf{z}}\tilde{\mathbf{w}}}||_\infty$ reach a desired tolerance.

4.4.3 Performance measures $\tilde{\mathbf{z}}$ to be considered

For the characterization of the present closed-loop systems, two separate performance measures $\tilde{\mathbf{z}}$ will be considered. The first performance measure $\tilde{\mathbf{z}}_1$, obtained by setting $C_1 = Q^{1/2}$ and $D_{12} = 0$ (and thus $\tilde{\mathbf{z}}_1^*\,\tilde{\mathbf{z}}_1 = \mathbf{x}^*\,Q\,\mathbf{x}$), allows us to evaluate the norms of the transfer function from the disturbance $\mathbf{w}$ to the energy of the state $\mathbf{x}$. For notational convenience, the transfer function from the disturbance $\mathbf{w}$ to the performance measure $\tilde{\mathbf{z}}_1$ is denoted $T_{\mathbf{xw}}$ in the remainder of this work.

The second performance measure $\tilde{\mathbf{z}}_2$, obtained by setting $C_1 = 0$ and $D_{12} = I$ (and thus $\tilde{\mathbf{z}}_2^*\,\tilde{\mathbf{z}}_2 = \mathbf{u}^*\,\mathbf{u}$), allows us to evaluate the norms of the transfer function from the disturbance $\mathbf{w}$ to the control $\mathbf{u}$. For notational convenience, the transfer function from the disturbance $\mathbf{w}$ to the performance measure $\tilde{\mathbf{z}}_2$ is denoted $T_{\mathbf{uw}}$ in the remainder of this work. Note that, since $\mathbf{z}^*\,\mathbf{z} = \mathbf{x}^*\,Q\,\mathbf{x} + \ell^2\,\mathbf{u}^*\mathbf{u}$ by (3.4), it follows that the 2-norm of the transfer function from the disturbance to the performance measure $\mathbf{z}$ actually used in the computation of the controller is just

$$||T_{\mathbf{zw}}||_2^2 = ||T_{\mathbf{xw}}||_2^2 + \ell^2||T_{\mathbf{uw}}||_2^2. \tag{4.8}$$

4.5 Systems to be analyzed

Four systems are now described and algebraically manipulated into the generic system form (4.1) presented at the beginning of this chapter. By so doing, any of the analysis techniques described above may be readily applied to any of the systems described below simply by appropriate definition of the tilde (˜) variables in (4.1). This versatile analysis approach is exploited in subsequent chapters to characterize the open-loop and closed-loop systems, and is a significant design advantage of modern control theory.

System #1. Open-loop plant (3.1 with 3.4b):

$$\boxed{\begin{aligned} \dot{\mathbf{x}} &= A\,\mathbf{x} + B_1\,\mathbf{w} + B_2\,\mathbf{u} \\ \mathbf{z} &= C_1\mathbf{x} + D_{12}\mathbf{u} \\ \mathbf{y} &= C_2\mathbf{x} + D_{21}\mathbf{w}. \end{aligned}} \tag{4.9}$$

System #2. Closed-loop plant with controller and full state information (3.1 with 3.4b & 3.3 augmented with extra control feedback term $\mathbf{u}'$, assuming $\hat{\mathbf{x}} = \mathbf{x}$):

$$\begin{aligned} &\text{Plant:} && \begin{cases} \dot{\mathbf{x}} = A\,\mathbf{x} + B_1\mathbf{w} + B_2\,\mathbf{u} \\ \mathbf{z} = C_1\,\mathbf{x} + D_{12}\,\mathbf{u} \end{cases} \\ &\text{Controller:} && \{\ \mathbf{u} = K\,\mathbf{x} + \mathbf{u}', \end{aligned}$$

Simple algebraic manipulation yields the generic form for analysis:

$$\boxed{\begin{aligned} \dot{\mathbf{x}} &= (A + B_2K)\,\mathbf{x} + B_1\,\mathbf{w} + B_2\,\mathbf{u}' \\ \mathbf{z} &= (C_1 + D_{12}K)\,\mathbf{x} + D_{12}\,\mathbf{u}' \\ \mathbf{y} &\triangleq \mathbf{x} \end{aligned}} \tag{4.10}$$

System #3. Closed-loop plant with estimator and no control (3.1 & 3.2 augmented with extra estimator feedback term $\hat{\mathbf{u}}'$, assuming $\mathbf{u} = \mathbf{0}$):

$$\begin{aligned} &\text{Plant:} && \begin{cases} \dot{\mathbf{x}} = A\,\mathbf{x} + B_1\,\mathbf{w} \\ \mathbf{y} = C_2\,\mathbf{x} + D_{21}\,\mathbf{w} \end{cases} \\ &\text{Estimator:} && \begin{cases} \dot{\hat{\mathbf{x}}} = A\,\hat{\mathbf{x}} - \hat{\mathbf{u}} \\ \hat{\mathbf{y}} = C_2\,\hat{\mathbf{x}} \\ \hat{\mathbf{u}} = L\,(\mathbf{y} - \hat{\mathbf{y}}) + \hat{\mathbf{u}}' \end{cases} \end{aligned}$$

Defining $\mathbf{x}_E$ as the state estimation error $\mathbf{x}_E \triangleq \mathbf{x} - \hat{\mathbf{x}}$ and and $\mathbf{y}_E$ as the measurement error $\mathbf{y}_E \triangleq \mathbf{y} - \hat{\mathbf{y}}$, simple algebraic manipulation yields the generic form for analysis:

$$\boxed{\begin{aligned} \dot{\mathbf{x}}_E &= (A + LC_2)\,\mathbf{x}_E + (B_1 + LD_{21})\,\mathbf{w} + \hat{\mathbf{u}}' \\ \mathbf{z}_E &\triangleq C_1\,\mathbf{x}_E \\ \mathbf{y}_E &= C_2\,\mathbf{x}_E + D_{21}\,\mathbf{w}. \end{aligned}} \tag{4.11}$$

System #4. Closed-loop plant with estimator and controller (3.1 with 3.4b, 3.2, & 3.3 augmented with extra control feedback term $\mathbf{u}'$):

$$\text{Plant:}\quad \begin{cases} \dot{\mathbf{x}} = A\,\mathbf{x} + B_1\,\mathbf{w} + B_2\,\mathbf{u} \\ \mathbf{z} = C_1\,\mathbf{x} \qquad\qquad + D_{12}\mathbf{u} \\ \mathbf{y} = C_2\,\mathbf{x} + D_{21}\mathbf{w} \end{cases}$$

$$\text{Estimator:}\quad \begin{cases} \dot{\hat{\mathbf{x}}} = A\,\hat{\mathbf{x}} - \hat{\mathbf{u}} + B_2\mathbf{u} \\ \hat{\mathbf{y}} = C_2\,\hat{\mathbf{x}} \\ \hat{\mathbf{u}} = L\,(\mathbf{y} - \hat{\mathbf{y}}) \end{cases}$$

$$\text{Controller:}\quad \{\ \ \mathbf{u} = K\,\hat{\mathbf{x}} + \mathbf{u}'$$

Simple algebraic manipulation yields the generic form for analysis:

$$\boxed{\begin{aligned} \begin{pmatrix} \dot{\mathbf{x}} \\ \dot{\mathbf{x}}_E \end{pmatrix} &= \begin{pmatrix} A + B_2 K & -B_2\,K \\ 0 & A + L\,C_2 \end{pmatrix} \begin{pmatrix} \mathbf{x} \\ \mathbf{x}_E \end{pmatrix} + \begin{pmatrix} B_1 \\ B_1 + LD_{21} \end{pmatrix} \mathbf{w} + \begin{pmatrix} B_2 \\ 0 \end{pmatrix} \mathbf{u}' \\ \mathbf{z} &= \begin{pmatrix} C_1 + D_{12}K & -D_{12}K \end{pmatrix} \begin{pmatrix} \mathbf{x} \\ \mathbf{x}_E \end{pmatrix} + D_{12}\ \mathbf{u}' \\ \mathbf{y}_E &= \begin{pmatrix} 0 & C_2 \end{pmatrix} \begin{pmatrix} \mathbf{x} \\ \mathbf{x}_E \end{pmatrix} + D_{21}\ \mathbf{w} \end{aligned}} \tag{4.12}$$

4.6 Analysis of semi-proper proportionally-controlled systems

When a proportional controller, such as that proposed in §3.3, is applied to the present problem, the resulting system may be written in the form

$$\dot{\mathbf{x}} = A\,\mathbf{x} + B_1\,\mathbf{w} + B_2\,\mathbf{u} \tag{4.13}$$

$$\mathbf{z} = C_1\,\mathbf{x} \qquad\qquad + D_{12}\mathbf{u} \tag{4.14}$$

$$\mathbf{y}_m = C_2\,\mathbf{x} + D_{21}\mathbf{w} + D_{22}\mathbf{u} \tag{4.15}$$

$$\mathbf{u} = K\,\mathbf{y}_m \tag{4.16}$$

with K of a simple form, such as that in (3.7). Combining to eliminate $\mathbf{u}$ and $\mathbf{y}_m$ gives

$$\begin{aligned} \dot{\mathbf{x}} &= [A + B_2\,(I - K\,D_{22})^{-1} K\,C_2]\,\mathbf{x} + [B_1 + B_2(I - K\,D_{22})^{-1} K\,D_{21}]\mathbf{w} \\ \mathbf{z} &= [C_1 + D_{12}(I - K\,D_{22})^{-1} K\,C_2]\mathbf{x} + \ [D_{12}\,(I - K\,D_{22})^{-1} K\,D_{21}]\,\mathbf{w}, \end{aligned}$$

which we may write more simply as

$$\begin{aligned}\dot{\mathbf{x}} &\triangleq \tilde{A}\,\mathbf{x} + \tilde{B}_1\,\mathbf{w}\\ \mathbf{z} &\triangleq \tilde{C}_1\mathbf{x} + \tilde{D}_{11}\mathbf{w}.\end{aligned}$$

The eigenvalues and eigenvectors of $\tilde{A}$ may be examined to characterize the behaviour of the closed-loop system in the absence of disturbances $\mathbf{w}$ and quantify the maximum transient energy growth using the techniques of §4.2 and §4.3.

Given this type of control, the transfer function from $\mathbf{w}(s)$ to $\mathbf{z}(s)$ is now

$$\mathbf{z}(s) = [\tilde{C}_1\,(\,s\,I - \tilde{A}\,)^{-1}\,\tilde{B}_1 + \tilde{D}_{11}]\mathbf{w}(s)\ \triangleq\ T_{\mathbf{zw}}(s)\,\mathbf{w}(s).$$

Setting $C_1 = Q^{1/2}$ and $D_{12} = 0$, and thus $\mathbf{z}^*\,\mathbf{z} = \mathbf{x}^*\,Q\,\mathbf{x}$ (our first performance measure), the norms of the transfer function from the disturbance $\mathbf{w}$ to the energy of the state $\mathbf{x}$, $||T_{\mathbf{xw}}||_2$ and $||T_{\mathbf{xw}}||_\infty$, can be evaluated using the techniques of §4.4. Note that, in this case, $\tilde{D}_{11} = 0$.

Setting $C_1 = 0$ and $D_{12} = I$, and thus $\mathbf{z}^*\,\mathbf{z} = \mathbf{u}^*\,\mathbf{u}$ (our second performance measure), we see that the transfer function from the disturbance $\mathbf{w}$ to the control $\mathbf{u}$ is not "strictly proper" (Skogestad & Postlethwaite 1996, pg. 5), as there is a direct feedthrough term from the disturbance $\mathbf{w}$ to the control $\mathbf{u}$; in this case, $\tilde{D}_{11} \neq 0$. As there is a term of $T_{\mathbf{uw}}(s)$ which is constant for all s, the system is termed "semi-proper", and thus, by its definition in (4.6), it is clear that $||T_{\mathbf{uw}}||_2 = \infty$.

The main point here is that a controller with a proportional component, such as the PI controller proposed by Joshi, Speyer, & Kim (1997), will not have built-in high frequency roll-off of the controller response, and measurement noise will feed *directly* through to the controller input. Thus, the rms value of the control $\mathbf{u}$ in response to a unit variance white Gaussian disturbance $\mathbf{w}$ is infinite. In practice, limitations in the response of the actuators and the controlling electronics would limit the rms response of a proportional controller to white-noise disturbances. An *ad hoc* low-pass filter is required to achieve high-frequency roll-off of the proportional component of a PI controller below those frequencies set by the implementation hardware itself. An advantage of the optimal and robust approaches developed in this article is that the resulting systems are strictly proper, and thus an appropriate amount of high frequency roll-off is built-in as a natural result of the control formulation (i.e., $T_{\mathbf{uw}}(j\omega) \to 0$ appropriately quickly as $\omega \to \infty$). Simulations of the idealized optimal and robust closed-loop systems developed in this article can be used to determine what high frequency performance of the implementation hardware is necessary for the desired performance of a given system.

Chapter 5

Analysis of uncontrolled, open-loop system

The uncontrolled ("open-loop") system is now examined in detail using the methods of analysis of §4 by consideration of system #1 in §4.5.

5.1 System Gramians

For both case (i) and case (ii) of the present system, the smallest eigenvalues of both system Gramians, L_c and L_o, are computed to be near machine zero, indicating that these systems are both uncontrollable and unobservable. To obtain information on stabilizability and detectability, analysis of the individual eigenmodes is necessary.

5.2 Eigenmode analysis

5.2.1 Eigenmode analysis of case (i)

The least-stable eigenvalues of A for case (i) are plotted in figure 1a and tabulated, along with the corresponding control and observation residuals f_κ and g_κ, in table 1. Figure 1b shows the shape of the eigenvectors corresponding to the 6 least-stable eigenvalues along with an example of a spurious mode as discussed in §3.4.1.

An important observation from figure 1b is that eigenvalues in the upper branch of figure 1a have corresponding eigenvectors with variations primarily in the centre of the channel, and thus it may be expected that these modes will be less controllable via wall transpiration and less observable via

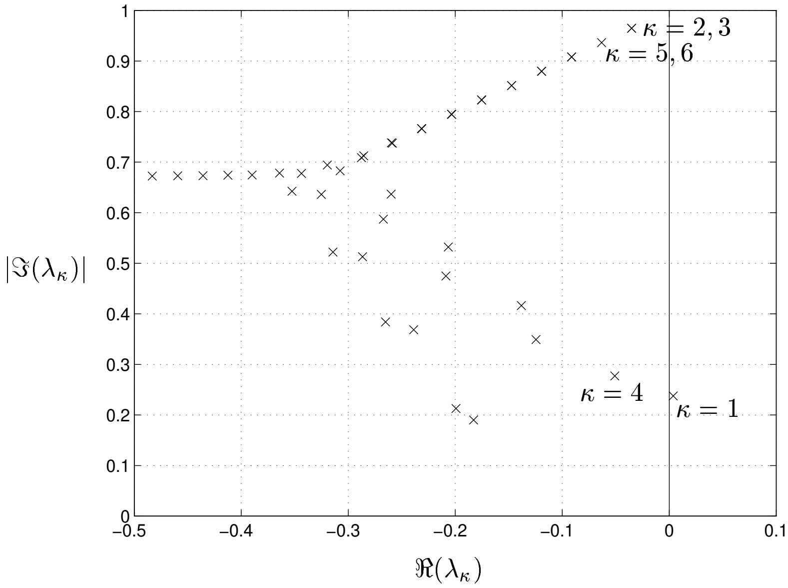

(a) Least-stable eigenvalues. The six least-stable eigenmodes are labeled.

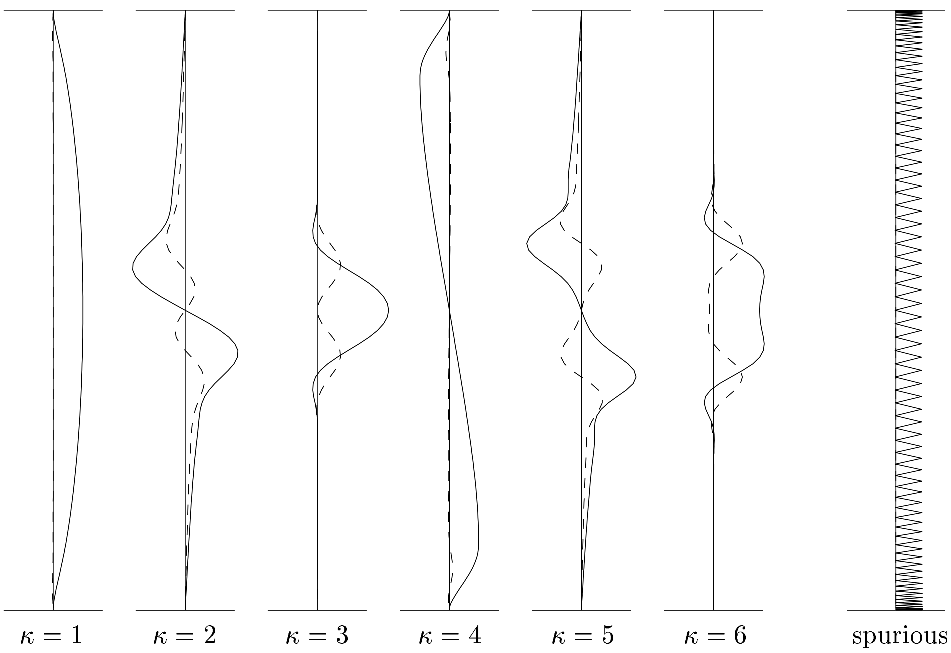

(b) Real (solid) and imaginary (dashed) parts of the $\mathbf{v}$ component of the eigenvectors corresponding to the six eigenvalues labeled in figure 1a and the spurious, unresolved eigenmode discussed in §3.4.1 (initially located at $\lambda = -0.0214 + 1.514\,i$ and later damped to remove its influence), plotted as a function of y from the lower wall (bottom) to the upper wall (top). The corresponding $\boldsymbol{\omega}$ components of these eigenvectors are zero.

Figure 1: Least-stable eigenmodes of A for case (i).

κ	λ_κ	f_κ	g_κ
1	$0.00373967 - 0.23752649\,i$	0.266545	102.61
2	$-0.03516728 - 0.96463092\,i$	0.000215	72.85
3	$-0.03518658 - 0.96464251\,i$	0.000005	1.45
4	$-0.05089873 - 0.27720434\,i$	0.026606	347.98
5	$-0.06320150 - 0.93631654\,i$	0.000513	81.39
6	$-0.06325157 - 0.93635178\,i$	0.000021	2.90
7	$-0.09122274 - 0.90798305\,i$	0.000931	83.36
8	$-0.09131286 - 0.90805633\,i$	0.000056	4.32
9	$-0.11923285 - 0.87962729\,i$	0.001587	77.67
10	$-0.11937073 - 0.87975570\,i$	0.000124	5.37
11	$-0.12450198 - 0.34910682\,i$	0.171859	69.50
12	$-0.13822653 - 0.41635102\,i$	0.037660	252.09
13	$-0.14723393 - 0.85124584\,i$	0.002833	63.31
14	$-0.14742560 - 0.85144938\,i$	0.000268	5.59
15	$-0.17522868 - 0.82283504\,i$	0.005581	44.14
$\vdots$	$\vdots$	$\vdots$	$\vdots$
37	$-0.32519719 - 0.63610486\,i$	5.659801	0.78
38	$-0.34373267 - 0.67764346\,i$	4.685315	0.64
$\vdots$	$\vdots$	$\vdots$	$\vdots$
52	$-0.66286552 - 0.67027520\,i$	0.259581	11.58
$\vdots$	$\vdots$	$\vdots$	$\vdots$

Table 1: Least-stable eigenmodes of A for case (i) and the associated control and observation residuals. Calculation used Chebyshev collocation technique with $N = 140$ in quad precision. The only unstable mode ($\kappa = 1$) is both sensitive to the control u and easily detected by the observations y.

κ	λ_κ	f_κ	g_κ
1	-0.00132907	0.9619	1.0396
2	-0.00205172	0.9932	1.8656
3	-0.00280951	0.5092	1.9641
4	-0.00444971	1.0457	2.3710
5	-0.00527691	0.3478	2.8749
6	-0.00794734	0.9150	2.9317
7	-0.00873127	0.2646	3.7789
8	-0.01233325	0.8009	3.5058
9	-0.01317259	0.2137	4.6786
10	-0.01781312	0.6841	4.1763
11	-0.01860088	0.1794	5.5751
$\vdots$	$\vdots$	$\vdots$	$\vdots$

Table 2: Least-stable eigenmodes of A for case (ii) and the associated control and observation residuals. Calculation used Chebyshev collocation technique with $N = 70$ in quad precision. All modes are stable and all eigenvalues real.

wall measurements than eigenmodes in the lower branch. This observation is quantified by smaller values of f_κ and g_κ for these modes.

Note from table 1 that the third eigenmode is five orders of magnitude less sensitive than the first eigenmode to modifications in the control. In general, those modes in the upper branch of figure 1a (large $|\Im(\lambda)|$) are much less sensitive to control than those in the lower branch (small $|\Im(\lambda)|$). Near the intersection of the two branches ($\Re(\lambda) \approx -0.3$), the control residual is maximum, while it decreases slowly to the left of this intersection ($\Re(\lambda) < -0.3$). It can be predicted that the closed-loop eigenmodes corresponding to the largest f_κ might be affected most upon application of controller feedback. Indeed, Joshi, Speyer, & Kim (1997) report difficulty with the destabilization of mode $\kappa = 37$, the mode with the largest f_κ, by application of their PI controller.

Note also from table 1 that the flow measurements are two orders of magnitude less sensitive to the third eigenmode than they are to the first eigenmode. It can be predicted that the closed-loop eigenmodes corresponding to the largest g_κ might be affected most upon application of estimator feedback.

5.2.2 Eigenmode analysis of case (ii)

The least-stable eigenvalues of A for case (ii) are plotted in figure 2a and tabulated, along with the corresponding control and observation residuals f_κ and g_κ, in table 2. Figure 2b shows the shape of the eigenvectors corresponding to the 9 least-stable eigenvalues. Note that all eigenmodes shown span the entire channel, and thus f_κ and g_κ are all $O(1)$; i.e., the least-stable eigenmodes are both observable and controllable.

An important observation from figure 2 is that the eigenvalues in this case tend to come in nearly identical pairs, and the corresponding eigenvectors are nearly parallel. This structure may be explained by examination of the governing equations. Defining $\Delta_v \triangleq \mathscr{D}\,\tilde{\mathscr{D}} - k_z^2 I$ and $\Delta_\omega \triangleq \mathscr{D}\,\mathscr{D} - k_z^2 I$, the discrete form of (2.4) when $k_x = 0$ is:

$$\begin{aligned} \Delta_v\,\dot{\mathbf{v}} &= \{\Delta_v(\Delta_v/Re)\}\;\mathbf{v} \\ \dot{\boldsymbol{\omega}} &= \{-i\,k_z\,U'\}\;\mathbf{v} + \{\Delta_\omega/Re\}\;\boldsymbol{\omega}. \end{aligned} \quad\Rightarrow\quad \begin{aligned} \dot{\mathbf{v}} &= \mathscr{L}\,\mathbf{v} \\ \dot{\boldsymbol{\omega}} &= \mathscr{C}\,\mathbf{v} + \mathscr{S}\,\boldsymbol{\omega} \end{aligned} \quad\Rightarrow\quad \dot{\mathbf{x}} = A\mathbf{x} + B\mathbf{u},$$

where $\mathscr{L} = \Delta_v/Re$, $\mathscr{C} = -i\,k_z\,U'\,I$, and $\mathscr{S} = \Delta_\omega/Re$, and $\mathscr{L}_c$, $\mathscr{C}_c$, and $\mathscr{S}_c$ are the centre blocks of $\mathscr{L}$, $\mathscr{C}$, and $\mathscr{S}$ respectively, as discussed in §2.2. Note that the only difference between $\mathscr{S}$ and $\mathscr{L}$ is the treatment of boundary conditions in the derivative operators of Δ_v and Δ_ω. The eigenvalues of the system matrix A are the union of the eigenvalues of $\mathscr{S}_c$ and the eigenvalues of $\mathscr{L}_c$. Due to the similarity of these two matrices when $k_x = 0$, the eigenvalues of A tend to come in nearly identical pairs, as shown in figure 2a.

Note that half of the eigenvectors of $A\,\mathbf{x} = \lambda\,\mathbf{x}$ correspond to the eigenvectors of $\mathscr{S}\,\boldsymbol{\omega} = \lambda\,\boldsymbol{\omega}$ with

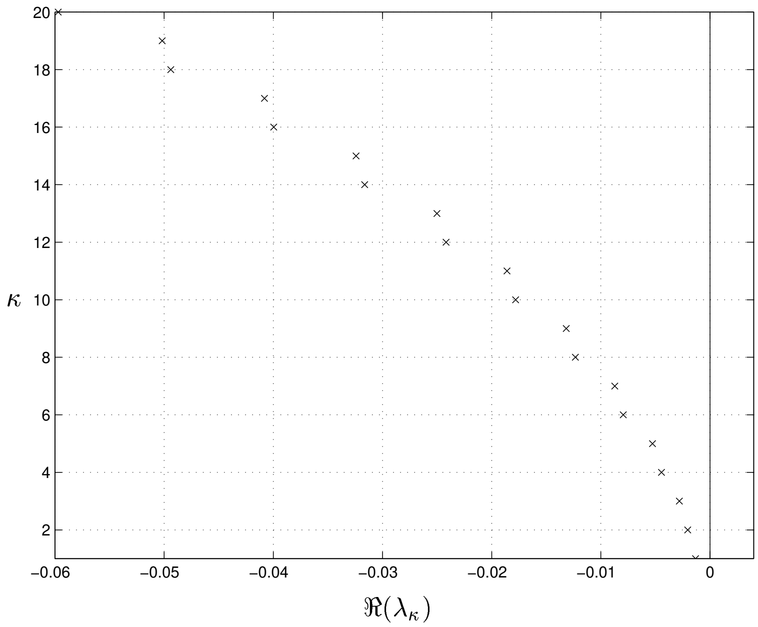

(a) Least-stable eigenvalues. Imaginary components of all eigenvalues are negligible.

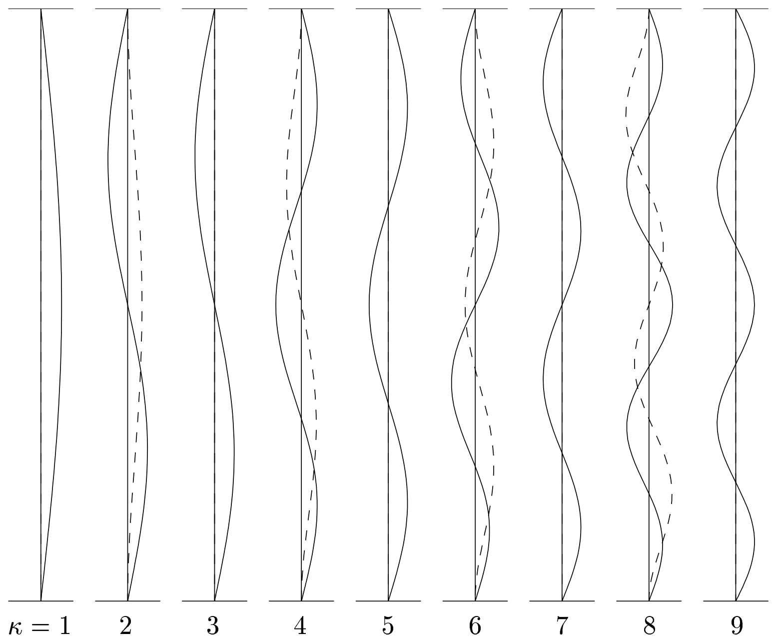

(b) Real part of the $\boldsymbol{\omega}$ component of the eigenvectors (solid) and 1000 times the imaginary part of the $\mathbf{v}$ component of the eigenvectors (dashed) corresponding to the least-stable eigenvalues of figure 2a, plotted as a function of y from the lower wall (bottom) to the upper wall (top). Imaginary part of the $\boldsymbol{\omega}$ components and real part of the $\mathbf{v}$ components of these eigenvectors are negligible.

Figure 2: Least-stable eigenmodes of A for case (ii).

$\mathbf{v} = \mathbf{0}$. The other half of the eigenvectors of A correspond to the eigenvectors of $\mathscr{L}\,\mathbf{v} = \lambda\,\mathbf{v}$ with $\boldsymbol{\omega} = -(\mathscr{S} - \lambda\,I)^{-1}\,\mathscr{C}\,\mathbf{v}$. Since the matrix $(\mathscr{S} - \lambda\,I)$ is nearly singular, $||\mathbf{v}||/||\boldsymbol{\omega}|| \ll 1$ in this second set of eigenvectors. Further, as the eigenvalues of the second set are near those of the first set, the (dominant) $\boldsymbol{\omega}$ components of the two sets of eigenvectors are nearly parallel, as shown in figure 2b.

5.3 Transient energy growth

The exponential energy growth possible in case (i), as shown in figure 3a, is well predicted by examining the eigenvalues for this case in figure 1a, as a system eigenvalue in the right half plane implies an unstable mode. The eigenvalues move to the left half plane as stabilizing estimators and controllers are applied to the system.

The large but finite transient energy growth possible in case (ii), which reaches a maximum of $\mathscr{E}(\tau)/\mathscr{E}(0) = 4897$ for the uncontrolled system as shown in figure 3b, can *not* be predicted by examination of the eigenvalues for this case in figure 2a. Such a large transient energy growth in a linearly stable system is possible because the eigenvectors of case (ii) are highly nonorthogonal, as shown in figure 2b. The mechanism for this large energy growth is explained in physical terms in figure 4. For small but finite initial flow perturbations, $O(Re)$ transient energy growth may be large enough to stimulate nonlinear instabilities in the flow and instigate transition to turbulence. In §6.4, the maximum transient energy growth for case (ii), $\max_{\tau,x(0)}\{\mathscr{E}(\tau)/\mathscr{E}(0)\}$, is shown to be significantly reduced as estimators and controllers are applied to the system.

5.4 Transfer function norms

As described in §4.4, in order to quantify the behaviour of the state response to disturbances and the control response to disturbances separately, norms of the transfer functions $T_{\mathbf{xw}}$ and $T_{\mathbf{uw}}$ will be computed separately. Three norms will be considered: $||T_{\mathbf{xw}}||_2$ is a measure of the state response to Gaussian disturbances, $||T_{\mathbf{xw}}||_\infty$ is a measure of the state response to worst-case disturbances, and $||T_{\mathbf{uw}}||_2$ is a measure of the control used in response to Gaussian disturbances. These transfer function norms will be used as benchmarks in §6.1 to quantify the effects of control and estimation for the present systems.

For the uncontrolled cases, of course, $T_{\mathbf{uw}} = 0$. For case (i), as the uncontrolled system is unstable, $||T_{\mathbf{xw}}||_2$ and $||T_{\mathbf{xw}}||_\infty$ are infinite; any slight excitation of the unstable mode of the system results in an unbounded response. For case (ii), the uncontrolled system has $||T_{\mathbf{xw}}||_2 = 524.8$ and $||T_{\mathbf{xw}}||_\infty = 15388$. Note that these numbers are large; due to the nonorthogonality of the eigenvectors of case (ii), the state is sensitive to small disturbances of a particular structure. Note also that the system response for the two different types of disturbances (Gaussian and worst case) differ by a factor of 30; Gaussian analysis alone is not sufficient to completely characterize the system.

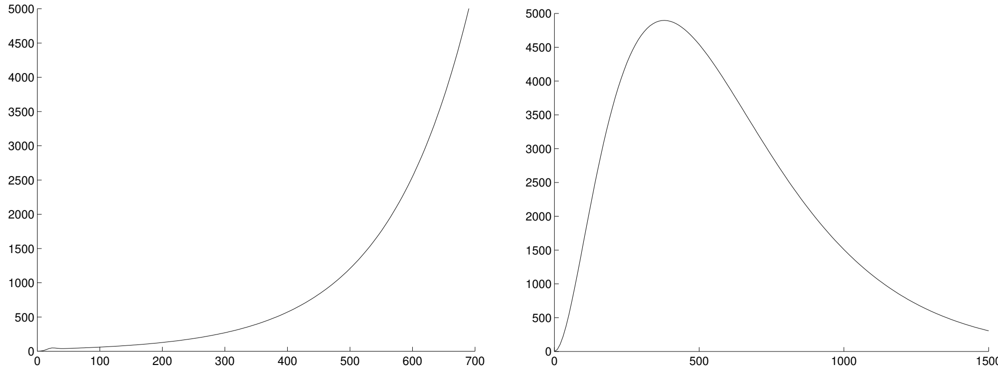

(a) Case (i), unstable.

(b) Case (ii), stable. Transient energy growth at $\tau = 379$ is $\mathscr{E}(\tau)/\mathscr{E}(0) = 4897$.

Figure 3: Maximum energy growth for open-loop, uncontrolled systems: $\mathscr{E}(t)/\mathscr{E}(0)$ versus t.

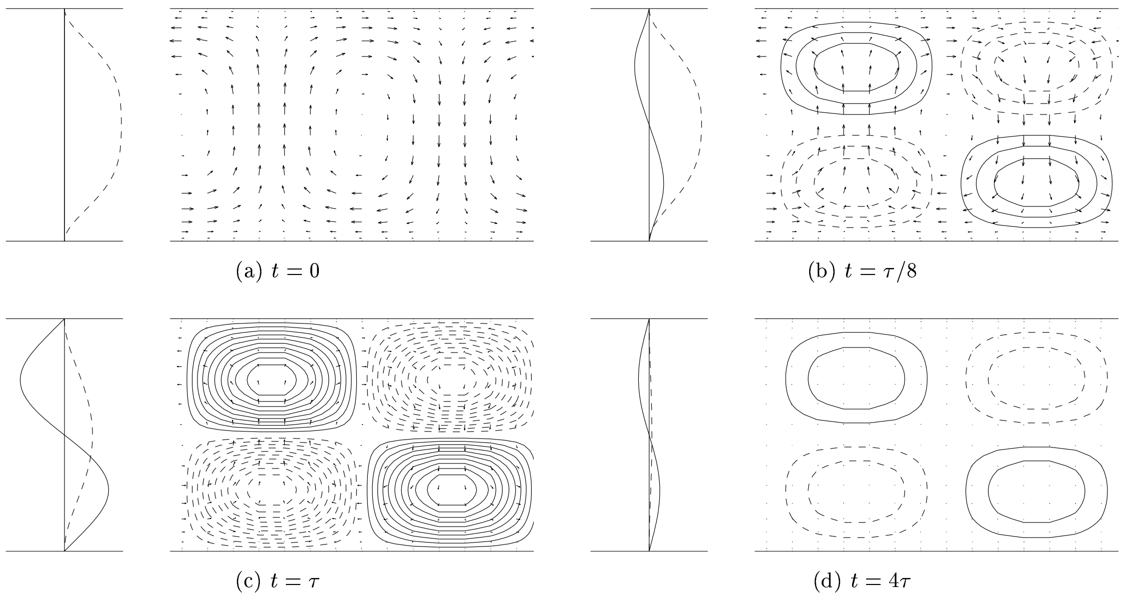

(a) $t = 0$

(b) $t = \tau/8$

(c) $t = \tau$

(d) $t = 4\tau$

Figure 4: Shape of the flow perturbation with the largest transient energy growth for case (ii), as plotted in figure 3b. At the left of each subfigure is the perturbation plotted as in figure 2b, with the $\mathbf{v}$ component (dashed) magnified by a factor of 250 as compared with the $\boldsymbol{\omega}$ component (solid). The corresponding flow perturbation in a cross-flow plane is shown at the right of each subfigure, with the cross-flow velocity vectors shown as arrows and the streamwise velocity as contours; recall that the flow perturbations for case (ii), with $k_x = 0$, have no streamwise variation. The initial perturbation (a superposition of several eigenmodes) is a streamwise vortex filling the channel with zero streamwise velocity component. The streamwise vorticity diminishes with time, during which very large streamwise velocity fluctuations are induced by its action on the mean streamwise velocity profile $U(y)$. Positive streamwise velocity regions ("sweeps") are indicated with solid contours, and negative streamwise velocity regions ("ejections") are indicated with dashed contours. The streamwise velocity fluctuations eventually decay, after the streamwise vorticity inducing them is sufficiently reduced.

Chapter 6

Analysis of closed-loop systems

The controlled ("closed-loop") systems are now examined in detail using the analysis methods of §4. Specifically, the behaviour of the flow and the estimator/controllers (or portions thereof) operating together as a single dynamical system is characterized.

6.1 Quantitative comparison of various closed-loop systems

Tables 3 and 4 summarize a parametric study of a variety of control schemes applied to cases (i) and (ii), respectively, using the transfer function norms described in §4.4 to provide a *quantitative* comparison between $\mathcal{H}_2$, $\mathcal{H}_\infty$, and proportional controllers.

The first two columns in these tables list the settings of the relevant parameters used to determine the controller and/or estimator. The remaining columns contain data on the response of the state in the closed-loop system to Gaussian disturbances and worst-case disturbances, the maximum transient energy growth, and the level of control effort used to attain this closed-loop performance. Specifically, the third column contains $||T_{\mathbf{xw}}||_2$, which indicates the square-root of the expected energy of the state, $E[\mathbf{x}^* Q\,\mathbf{x}]$, in response to white Gaussian disturbances $\mathbf{w}$. The fourth column contains $||T_{\mathbf{xw}}||_\infty$, which indicates the square-root of the expected energy of the state in response to worst-case disturbances $\mathbf{w}$ with unit norm. For comparison, the fifth column contains the maximum transient energy growth of the closed-loop system. The sixth column contains $||T_{\mathbf{uw}}||_2$, which indicates the rms value of the control $\mathbf{u}$ in response to white Gaussian disturbances $\mathbf{w}$. Recall that, by (4.8), $||T_{\mathbf{zw}}||_2^2 = ||T_{\mathbf{xw}}||_2^2 + \ell^2||T_{\mathbf{uw}}||_2^2$. For consistency, all transfer function norms tabulated are computed under the assumption that $\alpha = 1$ in the determination of the norm, though the estimator feedback L is determined with the value of α cited in the table. Of course, the analyses may be conducted easily for other values of α which better describe a particular system of interest.

control type		control parameters	$\|\|T_{\mathbf{xw}}\|\|_2$	$\|\|T_{\mathbf{xw}}\|\|_\infty$	$\max_{\tau,x(0)} \left\{ \frac{\mathscr{E}(\tau)}{\mathscr{E}(0)} \right\}$	$\|\|T_{\mathbf{uw}}\|\|_2$
(no control)		–	∞	∞	∞	0
$\mathcal{H}_2$ control $\gamma \to \infty$	full information controller	$\ell = 1000$	589.8	13357	24.4	20.29
		$\ell = 100$	574.8	12421	24.4	20.31
		$\ell = 30$	522.0	9163	23.9	20.93
		$\ell = 10$	498.5	7114	23.5	22.44
		$\ell = 1$	497.2	6673	23.4	23.07
		$\ell = 0.1$	497.2	6668	23.5	23.08
	state estimator†	$\alpha = 1000$	461.6	10248	55.5	0
		$\alpha = 100$	339.0	5273	53.4	0
		$\alpha = 10$	133.8	563	33.4	0
		$\alpha = 1$	89.2	160	25.4	0
		$\alpha = 0.1$	90.1	158	25.4	0
	composite estimator/ controller‡	$\alpha = 100,\quad \ell = 100$	867.3	22565	57.2	24.05
		$\alpha = 10,\quad \ell = 30$	548.5	9879	47.8	20.94
		$\alpha = 1,\quad \ell = 1$	501.2	6730	50.4	23.17
$\mathcal{H}_\infty$ control $\alpha = 10$ $\ell = 30$	full information controller	$\gamma = \infty$	522.0	9163	23.9	20.93
		$\gamma = 10000$	538.8	5129	23.3	28.35
		$\gamma = 8500$	884.1	4254	23.3	50.53
		$\gamma = 8200$	1807.9	4091	23.3	104.54
		$\gamma = \gamma_0 = 8122$	16522.7	4052	23.2	956.87
	state estimator†	$\gamma = \infty$	133.8	563	33.4	0
		$\gamma = \gamma_0 = 704$	117.6	310	22.5	0
	composite estimator/ controller‡	$\gamma = \infty$	548.5	9879	47.8	20.94
		$\gamma_{\text{controller}} = 8500$ $\gamma_{\text{estimator}} = 704$	**1047.2**	**4543**	**335.8**	**60.07**
proportional control $\phi_1 = \phi_2 = 0$		$k_1 = k_2 = 2$¶	3549	62248	8.5	∞
		$k_1 = k_2 = 10$	4641	6047	167	∞
		$k_1 = k_2 = 60$	6993	4577	7410	∞
		$k_1 = k_2 = 100$	7908	5253	17800	∞
		$k_1 = k_2 = 1000$	17596	61341	58600	∞
		$k_1 = k_2 = 10000$	43736	456491	86800	∞

Table 3: Performance of various controllers, case (i): $Re = 10{,}000$, $k_x = 1$, $k_z = 0$.
† State estimator: transfer function to x_E and max growth of $\mathscr{E} \triangleq x_E^* \, Q \, x_E$ reported.
‡ Composite estimator/controller: max growth of $\mathscr{E} \triangleq x^* \, Q \, x + x_E^* \, Q \, x_E$ reported.
¶ The minimum k_i which stabilize the proportionally-controlled closed-loop system.

control type		control parameters	$\|\|T_{\mathbf{xw}}\|\|_2$	$\|\|T_{\mathbf{xw}}\|\|_\infty$	$\max\limits_{\tau, x(0)} \left\{ \dfrac{\mathscr{E}(\tau)}{\mathscr{E}(0)} \right\}$	$\|\|T_{\mathbf{uw}}\|\|_2$
(no control)		–	524.8	15388	4897	0
$\mathcal{H}_2$ control $\gamma \to \infty$	full information controller	$\ell = 1000$	523.2	15307	4858	0.03
		$\ell = 100$	426.5	10796	943	1.93
		$\ell = 30$	284.8	5163	155	6.35
		$\ell = 10$	226.1	3616	185	11.59
		$\ell = 1$	212.6	3353	161	18.25
		$\ell = 0.1$	212.6	3350	159	18.49
	state estimator†	$\alpha = 1000$	524.6	15376	4894	0
		$\alpha = 100$	507.6	14333	4667	0
		$\alpha = 30$	415.7	9412	3448	0
		$\alpha = 10$	271.8	4853	1779	0
		$\alpha = 1$	155.9	2450	762	0
		$\alpha = 0.1$	248.7	2383	690	0
	composite estimator/controller‡	$\alpha = 100, \quad \ell = 100$	522.4	15135	4844	0.07
		$\alpha = 10, \quad \ell = 30$	398.8	7988	2679	3.49
		$\alpha = 1, \quad \ell = 1$	271.3	4528	1313	15.50
$\mathcal{H}_\infty$ control $\alpha = 10$ $\ell = 30$	full information controller	$\gamma = \infty$	284.8	5163	155	6.35
		$\gamma = \gamma_0 = 5340$	260.8	3558	277	8.86
	state estimator†	$\gamma = \infty$	271.8	4853	1779	0
		$\gamma = \gamma_0 = 5058$	234.5	3284	1473	0
	composite estimator/controller‡	$\gamma = \infty$	398.8	7988	2679	3.49
		$\gamma_{\text{controller}} = 5340$ $\gamma_{\text{estimator}} = 5058$	**353.2**	**5797**	**2357**	**5.56**
proportional control $\phi_1 = \phi_2 = 0$		$k_1 = k_2 = 0.1$	543	15028	4821	∞
		$k_1 = k_2 = 1$	1685	12885	4327	∞
		$k_1 = k_2 = 10$	16175	9219	3270	∞
		$k_1 = k_2 = 100$	161680	8181	2905	∞
		$k_1 = k_2 = 1000$	1616300	8058	2860	∞
		$k_1 = 10,\ k_2 = 0$	11443	13405	4219	∞

Table 4: Performance of various controllers, case (ii): $Re = 5{,}000$, $k_x = 0$, $k_z = 2.044$.
† State estimator: transfer function to x_E and max growth of $\mathscr{E} \triangleq x_E^* \, Q \, x_E$ reported.
‡ Composite estimator/controller: max growth of $\mathscr{E} \triangleq x^* \, Q \, x + x_E^* \, Q \, x_E$ reported.

6.1.1 Full information controllers

To investigate the behaviour of the $\mathcal{H}_2$ and $\mathcal{H}_\infty$ controllers separately from that of the estimator, consider the closed-loop system #2 in (4.10) for the controlled state $\mathbf{x}$, obtained by combining the open-loop plant with the controller and assuming full state information is available.

It is seen from tables 3 and 4 that full information controllers do an excellent job of reducing both $||T_{\mathbf{xw}}||_2$ and $||T_{\mathbf{xw}}||_\infty$, while maintaining finite values of $||T_{\mathbf{uw}}||_2$. The full information $\mathcal{H}_2$ controllers minimize the 2-norm of the transfer function from the disturbance $\mathbf{w}$ to the performance measure $\mathbf{z}$, namely, $||T_{\mathbf{zw}}||_2^2 = ||T_{\mathbf{xw}}||_2^2 + \ell^2||T_{\mathbf{uw}}||_2^2$; this is, in fact, the $\mathcal{H}_2$ design objective. As the control is made cheaper (ℓ is reduced), the state $\mathbf{x}$ contributes relatively more to the performance measure $\mathbf{z}$, causing the $\mathcal{H}_2$ controller to drive $||T_{\mathbf{xw}}||_2$ to the minimum value possible, though the control effort required, $||T_{\mathbf{uw}}||_2$, generally increases; these trends are all confirmed in the tables.

At a fixed price for the control ($\ell = 30$), the introduction of a worst-case disturbance in the design of an $\mathcal{H}_\infty$ controller (by the reduction of γ) results in a system which does not necessarily further reduce $||T_{\mathbf{xw}}||_2$, but which reduces the ∞-norm of the transfer function from the disturbance $\mathbf{w}$ to the performance measure $\mathbf{z}$, namely, $||T_{\mathbf{zw}}||_\infty$; this is, in fact, the $\mathcal{H}_\infty$ design objective. For vanishing values of ℓ, the absolute minimum value for $||T_{\mathbf{xw}}||_\infty$ may be obtained by reducing γ of the $\mathcal{H}_\infty$ controller to its minimum value γ_0. However, such a controller may require more control effort, $||T_{\mathbf{uw}}||_2$, and/or have worse response to Gaussian disturbances, $||T_{\mathbf{xw}}||_2$, than desirable for a particular implementation. To compensate, intermediate values of γ and ℓ may be chosen. The two parameters γ and ℓ provide the flexibility needed to achieve the desired trade-off between a) Gaussian disturbance response, b) worst-case disturbance response, and c) control effort required.

Note that $\ell \to 0$ limits exist for all norms listed for both case (i) and case (ii). As the present systems are stabilizable but not controllable, as remarked in §5.1, there are diminishing returns to be gained by increasing the feedback gains K. The optimal controllers do not attempt to push the closed-loop system beyond the limits imposed by uncontrollable modes. This topic is quantified further in §6.5 using the modal control residuals defined in §4.2.

6.1.2 State estimators

To investigate the behaviour of the $\mathcal{H}_2$ and $\mathcal{H}_\infty$ estimators separately from that of the controller, consider the closed-loop system #3 in (4.11) for the estimation error $\mathbf{x}_E \triangleq \mathbf{x} - \hat{\mathbf{x}}$, obtained by combining the open-loop plant with the estimator and assuming no control is applied.

It is seen from tables 3 and 4 that the state estimators (based on measurements at the wall only) do an excellent job of regulating the response of the estimation error $\mathbf{x}_E$ to both Gaussian disturbances ($||T_{\mathbf{xw}}||_2$) and worst-case disturbances ($||T_{\mathbf{xw}}||_\infty$). As the measurements are assumed to be increasingly accurate in the design of the estimator (α is reduced), the estimator feedback is increased, and it is seen that the $\mathcal{H}_2$ estimator drives $||T_{\mathbf{xw}}||_2$ to small values, though the estimator feedback (not tabulated) generally increases. Note that the behaviour of $||T_{\mathbf{xw}}||_2$ is not quite monotonic with respect to α for both case (i) and case (ii). This is because the $\mathcal{H}_2$ estimator is designed to reduce the expected value of $\mathbf{x}_E^* \mathbf{x}_E$, though, in the tables, $||T_{\mathbf{xw}}||_2$ represents the transfer function related to the expected value of $\mathbf{x}_E^* Q \mathbf{x}_E$ for consistency. The difference between these two types of measures is discussed further in §6.2.

At a fixed relative magnitude of measurement noise, $\alpha = 10$, the introduction of a worst-case disturbance in the design of an $\mathcal{H}_\infty$ estimator (by the reduction of γ) results in a system which reduces $||T_{\mathbf{zw}}||_\infty$, in a manner analogous to that of the $\mathcal{H}_\infty$ controller. For small values of α (reliable measurements), high levels of estimator feedback may result. Note that high levels of estimator feedback (or, for that matter, controller feedback) can cause problems if the state model A in the estimator (3.2a) is inaccurate. Though this topic is beyond the scope of the present discussion, it suffices to say that small levels of estimator feedback are desirable from the standpoint of reduced sensitivity to modeling errors. The two parameters γ and α provide the flexibility needed to achieve the desired trade-off between a) Gaussian disturbance response, b) worst-case disturbance response, and c) estimator feedback required. Future work recommended in this area would be a μ-synthesis approach to the present control problem to account rigorously for the sensitivity of the system to modeling uncertainties (Skogestad & Postlethwaite 1996).

6.1.3 Composite estimator/controllers

To investigate the behaviour of the estimator and controller acting together, consider the closed-loop composite system #4 in (4.12), in which the state is formed by the union of $\mathbf{x}$ and $\mathbf{x}_E$ and the system is obtained by combining the open-loop plant with both the estimator and the controller. It is seen from tables 3 and 4 that the transfer function norms $||T_{\mathbf{xw}}||_2$ and $||T_{\mathbf{xw}}||_\infty$ for the controlled systems based on estimated state information $\hat{\mathbf{x}}$ are slightly degraded from the controlled systems using the corresponding full-information controllers.

Some degradation of performance in the composite system (as compared with the full-information system) is expected, as the system dynamics of the composite system are of increased complexity. To characterize the dynamics of the composite system when no disturbances are present, the eigenmodes of

$$\tilde{A} = \begin{pmatrix} A + B_2 K & -B_2 K \\ 0 & A + L C_2 \end{pmatrix}$$

may be considered. The closed-loop eigenvalues of the composite system matrix $\tilde{A}$ are simply the union of the eigenvalues of the controlled system $(A + B_2 K)$ and the eigenvalues of the estimated system $(A + L C_2)$ discussed in the previous two sections.

Half of the eigenvectors of $\tilde{A}$ are formed by the eigenvectors of the controlled system $(A + B_2 K)\mathbf{x} = \lambda \mathbf{x}$ with $\mathbf{x}_E = \mathbf{0}$. Thus, in the closed-loop composite system with no disturbances, if the initial state estimate is correct ($\mathbf{x}_E(0) = \mathbf{0}$), then the state estimate will remain correct ($\mathbf{x}_E(t) = \mathbf{0}$) and the dynamics of the (decoupled) system as it is regulated to zero will simply be the dynamics of the controlled plant provided with full state information. The other half of the eigenvectors of $\tilde{A}$ are formed by the eigenvectors of the estimated system $(A + L\,C_2)\,\mathbf{x}_E = \lambda\,\mathbf{x}_E$ with $\mathbf{x} = (A + B_2\,K - \lambda I)^{-1}\,B_2\,K\,\mathbf{x}_E$. Thus, any errors in the initial state estimate ($\mathbf{x}_E(0) \neq \mathbf{0}$) will induce perturbations in the state itself ($\mathbf{x}(t) \neq \mathbf{0}$) as the entire coupled system is regulated back to zero.

6.1.4 Comparison with proportional control

Proportional controllers, though simpler in their design, are not nearly as effective as the $\mathcal{H}_2$ and $\mathcal{H}_\infty$ controllers. The most important flaw of any controller with a proportional component, as described in §4.6, is that it has no high-frequency roll-off in the controller's response to measurement noise, so the rms of the control response $\mathbf{u}$ to white noise ($||T_{\mathbf{uw}}||_2$) is unbounded.

The best $\mathcal{H}_\infty$ composite estimator/controllers tested, shown in boldface in tables 3 and 4, are seen to perform better than all proportional controllers tested with respect to the response of the state $\mathbf{x}$ to both white noise disturbances ($||T_{\mathbf{xw}}||_2$) and worst case disturbances ($||T_{\mathbf{xw}}||_\infty$). This is remarkable, as the $\mathcal{H}_\infty$ estimator/controllers use significantly less control energy than the proportional controllers, as indicated by their bounded values of $||T_{\mathbf{uw}}||_2$.

6.2 System eigenvalue ("root locus") analyses

By examining root locus plots which map the movement of the closed-loop system eigenvalues with respect to the scalar parameters of the system (for the $\mathcal{H}_\infty$ controller, γ, α, or ℓ; for the proportional controller, $k_1 = k_2 = k$), the effect of an estimator/controller applied to a large MIMO linear system may be partially characterized.

The eigenmodes of $\tilde{A} = A + B_2\,K$ describe the dynamics of the closed-loop system #2 in (4.10) when $\mathbf{u}' = \mathbf{w} = \mathbf{0}$. The movement of these eigenvalues as a function of ℓ and γ, the free parameters of the $\mathcal{H}_\infty$ controller, for case (i) are examined in figures 5a, 5b, and 5c. The eigenvalues for $\ell \to \infty$ are very near those of the uncontrolled system A in figures 5a and 5b, with the previously unstable mode reflected just to the left of the imaginary axis; this solution represents the "expensive control" limit that uses the minimum control necessary to marginally stabilize the system. The eigenvalues generally move to the left as ℓ, the "price" of the control, is decreased.

For $C_1 = (Q^{1/2}\ \ 0)^*$, the definition given in (3.4) and used throughout this article, the root locus for an $\mathcal{H}_2$ controller with respect to ℓ is given in figure 5a; note that the eigenvalues move only slightly with the application of $\mathcal{H}_2$ control. For $C_1 = (I\ \ 0)^*$, a definition which weighs all of the discretized values of the state $\mathbf{x}$ equally, more eigenvalue movement is seen in the root locus with respect to ℓ, as shown in figure 5b. However, the physically relevant energy norm, $||T_{\mathbf{zw}}||_2$, is reduced less effectively by this modified $\mathcal{H}_2$ controller. The modified definition of C_1 results in extra weighting in the performance measure on those regions of flow where the grid points are clustered. In the present case, this weighting takes the form $\eta(y) = (1 - y^2)^{-1/2}$, as discussed in §2.4. This is a very large weighting on the eigenfunctions near the wall, and thus this performance measure results in very large movement of all of the controllable eigenmodes which are nonzero in the heavily weighted region near the wall when the corresponding optimal controller is applied. The weighting given by $\eta(y)$ is not physically based, and thus, in the opinion of the authors, should not be used to define the performance measure. If a rigorous analysis indicates a Lyapunov function more relevant to secondary instability than the energy norm, that function may easily be used to replace Q in the present development. However, the *ad hoc* weighting implied by $\eta(y)$ is almost certainly not such a function, and performance measures based on the kinetic energy density, as used here, are preferred.

Figure 5c shows the movement of the closed-loop system eigenvalues as a function of γ, taking $\ell = 30$. Starting from a stable closed-loop $\mathcal{H}_2$ system ($\gamma = \infty$) with an intermediate value for the price of the control ($\ell = 30$), it is observed that the introduction of an unstructured disturbance into the controller computation (reducing γ) affects *only* the least-stable component of the system. Compare this with the $\mathcal{H}_2$ controller in figures 5a and 5b, which show that *all* controllable modes of the system are modified when ℓ is reduced.

Figure 5d shows the movement of the closed-loop system eigenvalues when MIMO proportional control is applied. For $k \geq 2$, the system is stable (i.e., the unstable eigenvalue moves to the left-half plane), and the eigenmodes *appear* to be effectively controlled right up to the large gain limit. Note also that a new, distinct ($\prec$)-shaped structure to the locus of eigenvalues emerges for case (i) with a MIMO proportional controller in the large gain limit, as indicated by the eigenvalues marked with an (o) in figure 5d. The simple pattern of eigenvalues in the lower branch, which is reminiscent of the pattern of eigenvalues of the (uncontrollable) centre modes in the upper branch, apparently emerges due to a fundamental shift to a simple boundary condition in this limit, as discussed in the following section.

Though root locus plots do reveal some important trends, they do *not* indicate the important effects of the nonorthogonality of the eigenvectors or the effect of the control on the physically relevant norms of interest. For systems (such as the present) with highly nonorthogonal eigenvectors, a root locus characterization can therefore be misleading, as established above by the apparently good behaviour of the proportional controller in the large gain limit, indicated by figure 5d, but its *terrible* disturbance response in this limit, reported in table 3. Note that Trefethen *et al.* (1993) have proposed an interesting extension to the root locus approach, referred to as pseudospectra, which extends the root locus analysis to reflect the sensitivity of a system to external forcing. In the future, such a technique should be explored in a closed-loop framework in an attempt to obtain a graphical characterization of different control approaches.

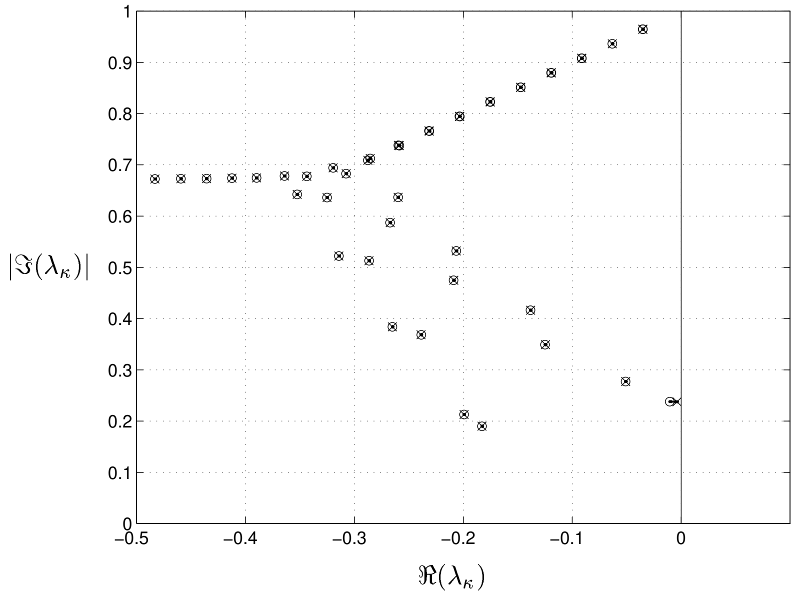

(a) Locus of least-stable eigenvalues of the $\mathcal{H}_2$ controller ($\gamma \to \infty$) as a function of ℓ. Eigenvalues for $\ell \to \infty$ are marked with an (x), and those for $\ell \to 0$ are marked with an (o). Note that eigenvalues barely move in this plot, though $||T_{\mathbf{zw}}||_2$, for which this controller is designed, is effectively minimized.

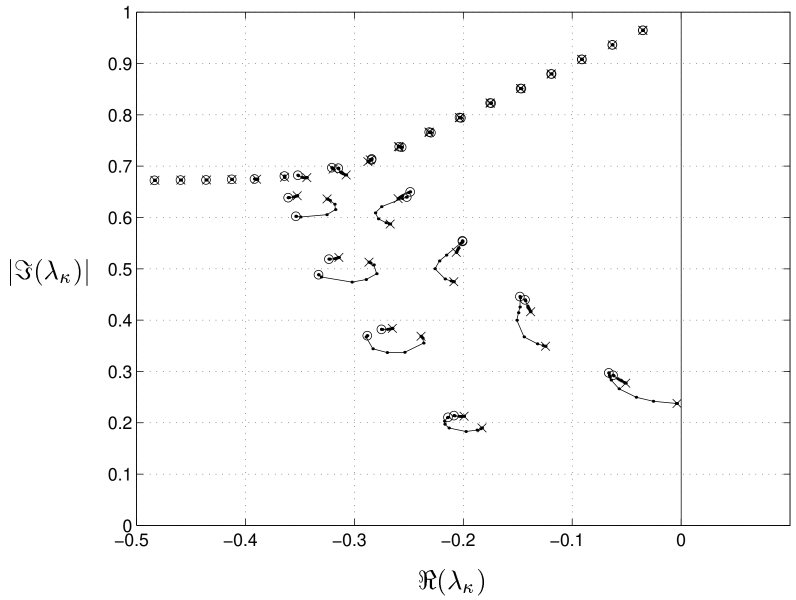

(b) Locus of least-stable eigenvalues of a modified $\mathcal{H}_2$ controller, taking (for this plot only) $C_1 = (I \quad 0)^*$. Eigenvalues are marked as in figure 5a. Note that the eigenvalues in the lower branch are significantly moved by this modified $\mathcal{H}_2$ controller. However, the physically relevant transfer function norms are more effectively reduced by controllers which are specifically designed taking the energy of the state into account, i.e., by those which take $C_1 = (Q^{1/2} \quad 0)^*$. As shown in figure 5a, such controllers may result in significantly *less* eigenvalue movement in a root locus plot. This implies that root locus plots themselves, which characterize eigenvalues but not eigenvectors or closed-loop transfer function norms, do not give the complete picture of system performance.

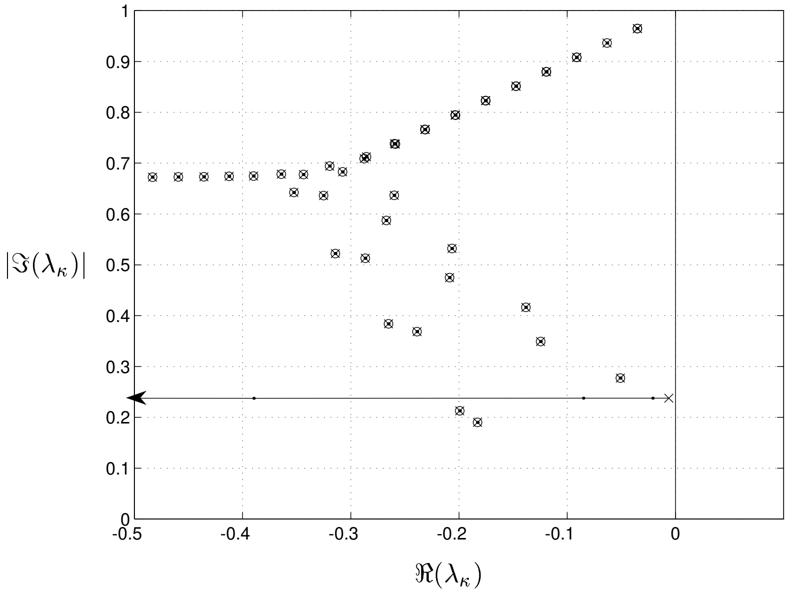

(c) Locus of least-stable eigenvalues of the $\mathcal{H}_\infty$ controller as a function of γ, taking $\ell = 30$. Eigenvalues for the $\mathcal{H}_2$ limit ($\gamma \to \infty$) are marked with an (x), and those for $\gamma \to \gamma_0$ are marked with an (o). The introduction of the unstructured disturbance in the $\mathcal{H}_\infty$ controller modifies only the least-stable eigenmode of an $\mathcal{H}_2$ result, without expending any extra feedback to control those eigenmodes not associated with the maximally unstable component of the system..

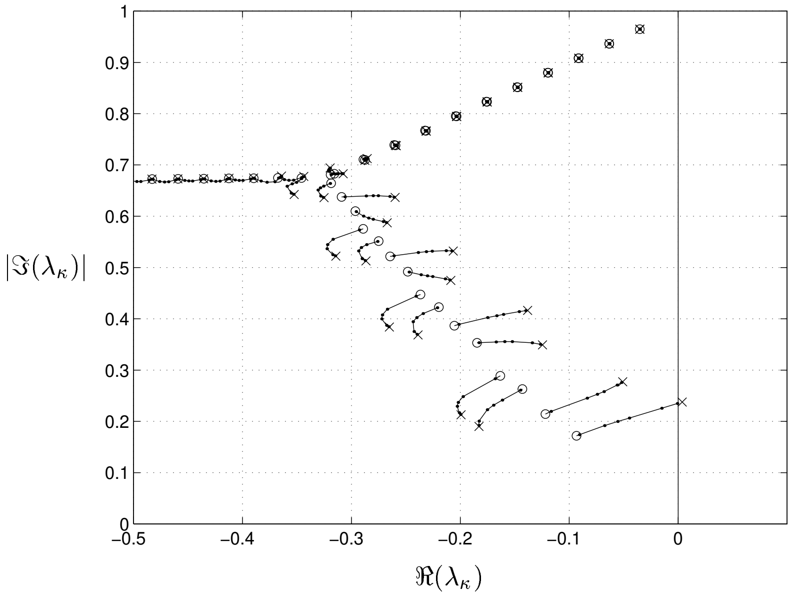

(d) Locus of least-stable eigenvalues of the MIMO proportional controller as a function of $k_1 = k_2 = k$, taking $\phi_1 = \phi_2 = 0$. Eigenvalues for $k = 0$ are marked with an (x), and those for $k \to \infty$ are marked with an (o). Note that, in the large gain limit, the eigenvalues in the lower branch align on a diagonal line.

Figure 5: Representative root loci demonstrating the movement of the least-stable eigenvalues of several closed-loop systems as a function of controller parameters.

6.3 Modification of eigenvectors by application of control

The modified shapes of the closed-loop eigenvectors for case (i) by application of $\mathcal{H}_\infty$ control and proportional control are shown in figure 6. Only the $\kappa = 1$ mode is significantly modified by the $\mathcal{H}_\infty$ controller, whereas all controllable eigenmodes are modified by the proportional controller. For case (ii), however, it is seen that the $\mathcal{H}_2$ (and $\mathcal{H}_\infty$) controllers modify all of the eigenvectors, as shown in figure 7. In this case, the critical issue is the nonorthogonality of the set of eigenvectors, not the real component of any particular eigenvalue, and thus the optimal control acts to make the set of eigenvectors more orthogonal.

Recall from §2 that the boundary conditions on the uncontrolled Orr-Sommerfeld problem are $v = 0$ and $\partial v/\partial y = 0$ at the walls. Consider the proportional controller of the form $\mathbf{u} = K\mathbf{y}_m$ given in (3.7), taking $k_1 = k_2 = k$ and $\phi_1 = \phi_2 = \phi$. By (2.5), noting that $k_z = 0$ for this case, the homogeneous Dirichlet boundary conditions at each wall are replaced by

$$v = k\, e^{i\phi}\, \frac{1}{Re}\, \frac{\partial u}{\partial y} = k \left(\frac{i\, k_x\, e^{i\phi}}{k_x^2 + k_z^2}\, \frac{1}{Re} \right) \frac{\partial^2 v}{\partial y^2} = k\, C\, \frac{\partial^2 v}{\partial y^2},$$

where C is some constant. Note that the homogeneous Neumann boundary condition still applies due to continuity. In the limit for which the feedback gain $k \to \infty$, assuming the eigenvectors remain finite (confirmed *a posteriori*), the Dirichlet boundary condition is equivalent to a homogeneous boundary condition on the *second* derivative of v, i.e.

$$\frac{\partial v}{\partial y} = 0 \quad \text{and} \quad \frac{\partial^2 v}{\partial y^2} = 0 \quad \text{when} \quad k \to \infty.$$

These simple boundary conditions on the closed-loop eigenvectors are verified by the plots of the computed eigenvectors for the proportional controller with large k in figure 6b for case (i), which clearly shows that both the slope and the curvature of the closed-loop eigenvectors go to zero near the wall. It is inferred that these simple homogeneous boundary conditions are related to the simple eigenvalue structure which emerges in this limit, as shown in figure 5d.

6.4 Reduction of maximum transient energy growth

The effect of the control on the worst-case transient energy growth is tabulated along with the transfer function norms in tables 3 and 4. Though large values of $||T_{\mathbf{zw}}||_\infty$ and large values of transient energy growth are both due, in part, to non-orthogonality of the eigenvectors, they do not always correlate closely as the various control parameters are altered. It is the excitation by external disturbance forcing, and not the growth from a particularly deleterious set of initial conditions, which is the primary topic of interest in the present control problem. Thus, transfer function norms, which quantify the response of the state and the control to external disturbance forcing, are used in the

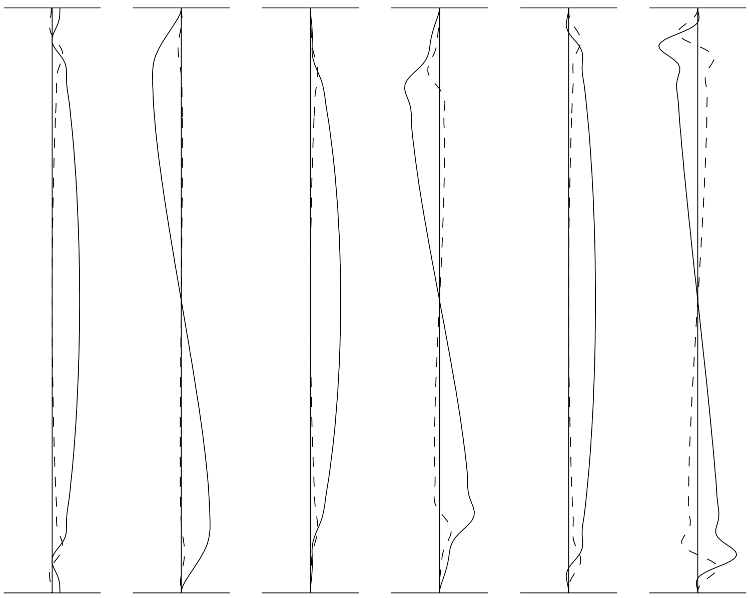

(a) Closed-loop eigenvectors of the system obtained with an $\mathcal{H}_\infty$ controller with $\ell = 30$ and $\gamma = 8300$. Only the least-stable mode is significantly modified.

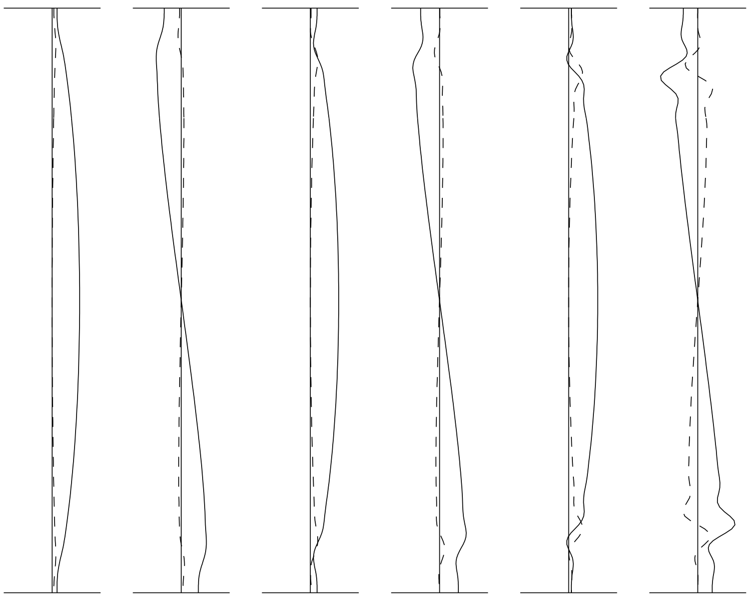

(b) Closed-loop eigenvectors of the system obtained with a MIMO proportional controller with $k_1 = k_2 = 10000$. All controllable eigenmodes are significantly modified.

Figure 6: Modified shape of closed-loop eigenvectors for case (i) by application of $\mathcal{H}_\infty$ control (top) and proportional control (bottom). Eigenvectors scaled as in figure 1b. Note that only eigenvectors with wall support, corresponding to the six least-stable eigenmodes from the lower branch, are plotted above; the uncontrollable eigenmodes from the upper branch are not modified by the control and are not shown. Those eigenmodes which have been modified by the control show a nonzero value of $\mathbf{v}$ at the wall in the above plots.

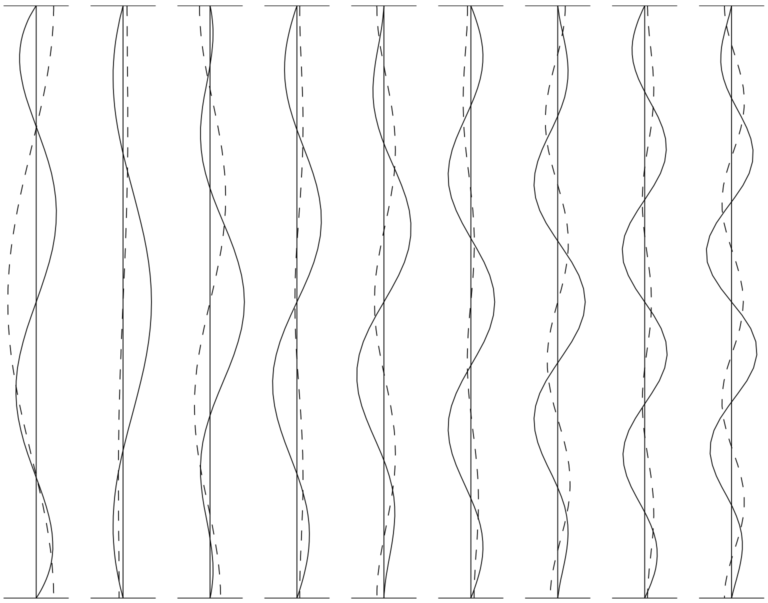

Figure 7: Modified shape of the nine least-stable closed-loop eigenvectors for case (ii) by application of $\mathcal{H}_2$ control with $\ell = 1$. Eigenvectors plotted as in figure 2b, with the **v** component (dashed) magnified by a factor of 300 rather than a factor of 1000. The eigenvectors are made more orthogonal by the application of control, to the point that a one-to-one correspondence of the above eigenmodes to the uncontrolled eigenmodes of figure 2b is barely distinguishable.

present work to formulate the control objective. However, a side effect of the control application in the present problem is that the maximum transient energy growth of the system is reduced effectively. For example, the maximum transient energy growth in case (ii), which is reduced from an uncontrolled value of $\mathscr{E}(\tau)/\mathscr{E}(0) = 4897$ to a value of 2860 by the proportional controller, is reduced to a value of 1313 by the wall-information $\mathcal{H}_2$ controller, and is reduced to a value of 155 by the full-information $\mathcal{H}_2$ controller, as tabulated in table 4 and shown in figure 8. The mechanism for the large reduction in energy growth is explained in physical terms in figure 9. Finite-horizon terminal controllers, in both an $\mathcal{H}_2$ and $\mathcal{H}_\infty$ setting (Green & Limebeer 1995), may be proposed to minimize the transient energy growth of a closed-loop system over a time interval τ in a rigorous manner. However, such is not the objective of the present control problem.

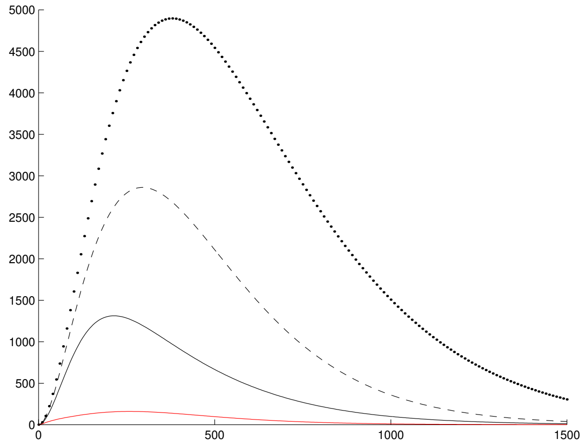

Figure 8: Reduction of maximum transient energy growth by application of control to case (ii): $\mathscr{E}(t)/\mathscr{E}(0)$ versus t. Top to bottom: no control, proportional control ($k = 1000$), wall-information $\mathcal{H}_2$ control ($\gamma = \infty$, $\alpha = 1$, $\ell = 1$), full-information $\mathcal{H}_2$ control ($\gamma = \infty$, $\ell = 30$).

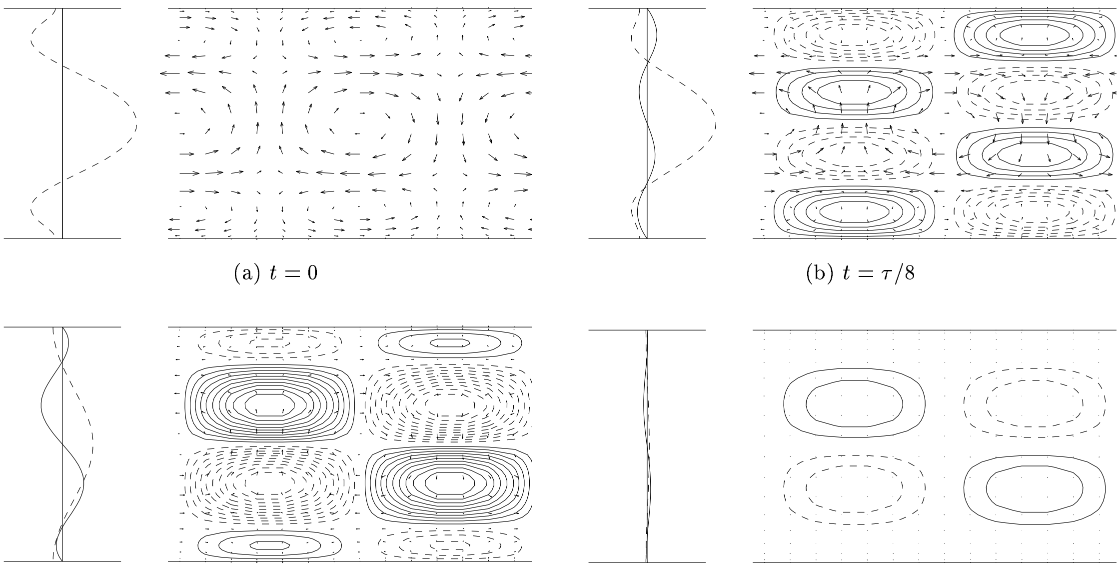

(a) $t = 0$

(b) $t = \tau/8$

(c) $t = \tau$

(d) $t = 4\tau$

Figure 9: Shape of the modified flow perturbation with the largest transient energy growth for the closed-loop case (ii) with full-information $\mathcal{H}_2$ control. A thirty-fold reduction of transient energy growth is obtained (figure 8) as compared with perturbations to the uncontrolled flow (figure 4). Subfigures plotted as in figure 4, with the contours of streamwise velocity rescaled to show detail. The control at the wall acts to create small "buffer" vortices near each wall, thereby reducing the extent of the streamwise vortex at the centre of the channel. The reduction in energy growth is compounded by the fact that this reduced centre vortex acts over a reduced range in mean streamwise velocity $U(y) = 1 - y^2$ between the centre and the edge of the vortex, thereby reducing its effectiveness at inducing streamwise velocity fluctuations.

κ	λ_κ	f_κ
1	$-0.01047924 - 0.23786793i$	0.000148105
2	$-0.03516736 - 0.96463100i$	0.000000125
3	$-0.03518658 - 0.96464251i$	0.000000003
4	$-0.05096577 - 0.27721190i$	0.000015360
5	$-0.06320167 - 0.93631678i$	0.000000297
6	$-0.06325157 - 0.93635179i$	0.000000012
7	$-0.09122298 - 0.90798352i$	0.000000538
8	$-0.09131286 - 0.90805636i$	0.000000033
9	$-0.11923315 - 0.87962804i$	0.000000918
10	$-0.11937073 - 0.87975574i$	0.000000072
11	$-0.12496333 - 0.34921218i$	0.000106622
12	$-0.13828462 - 0.41636473i$	0.000021774
13	$-0.14723423 - 0.85124693i$	0.000001639
14	$-0.14742558 - 0.85144947i$	0.000000156
15	$-0.17522893 - 0.82283652i$	0.000003228

(a) Least-stable eigenmodes of the closed-loop system $(A + B_2K)$ and their sensitivity to modifications of the control rule for the $\mathcal{H}_2$ controller in the limit of cheap control ($\ell = 0.01$). The numbering of the eigenvalues shown is the same as the numbering of the eigenvalues of table 1 to which they are connected by the root locus of figure 5a. In the $\ell \to 0$ limit, the control feedback modifies the closed-loop system eigenmodes until they are insensitive to further modifications of the control feedback, as illustrated by vanishing values of the control residual f_κ.

κ	λ_κ	g_κ
2	$-0.03505745 - 0.96474092i$	0.0000568
3	$-0.03518656 - 0.96464253i$	0.0000004
5	$-0.06287933 - 0.93668082i$	0.0000644
6	$-0.06325135 - 0.93635193i$	0.0000008
4	$-0.08362192 - 0.25066956i$	0.0002858
7	$-0.09059623 - 0.90874809i$	0.0000673
8	$-0.09131193 - 0.90805687i$	0.0000011
1	$-0.09588644 - 0.17888614i$	0.0000118
9	$-0.11823783 - 0.88095109i$	0.0000646
10	$-0.11936798 - 0.87975705i$	0.0000014
11	$-0.14135187 - 0.25722461i$	0.0000176
13	$-0.14584721 - 0.85329546i$	0.0000549
14	$-0.14741907 - 0.85145213i$	0.0000014
15	$-0.17347709 - 0.82577391i$	0.0000399
12	$-0.17418704 - 0.40314739i$	0.0002002

(b) Least-stable eigenmodes of the closed-loop system $(A + LC_2)$ and their sensitivity to modifications of the estimator feedback for the $\mathcal{H}_2$ estimator in the limit of vanishing measurement noise ($\alpha = 0.000001$). The numbering of the eigenvalues shown is the same as the numbering of the eigenvalues of table 1 to which they are connected by the appropriate root locus with respect to α. In the $\alpha \to 0$ limit, the estimator feedback modifies the closed-loop system eigenmodes until they are insensitive to further modifications of the estimator feedback, as illustrated by vanishing values of the observation residual g_κ.

Table 5: Vanishing values of the control and observation residuals f_κ and g_κ in the $\ell \to 0$ and $\alpha \to 0$ limits of the $\mathcal{H}_2$ controller and estimator.

6.5 Sensitivity of optimal estimator/controllers to further modification

The sensitivity of the closed-loop system eigenmodes to further modification of the $\mathcal{H}_2$ controller ($\gamma \to \infty$) in the cheap control limit ($\ell \to 0$) is shown in table 5a. This table shows that, in the cheap control limit, the closed-loop system matrix is modified to the point that the eigenmodes are no longer sensitive to further modification of the controller feedback. All of the controllable dynamics of the system have been used by the controller feedback in this limit. This demonstrates that the optimal ($\mathcal{H}_2$) controller extracts the best possible performance from a given system assumed to have no state disturbances and full, accurate state information.

The sensitivity of the closed-loop system eigenmodes to further modification of the $\mathcal{H}_2$ estimator ($\gamma \to \infty$) in the low measurement noise limit ($\alpha \to 0$) is shown in table 5b. This table shows that, in the limit of precise flow measurements, the closed-loop system matrix is modified to the point that the eigenmodes are no longer sensitive to further modification of the estimator feedback. All of the observable dynamics of the system have been used by the estimator feedback in this limit. This demonstrates that the optimal ($\mathcal{H}_2$) estimator (also known as a Kalman-Bucy filter) extracts the best possible state estimate from a given set of measurements when no control is applied and the system matrix A is modeled exactly.

Note, however, that the locations of the closed-loop eigenvalues in the $\ell \to 0$ and $\alpha \to 0$ limits depend upon the definition of performance measure, and thus are not unique. This can be seen by noting that, in the $\ell \to 0$ limit, the eigenvalue locations obtained by the two optimal controllers in figures 5a and 5b are very different. Thus, though the modal control and observation residuals f_κ and g_κ are useful from a qualitative standpoint to understand the limiting processes involved, they do not provide quantitative measures for how far a given eigenvalue will move upon application of feedback.

Chapter 7

Summary and conclusions

Optimal ($\mathcal{H}_2$) and robust ($\mathcal{H}_\infty$) control theories have been applied to the equations governing linear instabilities and disturbance amplification in laminar flows. Two cases, one supercritical and one subcritical (with highly nonorthogonal eigenmodes), have been studied in detail. The disturbance response in both cases is effectively reduced by the modern control approaches, and it is shown that approaches based on modern control theory significantly outperform classical proportional control approaches. Several different analysis approaches are used to quantify the behaviour of the controlled systems. Transfer function norms are the most natural measure to characterize the relevant properties of the systems at hand. Maximum transient energy growth also characterizes eigenmode nonorthogonality, but does not characterize well the degree to which external disturbances excite flow perturbations. Root locus analyses alone, which account only for system eigenvalues and not the nonorthogonality of system eigenvectors, are inadequate to characterize the present systems.

A convenient new scaling to the $\mathcal{H}_\infty$ estimation problem has been introduced such that three scalar parameters $\{\gamma, \alpha, \ell\}$ may be individually adjusted to achieve desired closed-loop system characteristics in large MIMO systems, and the performance of a family of $\mathcal{H}_2$ and $\mathcal{H}_\infty$ controllers applied to the flow stability problem is thoroughly characterized. With this new scaling, the magnitude of α required for good estimator performance is a quantitative measure of how "clean" the measurements have to be (relative to the magnitude of the state disturbances) to achieve the desired closed-loop performance of the $\mathcal{H}_2$ estimator. The dual structure of the control and estimation problems is retained with this scaling, clearly indicating the coupling and decoupling of the two problems as the three scalar parameters are varied.

Given control of the wall-normal component of boundary velocity only, the flow system is found to be stabilizable but not controllable. Given measurements of wall skin-friction only, the flow system is found to be detectable but not observable. It is shown that $\mathcal{H}_2$ estimators and controllers maximize closed-loop system performance with respect to Gaussian disturbances by minimizing the 2-norm of the transfer function from the disturbances $\mathbf{w}$ to an appropriate performance measure $\mathbf{z}$, denoted

$||T_{\mathbf{zw}}||_2$. In contrast, $\mathcal{H}_\infty$ estimators and controllers modify the corresponding $\mathcal{H}_2$ systems in their response to worst case disturbances by bounding the ∞-norm of the transfer function from the disturbances to the performance measure, denoted $||T_{\mathbf{zw}}||_\infty$. Reducing γ to the minimum value γ_0 for which a solution to the resulting Riccati equations exists results in the minimization of $||T_{\mathbf{zw}}||_\infty$.

By reducing γ, the structured disturbance term of an $\mathcal{H}_\infty$ estimator/controller identifies and stabilizes the response of the corresponding $\mathcal{H}_2$ closed-loop system to the particular disturbance to which it is most sensitive, and thus uses smaller amounts of feedback to attain the same level of worst-case system performance than would be necessary by reducing ℓ or α alone. Such reduced feedback results in smaller demands on the actuators used to achieve the closed-loop forcing and improved robustness to inaccuracies in the system model; the reduced feedback applied in the $\mathcal{H}_\infty$ approach results in reduced opportunity for improper feedback to disrupt the closed-loop system. Together, the scalar parameters $\{\gamma, \alpha, \ell\}$ provide a large degree of flexibility in the design of the $\mathcal{H}_\infty$ estimator/controllers to obtain the best trade-offs possible in the closed-loop systems between Gaussian disturbance response, worst case disturbance response, and feedback levels required.

REFERENCES

ABERGEL, F., & TEMAM, R. 1990 On some control problems in fluid mechanics. *Theor. and Comp. Fluid Dyn.* **1**, 303-325.

ANDERSON, E., BAI, Z., BISCHOF, C., DEMMEL, J., DONGARRA, J., DU CROZ, J., GREENBAUM, A., HAMMARLING, S., MCKENNEY, A., OSTROUCHOV, S., & SORENSEN, D. 1995 *LAPACK Users' Guide.* SIAM.

BAMIEH, B. 1997 The structure of optimal controllers of spatially-invariant distributed parameter systems. *Proceedings of the 36th IEEE Conference on Decision and Control*, Dec 8-12, San Diego.

BARTELS, R.H., & STEWART, G.W. 1972 Solution of the matrix equation $AX + XB = C$. *Communications of the ACM* **15**, 9, 820-826.

BEWLEY, T.R., & AGARWAL, R. 1996 Optimal and robust control of transition. *Proceedings of the 1996 CTR Summer Program*, Center for Turbulence Research, Stanford University/NASA Ames.

BEWLEY, T.R., MOIN, P., & TEMAM, R. 1997 Optimal and robust approaches for linear and nonlinear regulation problems in fluid mechanics. *AIAA Paper No.* 97-1872.

BEWLEY, T.R., & TEMAM, R., & ZIANE, M. 1998 A general framework for robust control in fluid mechanics. Accepted for publication in *Physica D*.

BRIDGES, T.J., & MORRIS, P.J. 1984 Differential eigenvalue problems in which the parameter appears nonlinearly. *J. Comput. Phys.* **55**, 437-460.

BUTLER, K.M., & FARRELL, B.F. 1992 Three-dimensional optimal perturbations in viscous shear flows. *Phys. Fluids A* **4**, 8, 1637-1650.

CANUTO, C., HUSSAINI, M.Y., QUARTERONI, A., & ZANG, T.A. 1988 *Spectral Methods in Fluid Dynamics.* Springer.

DAILEY, R.L., DOYLE, J.C., STEIN, G., BANDA, S.S., & YEH, H.H. 1990 *Lecture Notes for the Workshop on $\mathcal{H}_\infty$ and μ Methods for Robust Control.* Presented at 1990 American Control Conference, May 21-22, San Diego.

DOYLE, J.C., FRANCIS, B.A., & TANNENBAUM, A.R. 1992 *Feedback Control Theory.* Macmillan.

DOYLE, J.C., GLOVER, K., KHARGONEKAR, P.P., & FRANCIS, B.A. 1989 State-Space Solutions to Standard $\mathcal{H}_2$ and $\mathcal{H}_\infty$ Control Problems. *IEEE Trans. Auto. Control* **34**, 8, 831-847.

DRAZIN, P.G., & REID, W.H. 1992 *Hydrodynamic Stability.* Cambridge.

FRANKLIN, G.F., POWELL, J.D., & EMAMI-NAEINI, A. 1991 *Feedback Control of Dynamic Systems.* Addison-Wesley.

GRACE, A., LAUB, A.J., LITTLE, J.N., & THOMPSON, C.M. 1992 *Control System Toolbox User's Guide.* The MathWorks, Inc.

GREEN, M., & LIMEBEER, D.J.N. 1995 *Linear robust control.* Prentice-Hall.

GUSTAVSSON, L.H., & HULTGREN, L.S. 1980 A resonanace mechanism in plane Couette flow. *J. Fluid Mech.* **98**, 149-159.

HU, H.H., & BAU, H.H. 1994 Feedback control to delay or advance linear loss of stability in planar Poiseuille flow. *Proc. R. Soc. Lond.* A **447**, 299-312.

JOSHI, S.S., SPEYER, J.L., & KIM, J. 1995 Modelling and control of two dimensional Poiseuille flow. *34th IEEE Conference on Decision and Control*, 921-927.

JOSHI, S.S., SPEYER, J.L., & KIM, J. 1997 A systems theory approach to the feedback stabilization of infinitesimal and finite-amplitude disturbances in plane Poiseuille flow. *J. Fluid Mech.* **332**, 157-184.

JOSLIN, R.D., GUNZBURGER, M.D., NICOLAIDES, R.A., ERLEBACHER, G., & HUSSAINI, M.Y. 1997 Self-contained automated methodology for optimal flow control *AIAA J.* **35**, 816-824.

KAILATH, T. 1980 *Linear Systems.* Prentice-Hall.

KHORRAMI, M.R., MALIK, M.R., & ASH R.L. 1989 Application of spectral collocation technique to the stability of swirling flows *J. Comput. Phys.* **81**, 206-229.

KIM, J., MOIN, P., & MOSER, R. 1987 Turbulence statistics in fully developed channel flow at low Reynolds number. *J. Fluid Mech.* **177**, 133-166.

LAUB, A.J. 1991 Invariant subspace methods for the numerical solution of Riccati equations. In *The Riccati Equation* (ed. Bittaini, Laub, & Willems) 163-196. Springer.

LEWIS, F.L., & SYRMOS, V.L. 1995 *Optimal Control.* Wiley.

MOIN, P., & BEWLEY, T.R. 1995 Application of control theory to turbulence *Twelfth Australasian Fluid Mechanics Conference*, Dec. 10-15, Sydney, 109-117.

ORSZAG, S.A. 1971 Accurate solution of the Orr-Sommerfeld stability equation *J. Fluid Mech.* **50**, 4, 689-703.

ORSZAG, S.A., & PATERA, A.T. 1983 Secondary instability of wall-bounded shear flows *J. Fluid Mech.* **128**, 347-385.

REYNOLDS, W.C., & KASSINOS, S.C. 1995 One-point modeling of rapidly deformed homogeneous turbulence *Proc. R. Soc. Lond.* A **451**, 87-104.

SKOGESTAD, S., & POSTLETHWAITE, I. 1996 *Multivariable Feedback Control.* Wiley.

TREFETHEN, L.N., TREFETHEN, A.E., REDDY, S.C., & DRISCOLL, T.A. Hydrodynamic stability without eigenvalues *Science* **261**, 578-584.

ZHOU, K., DOYLE, J.C., & GLOVER, K. 1996 *Robust and Optimal Control.* Prentice-Hall.

Part II

Linear control and estimation of nonlinear chaotic convection: harnessing the butterfly effect

Part II has been published as

BEWLEY, T.R. 1998 Linear control and estimation of nonlinear chaotic convection: harnessing the butterfly effect. *Phys. Fluids* **11**, 1169-1186.

Abstract

This article examines the application of linear optimal/robust control theory to a low-order nonlinear chaotic convection problem. Linear control feedback is found to be fully effective only when it is switched off while the state is far from the desired equilibrium point, relying on the attractor of the system to bring the state into a neighborhood of the equilibrium point before control is applied. Linear estimator feedback is found to be fully effective only when *a*) the Lyapunov exponent of the state estimation error is negative, indicating that the state estimate converges to the uncontrolled state, and *b*) the estimator is stable in the vicinity of the desired equilibrium point.

The aim in studying the present problem is to understand better some possible pitfalls of applying linear feedback to nonlinear systems in a low-dimensional framework. Such an exercise foreshadows problems likely to be encountered when applying linear feedback to infinite-dimensional nonlinear systems such as turbulence. It is important to understand these problems and the remedies available in a low-dimensional framework before moving to more complex systems.

Chapter 1

Aim & Scope

The high sensitivity of nonlinear chaotic systems, such as fluid convection and turbulence, to small levels of external forcing may be exploited to stabilize such systems with small levels of coordinated feedback. It is demonstrated in this article that linear control feedback is capable of regulating a nonlinear convection problem from an arbitrary initial fluid state by modulation of the rate of heating applied to the system. It is similarly demonstrated that a nonlinear estimator with linear measurement feedback is capable of estimating the nonlinear convection problem based on measurements of the lateral temperature fluctuations in the fluid. As we will show, special care must be taken in both cases, as the nonlinearity of the system has important consequences. Finally, a state estimator and a controller may be combined to regulate the present nonlinear convection problem to the desired flow state based on limited state measurements.

The aptness of linear state feedback for regulating the nonlinear convection system with full state information is first characterized. It is shown that linear control feedback that is sufficient to linearly stabilize the desired flow state is capable of globally stabilizing the convection phenomenon. An important difficulty with the direct application of linear feedback to the nonlinear problem is identified: specifically, an aggravated undesired flow state is stabilized by the linear feedback in addition to the desired flow state, and the domain of convergence to this undesired state is large. Further, closed-loop system response when strong linearly-stabilizing control is applied may even be unbounded, though the desired flow state is endowed with a high degree of linear stability. An effective solution to this problem is demonstrated: namely, the convection system may be "caught" with a linear controller by applying control only when the state is "near" the desired state, relying on the chaotic dynamics of the uncontrolled system to bring the state into such a neighborhood before control is applied.

The aptness of nonlinear estimators forced with linear measurement feedback for estimating the nonlinear convection system with limited noisy measurements is then characterized. The nonlinearity makes the estimation problem fundamentally different than the control problem: more than just linear stability of infinitesimal estimation errors at a single location in phase space is required to build an estimator which is effective for the uncontrolled nonlinear system. However, convergence of the estimator is possible with direct linear feedback when appropriate feedback gains are used even if the estimator so constructed is not stable over the entire attractor of the uncontrolled system. The nature of the estimation problem is examined, conditions for effective estimator behavior are established, and an effective state estimator is determined.

Finally, conclusions are drawn and related questions are raised about the implications of the present work on the application of linear control theory to the infinite-dimensional nonlinear problem of turbulence.

Chapter 2

Background

2.1 Nominal behavior of the convection system

By major simplification of a buoyancy-driven flow problem governed by the Navier-Stokes equation (Lorenz 1963; Saltzman 1962), Edward Lorenz derived and characterized a simple set of ordinary differential equations which models a fluid convection problem (figure 1) and exhibits chaotic behavior (figure 2). This system may be expressed as

$$\begin{aligned} \dot{x}_1 &= \sigma\,(x_2 - x_1) \\ \dot{x}_2 &= -x_2 - x_1 x_3 \\ \dot{x}_3 &= -b\,x_3 + x_1 x_2 - b\,r, \end{aligned} \tag{2.1}$$

where x_1 is proportional to the intensity of the fluid motion, x_2 is proportional to the lateral temperature fluctuations in the fluid, and x_3 is proportional to the vertical temperature fluctuations in the fluid. The loop Rayleigh number r is proportional to the heating rate at the bottom of the convective system, the loop Prandtl number σ is related to the fluid's kinematic viscosity and thermal conductivity, the quantity b is related to the fluid's thermal expansion coefficient, and all variables have been nondimensionalized (Lorenz 1963). Lorenz showed that fluid motion in this system is chaotic for a sufficiently high rate of heating $r > r_H = \sigma(\sigma + b + 3)/(\sigma - b - 1)$. In this article, all computations are carried out for parameter values typical for a laboratory-scale implementation (Wang, Singer, & Bau 1992) of the geometry of figure 1b in the chaotic regime, nominally, $\sigma = 4$, $b = 1$, and $r = 3r_H = 48$.

The Lorenz equation was originally derived as a first-order approximation of the semi-infinite convection phenomenon illustrated in figure 1a, roughly modeling the solar heating at the bottom of a layer of convection cells in the earth's atmosphere (Lorenz 1963; Saltzman 1962). Unfortunately, the Lorenz equation models accurately only simple roll convection for $r < r_H$, when the

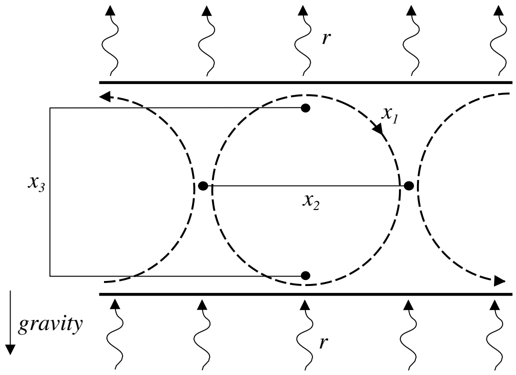

(a) Semi-infinite 2D convection rollers.

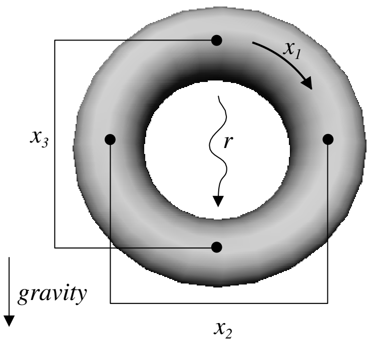

(b) Closed convection loop.

Figure 1: Geometry of two chaotic convection problems, approximately governed by (2.1), to which unsteady heating $r = \bar{u} + u'$ may be applied in order to stabilize a stationary convection state. Only the convection in the toroidal loop illustrated in figure 1b, which is restricted by the geometry to a single mode, is accurately governed by (2.1) when the steady-state heating rate is sufficiently high ($\bar{u} > r_H$) that the convection phenomenon is chaotic (Widmann, Gorman, & Robins 1989).

steady two-dimensional convection rollers are stable (Gleick 1987). Chaotic motion in this system is characterized by a superposition of several Fourier modes, and thus is not adequately modeled by (2.1).

However, as shown by Yorke & Yorke (1982) and Gorman, Widmann, & Robins (1986, 1989), a confined toroidal geometry, as illustrated in figure 1b, prevents other major convection modes from forming. When heated from below and cooled at the same rate from above (*e.g.*, with a simple heat pump), this system is approximately governed by (2.1) well into the chaotic regime $r > r_H$. (Note that the present work assumes a laminar drag law in the derivation of the governing equation (Widmann, Gorman, & Robins 1989). Note also that, for implementations in which the heating and cooling rates are not identical, a fourth equation should be incorporated into the governing set of equations to account for fluctuations in the average temperature in the loop (Hart 1984; Widmann, Gorman, & Robins 1989).) Its simple geometry and construction makes this model system a prime candidate for the study of the feedback control of chaotic fluid phenomena, much as the inverted pendulum has become a standard testbed for the control of unstable systems in dynamics. Both problems represent easily-constructed minimum realizations of important unstable phenomena in large-scale systems, and thus a thorough understanding of the estimation and control of these model systems is illuminating.

The chaotic behavior of the uncontrolled system (see figure 2) is well understood (Lorenz 1963, Sparrow 1982, Gleick 1987, Lorenz 1993). Under the present conditions, the trajectory of the state meanders deterministically but nonperiodically around two unstable focus points $\bar{\mathbf{x}}$ and $\bar{\mathbf{x}}'$ and an unstable saddle point $\bar{\mathbf{x}}''$, where, defining $c = \sqrt{b(r-1)}$,

$$\bar{\mathbf{x}} = \begin{pmatrix} c \\ c \\ -1 \end{pmatrix}, \quad \bar{\mathbf{x}}' = \begin{pmatrix} -c \\ -c \\ -1 \end{pmatrix}, \quad \text{and} \quad \bar{\mathbf{x}}'' = \begin{pmatrix} 0 \\ 0 \\ -r \end{pmatrix}.$$

The system takes from one to several cycles around each focus point alternately. The unstable focus $\bar{\mathbf{x}}$ corresponds to uniform clockwise fluid motion, the unstable focus $\bar{\mathbf{x}}'$ corresponds to uniform anti-clockwise fluid motion, and the unstable saddle $\bar{\mathbf{x}}''$ corresponds to zero fluid motion.

Note that figure 2c illustrates that the sheet containing the attractor is twisted in such a way that the intermittent maxima in x_3 along the state trajectory in the quadrant near either focus point may occur on either of two lobes. This results in the multiple-valued Poincaré map of figure 3 (*i.e.*, draw a vertical line and, in places, it intersects the curve at least four times). Note that the smaller of the two lobes is visited very infrequently; over 40,000 peaks in x_3 were computed in order to produce the plot shown in figure 3.

The chaotic motion of the present convection system is characterized by trajectories which, when integrated over the attractor, diverge exponentially. The system, therefore, is highly sensitive to small disturbances. Such disturbances may arise from a variety of sources, including:

a.) modification of the initial conditions,

b.) unmodeled perturbations to the control applied (in this case taken to be the heating rate), and

c.) unmodeled perturbations to the governing equation (such as those resulting from secondary flows and other unmodeled system dynamics).

For PDE systems such as turbulence, the sources of disturbance may be identified as perturbations to the initial conditions, the boundary conditions, and the PDE itself. This sensitivity to perturbations is loosely referred to in the popular literature as the "butterfly effect" (Gleick 1987; Lorenz 1993; Shinbrot *et al.* 1993):

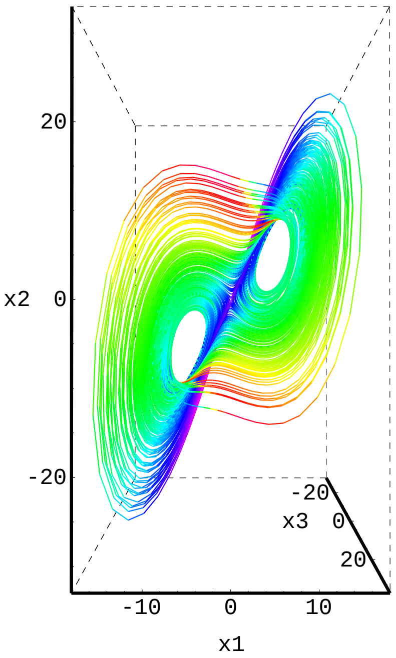

(a) Top view.

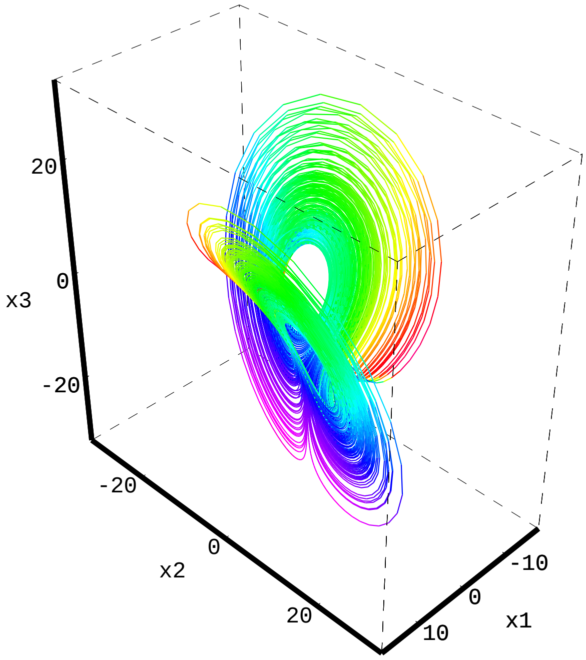

(b) Oblique view.

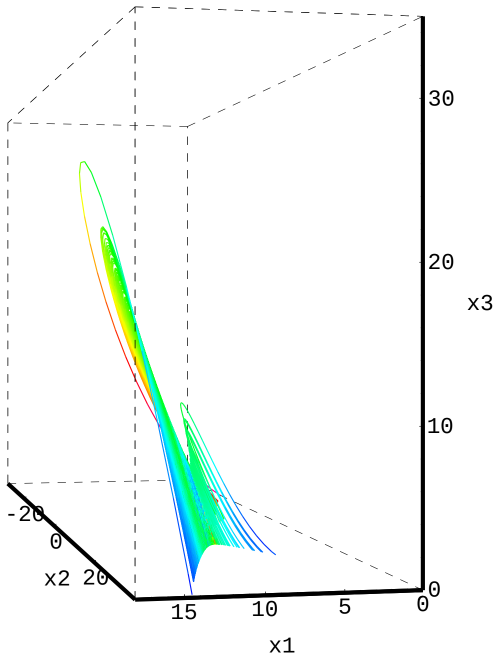

(c) Detailed oblique view of the $(x_1 > 0, x_3 > 0)$ quadrant, illustrating that the sheet of the attractor is twisted.

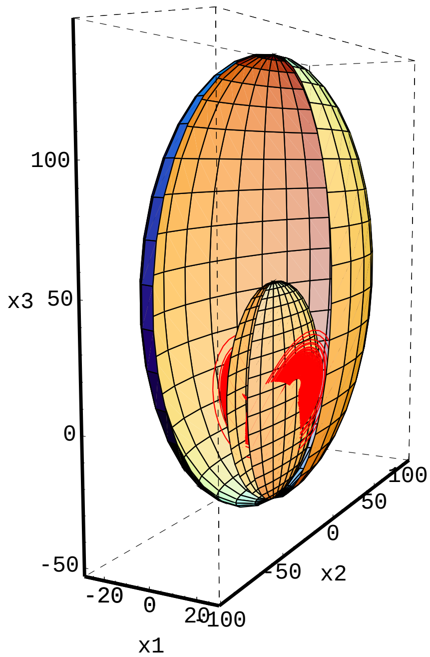

(d) Surface of absorbing ball (outer ellipsoid) and chaotic trajectory of state (red). (see App. A)

Figure 2: Trajectory of the state $\mathbf{x}$ in phase space for a convection problem governed by the Lorenz equation with $\sigma = 4$, $b = 1$, and $r = 48$. In figures 2a-2c, violet/blue indicates the portion of the attractor with positive local Lyapunov exponent (diverging trajectories) whereas red/yellow indicates the portion of the attractor with negative local Lyapunov exponent (converging trajectories).

> *disturbances of magnitude commensurate with the flap of a butterfly's wing are sufficient to alter substantially the trajectory of the system over a long time interval.*

Note that the trajectory from two almost identical initial states may take a long time to diverge, though the exponential divergence of the system will eventually dominate under most circumstances.

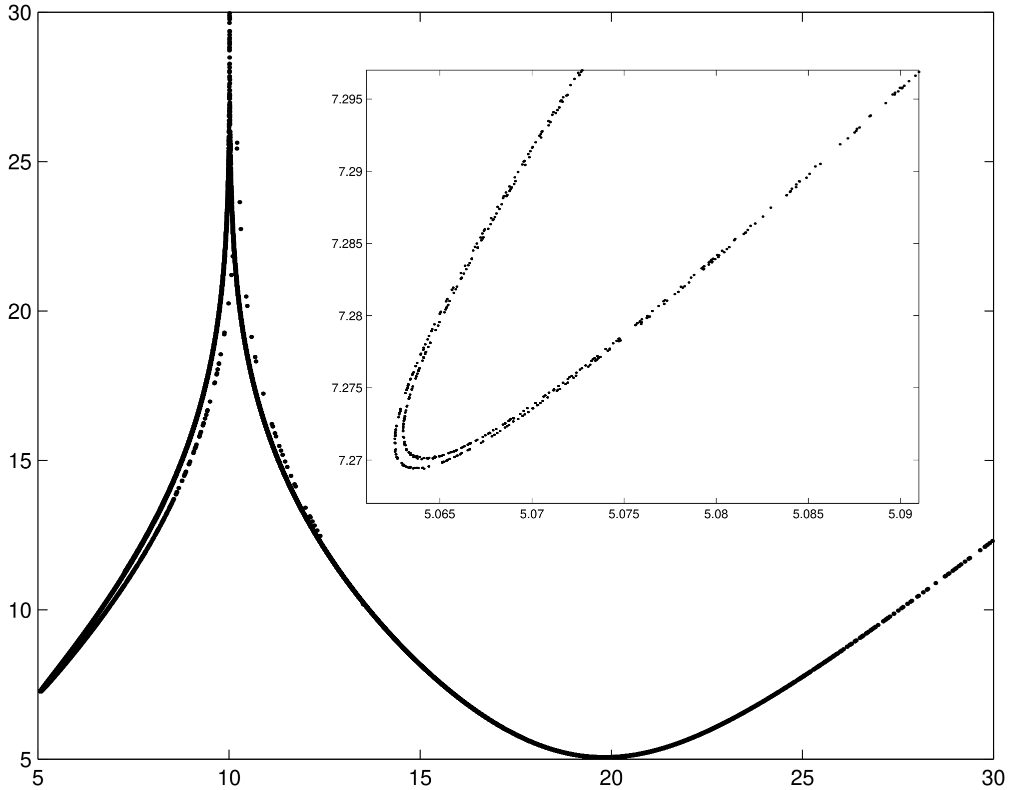

Figure 3: Poincaré map of the uncontrolled Lorenz system ($\sigma = 4$, $b = 1$, $\bar{u} = 48$, $u' = 0$). The j'th maximum of $x_3(t)$ is plotted as a function of the $(j-1)$'th maximum of $x_3(t)$, a common technique used to characterize the nature of a chaotic system (Lorenz 1963). Note that the map is multiple valued. Points to the right of each cusp are accompanied by a change in sign of x_1, whereas points to the left of each cusp are accompanied by no change in sign of x_1. Near the lower-left corner of the map, as illustrated in greater detail in the inset, the curvature is smooth (not cusped) and the map is at least quadruple valued.

The convergence or divergence of system trajectories is made precise by the Lyapunov exponent and the local Lyapunov exponent (Nese 1989; Eckhardt & Yau 1993; Farrell & Ioannou 1996). Consider an infinitesimal perturbation $\delta\mathbf{x}(0)$ of an initial state $\mathbf{x}(0)$. The perturbation $\delta\mathbf{x}(t)$ evolves in the tangent space of $\mathbf{x}(t)$ according to the linearization of (2.1), which is given by

$$\begin{aligned}\dot{\delta x_1} &= \sigma\,(\delta x_2 - \delta x_1)\\ \dot{\delta x_2} &= -\delta x_2 - x_1\,\delta x_3 - x_3\,\delta x_1\\ \dot{\delta x_3} &= -b\,\delta x_3 + x_1\,\delta x_2 + x_2\,\delta x_1.\end{aligned}$$

The Lyapunov exponent λ_∞ is defined as

$$\lambda_\infty = \lim_{T\to\infty}\frac{1}{T}\log\frac{||\delta\mathbf{x}(T)||}{||\delta\mathbf{x}(0)||}$$

for almost all initial states $\mathbf{x}(0)$ and initial infinitesimal perturbations $\delta\mathbf{x}(0)$. The Lyapunov exponent thus measures the exponential rate of convergence ($\lambda_\infty < 0$) or divergence ($\lambda_\infty > 0$) of perturbed trajectories of the system when averaged over long time intervals ($T \to \infty$). For the present parameter values, the Lyapunov exponent was calculated to be $\lambda_\infty = 0.707$. The local Lyapunov exponent $\lambda_\epsilon(\mathbf{x}(t))$ is defined as

$$\lambda_\epsilon(\mathbf{x}(t)) = \lim_{T\to 0}\frac{1}{T}\log\frac{||\delta\mathbf{x}(t+T)||}{||\delta\mathbf{x}(t)||}$$

for t sufficiently large that $\mathbf{x}(t)$ lies on the attractor and $\delta\mathbf{x}(t)$ points along the expanding direction in tangent space (Eckhardt & Yau 1993). The local Lyapunov exponent thus measures the local exponential rate of convergence or divergence of trajectories on the attractor, and the Lyapunov exponent is the long-time average along the system trajectory $\mathbf{x}(t)$ of the local Lyapunov exponent (see figures 2 and 4). It is shown in Appendix D that the Lyapunov exponent is a general property of the system in the sense that it is independent of the choice of norm used in its definition, though this is not true of the local Lyapunov exponent. These quantities will be extended in §4 to examine the convergence or divergence of the state estimation error when linear feedback is applied.

2.2 The control problem

Recently interest in the convection model of Lorenz has been rekindled by attempts to control convection phenomena. As shown in this article, the system sensitivity described above may be harnessed to control the present problem with small amounts of linear feedback.

In the present control problem, a steady-state heating rate $\bar{u}$ is modulated by an unsteady control u' such that

$$r = \bar{u} + u'.$$

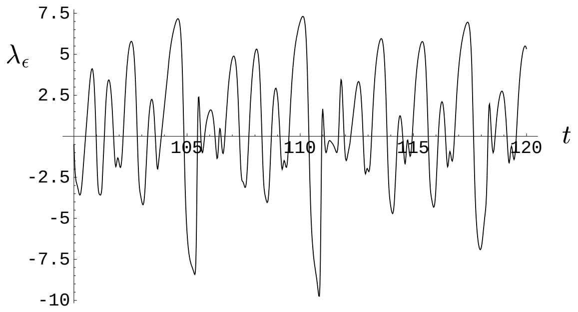

Figure 4: The local Lyapunov exponent $\lambda_\epsilon(t)$ for the uncontrolled system (as computed with the Euclidian norm) as the state moves on the attractor. The average of the local Lyapunov exponent integrated over the path of the attractor gives the Lyapunov exponent $\lambda_\infty = 0.707$, indicating that perturbed trajectories diverge exponentially.

The control problem considered here is to find an algorithm for computing the control u' (modulation of the cooling/heating rate at the top/bottom of the apparatus) based on limited observations of the state (specifically, noisy measurements of x_2) in order to stabilize the focus point corresponding to time-invariant clockwise motion of the fluid $\bar{\mathbf{x}}$, which is stationary but linearly unstable in the uncontrolled ($u' = 0$) Lorenz system for $\bar{u} > r_H$. This model control problem, introduced in the linear optimal context by Vincent (1997) and Yuen & Bau (1998), has been the topic of several recent investigations (Vincent & Yu 1991; Wang & Abed 1992; Wang, Singer, & Bau 1992; Shinbrot *et al.* 1993; Wan & Bernstein 1995; Yuen & Bau 1996; Vincent 1997; Yuen & Bau 1998; etc.). The present study characterizes certain problems which arise when linear feedback is used for the estimation and control of the Lorenz system. These issues should be well understood on this model nonlinear system before applying linear feedback to more complex nonlinear systems such as turbulence, as discussed in §4.

2.3 State disturbances and measurement noise

State disturbances are inevitable in the present system, and come from sources such as unmodeled heat transfer and secondary flows. Noise of some level in the measurement is also inevitable, and arises from inaccuracies of the thermocouples measuring the temperature difference x_2 and from the electronics processing their signals, which are often quite low voltage. These "disturbances", as they shall generically be referred to, are now accounted for in a general form; details of the disturbance scaling outlined here, using the same notation as the present development, may be found in Bewley & Liu (1998).

Define G_1 as the square root of the expected covariance of the state disturbances to be added to the three components of (2.1) and α as the rms amplitude of the noise of the (scalar) temperature measurement. It is assumed that G_1 and α are time invariant. In the present problem, as nothing is known about the state disturbances *a priori*, they are assumed to have the simple covariance $G_1 \triangleq I$. Known structure of the covariance of the state disturbance (for example, knowledge of where the unmodeled heat transfer is likely to occur) is accounted for by replacing $G_1 = I$ with an appropriate matrix of unit maximum singular value, retaining the quantity α to reflect the ratio between the magnitude of the measurement noise and the magnitude of the state disturbance (Bewley & Liu 1998). As any covariance of the disturbances known in advance is accounted for in G_1 and α, the external disturbance vector $\mathbf{w}$ taken to drive this problem is assumed to be, in the optimal case, an uncorrelated, zero-mean, white Gaussian process and, in the robust case, an unstructured disturbance with equal weighting on all states.

The externally-disturbed system equation for $\dot{\mathbf{x}}$ and the equation for the noisy flow measurement $\mathbf{y}$ of the left/right temperature difference x_2 are written in matrix form as

$$\dot{\mathbf{x}} = A\,\mathbf{x} + N(\mathbf{x}) + B_1\,\mathbf{w} + B_2\,\mathbf{u} + \mathbf{r} \tag{2.2a}$$

$$\mathbf{y} = C_2\mathbf{x} \qquad\qquad + D_{21}\,\mathbf{w}, \tag{2.2b}$$

with

$$\mathbf{x} \triangleq \begin{pmatrix} x_1 \\ x_2 \\ x_3 \end{pmatrix}, \qquad \mathbf{u} \triangleq \begin{pmatrix} u' \end{pmatrix}, \qquad \mathbf{r} \triangleq \begin{pmatrix} 0 \\ 0 \\ -b\,\bar{u} \end{pmatrix},$$

$$A \triangleq \begin{pmatrix} -\sigma & \sigma & 0 \\ 0 & -1 & 0 \\ 0 & 0 & -b \end{pmatrix}, \qquad N(\mathbf{x}) \triangleq \begin{pmatrix} 0 \\ -x_1 x_3 \\ x_1 x_2 \end{pmatrix},$$

$$B_1 \triangleq \begin{pmatrix} G_1 & 0 \end{pmatrix}, \qquad B_2 \triangleq \begin{pmatrix} 0 \\ 0 \\ -b \end{pmatrix},$$

$$C_2 \triangleq \begin{pmatrix} 0 & 1 & 0 \end{pmatrix}, \qquad \text{and} \qquad D_{21} \triangleq \begin{pmatrix} 0 & \alpha\, I \end{pmatrix}.$$

The appropriate transfer function norms, reflecting the response of the closed-loop systems to be developed to small (linear) disturbances $\mathbf{w}$, are tabulated in the following two sections. For clarity, the simulations of the full nonlinear systems in the present work are performed with the disturbance vector $\mathbf{w} = \mathbf{0}$. In this way, we analyze the nonlinear dynamics of the closed-loop systems separately from their small-disturbance response characteristics.

Chapter 3

Determination of an effective control strategy

In this section, we present an effective control strategy for the nonlinear system (2.2a) when full state information is available, $\mathbf{y} = \mathbf{x}$. Initially, linear optimal/robust control theory is used to compute control feedback which linearly stabilizes the desired state. Subsequently, the resulting (linear) control feedback is applied to the full nonlinear problem, as discussed in the introduction.

Define a perturbation $\boldsymbol{\xi}$ of the state $\mathbf{x}$ from the desired state $\bar{\mathbf{x}}$ such that

$$\boldsymbol{\xi} \triangleq \mathbf{x} - \bar{\mathbf{x}}.$$

The stabilization of uniform clockwise motion is equivalent to the regulation of the perturbation $\boldsymbol{\xi}$ to zero. We would like to accomplish this regulation with a limited amount of control $\mathbf{u}$. In the robust setting, we would even like to accomplish such regulation in the presence of a finite disturbance $\mathbf{w}$ which maximally spoils the control objective. Thus, following the approach of standard linear optimal/robust control theory, the problem under consideration is expressed as the <u>minimization</u> of a control objective $\mathcal{J}$ with respect to the control $\mathbf{u}$ and the simultaneous <u>maximization</u> of the control objective $\mathcal{J}$ with respect to the disturbance $\mathbf{w}$, where

$$\begin{aligned} \mathcal{J} &= E\Big[\boldsymbol{\xi}^*\, Q\, \boldsymbol{\xi} + \ell^2\, \mathbf{u}^* \mathbf{u} - \gamma^2\, \mathbf{w}^* \mathbf{w}\Big] \\ &= E\Big[\mathbf{z}^* \mathbf{z} - \gamma^2\, \mathbf{w}^* \mathbf{w}\Big]. \end{aligned}$$

The expectation value is defined such that

$$E[\cdot] \triangleq \lim_{T\to\infty} \frac{1}{T} \int_0^T [\cdot]\, dt,$$

and the performance measure $\mathbf{z}$ is defined such that

$$\mathbf{z} = C_1 \boldsymbol{\xi} + D_{12} \mathbf{u}, \tag{3.1}$$

with

$$C_1 \triangleq \begin{pmatrix} Q^{1/2} \\ 0 \end{pmatrix} \quad \text{and} \quad D_{12} \triangleq \begin{pmatrix} 0 \\ \ell I \end{pmatrix}.$$

As all elements of the state $\mathbf{x}$ are similarly scaled, it is reasonable to take $Q = I$. The parameter ℓ^2 denotes the price of the control. Reduced values of ℓ penalize the cost function less upon the application of control, and thereby tend to result in larger control magnitudes, $E[\,\mathbf{u}^* \,\mathbf{u}\,]$, and smaller excursions of the perturbation, $E[\,\boldsymbol{\xi}^*\, Q\, \boldsymbol{\xi}\,]$. Similarly, the parameter γ^2 denotes the "price" of the disturbance, in the spirit of a noncooperative game. Note that setting $\gamma \to \infty$ eliminates the disturbance from the noncooperative game ($\mathbf{w} \to \mathbf{0}$ in the maximization w.r.t. $\mathbf{w}$), resulting in the optimal control result. Reduced values of γ introduce a finite component of the worst-case disturbance to the problem, generally resulting in larger feedback gains targeted at stabilizing the system response to the worst-case disturbance. Further discussion of the nature of this noncooperative game is deferred to Bewley & Liu (1998).

The equation governing the state perturbation $\boldsymbol{\xi}$ (for any reference point $\bar{\mathbf{x}}$) is easily derived (Lorenz 1963) from (2.2a) and written in matrix form as

$$\dot{\boldsymbol{\xi}} = \bar{A}\,\boldsymbol{\xi} + N(\boldsymbol{\xi}) + B_1\,\mathbf{w} + B_2\,\mathbf{u} + \bar{\mathbf{r}}, \tag{3.2}$$

where the linearized system matrix $\bar{A}$ and the constant vector $\bar{\mathbf{r}}$ take the form

$$\bar{A} \triangleq A + \begin{pmatrix} 0 & 0 & 0 \\ -\bar{x}_3 & 0 & -\bar{x}_1 \\ \bar{x}_2 & \bar{x}_1 & 0 \end{pmatrix}, \qquad \bar{\mathbf{r}} \triangleq A\,\bar{\mathbf{x}} + N(\bar{\mathbf{x}}) + \mathbf{r}.$$

Note that $\bar{\mathbf{r}} = \mathbf{0}$ because $\bar{\mathbf{x}}$ is taken to be a stationary point of the uncontrolled system (2.1). For sufficiently small perturbations $\boldsymbol{\xi}$, the nonlinear term $N(\boldsymbol{\xi})$ is small compared with the linear terms. Thus, for a state $\mathbf{x}$ in a sufficiently small neighborhood of the desired state $\bar{\mathbf{x}}$, the controller feedback $\mathbf{u}$ solving the noncooperative game discussed above for the nonlinear system (2.2a) may be determined by analysis of just the linear terms of (3.2).

The linear operator $\bar{A}$ is unstable for $r > r_H$. For the present parameter values, the eigenvalues of $\bar{A}$ are $\{-6.66, 0.33 \pm 7.50i\}$. As the complex eigenvalues have positive real parts, a small perturbation to the state $\mathbf{x}$ from the stationary point $\bar{\mathbf{x}}$ causes the state to spiral away from the stationary point in the uncontrolled system.

A linear controller of the form

$$\mathbf{u} = K\boldsymbol{\xi} = K(\mathbf{x} - \bar{\mathbf{x}}) \tag{3.3a}$$

solving the noncooperative game discussed above for the linearization of the system (3.2) governing the state perturbation $\boldsymbol{\xi}$ is given by the controller feedback

$$K = -\frac{1}{\ell^2} B_2^* X, \tag{3.3b}$$

where

$$X = \mathrm{Ric}\begin{pmatrix} \bar{A} & \dfrac{1}{\gamma^2} B_1 B_1^* - \dfrac{1}{\ell^2} B_2 B_2^* \\ -C_1^* C_1 & -\bar{A}^* \end{pmatrix} \tag{3.3c}$$

and Ric$(\cdot)$ denotes the solution of the associated Riccati problem (Laub 1991), in accordance with standard linear optimal/robust control theory (Doyle *et al.* 1989; Lewis & Syrmos 1995; Green & Limebeer 1995; Bewley & Liu 1998). Resulting feedback matrices K for representative ℓ and γ are given in tables 1 and 2.

Inserting a linear controller of the form $\mathbf{u} = K\boldsymbol{\xi}$ into (3.2) and rearranging, the closed-loop system matrix takes the form $\bar{A} + B_2 K$. For the present parameter values with, for example, $\ell = 0.25$ and $\gamma = \infty$ and K computed from (3.3), the eigenvalues of $\bar{A} + B_2 K$ are $\{-6.70, -2.48 \pm 7.39i\}$. As all eigenvalues now have negative real parts, any small perturbation to the state $\mathbf{x}$ from the stationary point $\bar{\mathbf{x}}$ causes the state to spiral back to the stationary point in the controlled system.

The linear (*i.e.*, small) disturbance rejection of the various controllers K near the desired stationary point $\mathbf{x} \approx \bar{\mathbf{x}}$ is quantified by the appropriate transfer function norms (Skogestad & Postlethwaite 1996). The precise mathematical description of these transfer function norms is summarized in Bewley & Liu (1998). In short,

$\|T_{\boldsymbol{\xi}\mathbf{w}}\|_2$ measures the rms value of the state perturbation $\boldsymbol{\xi}$ in response to small white Gaussian disturbances $\mathbf{w}$,

$\|T_{\boldsymbol{\xi}\mathbf{w}}\|_\infty$ measures the rms value of the state perturbation $\boldsymbol{\xi}$ in response to small disturbances $\mathbf{w}$ with the worst-case structure, and

$\|T_{\mathbf{u}\mathbf{w}}\|_2$ measures the rms value of the control $\mathbf{u}$ in response to small white Gaussian disturbances $\mathbf{w}$.

As seen in table 1, decreasing the parameter ℓ results in increased control feedback ($\|T_{\mathbf{u}\mathbf{w}}\|_2$) to counteract disturbances with stronger control, thereby resulting in a smaller state response to Gaussian disturbances ($\|T_{\boldsymbol{\xi}\mathbf{w}}\|_2$). Decreasing ℓ also happens to reduce the state response to worst-case disturbances ($\|T_{\boldsymbol{\xi}\mathbf{w}}\|_\infty$) fairly effectively.

ℓ	K			$\|\|T_{\boldsymbol{\xi}\mathbf{w}}\|\|_2$	$\|\|T_{\boldsymbol{\xi}\mathbf{w}}\|\|_\infty$	$\|\|T_{\mathbf{uw}}\|\|_2$
1000	(0.3222	−0.3222	1.3277)	1.848	3.173	1.946
10	(0.3247	−0.3254	1.3392)	1.832	3.120	1.946
1†	(0.4696	−0.5424	2.0719)	1.296	1.512	2.083
0.50	(0.6541	−0.9428	3.2341)	0.994	0.847	2.400
0.25	(0.8722	−1.9933	5.6581)	0.774	0.466	2.980
0.10	(0.4843	−6.4708	12.7740)	0.622	0.269	4.128
0.050	(−1.8511	−15.8700	23.8717)	0.575	0.271	5.311
0.025	(−8.1871	−36.3081	44.8130)	0.551	0.273	7.049
0.010	(−29.1673	−99.2058	105.5891)	0.536	0.268	10.759

Table 1: Optimal controller feedback gains ($\gamma = \infty$) and linear disturbance rejection near desired fixed point ($\mathbf{x} = \bar{\mathbf{x}}$). Transfer function norms reported measure the linearized response of the closed-loop system to state disturbances when the system is near the linearization point $\mathbf{x} = \bar{\mathbf{x}}$ for which the controllers were designed. †Case studied by Yuen & Bau (1998).

γ	K			$\|\|T_{\boldsymbol{\xi}\mathbf{w}}\|\|_2$	$\|\|T_{\boldsymbol{\xi}\mathbf{w}}\|\|_\infty$	$\|\|T_{\mathbf{uw}}\|\|_2$
∞	(0.3247	−0.3254	1.3392)	1.832	3.118	1.946
25	(0.5151	−0.7188	2.4580)	1.161	1.193	2.189
20	(0.6855	−1.8348	4.7175)	0.832	0.556	2.775
18	(−0.5661	−8.7956	13.0871)	0.619	0.257	4.246
17.5	(−11.2060	−41.0934	39.9697)	0.554	0.248	7.316
17.35	(−128.2235	−365.7229	285.2543)	0.533	0.243	20.442
$\gamma_0 \approx 17.33$	(−3377.5645	−9338.9540	7028.6511)	0.530	0.242	102.676

Table 2: Robust controller feedback gains ($\ell = 10$) and linear disturbance rejection near desired fixed point (see legend of table 1).

Table 2 illustrates the effect of accounting for a finite component of the worst-case disturbance in the control problem by reducing γ. Starting from one of the optimal controllers of table 1 (specifically, the one with $\ell = 10$), reducing γ effectively reduces the response of the state to worst-case disturbances ($\|T_{\boldsymbol{\xi}\mathbf{w}}\|_\infty$). There is a minimum value $\gamma = \gamma_0$ below which the Riccati equation (3.3c) cannot be solved. For γ close to this value, the feedback gains are quite large, though such increased feedback has only a small effect on $\|T_{\boldsymbol{\xi}\mathbf{w}}\|_\infty$. Due to the possibility of system uncertainties, actuator saturation, and measurement noise, large feedback gains are not desirable, and intermediate values of both ℓ and γ are preferred. In the present system, there are few degrees of freedom, and the robust controllers do not provide much beyond what the optimal controllers provide. Notice, for example, the similar weights K and the similar transfer function norms attained with the $\ell = 0.025$, $\gamma = \infty$ ("optimal") case in table 1 and the $\ell = 10$, $\gamma = 17.5$ ("robust") case in table 2. This similarity in performance of the optimal and robust controllers is in sharp contrast with the results of the high-dimensional, highly non-orthogonal problems studied in the transition control problem of Bewley & Liu (1998), in which the robust component in the control problem is much more significant.

Appendix B derives sufficient conditions on the feedback K for boundedness of the closed-loop nonlinear system which is obtained by application of the linear feedback (3.3a) to the undisturbed nonlinear plant (2.2a). For control feedback determined from (3.3) which happens to satisfy these constraints, as shown in figure 5, direct application of linear feedback stabilizes both the desired state $\bar{\mathbf{x}}$ (indicated by the black trajectories of figure 5) and an undesired state, which is near the aforementioned point $\bar{\mathbf{x}}'$ for small values of K (indicated by the green trajectories of figure 5). An unstable manifold exists between these two stabilized points, as indicated by the contorted blue/red surfaces in figure 5. Any initial state on the blue side of this manifold will converge to the desired state, and any initial state on the red side of this manifold will converge to the undesired state. It is mathematically possible that an unstable chaotic system trajectory still exists which is confined to the manifold separating these two regions of attraction. In a practical (disturbed) system, however, the state will never remain on this unstable manifold. Note that the unstable manifold includes the $x_1 = x_2 = 0$ axis, which is indicated with white lines in figure 5.

As seen in figure 5, for increased feedback magnitude K (*e.g.*, decreased ℓ), the undesired stabilized state moves farther from the origin, and the domain of convergence of the undesired state remains large; the closed-loop system eventually becomes unbounded for sufficiently large feedback K. Some form of nonlinearity in the feedback rule is required to eliminate this undesired behavior. An effective technique is to apply control of the form

$$\mathbf{u} = H(R - |\mathbf{x} - \bar{\mathbf{x}}|)\, K\boldsymbol{\xi}, \qquad H(\zeta) = \begin{cases} 0 & \text{for } \zeta \le 0 \\ 1 & \text{for } \zeta > 0, \end{cases}$$

such that the control is turned on only when the state $\mathbf{x}(t)$ is inside a sphere of radius R, centered at

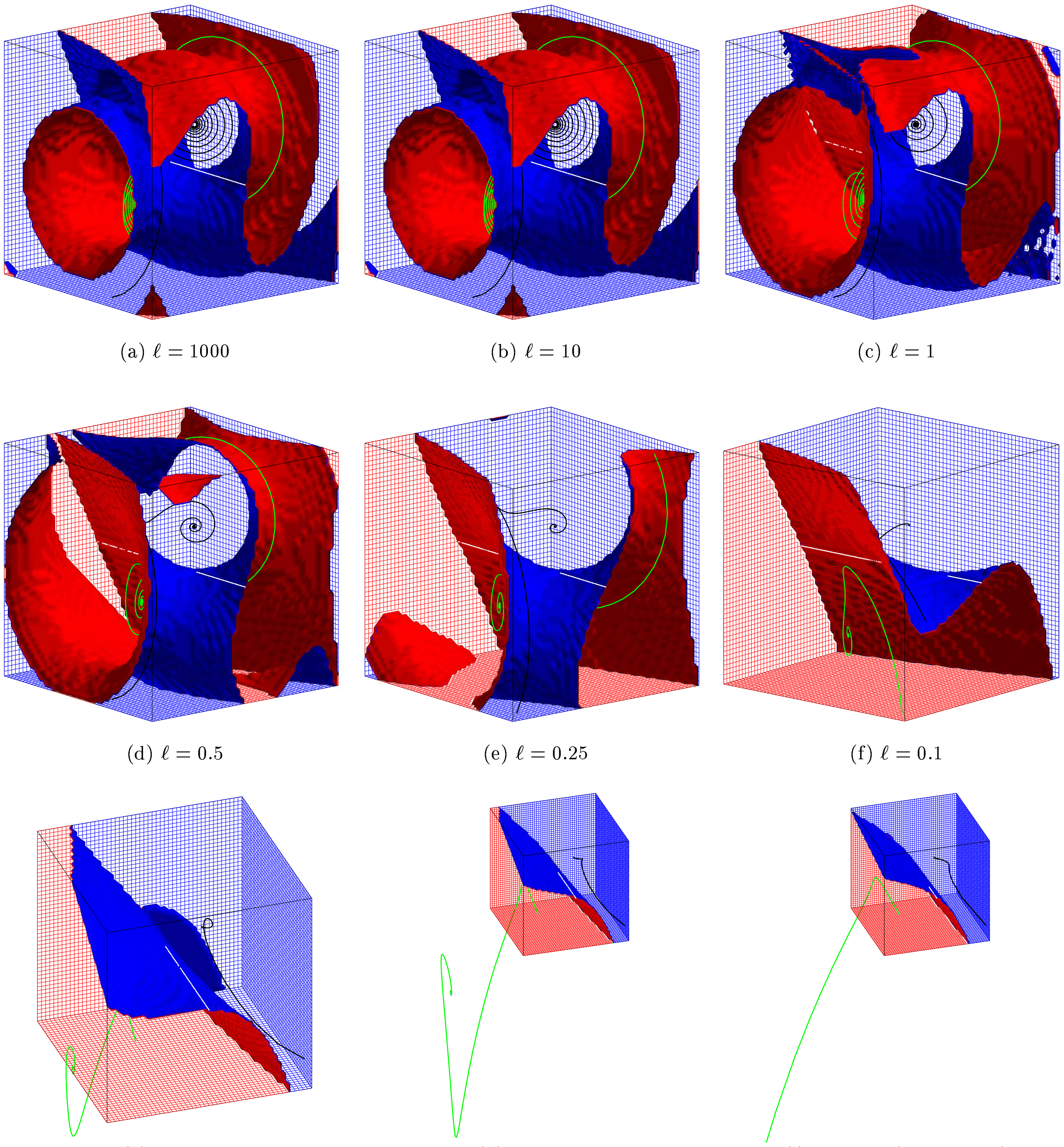

(a) $\ell = 1000$ (b) $\ell = 10$ (c) $\ell = 1$

(d) $\ell = 0.5$ (e) $\ell = 0.25$ (f) $\ell = 0.1$

(g) $\ell = 0.05$ (h) $\ell = 0.025$ (i) $\ell = 0.01$ (unbounded)

Figure 5: Regions of attraction of desired (blue) and undesired (red) stationary points in linearly-controlled convection system and typical trajectories in each region (black and green respectively). The cubical domain illustrated is $\Omega = (-25, 25)^3$ in all nine subfigures; for clarity, slightly different viewpoints are used in each subfigure.

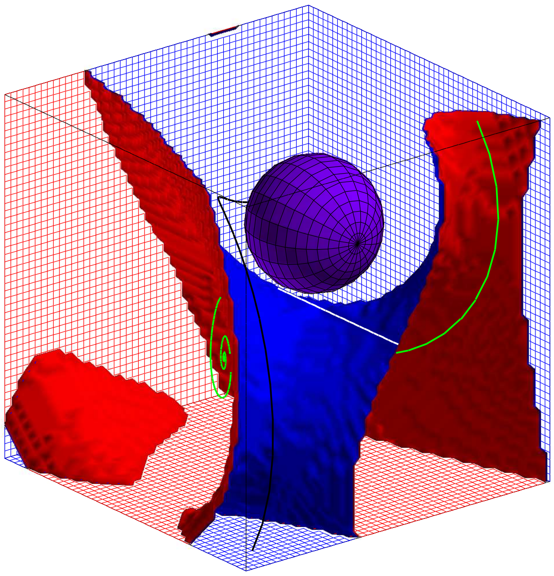

(a) Definition of a subdomain (violet) completely contained in the (blue) domain of convergence of the desired fixed point when linear optimal control with $\ell = 0.25$ is applied. It is possible to define a subdomain so contained which is larger than the example shown.

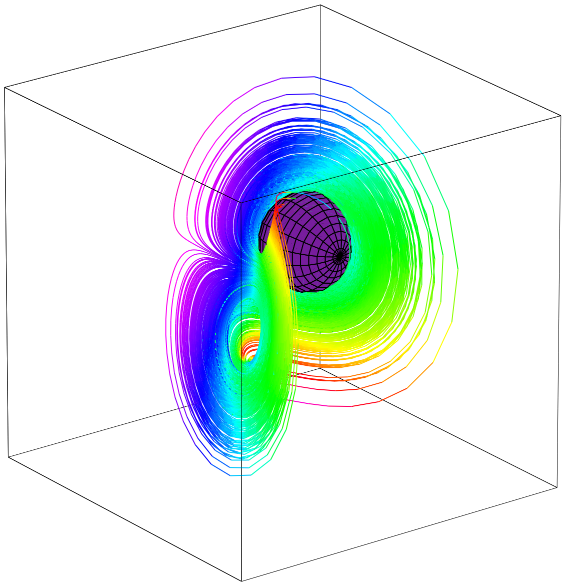

(b) The subdomain defined (violet) contains a substantial portion of the chaotic attractor of the uncontrolled system. Thus, the uncontrolled system will eventually move inside the subdomain where linear control is effective.

Figure 6: Combination of the linear controller with an on/off switch. No control is applied when the state is outside the violet subdomain shown. The chaotic uncontrolled system eventually brings the state inside the subdomain shown. Linear control is then applied to "catch" the system, drawing it to the desired stabilized state.

$\bar{\mathbf{x}}$, completely contained in the domain of convergence of the desired stationary point in the linearly-controlled system. Such a subdomain is denoted by a violet sphere in figure 6a. The chaotic dynamics of the uncontrolled system will bring the system into this subdomain in finite time, as depicted by figure 6b, after which control may be applied to "catch" the state at the desired equilibrium point. Similar switched approaches were recommended by Vincent & Yu (1991), Wang & Abed (1992), and Vincent (1997) for the Lorenz problem, and may also be applied to swing up and catch an inverted pendulum, as demonstrated by Malmborg, Bernhardsson, & Åström (1996). The key to the effectiveness of this approach is the determination a feedback control which makes the subdomain in which the linear control may be applied successfully as large as possible, so that the uncontrolled state $\mathbf{x}(t)$, moving along the attractor of the system, enters this subdomain in a short amount of time (Vincent 1997).

Chapter 4

Determination of an effective state-estimation strategy

When full state information is not available, one may first develop a state estimate based on the available state measurements, then feed this state estimate back through a full-state controller, such as one of the controllers of §3, to control the system. This chapter discusses how to determine an effective state estimator for the present problem. Details of how the synthesized estimator/controller is assembled are given in §5.

A reasonable requirement of the state estimator is that its dynamics be at least similar to the dynamics of the state itself when no feedback is applied. To achieve this, the state estimator itself must be nonlinear. Since the state equation (2.2a) and the measurement equation (2.2b) are well known in the present problem, we will model them closely in our estimator equations such that

$$\dot{\hat{\mathbf{x}}} = A\,\hat{\mathbf{x}} + N(\hat{\mathbf{x}}) + B_2\,\mathbf{u} + \mathbf{r} - \hat{\mathbf{u}} \tag{4.1a}$$

$$\hat{\mathbf{y}} = C_2\hat{\mathbf{x}}. \tag{4.1b}$$

The disturbance $\mathbf{w}$ that drives the flow system (2.2), which is unmeasurable, is not available to force the model system (4.1). Instead, a forcing term $\hat{\mathbf{u}}$ is computed based on the flow measurements $\mathbf{y}$ and added to the rhs of (4.1a) to force the state estimate $\hat{\mathbf{x}}$ in the estimator towards the state $\mathbf{x}$ itself, correcting for the state disturbances $B_1\mathbf{w}$ in (2.2a) while accounting for the measurement noise $D_{21}\mathbf{w}$ in (2.2b). The task at hand is to determine the feedback $\hat{\mathbf{u}}$ as a function of the measurements $\mathbf{y}$ such that this goal is attained. As in the previous section, the feedback will be determined by application of linear optimal/robust control theory, though this feedback is applied, in the end, to the *nonlinear* estimator given by (4.1). Since the state estimate is computed in the controlling electronics in any implementation, all three components of the model equation (4.1a) may be forced by the estimator feedback $\hat{\mathbf{u}} = (\hat{u}_1\ \hat{u}_2\ \hat{u}_3)^*$ with no difficulty in the implementation.

Consider the deviations $\boldsymbol{\eta}$ and $\hat{\boldsymbol{\eta}}$ of the state $\mathbf{x}$ and the state estimate $\hat{\mathbf{x}}$ from some (as yet undetermined) reference state $\tilde{\mathbf{x}}$ such that

$$\boldsymbol{\eta} = \mathbf{x} - \tilde{\mathbf{x}} \quad \text{and} \quad \hat{\boldsymbol{\eta}} = \hat{\mathbf{x}} - \tilde{\mathbf{x}}. \tag{4.2}$$

The equations governing $\boldsymbol{\eta}$ and $\hat{\boldsymbol{\eta}}$ are easily derived from (2.2a) and (4.1a) such that

$$\dot{\boldsymbol{\eta}} = \tilde{A}\,\boldsymbol{\eta} + N(\boldsymbol{\eta}) + B_1\,\mathbf{w} + B_2\,\mathbf{u} + \tilde{\mathbf{r}} \tag{4.3a}$$
$$\dot{\hat{\boldsymbol{\eta}}} = \tilde{A}\,\hat{\boldsymbol{\eta}} + N(\hat{\boldsymbol{\eta}}) \qquad\qquad + B_2\,\mathbf{u} + \tilde{\mathbf{r}} - \hat{\mathbf{u}}, \tag{4.3b}$$

where the linearized system matrix $\tilde{A}$ and the constant vector $\tilde{\mathbf{r}}$ take the form

$$\tilde{A} = A + \begin{pmatrix} 0 & 0 & 0 \\ -\tilde{x}_3 & 0 & -\tilde{x}_1 \\ \tilde{x}_2 & \tilde{x}_1 & 0 \end{pmatrix} \quad \text{and} \quad \tilde{\mathbf{r}} = A\,\tilde{\mathbf{x}} + N(\tilde{\mathbf{x}}) + \mathbf{r}.$$

Note that $\tilde{\mathbf{x}}$ need not be a stationary point, and thus $\tilde{\mathbf{r}}$ is not necessarily zero. Defining the estimation error $\mathbf{x}_e \triangleq \mathbf{x} - \hat{\mathbf{x}} = \boldsymbol{\eta} - \hat{\boldsymbol{\eta}}$ and the measurement error $\mathbf{y}_e \triangleq \mathbf{y} - \hat{\mathbf{y}}$ and subtracting (4.3b) from (4.3a) and (4.1b) from (2.2b), it is seen that $\mathbf{x}_e$ and $\mathbf{y}_e$ obey the equations

$$\dot{\mathbf{x}}_e = \tilde{A}\,\mathbf{x}_e + N(\boldsymbol{\eta}) - N(\hat{\boldsymbol{\eta}}) + B_1\,\mathbf{w} + \hat{\mathbf{u}} \tag{4.4a}$$
$$\mathbf{y}_e = C_2\mathbf{x}_e \qquad\qquad + D_{21}\mathbf{w}. \tag{4.4b}$$

The nonlinear term in this equation may be written

$$\begin{aligned} N(\boldsymbol{\eta}) - N(\hat{\boldsymbol{\eta}}) &= M(\hat{\boldsymbol{\eta}})\mathbf{x}_e + N(\mathbf{x}_e) \\ &= M(\boldsymbol{\eta})\mathbf{x}_e - N(\mathbf{x}_e), \end{aligned} \tag{4.5}$$

where

$$M(\boldsymbol{\eta}) = \begin{pmatrix} 0 & 0 & 0 \\ -\eta_3 & 0 & -\eta_1 \\ \eta_2 & \eta_1 & 0 \end{pmatrix}.$$

For sufficiently small $\boldsymbol{\eta}$ and $\mathbf{x}_e$, the linear terms of (4.4a) dominate the nonlinear term $N(\boldsymbol{\eta}) - N(\hat{\boldsymbol{\eta}})$ (see (4.5)). Thus, for sufficiently small estimator error $\mathbf{x}_e$ and for the state $\mathbf{x}$ in a sufficiently small neighborhood of the reference state $\tilde{\mathbf{x}}$, the estimator feedback $\hat{\mathbf{u}}$ minimizing the estimation error $\mathbf{x}_e$ may be determined by analysis of just the linear terms of (4.4).

Linear estimator feedback of the form

$$\hat{\mathbf{u}} = L\mathbf{y}_e = L(\mathbf{y} - \hat{\mathbf{y}}) \tag{4.6a}$$

solving the dual of the noncooperative game discussed in §3 for the linearization of the system (4.4a) governing the estimation error $\mathbf{x}_e$ is given by the estimator feedback

$$L = -\frac{1}{\alpha^2}\, Y\, C_2^*, \tag{4.6b}$$

where

$$Y = \mathrm{Ric}\begin{pmatrix} \tilde{A}^* & \dfrac{1}{\gamma^2}\, C_1^*\, C_1 - \dfrac{1}{\alpha^2}\, C_2^*\, C_2 \\ -B_1\, B_1^* & -\tilde{A} \end{pmatrix}, \tag{4.6c}$$

in accordance with standard linear theory (Doyle *et al.* 1989; Lewis & Syrmos 1995; Green & Limebeer 1995; Bewley & Liu 1998). Note that an “optimal estimator”, determined with $\gamma = \infty$, is usually referred to as a Kalman-Bucy filter. Resulting feedback matrices L for representative α and γ are given in tables 3 and 4.

The linear (*i.e.*, small) disturbance rejection of the closed-loop system (4.4) with the estimator feedback (4.6a) applied, given that the state $\mathbf{x}$ and the state estimate $\hat{\mathbf{x}}$ are near a known reference point, is (again) quantified by the appropriate transfer function norms (Skogestad & Postlethwaite 1996; Bewley & Liu 1998). In short,

$\|T_{\mathbf{x}_e\mathbf{w}}\|_2$ measures the rms value of the estimation error $\mathbf{x}_e$ in response to small white Gaussian disturbances $\mathbf{w}$,

$\|T_{\mathbf{x}_e\mathbf{w}}\|_\infty$ measures the rms value of the estimation error $\mathbf{x}_e$ in response to small disturbances $\mathbf{w}$ with the worst-case structure, and

$\|T_{\hat{\mathbf{u}}\mathbf{w}}\|_2$ measures the rms value of the estimator feedback $\hat{\mathbf{u}}$ in response to small white Gaussian disturbances $\mathbf{w}$.

The dependence of the performance of the estimation error system (4.4) on α and γ near the design point $\mathbf{x} \approx \hat{\mathbf{x}} \approx \tilde{\mathbf{x}}$ is similar to the dependence of the design-point performance of the controlled system on ℓ and γ studied in §3. The estimators summarized in tables 3 and 4 are designed with the feedback L determined according to (4.6) with $\tilde{\mathbf{x}} = \mathbf{0}$. In tables 3 and 4, we investigate the linear disturbance rejection of the closed-loop estimation error system near the desired fixed point $\mathbf{x} \approx \hat{\mathbf{x}} \approx \bar{\mathbf{x}}$, conditions which are *off* the design point for the estimator. For large α, the feedback determined is not sufficient to stabilize the estimator near the desired fixed point $\mathbf{x} \approx \hat{\mathbf{x}} \approx \bar{\mathbf{x}}$, and the transfer function norms reported are unbounded. Decreasing the parameter α results in increased estimator feedback gains L and eventually stabilizes the estimation error near the desired fixed

α	L^*	κ_∞	$\lVert T_{\mathbf{x}_e\mathbf{w}}\rVert_2$	$\lVert T_{\mathbf{x}_e\mathbf{w}}\rVert_\infty$	$\lVert T_{\hat{\mathbf{u}}\mathbf{w}}\rVert_2$
100	(−0.00004 −0.00005 0.0)	0.70	∞	∞	∞
10	(−0.0040 −0.0050 0.0)	0.70	∞	∞	∞
1	(−0.3060 −0.4142 0.0)	0.45	∞	∞	∞
0.50	(−0.7929 −1.2361 0.0)	0.04	1.690	2.599	1.555
0.25	(−1.5379 −3.1231 0.0)	−1.04	0.977	0.777	2.049
0.10	(−2.5765 −9.0499 0.0)	−3.95	0.747	0.401	3.384
0.050	(−3.1675 −19.0250 0.0)	−3.67	0.784	0.602	4.927
0.025	(−3.5456 −39.0125 0.0)	−1.82	0.913	0.915	6.851
0.010	(−3.8077 −99.0050 0.0)	0.01	1.101	1.361	9.814

Table 3: Optimal estimator (a.k.a. Kalman-Bucy filter) feedback gains ($\gamma = \infty$), Lyapunov exponent characterizing estimator convergence to uncontrolled state, and linear disturbance rejection near desired fixed point. The Lyapunov exponent κ_∞ denotes the rate of convergence ($\kappa_\infty < 0$) or divergence ($\kappa_\infty > 0$) of the state estimate to the state as the state moves on the attractor when the estimation error $\mathbf{x}_e$ is small. Transfer function norms reported measure linearized response, near $\mathbf{x} = \hat{\mathbf{x}} = \bar{\mathbf{x}}$, of estimator error to state disturbances, though the estimator feedback was designed with linear theory by linearization about $\mathbf{x} = \hat{\mathbf{x}} = 0$ (*i.e.*, transfer function norms are reported at conditions which are *off* the design point). Necessary conditions for effective estimator behavior are: *a.*) κ_∞ must be negative, and *b.*) the transfer function norms reported must be bounded.

γ	L^*	κ_∞	$\lVert T_{\mathbf{x}_e\mathbf{w}}\rVert_2$	$\lVert T_{\mathbf{x}_e\mathbf{w}}\rVert_\infty$	$\lVert T_{\hat{\mathbf{u}}\mathbf{w}}\rVert_2$
∞	(−0.3060 −0.4142 0.0)	0.45	∞	∞	∞
2	(−0.3384 −0.4413 0.0)	0.44	∞	∞	∞
1.5	(−0.3729 −0.4696 0.0)	0.43	∞	∞	∞
1.1	(−0.5091 −0.5781 0.0)	0.38	4.778	21.57	2.326
1.02	(−0.7062 −0.7294 0.0)	0.29	2.597	6.290	1.670
$\gamma_0 \approx 1.016$	(−0.7879 −0.7909 0.0)	0.24	2.292	4.868	1.621

Table 4: Robust estimator feedback gains ($\alpha = 1$), Lyapunov exponent characterizing estimator convergence to uncontrolled state, and linear disturbance rejection near desired fixed point (see legend of table 3).

point. This results in finite values of the transfer function norms reported in table 3 for $\alpha \leq 0.5$. Decreasing the parameter α from 0.5 to 0.1 results in increased estimator feedback ($\|T_{\hat{\mathbf{u}}\mathbf{w}}\|_2$) to account for disturbances more rapidly, thereby resulting in a smaller response of the estimation error to Gaussian disturbances ($\|T_{\mathbf{x}_e\mathbf{w}}\|_2$). The worst-case response of the estimation error ($\|T_{\mathbf{x}_e\mathbf{w}}\|_\infty$) in this problem, which has few degrees of freedom, follows trends which closely match the estimation error response to Gaussian disturbances ($\|T_{\mathbf{x}_e\mathbf{w}}\|_2$), and introducing the robust component (table 4) does not provide much beyond what the optimal approach can provide. The large feedback gains L for the estimators with $\alpha < 0.1$ are not effective in reducing further the system response under these off-design conditions; as for the controller, intermediate values of both α and γ are preferred.

By applying the linear measurement feedback (4.6a) to the undisturbed estimation error equations (4.4), noting (4.5), the closed-loop equation for the estimation error may be written in the form

$$\begin{aligned}\dot{\mathbf{x}}_e &= \left(\tilde{A} + LC_2\right)\mathbf{x}_e - N(\mathbf{x}_e) + M(\boldsymbol{\eta}(t))\,\mathbf{x}_e \\ &= \left(A + LC_2 + M(\mathbf{x}(t))\right)\mathbf{x}_e - N(\mathbf{x}_e)\end{aligned} \tag{4.7}$$

Conservative sufficient conditions for convergence of the nonlinear closed-loop system (4.7) are established in Appendix C. Unfortunately, it does not appear possible to select time-invariant linear estimator feedback L such that the estimator error decreases uniformly as the uncontrolled state $\mathbf{x}(t)$ moves along the trajectory of the attractor, as the term $M(\mathbf{x}(t))$ is destabilizing over a portion of the attractor. However, this does not imply that the estimator will necessarily diverge; effective estimators may still be found, as will now be shown.

The convergence or divergence of the state estimator for the uncontrolled system, when the estimation error $\mathbf{x}_e$ is small, may be made precise by extensions of the Lyapunov exponent λ_∞ and the local Lyapunov exponent $\lambda_\epsilon(\mathbf{x}(t))$ used to characterize the uncontrolled system in §2.1. Consider an infinitesimal perturbation $\delta\mathbf{x}_e(0) = \mathbf{x}_e(0)$ of the state estimation error such that $|\delta\mathbf{x}_e(0)| = |\mathbf{x} - \hat{\mathbf{x}}| \ll 1$. The perturbation $\delta\mathbf{x}_e(t)$ evolves according to the linearization of (4.7), which is given by

$$\dot{\delta\mathbf{x}}_e = \left(A + LC_2 + M(\mathbf{x}(t))\right)\delta\mathbf{x}_e.$$

The Lyapunov exponent κ_∞ is defined as

$$\kappa_\infty = \lim_{T\to\infty}\frac{1}{T}\log\frac{\|\delta\mathbf{x}_e(T)\|}{\|\delta\mathbf{x}_e(0)\|}$$

for almost all initial states $\mathbf{x}(0)$ and estimator perturbations $\delta\mathbf{x}_e(0)$. The Lyapunov exponent κ_∞ thus measures the exponential rate of convergence ($\kappa_\infty < 0$) or divergence ($\kappa_\infty > 0$) of the state estimator when averaged over long time intervals ($T \to \infty$). Calculated values of the Lyapunov exponent κ_∞ for the present estimators are tabulated in tables 3 and 4. The local Lyapunov exponent $\kappa_\epsilon(\mathbf{x}(t))$ is defined as

$$\kappa_\epsilon(\mathbf{x}(t)) = \lim_{T\to 0} \frac{1}{T} \log \frac{\|\delta\mathbf{x}_e(t+T)\|}{\|\delta\mathbf{x}_e(t)\|}$$

for t sufficiently large, in a manner analogous to the local Lyapunov exponent $\lambda_\epsilon(\mathbf{x}(t))$ of the uncontrolled system. The local Lyapunov exponent $\kappa_\epsilon(\mathbf{x}(t))$ of the state estimation error thus measures the local exponential rate of convergence or divergence of state and the state estimate when the estimation error is small. The Lyapunov exponent κ_∞ is the long-time average along the system trajectory $\mathbf{x}(t)$ of the local Lyapunov exponent $\kappa_\epsilon(\mathbf{x}(t))$ (see figure 7). As the estimator equation (4.1a) accurately models the state equation (2.2a), the Lyapunov exponent for the estimator κ_∞ reduces to the Lyapunov exponent for the uncontrolled state $\lambda_\infty = 0.707$ when the estimator feedback L is made small, as shown in table 3.

It is demonstrated in simulations (see, for example, figure 8) that, for α sufficiently small that $\kappa_\infty < 0$ (table 3), the estimator feedback globally stabilizes the estimation error $\mathbf{x}_e$ to zero even for initial conditions on the estimation error $\mathbf{x}_e(0)$ which are not small. As opposed to the control problem, no undesired stabilized states other than $\mathbf{x}_e = 0$ were detected in the closed-loop nonlinear system for the estimation error.

It was found (compare figures 7b and 7c) that choosing a (time-invariant) reference state $\tilde{\mathbf{x}}$ at the origin, which is the approximate "center of mass" of the orbits of the uncontrolled system (figure 2a-c), gave the best estimator performance for the range of initial conditions tested. This is reasonable, as the reference state $\tilde{\mathbf{x}}$, about which we linearize the system to determine the estimator feedback, should be as close as possible to the state $\mathbf{x}(t)$ at any instant for the linearization of the estimator error equation (specifically, the neglect of $M(\boldsymbol{\eta})$ in (4.7)) to be valid.

It was also found (compare figures 7b and 7d) that the nonlinear term $N(\hat{\mathbf{x}})$ in the estimator (4.1a) is essential for good estimator performance. Without it, the equation for a small perturbation $\delta\mathbf{x}_e(t)$ of the estimator (when we take $\tilde{\mathbf{x}} = \mathbf{0}$) takes the form

$$\dot{\delta\mathbf{x}}_e = \big(A + LC_2\big)\,\delta\mathbf{x}_e + N\big(\mathbf{x}(t)\big),$$

where the nonlinear term $N(\mathbf{x}(t))$ is not small as the state $\mathbf{x}(t)$ moves on the attractor. The linear estimator feedback $LC_2\,\delta\mathbf{x}_e$, which is proportional to the size of the estimation error perturbation, is not sufficient to stabilize this term. The estimator will continually be disrupted if the nonlinear term $N(\hat{\mathbf{x}})$ is not included in the equation for the estimator (4.1).

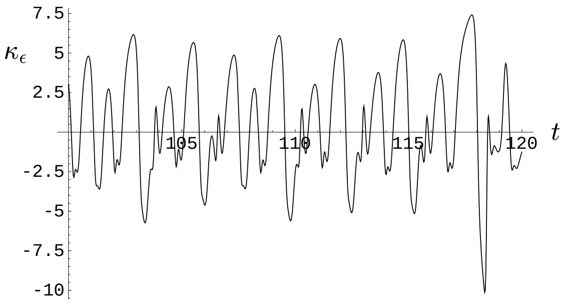

(a) Estimator designed with $\alpha = 1.0$, $\tilde{\mathbf{x}} = \mathbf{0}$. The value of the Lyapunov exponent κ_∞, which is the average value of the local Lyapunov exponent κ_ϵ plotted, is $\kappa_\infty = 0.45 > 0$. This indicates that the state estimator is unstable ($\kappa_\epsilon > 0$) more than it is stable ($\kappa_\epsilon < 0$), and thus the state estimate will not converge to the uncontrolled state.

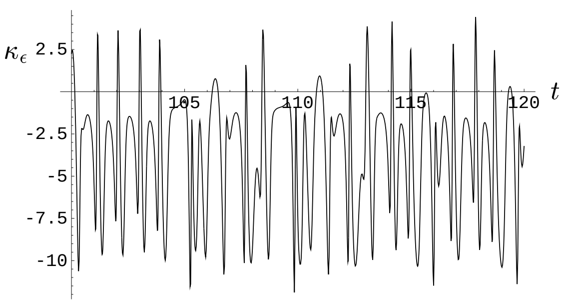

(b) Estimator designed with $\alpha = 0.1$, $\tilde{\mathbf{x}} = \mathbf{0}$. The value of the Lyapunov exponent is $\kappa_\infty = -3.95 < 0$. This indicates that the state estimator is stable more than it is unstable, and thus the state estimate will converge to the uncontrolled state when $\mathbf{x}_e$ is small. Note that estimator convergence is attained even though the estimator error does not decrease uniformly over the entire path of the attractor.

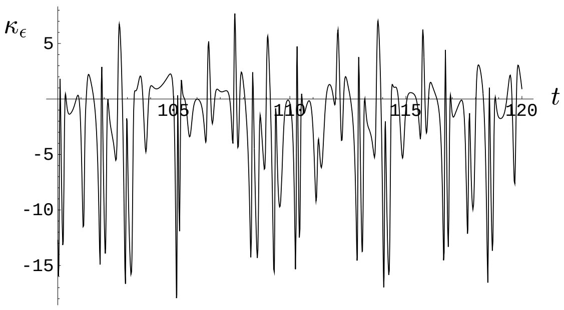

(c) Estimator designed with $\alpha = 0.1$, $\tilde{\mathbf{x}} = \bar{\mathbf{x}}$. Lyapunov exponent $\kappa_\infty = -2.33 < 0$. It is found that linear estimator feedback designed with $\tilde{\mathbf{x}} = \mathbf{0}$ has better convergence properties (cf. figure 7b).

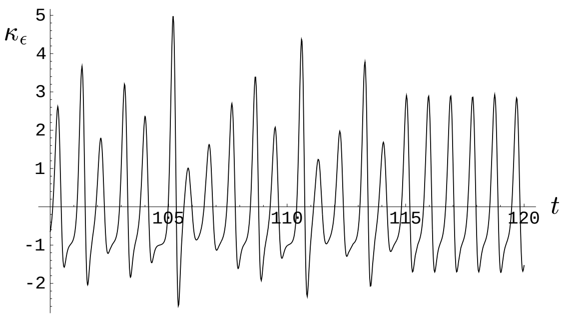

(d) Estimator designed with $\alpha = 0.1$, $\tilde{\mathbf{x}} = \mathbf{0}$, and the nonlinear term dropped from the estimator equation (4.1). Lyapunov exponent $\kappa_\infty = 0.01$. The nonlinear term in the estimator is essential for good performance (cf. figure 7b).

Figure 7: Local Lyapunov exponent $\kappa_\epsilon(t)$ describing the local growth or attenuation of small perturbations of the estimation error $\mathbf{x}_e(t)$ in the closed-loop system for the state estimator as the state $\mathbf{x}(t)$ moves along the attractor.

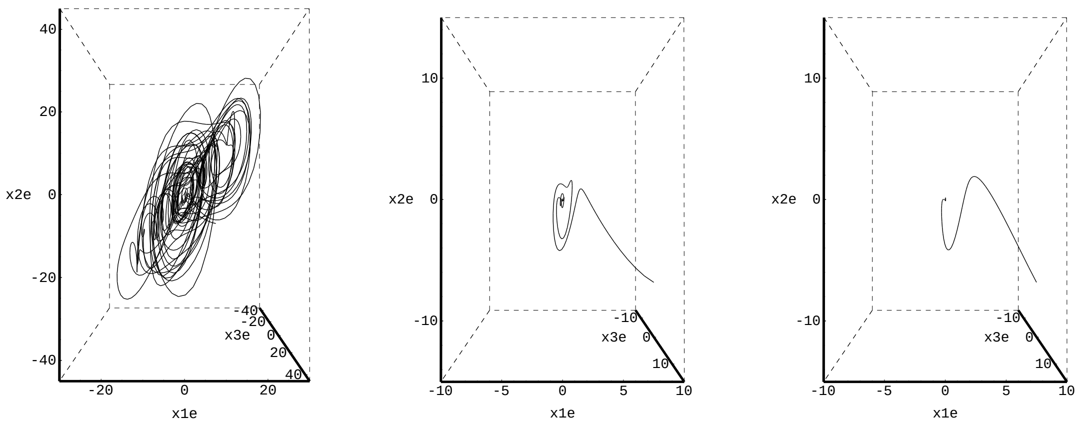

(a) $\alpha = 1.0$, $\kappa_\infty = 0.45$. (b) $\alpha = 0.25$, $\kappa_\infty = -1.04$. (c) $\alpha = 0.1$, $\kappa_\infty = -3.95$.

Figure 8: Trajectory of the estimation error $\mathbf{x}_e(t)$ for estimators determined with $\tilde{\mathbf{x}} = 0$ and three different values of α when applied to the uncontrolled, undisturbed convection system. The initial conditions on the state, $\mathbf{x}(0) = (5\ 1\ 0)^*$, and the state estimate, $\hat{\mathbf{x}}(0) = (-5\ 10\ 0)^*$, are separated significantly in these simulations. Even so, for estimators with $\kappa_\infty < 0$, the estimator feedback $\hat{\mathbf{u}}$ rapidly brings the state estimate $\hat{\mathbf{x}}$ in close proximity to the state $\mathbf{x}$ based on measurements of x_2 only. Such behavior is seen with all initial conditions tested. The approach of the estimated state to the actual state is more rapid for estimators with smaller values of κ_∞. After the state and the estimate are brought into proximity, nonlinear estimators with $\kappa_\infty < 0$ accurately track the chaotic trajectory of the state with little further estimator feedback required.

Better performance may be obtained in flow systems which prove to be more difficult to estimate using a *gain scheduling* approach to select the most suitable estimator feedback gains. Note that the simple switching function $H(\zeta)$ used for the controller feedback in the previous section is a crude example of a simple gain scheduling approach. For the estimator, a gain scheduling approach might entail a reference state which is a function of time, with the feedback gains $L(t)$ recomputed as the system evolves using the linearization $\tilde{\mathbf{x}}(t) = \hat{\mathbf{x}}(t)$. With such an approach, $\hat{\boldsymbol{\eta}}(t)$ and $M(\hat{\boldsymbol{\eta}}(t))$ are identically zero, and stability of the estimator error to small disturbances anywhere on the attractor is established by the local linear stability of the closed-loop system matrix $\tilde{A}(t) + L(t)\,C_2$, with a proof similar to that in Appendix B with $\tilde{\mathbf{r}} = \mathbf{0}$. A gain scheduling approach, however, is more difficult to implement than constant-gain feedback, requiring on-line computation of the estimator Riccati equation (4.6c), and is *not* required to stabilize the estimator error in the present system, given that the constant estimator feedback L selected is sufficient to provide $\kappa_\infty < 0$, as discussed above.

Chapter 5

Practical control approach

It is straightforward to combine the estimators and controllers of the two previous sections to obtain an estimator-based controller which may be implemented based on limited noisy measurements. The flow of information in this approach is illustrated schematically by the following standard block diagram.

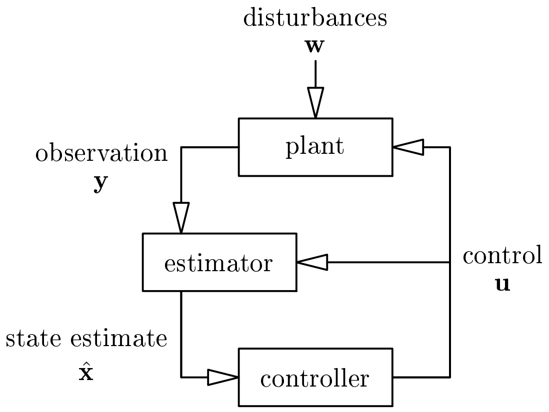

The plant, forced by external disturbances, has an internal state $\mathbf{x}$ which cannot be observed. Instead, a noisy observation $\mathbf{y}$ is made and an estimate of the state $\hat{\mathbf{x}}$ determined. This state estimate is then fed through the controller to determine the control $\mathbf{u}$ to be applied on the plant to regulate $\mathbf{x}$ to zero.

To summarize, the equations governing the plant (replaced in the implementation by the apparatus itself) are

$$\begin{aligned}\dot{\mathbf{x}} &= A\,\mathbf{x} + N(\mathbf{x}) + B_1\,\mathbf{w} + B_2\,\mathbf{u} + \mathbf{r}\\ \mathbf{y} &= C_2\mathbf{x} + D_{21}\mathbf{w},\end{aligned}$$

the (nonlinear) equations for the estimator (updated by the measurements $\mathbf{y}$ only) are

$$\begin{aligned}
\dot{\hat{\mathbf{x}}} &= A\,\hat{\mathbf{x}} + N(\hat{\mathbf{x}}) + B_2\,\mathbf{u} + \mathbf{r} - \hat{\mathbf{u}} \\
\hat{\mathbf{y}} &= C_2\hat{\mathbf{x}} \\
\hat{\mathbf{u}} &= H(t-t_1)\,L(\mathbf{y}-\hat{\mathbf{y}}),
\end{aligned}$$

and the equation for the controller (based now on the state estimate $\hat{\mathbf{x}}$) is

$$\mathbf{u} = H(t-t_2)\,H(R - |\hat{\mathbf{x}}-\bar{\mathbf{x}}|)\,K(\hat{\mathbf{x}}-\bar{\mathbf{x}}).$$

Values of K and L have been computed by application of linear control theory to the appropriate linearized problems and are reported in tables 1-4. Three parameters $\{\gamma, \alpha, \ell\}$ may be used to scale the magnitude of the estimator and controller feedback appropriately for particular implementations. Note that:

- estimator feedback is turned on only after an amount of time t_1 has elapsed which is sufficiently large that the state $\mathbf{x}(t)$ is near the attractor, after which the convergence of the estimator has been thoroughly verified, and
- control feedback is turned on only after both
  - *i.*) an amount of time $t_2 > t_1$ has elapsed which is sufficiently large that the state estimation error $\mathbf{x}_e(t) = \mathbf{x}(t) - \hat{\mathbf{x}}(t)$ is small, and
  - *ii.*) the state estimate $\hat{\mathbf{x}}(t)$ (and therefore the state $\mathbf{x}(t)$ itself) has meandered to a point within the subdomain, illustrated in figure 6, inside of which convergence of the linearly-controlled system to the desired state is assured.

For this approach to be effective, the estimator must be able to both

a.) track the uncontrolled state $\mathbf{x}(t)$ as it moves on the attractor, and

b.) track small perturbations of the controlled state in the vicinity of the desired fixed point.

It is found by simulation that, when the appropriate controllers and estimators are selected, the approach described above converges from all initial conditions tested. A particular case tested in detail took $t_1 = 0$, $t_2 = 5$, $R = 9$, $\hat{\mathbf{x}}(0) = \mathbf{0}$, estimator feedback computed with $\alpha = 0.1$ and $\gamma = \infty$, controller feedback computed with $\ell = 0.25$ and $\gamma = \infty$, and sampled a large range of initial conditions $\mathbf{x}(0)$ within the absorbing ball of figure 2d. The estimator converged properly and the control application successfully caught the state at the desired state in all cases tested.

Chapter 6

Conclusions and related questions in the turbulence problem

It has been demonstrated that, using linear optimal/ robust control theory, the Lorenz equation may be estimated effectively based on partial state measurements and controlled effectively with limited control authority. Linear control feedback is found to be fully effective only when it is switched off while the state is far from the desired equilibrium point, relying on the attractor of the system to bring the state into a neighborhood of the equilibrium point before control is applied. Linear estimator feedback is found to be fully effective only when *a*) the Lyapunov exponent of the state estimation error is negative, indicating that the state estimate converges to the uncontrolled state, and *b*) the estimator is stable in the vicinity of the desired equilibrium point. Fundamental limitations in the control and estimation of a nonlinear system by linear feedback have been characterized.

For the present nonlinear problem, nonlinear feedback controllers may be constructed which are superior in terms of their global convergence to the linear controllers examined here. Wang & Abed (1992) achieve effective control of the present system with a washout filter and control with a cubic nonlinearity, supplanting the linear controller (3.3) with

$$\begin{aligned} \dot{x}_4 &= x_3 - k_1 x_4 \\ u &= -k_2 (x_3 - k_1 x_4)^3. \end{aligned}$$

A controller of a similar form was implemented experimentally by Yuen & Bau (1996). Ezal, Pan, & Kokotović (1997) have shown that the integrator backstepping approach (which involves the recursive construction of appropriate Lyapunov functions for each scalar component of the governing equation) may be applied to compute nonlinear feedback controls for a certain class of nonlinear systems for global stabilization while maintaining local optimality. Systems that lend themselves to this approach may be written in the strict-feedback form

$$\begin{aligned}
\dot{x}_1 &= x_2 + f_1(x_1) &&+ h_1(x_1)\,w \\
\dot{x}_2 &= x_3 + f_2(x_1, x_2) &&+ h_1(x_1, x_2)\,w \\
&\vdots \\
\dot{x}_n &= u + f_n(x_1, \ldots, x_n) &&+ h_n(x_1, \ldots, x_n)\,w.
\end{aligned}$$

Such methods of constructive Lyapunov stabilization (Jankovic, Sepulchre, & Kokotović 1996) do extend to the Lorenz equation, at least in problems in which the control is applied to the equation for x_2 (the left/right temperature difference), as considered by Vincent & Yu (1991), Shinbrot *et al.* (1993), Wan & Bernstein (1995), and Jankovic (1997). In the problem considered in the present article and in Wang & Abed (1992), Wang, Singer, & Bau (1992), Yuen & Bau (1996), and elsewhere, control is applied to the equation for x_3 (the top/bottom temperature difference). This appears to be a slightly more difficult control problem: for instance, globally stabilizing linear controls, such as those found by Wan & Bernstein (1995), appear to be unavailable in the present case (see Appendix B). It remains to be seen whether or not the intriguing nonlinear approaches discussed above may be extended to more complex systems, such as those governed by the Navier-Stokes equation.

In this article, we have focused our attention on the fundamental limitations inherent to the application of linear feedback control to the present nonlinear system, as we are considering the Lorenz system as a model for more complex systems for which appropriate nonlinear feedback approaches are not yet available. As quoted by Petar Kokotović (1992), Richard Bellman is said to have compared one who designs linear controls for nonlinear systems with one who, "*having lost his watch in a dark alley, is searching for it under a lamp post*". To pursue this metaphor further, we are, indeed, waiting at the lamp post with our present approach; however, due to the chaotic behavior of the Lorenz system, we are confident that our watch will roll into view in finite time. Important open questions remain:

1. Are switched approaches, similar to the one required for the present convection problem, necessary for effective application of linear feedback to turbulence?

2. If the answer to question 1 is positive, under what conditions does turbulence flow into the view of linear controls, and what linear control algorithms illuminate the largest area?

3. If the conditions for the successful application of linear feedback to turbulence are overly restrictive, what forms of nonlinear feedback are best suited for the problem of turbulence?

To make these questions concrete, subcritical (*i.e.*, low Reynolds number) turbulent channel flow is an appropriate testbed (Moin & Bewley 1995). This flow is observed in simulation and experiment to have recurrent features, referred to as coherent structures (Robinson 1991, Jeong *et al.* 1997), characteristic of higher Reynolds number flows of practical engineering interest. The near-wall coherent structures are a major source of the turbulent cascade of energy, and may be eliminated by control actuation applied at the wall (blowing/suction). Globally stabilizing controls, however, are exceedingly difficult to determine and, to date, have been found only with nonlinear optimal control theory in an (entirely impractical) predictive control setting (Temam, Bewley, & Moin 1997). More practical control algorithms are necessary. At least three control approaches for this nonlinear problem come to mind:

1. Design a linear optimal/robust controller for increased linear stability of the laminar flow (Bewley & Liu 1998), possibly coupling with a reduced-order state estimator updated with linear measurement feedback. Such an approach is a direct extension of the approach used in the present manuscript, and similar problems should be expected. Note that uncontrolled subcritical turbulent channel flow remains at all times far from the stable equilibrium point of laminar channel flow at the same bulk velocity. Thus, the state of the uncontrolled system might never enter a subdomain inside of which the effectiveness of the linear controller can be assured (cf. figure 6).

2. Numerically optimize the undetermined coefficients in a simple (linear or nonlinear) output feedback rule for particular turbulent flow realizations, either with nonlinear optimal/robust control theory (Bewley, Moin, & Temam 1996; Bewley, Temam, & Ziane 1998) or with a heuristic training algorithm such as a neural network (Lee *et al.* 1997). Such optimizations must be performed on large ensembles of turbulent flows to achieve optimized *ad hoc* control rules which generalize to other turbulent flow realizations, and thus are numerically challenging to perform. Effective performance of such approaches can not be guaranteed, but can at least partially reduce the magnitude of the turbulent fluctuations (Lee *et al.* 1997).

3. Apply nonlinear feedback control theory for PDEs based on rigorous notions such as L2-gain and passivity (van der Schaft 1996; Isidori 1995) as such theory becomes available.

It is not certain which approach will most effectively bring turbulence into the light, and all three approaches will continue to be explored.

Appendix A

Boundedness of the state of the uncontrolled system

After an initial transient, the trajectory of the state $\mathbf{x}$ in the system (2.1) ultimately becomes confined (Lorenz 1993) to a bounded subspace of the three-dimensional phase space $\{x_1, x_2, x_3\}$, as indicated in figure 2, approaching the set referred to as the attractor of the system. The boundedness of the attractor is now established.

Lemma 1 *Given the uncontrolled open-loop system for the state* $\mathbf{x}$*, of the form*

$$\dot{\mathbf{x}} = \begin{pmatrix} \sigma\,(x_2 - x_1) \\ -x_2 - x_1 x_3 \\ -b\,x_3 + x_1 x_2 - b\,\bar{u} \end{pmatrix} = A\,\mathbf{x} + N(\mathbf{x}) + \mathbf{r}$$

with

$$A \triangleq \begin{pmatrix} -\sigma & \sigma & 0 \\ 0 & -1 & 0 \\ 0 & 0 & -b \end{pmatrix}, \quad N(\mathbf{x}) \triangleq \begin{pmatrix} 0 \\ -x_1 x_3 \\ x_1 x_2 \end{pmatrix}, \quad \mathbf{r} \triangleq \begin{pmatrix} 0 \\ 0 \\ -b\,\bar{u} \end{pmatrix},$$

for $\sigma \geq 1$*,* $0 < b < 2$*, and* $\bar{u} > 1$*. The existence of an absorbing ball may be established such that any trajectory of* $\mathbf{x}$ *originating outside of this ball will enter it in finite time, and any trajectory of* $\mathbf{x}$ *inside this ball will never leave it.*

Proof. (Outlined by Sparrow 1982.) Define a Lyapunov function (Graham & McRuer 1961; van der Schaft 1996) V such that

$$V \triangleq \frac{1}{2}\left[\bar{u}\,x_1^2 + \sigma\,x_2^2 + \sigma(x_3 - \bar{u})^2\right].$$

Differentiating V, it is easily shown that

$$\begin{aligned}\dot{V} &= \bar{u}\,x_1\,\dot{x}_1 + \sigma\,x_2\,\dot{x}_2 + \sigma\,(x_3 - \bar{u})\,\dot{x}_3 \\ &= -\sigma\,(\bar{u}\,x_1^2 + x_2^2 + b\,x_3^2 - b\,\bar{u}^2).\end{aligned}$$

Note that $\dot{V} < 0$ everywhere outside an ellipsoidal domain D, where D is defined by

$$\frac{x_1^2}{b\,\bar{u}} + \frac{x_2^2}{b\,\bar{u}^2} + \frac{x_3^2}{\bar{u}^2} \le 1 \qquad \forall\,\mathbf{x} \in D.$$

Define an ellipsoidal domain E such that

$$\frac{x_1^2}{4\,\sigma\,\bar{u}} + \frac{x_2^2}{4\,\bar{u}^2} + \frac{(x_3 - \bar{u})^2}{4\,\bar{u}^2} \le 1 + \epsilon \qquad \forall\,\mathbf{x} \in E$$

for some small but finite $\epsilon > 0$. Since D (the smaller ellipsoid of figure 2d) is completely contained in E (the larger ellipsoid of figure 2d), it follows that $\dot{V} \le -\delta(\epsilon)$ everywhere on and outside of E, for some finite $\delta(\epsilon) > 0$. Note that V is constant on the surface of E, with larger values outside and smaller values inside. It follows directly from these two conditions that

a.) any trajectory of the system originating outside of E will enter it in finite time, and

b.) all trajectories pass *inward* through the boundary of E, so any trajectory of the system inside E will never leave it.

The surface of E is thus referred to as an "absorbing ball" of the state $\mathbf{x}$. $\square$

Appendix B

Boundedness of the state of the controlled system

Lemma 2 *Given the linearly-controlled closed-loop system for $\boldsymbol{\eta} = \mathbf{x} - \tilde{\mathbf{x}}$, the deviation of the state $\mathbf{x}$ from a reference state $\tilde{\mathbf{x}}$, which may be written in the form*

$$\dot{\boldsymbol{\eta}} = (\tilde{A} + B_2 K)\,\boldsymbol{\eta} + N(\boldsymbol{\eta}) + \tilde{\mathbf{r}}$$

with

$$\tilde{A} + B_2 K \triangleq \begin{pmatrix} -\sigma & \sigma & 0 \\ -\tilde{x}_3 & -1 & -\tilde{x}_1 \\ \tilde{x}_2 - bk_1 & \tilde{x}_1 - bk_2 & -b - bk_3 \end{pmatrix},$$

$$K^* \triangleq \begin{pmatrix} k_1 \\ k_2 \\ k_3 \end{pmatrix}, \quad \tilde{\mathbf{x}} \triangleq \begin{pmatrix} 0 \\ bk_1 \\ \sigma \end{pmatrix}, \quad \bar{\mathbf{x}} \triangleq \begin{pmatrix} \sqrt{b(\bar{u}-1)} \\ \sqrt{b(\bar{u}-1)} \\ -1 \end{pmatrix},$$

$$\tilde{\mathbf{r}} \triangleq A\,\tilde{\mathbf{x}} + N(\tilde{\mathbf{x}}) + \mathbf{r} + B_2 K(\tilde{\mathbf{x}} - \bar{\mathbf{x}}),$$

where A, $N(\cdot)$, $\mathbf{r}$, σ, b, and $\bar{u}$ are defined as in Lemma 1. If $k_3 > -(1+b)/b$ and $k_2^2 < 4(1+k_3)/b$, the existence of an absorbing ball may be established such that any trajectory of $\boldsymbol{\eta}$ originating outside of this ball will enter it in finite time, and any trajectory of $\boldsymbol{\eta}$ inside this ball will never leave it.

Proof. Define a Lyapunov function V_c such that $V_c \triangleq \dfrac{1}{2}\boldsymbol{\eta}^*\boldsymbol{\eta}$. Differentiating V_c and noting that $\boldsymbol{\eta}^* N(\boldsymbol{\eta}) = 0$, it is easily shown that

$$\dot{V}_c = \boldsymbol{\eta}^*\dot{\boldsymbol{\eta}} = \boldsymbol{\eta}^*(\tilde{A} + B_2 K)\boldsymbol{\eta} + \boldsymbol{\eta}^*\tilde{\mathbf{r}}.$$

The nonzero part of the first term comes from the symmetric part of $\tilde{A} + B_2 K$, which is given by

$$S_c(\tilde{\mathbf{x}}) = \begin{pmatrix} -\sigma & \dfrac{\sigma - \tilde{x}_3}{2} & \dfrac{\tilde{x}_2 - bk_1}{2} \\ \dfrac{\sigma - \tilde{x}_3}{2} & -1 & \dfrac{-bk_2}{2} \\ \dfrac{\tilde{x}_2 - bk_1}{2} & \dfrac{-bk_2}{2} & -b - bk_3 \end{pmatrix},$$

A necessary and, with the present value of $\tilde{\mathbf{x}}$, sufficient condition for $S_c(\tilde{\mathbf{x}})$ to be negative definite is that the matrix

$$\begin{pmatrix} -1 & \dfrac{-bk_2}{2} \\ \dfrac{-bk_2}{2} & -b - bk_3 \end{pmatrix}$$

have negative eigenvalues, which is true iff

$$k_3 > -\frac{1+b}{b} \qquad \text{and} \qquad k_2^2 < \frac{4(1+k_3)}{b}. \tag{B.1}$$

Note that these inequalities are satisfied by some, but not all, of the values K computed by linear optimal/robust control theory and reported in tables 1 and 2.

Let λ_1 be the maximum eigenvalue of $S_c(\tilde{\mathbf{x}})$, and assume that the conditions of (B.1) are satisfied (*i.e.*, $\lambda_1 < 0$). It follows that

$$\begin{aligned} \dot{V}_c &= \boldsymbol{\eta}^*(\tilde{A} + B_2 K)\boldsymbol{\eta} + \boldsymbol{\eta}^* \tilde{\mathbf{r}} \\ &\leq \lambda_1 |\boldsymbol{\eta}|^2 + |\boldsymbol{\eta}||r| \end{aligned}$$

Define a spherical domain E_c such that

$$|\boldsymbol{\eta}| \leq \left| \frac{\tilde{\mathbf{r}}}{\lambda_1} \right| + \epsilon \qquad \forall\, \boldsymbol{\eta} \in E_c$$

for some small but finite $\epsilon > 0$. It follows that $\dot{V}_c \leq -\delta(\epsilon)$ everywhere on and outside of E_c, for some finite $\delta(\epsilon) > 0$. Note that V_c is constant on the surface of the spherical domain E_c, with larger values outside and smaller values inside. It therefore follows, as in the proof of Lemma 1, that the surface of E_c is an absorbing ball of the controlled state $\boldsymbol{\eta} = \mathbf{x} - \tilde{\mathbf{x}}$. □

If we take $\tilde{\mathbf{x}} = \bar{\mathbf{x}}$ in Lemma 2, it follows that $\tilde{\mathbf{r}} = \bar{\mathbf{r}} = \mathbf{0}$ (as in §3). Thus, if $S_c(\bar{\mathbf{x}})$ (*i.e.*, the symmetric part of $\bar{A} + B_2 K$) has all negative eigenvalues, we may shrink the absorbing ball E_c to a small neighborhood of $\mathbf{x} = \bar{\mathbf{x}}$, and thus the desired fixed point is globally asymptotically stable. Unfortunately, it does not appear to be possible to select a linear control feedback matrix K which provides this much stabilization to the present problem.

Appendix C

Convergence of the state estimation error

Lemma 3 *Given the closed-loop system (with linear measurement feedback) for the state estimation error* $\mathbf{x}_e = \mathbf{x} - \hat{\mathbf{x}}$*, the deviation of the state* $\mathbf{x}$ *from the state estimate* $\hat{\mathbf{x}}$*, which may be written in the form*

$$\dot{\mathbf{x}}_e = \big(A + LC_2 + M(\mathbf{x})\big)\,\mathbf{x}_e - N(\mathbf{x}_e)$$

with

$$A + LC_2 \triangleq \begin{pmatrix} -\sigma & \sigma + l_1 & 0 \\ 0 & -1 + l_2 & 0 \\ 0 & l_3 & -b \end{pmatrix},$$

$$L \triangleq \begin{pmatrix} l_1 \\ l_2 \\ l_3 \end{pmatrix}, \qquad M(\mathbf{x}) \triangleq \begin{pmatrix} 0 & 0 & 0 \\ -x_3 & 0 & -x_1 \\ x_2 & x_1 & 0 \end{pmatrix},$$

where A*,* $N(\cdot)$*,* σ*, and* b *are defined as in Lemma 1. The* L_2*-norm of the state estimation error* $\mathbf{x}_e$ *decreases uniformly in time whenever the linear feedback* L *and the state* $\mathbf{x}$ *are such that the eigenvalues of the symmetric part of* $A + LC_2 + M(\mathbf{x})$ *are negative.*

Proof. Define a Lyapunov function V_e such that $V_e = \dfrac{1}{2}\mathbf{x}_e^*\mathbf{x}_e$. Differentiating V_e and noting that $\mathbf{x}_e^* N(\mathbf{x}_e) = 0$, it is easily shown that

$$\dot{V}_e \triangleq \mathbf{x}_e^*\dot{\mathbf{x}}_e = \mathbf{x}_e^*\big(A + LC_2 + M(\mathbf{x})\big)\mathbf{x}_e.$$

The nonzero part of this expression comes from the symmetric part of $A + LC_2 + M(\mathbf{x})$, which is given by

$$S_e(\mathbf{x}) = \begin{pmatrix} -\sigma & \dfrac{\sigma + l_1 - x_3}{2} & \dfrac{x_2}{2} \\ \dfrac{\sigma + l_1 - x_3}{2} & -1 + l_2 & \dfrac{l_3}{2} \\ \dfrac{x_2}{2} & \dfrac{l_3}{2} & -b \end{pmatrix},$$

Let E_e contain only those points in $\mathbf{x}$ for which, for a given L and for all $\mathbf{x} \in E_e$, all eigenvalues of $S_e(\mathbf{x})$ are negative. (A necessary and sufficient condition for all eigenvalues to be negative may be established by applying the Routh-Hurwitz criterion to the expression for $\det(\lambda I - S_e(\mathbf{x}))$ expanded as a polynomial in λ.) It follows that, for $\mathbf{x} \in E_e$, we have

$$\begin{cases} \dot{V}_e = 0 & \text{at } \mathbf{x}_e = 0 \ (i.e., \ \hat{\mathbf{x}} = \mathbf{x}) \\ \dot{V}_e < 0 & \text{elsewhere.} \end{cases}$$

Thus, when $\mathbf{x} \in E_e$, the L_2-norm of the state estimation error $\mathbf{x}_e$ decreases uniformly in time. □

Note that E_e is non-empty for at least some L. For example, even for $L = 0$ (*i.e.*, no measurement feedback at all) the region near $x_3 = \sigma$, $x_1 = x_2 = 0$ has all negative eigenvalues.

Unfortunately, it does not appear (for the present parameter values) to be possible to select linear estimator feedback L such that the entire absorbing ball E of the state $\mathbf{x}$ (derived in Lemma 1) is contained in the domain E_e inside of which convergence of the estimator is assured (Lemma 3). Weaker conditions which result in an estimator which is sufficient for the present problem are discussed in §4.

Appendix D

Norm independence of the Lyapunov exponent

In this appendix, it is shown that, for finite-dimensional systems, the value of the Lyapunov exponent is independent of the norm used in its definition, though the local Lyapunov exponent is not. As the Lyapunov exponent is the time average of the local Lyapunov exponent, this is an interesting and perhaps counter-intuitive observation. In addition, when the Euclidean norm is used in its definition, a simple physical interpretation may be assigned to the local Lyapunov exponent.

We first note the norm equivalence principle: for any vector norm $||\mathbf{x}||$ of a finite-dimensional vector $\mathbf{x}$ satisfying

1. non-negativity $||\mathbf{x}|| \geq 0$ with $||\mathbf{x}|| = 0 \Leftrightarrow \mathbf{x} = \mathbf{0}$,

2. homogeneity $||\alpha\mathbf{x}|| = |\alpha| \cdot ||\mathbf{x}||$ for all complex scalars α, and

3. the triangle inequality $||\mathbf{x} + \mathbf{y}|| \leq ||\mathbf{x}|| + ||\mathbf{y}||$,

the following inequality holds:

$$C_1||\mathbf{x}||_2 \leq ||\mathbf{x}|| \leq C_2||\mathbf{x}||_2$$

where $||\mathbf{x}||_2$ denotes the Euclidian norm. Note that, as the dimension of the system under consideration increases, the ratio C_2/C_1 also increases, and thus these bounds are not very tight for high-dimensional systems.

Now consider bounds on the expression for λ_∞, as defined with any norm $\|\mathbf{x}\|$ satisfying the above listed properties, by a similar expression defined with the Euclidian norm $\|\mathbf{x}\|_2$. By the norm equivalence principle cited above, it follows that

$$P = \lim_{T\to\infty} \frac{1}{T} \log \frac{\|\delta\mathbf{x}(T)\|}{\|\delta\mathbf{x}(0)\|} \leq \lim_{T\to\infty} \frac{1}{T} \log \frac{C_2}{C_1} \frac{\|\delta\mathbf{x}(T)\|_2}{\|\delta\mathbf{x}(0)\|_2} = \lim_{T\to\infty} \frac{1}{T} \log \frac{\|\delta\mathbf{x}(T)\|_2}{\|\delta\mathbf{x}(0)\|_2} \triangleq Q.$$

By a similar calculation, it follows that

$$P = \lim_{T\to\infty} \frac{1}{T} \log \frac{\|\delta\mathbf{x}(T)\|}{\|\delta\mathbf{x}(0)\|} \geq \lim_{T\to\infty} \frac{1}{T} \log \frac{C_1}{C_2} \frac{\|\delta\mathbf{x}(T)\|_2}{\|\delta\mathbf{x}(0)\|_2} = \lim_{T\to\infty} \frac{1}{T} \log \frac{\|\delta\mathbf{x}(T)\|_2}{\|\delta\mathbf{x}(0)\|_2} = Q.$$

We have arrived at the inequality $Q \leq P \leq Q$, and thus it follows that $P = Q$, *i.e.*, the Lyapunov exponent computed with any norm satisfying the above listed properties is identical to that computed with the Euclidian norm in a finite-dimensional system. Note that the proof utilizes the $T \to \infty$ limit and thus a similar proof does not follow for the local Lyapunov exponent.

In the special case in which we use the Euclidean norm in its definition, we can assign the local Lyapunov exponent a simple physical interpretation:

$$\begin{aligned}
\lambda_\epsilon(\mathbf{x}(t)) &= \lim_{T\to 0} \frac{1}{T} \log \frac{\|\delta\mathbf{x}(t+T)\|_2}{\|\delta\mathbf{x}(t)\|_2} \\
&= \lim_{T\to 0} \frac{1}{2T} \log \frac{\left(\delta\mathbf{x}(t) + T\dot{\delta\mathbf{x}}(t)\right)^* \left(\delta\mathbf{x}(t) + T\dot{\delta\mathbf{x}}(t)\right)}{\delta\mathbf{x}(t)^*\,\delta\mathbf{x}(t)} \\
&= \lim_{T\to 0} \frac{1}{2T} \log \frac{\delta\mathbf{x}(t)^*\,\delta\mathbf{x}(t) + 2T\dot{\delta\mathbf{x}}(t)^*\,\delta\mathbf{x}(t) + T^2\dot{\delta\mathbf{x}}(t)^*\,\dot{\delta\mathbf{x}}(t)}{\delta\mathbf{x}(t)^*\,\delta\mathbf{x}(t)} \\
&= \frac{\dot{\delta\mathbf{x}}(t)^*\,\delta\mathbf{x}(t)}{\delta\mathbf{x}(t)^*\,\delta\mathbf{x}(t)} \\
&= \frac{\|\dot{\delta\mathbf{x}}(t)\|_2}{\|\delta\mathbf{x}(t)\|_2} \cos \sphericalangle\left(\dot{\delta\mathbf{x}}(t), \delta\mathbf{x}(t)\right).
\end{aligned}$$

The final expression is simply the ratio of the magnitudes of $\dot{\delta\mathbf{x}}(t)$ and $\delta\mathbf{x}(t)$ times the cosine of the angle between them. Naturally, if the cosine of this angle is positive, the magnitude of the perturbation in the Euclidean norm is increasing, and if it is negative, the magnitude of the perturbation is decreasing.

REFERENCES

BAU, H.H., & WANG, Y.Z. 1991 Chaos: a heat transfer perspective. *Annual Review of Heat Transfer* (ed. C.L. Tien), **4**, 1-50.

BEWLEY, T.R., & LIU, S. 1998 Optimal and Robust Control and Estimation of Linear Paths to Transition. *J. Fluid Mech.* **365**, 305-349.

BEWLEY, T.R., MOIN, P., & TEMAM, R. 1996 A method for optimizing feedback control rules for wall-bounded turbulent flows based on control theory. *Proceedings of the ASME Fluids Engineering Summer Meeting*, ASME FED **237**, p. 279-285.

BEWLEY, T.R., TEMAM, R., & ZIANE, M. 1998 A general framework for robust control in fluid mechanics. Submitted to *Physica D*.

DOYLE, J.C., GLOVER, K., KHARGONEKAR, P.P., & FRANCIS, B.A. 1989 State-Space Solutions to Standard $\mathcal{H}_2$ and $\mathcal{H}_\infty$ Control Problems. *IEEE Trans. Auto. Control* **34**, 8, 831-847.

ECKHARDT, B., & YAU, D. 1993 Local Lyapunov exponents in chaotic systems. *Physica* D, **65**, 100-108.

EZAL, K., PAN, Z., & KOKOTOVIĆ, P.V. 1997 Locally Optimal Backstepping Design. *Proceedings of the 36th IEEE Conference on Decision and Control*, San Diego.

FARRELL, B.F., & IOANNOU, P.J. 1996 Generalized stability theory. Part II: nonautonomous operators. *J. Atmos. Sci.*, **53**, (14) 2041-2053.

GLEICK, J. 1987 *Chaos: Making a New Science.* Viking.

GORMAN, M., WIDMANN, P.J., & ROBINS, K.A. 1986 Nonlinear Dynamics of a Convection Loop: a Quantitative Comparison of Experiment with Theory. *Physica* 19D, 255-267.

GRAHAM, D., & MCRUER, D. 1961 Analysis of nonlinear control systems. Wiley.

GREEN, M., & LIMEBEER, D.J.N. 1995 *Linear robust control.* Prentice-Hall.

HART, J.E. 1984 A new analysis of the closed loop thermosyphon. *Int. J. Heat Mass Transfer* **27**, (1) 125-136.

ISIDORI, A. 1995 *Nonlinear control systems.* Springer.

JANKOVIC, M., SEPULCHRE, R., & KOKOTOVIĆ, P.V. 1996 Constructive Lyapunov stabilization of nonlinear cascade systems. *IEEE Trans. Automat. Contr.* **41**, (12) 1723-1735.

JANKOVIC, M. 1997 Private communication.

JEONG, J., HUSSAIN, F., SCHOPPA, W., & KIM, J. 1997 Coherent structures near the wall in a turbulent channel flow. *J. Fluid Mech.* **332**, 185-214.

KOKOTOVIĆ, P.K. 1992 The Joy of Feedback: Nonlinear and Adaptive. *IEEE Control Systems Magazine*, **12**, (3) 7-17.

LAUB, A.J. 1991 Invariant subspace methods for the numerical solution of Riccati equations. In *The Riccati Equation* (ed. Bittaini, Laub, & Willems) 163-196. Springer.

LEWIS, F.L., & SYRMOS, V.L. 1995 *Optimal control.* Wiley.

LEE, C., KIM, J., BABCOCK, D., & GOODMAN, R. 1997 Application of neural network to turbulence control for drag reduction. *Phys. Fluids* **9** (6), 1740-1747.

LORENZ, E.N. 1963 Deterministic nonperiodic flow. *J. Atmos. Sci.* **20**, 130-141.

LORENZ, E.N. 1993 *The Essence of Chaos.* University of Washington Press.

MALMBORG, J., BERNHARDSSON, B., & ÅSTRÖM, K.J. 1996 A stabilizing switching scheme for multi controller systems. *Proceedings of the 13th World Congress of IFAC*, **F**, pp 229-234. San Francisco.

MOIN, P., & BEWLEY, T.R. 1995 Application of control theory to turbulence. *Twelfth Australasian Fluid Mechanics Conference*, Dec. 10-15, Sydney, 109-117.

NESE, J.M. 1989 Quantifying local predictability in phase space. *Physica* D, **35**, 237-250.

ROBINSON, S.K. 1991 Coherent motions in the turbulent boundary layer. *Ann. Rev. Fluid Mech.* **23**, 601-639.

SALTZMAN, B. 1962 Finite Amplitude Free Convection as an Initial Value Problem—I. *J. Atmos. Sci.* **19**, 329-341.

SHINBROT, T., GREBOGI, C., OTT, E., & YORKE, J.A. 1993 Using small perturbations to control chaos. *Nature*, **363**, 411-417.

SKOGESTAD, S., & POSTLETHWAITE, I. 1996 *Multivariable Feedback Control*. Wiley.

SPARROW, C. 1982 *The Lorenz Equations: Bifurcations, Chaos, and Strange Attractors.* Springer.

TEMAM, R., BEWLEY, T.R., & MOIN, P. 1997 Control of turbulent flows. *Proceedings of the 18th IFIP TC7 Conference on System Modelling and Optimization*, July 15, Detroit, Michigan.

VAN DER SCHAFT, A. 1996 L_2-gain and passivity techniques in nonlinear control. Springer.

VINCENT, T.L., & YU, J. 1991 Control of a Chaotic System. *Dynamic and Control*, **1**, (1) 35-52.

VINCENT, T.L. 1997 Control using chaos. *IEEE Control Systems Magazine*, **17**, (6) 65-76.

WAN, C.-J., & BERNSTEIN, D.S. 1995 Nonlinear Feedback Control with Global Stabilization. *Dynamics and Control*, **5**, (4) 321-346.

WANG, H., & ABED, E.H. 1992 Bifurcation Control of Chaotic Dynamical Systems. *U. of Maryland Institute for Sytems Research*, Technical Research Report 92-67.

WANG, Y.Z., SINGER, J., & BAU, H.H. 1992 Controlling Chaos in a Thermal Convection Loop. *J. Fluid Mech.* **237**, 479-498.

WIDMANN, P.J., GORMAN, M., & ROBINS, K.A. 1989 Nonlinear Dynamics of a Convection Loop II. Chaos in Laminar and Turbulent Flows. *Physica* D, **36**, 157-166.

YORKE, J.A., & YORKE, E.E. 1982 Chaotic Behavior and Fluid Dynamics. In: *Hydrodynamic Stability and the Transition to Turbulence* (eds. H.L. Swinney & J. Gollub), Topics in Applied Physics, **45**, 77-95. Springer.

YUEN, P.K., & BAU, H.H. 1996 Rendering a subcritical Hopf bifurcation supercritical. *J. Fluid Mech.* **317**, 91-109.

YUEN, P.K., & BAU, H.H. 1998 Optimal Control of Chaotic Convection—Theory and Experiments. Unpublished.

Part III

DNS-based predictive control of turbulence: an optimal benchmark for feedback algorithms

Part III has been submitted for publication as

Bewley, T.R., Moin, P., & Temam, R. 1999 DNS-based predictive control of turbulence: an optimal benchmark for feedback algorithms. Submitted to *J. Fluid Mech.*

Abstract

Direct numerical simulations (DNS) and optimal control theory are used in a predictive control setting to determine controls that effectively reduce the turbulent kinetic energy and drag of a turbulent flow in a plane channel at $Re_\tau = 100$ and $Re_\tau = 180$. Wall transpiration (unsteady blowing/suction) with zero net mass flux is used as the control. The algorithm used for the control optimization is based solely on the control objective and the nonlinear partial differential equation governing the flow, with no *ad hoc* assumptions beyond that of a finite prediction horizon, T, over which the control is optimized.

Flow relaminarization, accompanied by a drag reduction of over 50 percent, is obtained in some of the control cases with the predictive control approach in direct numerical simulations of subcritical turbulent channel flows. Such performance far exceeds what has been obtained to date in similar flows (using this type of actuation) via adaptive strategies such as neural networks, intuition-based strategies such as opposition control, and the so-called "suboptimal" strategies, which involve optimizations over a vanishingly small prediction horizon $T^+ \to 0$. To achieve flow relaminarization in the predictive control approach, it is shown that it is necessary to optimize the controls over a sufficiently long prediction horizon $T^+ \gtrsim 25$. Implications of this result are discussed.

The predictive control algorithm requires full flowfield information and is computationally expensive, involving iterative direct numerical simulations. It is, therefore, impossible to implement this algorithm directly in a practical setting. However, these calculations allow us to quantify the best possible system performance given a certain class of flow actuation and to qualify how optimized controls correlate with the near-wall coherent structures believed to dominate the process of turbulence production in wall-bounded flows. Further, various approaches have been proposed to distill practical feedback schemes from the predictive control approach without the suboptimal approximation, which is shown in the present work to restrict severely the effectiveness of the resulting control algorithm. The present work thus represents a further step towards the determination of optimally effective yet implementable control strategies for the mitigation or enhancement of the consequential effects of turbulence.

Chapter 1

Background

The recent development of the technology necessary to produce micro-scale mechanical devices, commonly referred to as Micro-Electro-Mechanical Systems (MEMS), has prompted researchers to investigate the possibility of using micro-scale actuation for the control of unstable flow phenomena in order to achieve macro-scale effects. Such leveraging of control effort is possible in chaotic systems (such as turbulence) due to the extreme sensitivity of such systems to small levels of control forcing. Of primary interest in such problems, of course, is the determination of when and where control should be applied to maximize the desired effect.

The original vision for the emergence of MEMS was given by Richard Feynman (1959), in his classic lecture at the American Physical Society entitled “There’s Plenty of Room at the Bottom”, in which Feynman foresaw many of the techniques and challenges encountered by the MEMS community today. Building on the technology developed for the fabrication of silicon chips, there has been a flurry of activity in MEMS for the last decade. For reviews of recent developments of MEMS technology which relate to micro-scale measurement and control in fluid mechanics, the reader is referred to Ho & Tai (1996, 1998), McMichael (1996), Gad El Hak (1996), and Moin & Bewley (1994). In these reviews, the reader will find a variety of sensors and actuators currently under development which are suitable for application in feedback control of turbulence. The primary questions in MEMS development today are how to design such devices to be durable in hostile environments and how to produce such devices at high yield and low cost.

Suffice it to say here that, in the near future, it might be possible to use MEMS technology to measure small-scale turbulent fluctuations of a flow and, subsequently, to apply coordinated small-scale forcing to the flow in order to achieve a desired large-scale effect. Examples of problems of particular interest include reducing drag, reducing heat transfer, delaying transition, delaying separation, increasing mixing, and reducing levels of wall-pressure fluctuations and/or radiated sound. For each of these problems, important questions arise:

1. How much do practical engineering designs stand to benefit if durable MEMS sensors and actuators can indeed be built in large arrays?

2. How and where should the control be applied?

3. Is feedback necessary? If so, what attainable flowfield measurements provide the most useful information? What feedback algorithms are most effective? Specifically,

- Are simple output feedback rules sufficient, or is low-order state estimation required?

- Is linear feedback effective for the control and estimation problems, or is a gain scheduling approach and/or some form of nonlinear feedback preferable?

Answers to most of these questions are not yet known. The present work implements a sensitivity analysis of the Navier-Stokes equation through the definition of an *adjoint field*. From this type of analysis, answers to some of these questions may begin to be sought. As discussed in Bewley *et al.* (1998) and Bewley, Temam, & Ziane (1999), the approach used in the present paper may be extended readily to a variety of problems in fluid mechanics, including the optimization of open-loop time-periodic forcing profiles for turbulent jets and the forecasting of chaotic fluid systems based on limited noisy flowfield measurements. Thus, the approach being developed is of interest even if vast arrays of durable MEMS devices are never realized for commercial use.

We now summarize a few of the recent approaches used to determine implementable feedback control algorithms for turbulent flows, categorizing these approaches to the feedback control problem by examining their mathematical dependence on the equation governing the system. This brief survey of this active field of research puts the present approach in context with a sampling of the other techniques currently under investigation. For a more thorough discussion along this line, see Moin & Bewley (1994).

1.1 Adaptive networks

The first class of schemes which may be proposed to achieve small scale flow control actually makes no explicit reference to the dynamics known to take place in the flow or the Navier-Stokes equation which governs these dynamics. Instead, a "reasonable" network is fashioned which takes as input those measurable flow quantities assumed to be most relevant to the control problem and produces as output the requisite control velocity. The coefficients of this network are then "trained" by applying the control network to the flow and gradually adjusting the coefficients in a heuristic manner based on the resulting evolution of the flow. (Note that there are many different approaches to adaptive control. Hertz, Krogh, & Palmer (1991) and Ioannou & Sun (1996) discuss several possible techniques.) The main advantage of the adaptive approach is that the feedback coefficients can adjust to compensate for changing characteristics of the system being controlled, such as modification of the mean flow speed and direction, the sensitivity of the sensors, and the responsiveness of the actuators.

As an example of one adaptive approach, an adaptive inverse technique has been applied by Lee *et al.* (1996) to a turbulent channel flow at $Re_\tau = 100$, providing approximately 20% drag reduction. This approach first develops an approximate "inverse model" between measurable flow quantities (as input) and the control forcing (as output) with an adaptive technique. This is done by forcing the system with small, "sufficiently rich" control signals which "push" the system a variety of different directions while monitoring the response of the measurements. From this data, a network is constructed which attempts to reproduce (model) the control used based on the measurements taken. (In an inherently nonlinear system such as turbulence, this is a challenging proposition, as any simple linear expression of this relationship would probably be highly nonstationary as the arrangement of the coherent structures near the wall evolves in time.) Each iteration of the adaptation for this inverse model consists of three steps: 1) computing the error of the model output with respect to the desired model output (the actual control forcing used), 2) determining the influence of the various weights in the model on this error, then 3) updating all the weights in the model a small amount in a manner that reduces the error. When applied to the nonlinear adaptive networks commonly used for this purpose, known as "neural networks", this is referred to as "back-propagation" of the error. Once (if) the approximate inverse model between the flow measurements and the control converges for the open-loop system, the inverse model is used to determine a control which will drive the flow measurements towards some desired state, this control is applied to the flow, and the inverse model is further trained to adapt it to the (now modified) characteristics of the closed-loop system. In the case of Lee *et al.* (1996), the desired state was chosen to be a state with reduced fluctuations of the spanwise wall shear; several other strategies may be considered and lead to schemes of varying degrees of effectiveness.

1.2 Schemes based on understanding of dominant physics

In situations in which the dominant physics is well understood, judgment can guide an engineer to design effective control schemes. Success is limited, however, by the engineer's understanding of the physical processes involved; in the case of turbulence, our understanding is still limited despite several decades of intense research.

As an example, an opposition strategy was used by Choi, Moin, & Kim (1994) to reduce the drag in a turbulent channel flow at $Re_\tau = 100$ by mitigating the effect of the near-wall vortices. By opposing near-wall vertical motions of the fluid with an equal and opposite control velocity at the wall, the motion of high momentum fluid towards the wall by the sweep events is abated, and the drag may be reduced by up to 25%.

In follow-on computations and flow visualizations by Hammond, Bewley, & Moin (1998) at

$Re_\tau = 180$, it was shown why this opposition strategy is effective only when the distance y between the detection plane and the wall is sufficiently small ($y^+ = 15$ works best). When the detection plane is too far from the wall, high speed fluid may be drawn in *on a skewed path* from a sweep event into the near-wall region and down towards the wall beneath a nearby ejection event, where the opposition scheme applies suction. For $y^+ > 15$, this mechanism of instability of the closed-loop system is possible, and the turbulence levels and mean drag of the flow are significantly increased. For $y^+ \lesssim 15$, the detection plane is too close to the wall for this mechanism of instability to be effective (as viscosity limits the cross-flow convection possible immediately adjacent to the wall), and the turbulence levels and mean drag are reduced.

Another promising intuition-based concept was proposed by Koumoutsakos (1997), in which the turbulence control problem is considered in terms of the minimization of the so-called "vorticity flux" (i.e., the wall-normal component of the vorticity gradient tensor) at the wall. The control algorithms considered in this framework may be constrained at the outset to depend on wall information only. The simulations of Koumoutsakos (1999) of a turbulent channel flow at $Re_\tau = 180$ indicate the formation of sustained spanwise-coherent fluid "rollers" near the wall with wall-normal blowing/suction via a control strategy targeting reduced gradients of vorticity near the wall, and drag reductions of 40% are reported. A related strategy has been proposed by Keefe (1997) in which the wall-normal gradients of wall-normal vorticity are reduced via the selective actuation of an array of small rotatable disks flush-mounted on the surface rather than a distribution of blowing/suction. Such a configuration might be more straightforward to implement in hardware than blowing/suction. Related channel-flow simulations, in which body forcing confined to the $x_2^+ < 6$ region was used instead of boundary forcing, has resulted in drag reductions of up to 35% (Keefe 1995).

1.3 Extrapolation of linear control theory

The application of linear control theory to the linearized Navier-Stokes equation in a channel is straightforward: see, e.g., Joshi, Speyer, & Kim (1997) for the application of classical control theory and Bewley & Liu (1998) for the application of modern control theory. There are a few critical issues concerning the development of practically implementable algorithms which are still being addressed, but these do not appear to be insurmountable.

One of the most important such issues is that the weights in the linear feedback controller must have compact support in physical space (even if it is designed in Fourier space) in order for the controller to be implementable (Bamieh 1997). It is important to note that many linear controllers designed in Fourier space do not satisfy this property. In flows which are not spatially periodic (as is the case with all real channel flows), an incorrect assumption of spatial periodicity in the application of a non-compact controller would result in a Gibbs phenomenon which would probably render the controller ineffective even if all other assumptions in the controller design were met in the experiment. On the other hand, a physical-space controller with compact spatial support is not affected by Gibbs phenomenon and therefore generalizes to a variety of periodic and non-periodic flows with similar near-wall dynamics.

Another important issue yet to be completely resolved is the most appropriate method for linear model reduction. Cortelezzi *et al.* (1999) addresses this topic and obtains a linear model reduction by truncating those linear eigenmodes with low observability or controllability from a model of a 2D unsteady channel flow. (Surprisingly, Cortelezzi *et al.* (1999) reports a drag reduction to 50% below the laminar level by application of a zero-net mass flux linear controller.) In the highly nonorthogonal (i.e., nearly defective) systems often encountered in 3D flows, model reduction schemes mindful of the transfer function of interest, such as the p, q Markov covariance equivalent realization (Villemagne & Skelton 1988) or optimal Hankel norm approximation (Zhou, Doyle, & Glover 1996), are well suited, and should be studied in future work.

Even with such questions remaining open, researchers are beginning to consider the extrapolation of the linear control feedback determined by linear control theory directly to the fully nonlinear problem of a turbulent flow. The first reason to try such an approach is simply because we can: due to the ease of determining and implementing linear control feedback, we should attempt to exploit everything we can from our ability to compute linear controls.

There is at least some justification in the fluids literature for such an approach. Though the significance of this result has been debated, Farrell & Ioannou (1993) have clearly shown that the linearized Navier-Stokes equation in a plane channel flow, when excited with the appropriate stochastic forcing, exhibits behaviour which is reminiscent of streamwise vortices and streamwise streaks characteristic of turbulent flows, though perhaps at a length scale which must be tuned by observation of the full nonlinear system. Whatever information the linearized equation actually contains about the real mechanisms for formation of streamwise vortices and streamwise streaks, the linear controllers should be able to exploit.

There is also some justification in the mathematical literature for such an approach. Interestingly, Barbu & Sritharan (1998) proved mathematically that solutions of the linear robust control problem for Navier-Stokes systems, such as those determined by Bewley & Liu (1998) for small perturbations to a laminar channel flow, are γ-suboptimal for the full (nonlinear) Navier-Stokes equation for finite (albeit sufficiently small) flow perturbations. However, important possible pitfalls of applying linear control feedback to stabilize *large* flow perturbations, such as those on a chaotic attractor (where the effects of the nonlinear terms are essential for describing the system behaviour), are illustrated for a simple model problem by Bewley (1999). It is shown in this reference that such an approach can lead to closed-loop systems which can either converge to the wrong state or even blow up unless the appropriate nonlinear switches are introduced.

1.4 A need for reduced-order nonlinear models

When considering the control of the multi-scale phenomenon of turbulence, it is clear that an accurate reduced-order nonlinear model (as an alternative to direct numerical simulation) would simplify the control problem greatly. At the very least, an efficient reduced-order *representation* of the near-wall turbulent state is probably a necessity if we are ever to attempt to implement an estimator-based control algorithm, as discussed in §2.4, even if the dynamics of such a reduced-order model does not follow closely the dynamics of the full Navier-Stokes system without substantial measurement feedback. Such reduced-order models for turbulent flows have been sought for years, though the suitability of current approaches for providing such models for a *controlled* turbulent flow (for which the dynamics is substantially altered from that of the uncontrolled turbulent flow) is still an open question.

In the framework of a reduced-order model, the movement of the near-wall longitudinal vortices when observed in a cross-flow plane is interpreted as the orbiting of a low-dimensional state. The complete passage of a coherent structure through the cross-flow plane of interest leads to a rapid jump in this state to a different state, representing a modified distribution of near-wall longitudinal vortices. Such a rapid jump between critical points (sometimes referred to in the fluids literature as a so-called "turbulent burst"), followed by a quiescent period in which the flow pattern remains largely unchanged, is referred to in the dynamical systems literature as a heteroclinic cycle. With a good reduced order model, one might hope to characterize the quiescent period, as the longitudinal legs of the near-wall coherent structures convect through a given cross-flow plane. However, it is much more difficult to capture the phase during which the end of a coherent structure passes through the cross-flow plane of interest and a new distribution of longitudinal vortices emerges. To decrease the frequency with which a reduced-order model must adjust to a new arrangement of near-wall longitudinal vortices, it is useful to utilize such models in a reference frame which convects at the average speed of the coherent structures.

The techniques of dynamical systems theory have encountered some success for analyzing and interpreting turbulence dynamics (Aubry *et al.* 1988; Holmes, Lumley, & Berkooz 1996). Due to their large range of spatial and temporal scales, however, turbulent flows are known to have relatively high dimensions in this framework even at fairly low Reynolds numbers, which makes analysis of these systems extremely difficult (Keefe, Moin, & Kim 1992).

An example of one approach for determining reduced-order models is the ongoing work of anatomizing the coherent structures of wall-bounded turbulence using the proper orthogonal decomposition (POD) (Berkooz, Holmes, & Lumley 1993). This decomposition provides a (numerically determined) set of modes which is particularly efficient in representing second-order turbulence statistics near a wall, at least when no control is applied to the flow. However, the equation expressing the evolution of and interaction between these modes is quite complex. Further, it remains to be determined the best way to extract POD modes for a controlled turbulent flow. Some sort of iterative technique, in which the control algorithm and the POD modes are sought simultaneously, might be required in order to extract a set of modes which efficiently captures the energetic structures actually present in the controlled flow. As the controlled flow is not statistically stationary, one might ultimately need a sequence of different POD models/control algorithms to completely relaminarize an initially turbulent flow, with the controller scheduling required based on an (evolving) bulk flow statistic such as total drag or TKE.

As a preliminary example of control using such a reduced-order model, Coller, Holmes, & Lumley (1994) consider the control of a simple model problem (developed by Aubry *et al.* 1988), governed by a two-component equation with dynamics similar to that of a POD model of near-wall longitudinal vortices. This model equation is subjected to random excitation to account (albeit, roughly) for unmodeled system dynamics and disturbances. A strategy is developed and demonstrated which delays heteroclinic transitions in this simple model as long as possible by sensing when the state is near an unstable fixed point and maintaining it there with feedback control for as long as possible. Once the state diverges from this fixed point, presumably due to the significant unmodeled dynamics of the flow (e.g., the passage of the head of a coherent structure), control is turned off until the state approaches the neighborhood of another unstable fixed point. Such a "chaos control" strategy is akin to that proposed by Ott, Grebogi, & Yorke (1990) and implemented in a turbulent channel flow setting by Keefe (1993). Preliminary work in the application of this type of strategy to low Reynolds number turbulent flows is reviewed by Lumley & Blossey (1998). To date, approximately 20% drag reduction has been obtained with this approach in turbulent flows.

1.5 A need for model-based control strategies

The complex, multi-scale nature of turbulent flows have largely thwarted efforts to subdue turbulence with feedback based on either adaptive "black boxes" or on physically-based notions and have frustrated efforts to develop reduced-order models from which effective controls may be determined. We are thus driven to derive turbulence control algorithms directly from the equation known to govern the problem at hand. The balance of this paper describes and demonstrates one approach of determining such control strategies via optimal control theory and iterative direct numerical simulations.

Chapter 2

Optimal and robust control in the predictive control framework

2.1 The seminal idea and an analogy to the game of chess

The general idea of the receding-horizon predictive control setting (as formulated in continuous time) is shown in figure 1. To put this approach into a more intuitive context, and to appreciate better the importance of the (somewhat mathematical) gradient-based optimization approach to the present problem, it is useful at the outset to compare and contrast the present approach to massively-parallel brute-force algorithms recently developed to play the game of chess. The parallels and the shortcomings of this analogy highlight well the problem at hand.

The goal when playing chess is to capture the other player's king through an alternating series of discrete moves with the opponent: at any particular turn, a player has to select one move out of at most thirty or so legal alternatives. Upon first inspection, this task seems quite simple compared to the problem of control of three-dimensional turbulence. Even once the problem is discretized in space and time, the turbulence control problem is generally a much higher-dimensional optimization problem, involving the coordination of a large array of actuators, where the effects of all control actions are intricately coupled via a high-dimensional, nonlinear, chaotic state governed by the Navier-Stokes equation.

To accomplish its optimization, a computer program designed to play the comparatively "simple" game of chess, such as *Deep Blue* (Newborn 1997), must, in the worst case, plan ahead by iteratively examining a tree of possible evolutions of the game several moves into the future[1] (Atkinson 1993). At each step, the program selects that move which leads to the best expected outcome, given that

[1] Note that extensive tables of opening sequences and endgame sequences are also stored in modern chess programs to assist with these phases of the game, though the bulk of the midgame must be examined essentially by brute force.

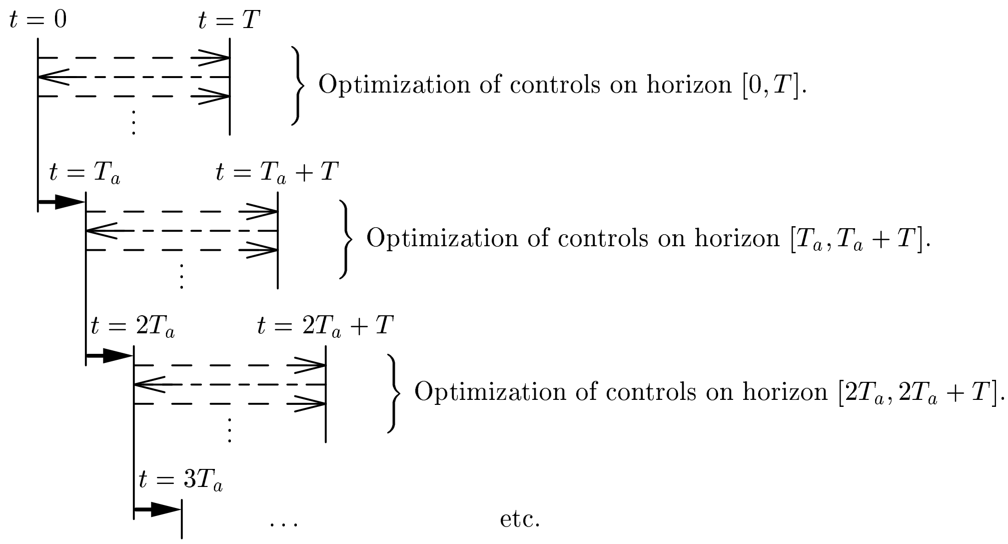

Figure 1: The sequence of events in receding-horizon predictive control. The heavy solid arrows indicate the flow advancement. The evolution of the "actual" flow response to several "test" distribution of controls is explored during the iterative flow prediction (dashed line) and adjoint computation (dot-dashed line) stages, during which the control is optimized by a gradient algorithm. Once this iteration converges, the flow is "advanced" some portion T_a of the period T over which the control was optimized, and the optimization process is begun anew.

the opponent is doing the same, in the spirit of a noncooperative game. The version of *Deep Blue* that defeated Garry Kasparov in 1997 was able to calculate up to 200 billion moves in the three minutes it was allowed to conduct each turn. Even with this extreme number of function evaluations at its disposal on this relatively simple problem, the algorithm was only about an even match with Kasparov's human intuition.

A similar brute-force optimization strategy based on function evaluations alone might be suggested for the problem of turbulence control. In this context, the so-called "genetic algorithms" (Michalewicz 1996) are the primary candidates. The primary strengths of these algorithms are their ease of programming and their ability to minimize pathological functions in which gradient information is of limited usefulness. Such algorithms are effective for low-dimensional optimization problems, even in situations for which the evolution equation governing the system at hand is not available, so long as the number of parameters to be optimized is not very large (Padmanabhan, Bowman, & Powell 1993; Koumoutsakos, Freund, & Parekh 1998). They may also be viable in high-dimensional optimization problems when function evaluations can be performed extremely quickly[2] and/or a very long time is given to conduct the optimization. In the case of the optimization (by

[2] Such is not the case with most direct numerical simulations, but may be realized experimentally for statistically-stationary optimization problems.

biological adaptation) of the drag-reducing ribbed surface on the scales of fast-swimming sharks (see, e.g., Choi, Moin, & Kim 1993 and Bechert *et al.* 1997), the optimization has taken, literally, millions of years. As the present optimization problem is very high dimensional (up to $O(10^7)$ control variables per optimization horizon) and function evaluations (direct numerical simulations) are very expensive, a more efficient optimization strategy is required.

An improved algorithm to the brute-force approach, suitable for optimizing the present problem in a reasonable amount of time, is available because

a.) we know the equation governing the evolution of the present system, and

b.) we can formulate the problem of interest as a functional to be minimized.

Taking these two facts together, we will devise and solve an iterative procedure based on gradient information, derived from an *adjoint field*, to optimize the controls for the desired purpose on the prediction horizon of interest in an efficient manner. Only by exploiting such gradient information can the high-dimensional optimization problem at hand be made tractable. Note that it is desirable that the optimization problems we will formulate be constructed in such a manner that they are as well-conditioned (i.e., non-pathological) as possible in order to make them amenable to efficient gradient-based numerical optimization algorithms. To this end, several different formulations of the present control problem are discussed in §6.

Clearly, in both the chess problem and the turbulence problem, the further into the future one can optimize the problem the better; however, both problems get exponentially harder to optimize as the prediction horizon is increased. Since only intermediate-term optimization is tractable, it is not always the best approach to represent the final objective in the cost functional. In the chess problem, though the final aim is to capture the other player's king, it is most effective to adopt a mid-game strategy of establishing good board position and achieving material advantage. Similarly, if the turbulence control objective is reducing drag, it is found (see §7) that it is most effective along the way to minimize a finite-horizon cost functional related to the turbulent kinetic energy of the flow, since the turbulent transport of momentum is responsible for inducing a substantial portion of the drag in a turbulent flow. In a sense, turbulence is the "cause" and high drag is the "effect", and it is most effective to target the "cause" in the cost functional when optimizations on only intermediate prediction horizons are possible.

In addition, a smart optimization algorithm allows for excursions in the short term if such a strategy leads to a long-term advantage. For example, in chess, a good player is willing to sacrifice a lesser piece if, by so doing, a commanding board position is attained and/or a restoring exchange is forced a few moves later. Similarly, by allowing a turbulence control scheme to increase (temporarily) the turbulent kinetic energy of a flow, a transient may ensue which, eventually, effectively diminishes the strength of the near-wall coherent structures. It is shown in §7 that terminal control strategies, aimed at minimizing the turbulence only at the end of each optimization period, appear to have an advantage over regulation strategies, which penalize excursions of the turbulent kinetic energy over the entire prediction horizon.

2.1.1 Related approaches

The use of adjoint-based techniques to optimize controls for nonlinear systems in the receding-horizon predictive control framework is well developed for both continuous-time and discrete-time problem formulations. References on these topics include: Bryson & Ho (1975), Garci, Prett, & Morari (1989), Mayne, & Michalska (1990), Soeterboek (1992), Clarke (1994), Muske & Edgar (1997), and Sutton & Bitmead (1999). These techniques are related to those used in (essentially time invariant) distributed optimization problems, such as the optimization of bioartificial arteries (Petzold *et al.* 1997), the prediction of bone hardening due to applied periodic loading (Jacobs *et al.* 1997), and the optimization of airfoils for aerodynamic design (Reuther *et al.* 1996).

In the active feedback control setting, the predictive control technique has found broad application and popular acceptance in applications for which the system of interest evolves but slowly, such as in the chemical process industry (Seborg, Edgar, & Mellichamp 1989). In such applications, the system evolves so slowly that it may be considered as "frozen" in time, and a fast computer may be used to predict the evolution of the system many times to determine iteratively the most suitable set of controls to apply to the system over the given time horizon T. As mentioned earlier, given that the governing equation is known and a mathematical statement of the control problem is available, it is a straightforward exercise to determine gradient information with which the controls may be efficiently updated. The predictive control approach is useful, for example, for determining a schedule of controls to switch effectively from one set point in a chemical process to another, while keeping rise time, overshoot, and settling time to a minimum. The predictive control approach is very versatile, and is effective in otherwise problematical systems, including those which are inherently nonlinear, those which contain saturation constraints and rate constraints on the actuators, and those which are characterized by significant time delays between application of the control and measurement of its effects (see, e.g., Yang & Polak 1993).

Note that the present approach is sometimes referred to as Model Predictive Control (MPC) in the controls literature. The "model" of the fluid flow used in the present work is direct numerical simulation, which is essentially an exact evolution of the Navier-Stokes equation governing the system of interest. As the word "model" in the fluids literature generally has the connotation of an *approximate* model, we have, for clarity, chosen to drop the word "model" from our description of the present approach.

2.2 Predictive control optimization in the fluid mechanical setting

Turbulent flows, by most measures, are *not* slowly-evolving systems. In a practical implementation, it is almost always impossible to predict iteratively several possible evolutions of a turbulent flow (resulting from several possible sequences of control application) during a period of time short enough that the actual flow may be considered as "frozen" in time. Thus, it is impossible to implement the predictive control algorithm directly in a practical setting for the problem of turbulence. However, we can perform such a procedure in a computer, where a turbulent flow may be (artificially) "frozen" in time. Such an exercise is not considered as simply an abstract *Gedankenexperiment*, as it allows us to quantify the best possible system performance given a certain class of flow actuation and qualify how optimized controls correlate with the near-wall coherent structures believed to dominate the process of turbulence production in wall-bounded flows. Further, various approaches have been proposed to distill practical feedback schemes from the predictive control approach, as discussed in §2.4. The present exercise is a necessary step in the development of such optimization algorithms for practical feedback control rules.

The mathematical details of optimal control theory applied to the Navier-Stokes equation and other nonlinear PDEs have a long and rich history which will not be expounded upon here. Significant early advances in this area are well documented by Morse & Feshbach (1953), Lions (1968), and Finlayson (1972). After somewhat of a hiatus in this area, there has been a resurgence of interest in the mathematical properties of these approaches, such as existence and uniqueness of solutions and proofs of convergence of proposed numerical algorithms. Abergel & Temam (1990), Gunzburger, Hou, & Svobodny (1990), Sritharan (1991, 1998), Gunzburger (1995), Lagnese, Russell, & White (1995), and Bewley, Temam, & Ziane (1999) discuss several of these recent advances.

Early attempts to implement predictive control with adjoint-based optimization approaches compromised on the length of the prediction horizon, taking $T^+ \lesssim 1$ (Bewley *et al.* 1993; Hill 1993; Lee, Kim, & Choi 1998; etc.). This approach has the dubious distinction of being dubbed the "suboptimal approximation". The main reason for making such an assumption is that it results in control rules which are easy to implement and solve, eliminating the tedious and impractical predictive control framework. Another advantage of this approach is that, by approximating the nonlinear terms with a Taylor series expansion of wall information (Hill 1993) or neglecting the nonlinear terms altogether (Lee, Kim, & Choi 1998), the resulting problem can be solved analytically, resulting in a control scheme in terms of wall information only. Though schemes of this "suboptimal" variety do give drag reductions in the neighborhood of 20% (Bewley *et al.* 1993; Hill 1993; Lee, Kim, & Choi 1998), this approach is recognized to neglect the nonlinear evolution central to the development of turbulent flows, and the importance of taking intermediate prediction horizons which at least partially capture the evolution of the near-wall coherent structures is now readily apparent (see §7).

2.3 Adjoint-based ensemble optimization of practical control algorithms—a preview

The present work is a first step towards developing finite-horizon, adjoint-based techniques for the optimization of practical feedback control rules for turbulent flows of the two types illustrated in figure 2. The (initially undetermined) coefficients of the feedback rules in both configurations may be optimized rigorously with predictive approaches based on the adjoint analysis developed here (Bewley, Moin, & Temam 1996). In this approach, an identical control rule is applied at large ensembles (thousands) of control points on the walls of a representative turbulent flow[3]. The gradient information determined by the adjoint approach is then used to determine the sensitivity of the cost functional to modification of the coefficients in this control rule (rather than modification of the control distribution itself). If the ensemble is large enough with respect to the complexity of the control rule being optimized, optimization via this approach should lead to a set of coefficients which generalizes well to other turbulent flow realizations with similar near-wall dynamics.

In the output feedback configuration, the flow is controlled using computationally inexpensive direct feedback from instantaneous flow measurements. Note that the structure of this feedback rule may be nonlinear and may incorporate a finite impulse response (FIR) filter to account for information from past measurements in the control rule.

In the estimator-based configuration, the filter used effectively establishes a time-evolving estimate of the flow state near the wall, assimilating appropriately the information contained in the available sequence of (noisy) flow measurements. The model used in the estimator may in fact be the full Navier-Stokes equation or (preferably) a reduced-order representation thereof, as discussed earlier. The flow is then controlled with a (possibly nonlinear) control rule based on this flow estimate. It is important that the system model used in the estimator at least roughly model the nonlinear dynamics of the full flow system (Bewley 1999).

In the linear case, the estimation problem and the control problem are linked only when they are optimized in the noncooperative game framework of "robust control", in which a finite component of "worst case" noise is introduced which is maximally detrimental to the control objective (Green & Limebeer 1995). Such an approach is well developed for linear problems, and is referred to as $\mathcal{H}_\infty$ control. Doyle *et al.* (1989) present a compact form of this approach which makes it straightforward to apply to linear problems, as illustrated in Bewley & Liu (1998) for the control of the linear stages of transition. This noncooperative game framework, which (albeit in the brute-force context) is essential to the success of the chess algorithm (which is, in fact, a noncooperative game!), is also useful in the present problem. As discussed in detail in Bewley & Liu (1998), this framework allows feedback gains to be kept to a minimum for components of the system not relevant to the control problem at hand. These reduced feedback gains result in reduced opportunity for improper feedback

[3]As the flow considered is statistically homogeneous in the streamwise and spanwise directions, this approach is reasonable.

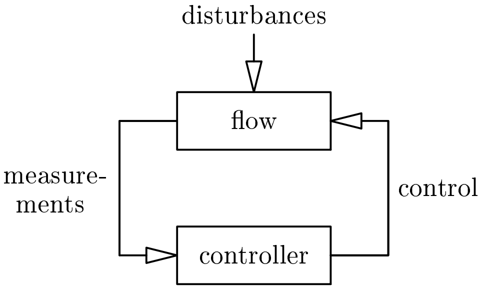

a) Output feedback configuration

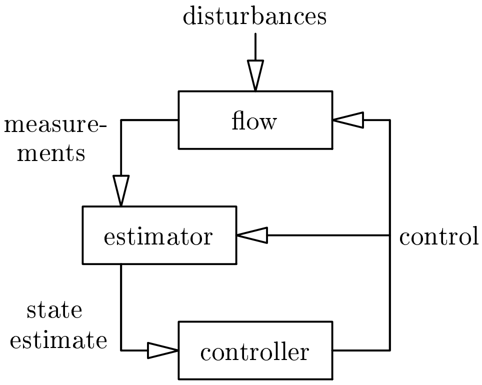

b) Estimator-based configuration

Figure 2: Examples of practical feedback control configurations based on limited noisy flow measurements. The unknown feedback coefficients in both configurations may be optimized numerically with the techniques based on the optimization approach developed in this paper.

to disrupt the closed-loop system.

New methods to apply the robust approach to distributed, fully nonlinear systems such as turbulence have also been mathematically investigated (Bewley, Temam, & Ziane 1999). It appears likely that the robust element in the nonlinear optimization framework will be key to the effective implementation of feedback control to turbulence when only limited noisy measurements are available.

Chapter 3

Governing equation

The problem we consider in the present paper is the control of a fully-developed turbulent channel flow with full flowfield information available to the control algorithm. The flow is governed by the incompressible Navier-Stokes equation inside a three-dimensional rectangular domain Ω with unsteady wall-normal velocity boundary conditions ϕ applied on the walls $\Gamma_2^{\pm}$ as the control, as depicted in figure 3. The extent of the computational domain is chosen to be large enough in the homogeneous directions (x_1 and x_3) that the convenient (though non-physical) periodic boundary conditions applied in these directions have minimal effect on the nature of the near-wall turbulence. This is illustrated qualitatively in figure 4 and quantitatively (by the decay of the spatial correlations of the turbulence to zero well before the edge of the computational domain) in plots such as those represented in figures 5a and 6a. Though this is an idealized geometry, it gives insight into the nature of near-wall turbulence which can later be exploited in more practical configurations, such as the control of a spatially-developing boundary layer with discrete wall-mounted actuators.

Three vector fields are first defined: the flow state $\mathbf{q}$, the flow perturbation state $\mathbf{q}'$, and the adjoint state $\mathbf{q}^*$:

$$\mathbf{q}(\mathbf{x},t) = \begin{pmatrix} p\,(\mathbf{x},t) \\ \mathbf{u}(\mathbf{x},t) \end{pmatrix}, \qquad \mathbf{q}'(\mathbf{x},t) = \begin{pmatrix} p'(\mathbf{x},t) \\ \mathbf{u}'(\mathbf{x},t) \end{pmatrix}, \qquad \mathbf{q}^*(\mathbf{x},t) = \begin{pmatrix} p^*(\mathbf{x},t) \\ \mathbf{u}^*(\mathbf{x},t) \end{pmatrix}.$$

Each of these vector fields is composed of a pressure component and a velocity component, all of which are continuous functions of space, $\mathbf{x}$, and time, t. The velocity components themselves are also vectors, with components in the streamwise direction x_1, the wall-normal direction x_2, and the spanwise direction x_3. Partial differential equations governing all three of these fields will be derived in due course, and the motivation for introducing $\mathbf{q}'$ and $\mathbf{q}^*$ will be given as the need for these fields arises in the control derivation. Only after the control problem has been derived completely

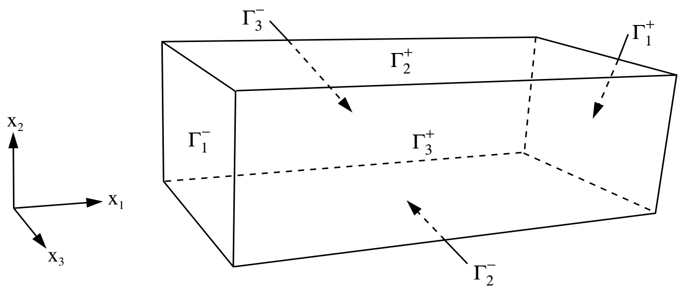

Figure 3: Channel flow geometry. The interior of the domain is denoted Ω and the boundaries of the domain in the x_i direction are denoted $\Gamma_i^{\pm}$. Unsteady wall-normal velocity boundary conditions are applied on the walls $\Gamma_2^{\pm}$ as the control, with periodic boundary conditions applied in the streamwise direction x_1 and spanwise direction x_3. An external pressure gradient P_x is applied to induce a mean flow in the x_1 direction.

in differential form is it discretized in space and time. For the current three-dimensional nonlinear problem (which necessitates a mixture of implicit and multi-step explicit schemes for accurate time advancement, with incompressibility enforced by an involved fractional step algorithm), this approach (referred to as "optimize then discretize") is found to yield adjoint systems which are the easiest to understand and to code. For simpler systems, such as the one-dimensional linear problem of transition control examined in Bewley & Liu (1998), the discrete control expressions derived from the discrete form of the governing equation are found to be tractable (a setting referred to as "discretize then optimize"). Note that the processes of optimization and discretization, in general, do not commute, and thus these two approaches are not necessarily equivalent even upon refinement of the space/time grid (Vogel & Wade 1995).

The governing equation may be written functionally as

$$\mathcal{N}(\mathbf{q}) = \begin{pmatrix} 0 \\ -\mathbf{r}\, P_x(\mathbf{x}, t) \end{pmatrix} \qquad \text{in } \Omega, \tag{3.1a}$$

where $\mathcal{N}(\mathbf{q})$ is defined below in (3.3) and $\mathbf{r}$ is a unit vector in the x_1 direction. The boundary conditions on the state $\mathbf{q}$ are periodic in the streamwise and spanwise directions, and a wall-normal control velocity is distributed over the walls such that

$$\mathbf{u} = -\phi\, \mathbf{n} \qquad \text{on } \Gamma_2^{\pm}, \tag{3.1b}$$

where $\mathbf{n}$ is the unit outward normal to the boundary $\partial\Omega$. Initial conditions on the velocity are prescribed such that

$$\mathbf{u} = \mathbf{u}_0 \qquad \text{at } t = 0. \tag{3.1c}$$

The flow is sustained by an externally-applied[1] mean pressure gradient (per unit mass) P_x in the streamwise direction; this mean pressure gradient may be either a fixed constant or modified at each time step in order to maintain a constant mass flux through the channel. The control ϕ is constrained to inject zero net mass at the walls, such that

$$\int_{\Gamma_2^+} \phi \, d\mathbf{x} = \int_{\Gamma_2^-} \phi \, d\mathbf{x} = 0 \qquad \forall t. \tag{3.2}$$

Note that boundary conditions and initial conditions on the pressure p are not needed for a well-posed problem formulation. Mathematically speaking (Temam 1984; Abergel & Temam 1990; Bewley, Temam, & Ziane 1999), the control derivation presented in this paper may be conducted on a divergence free submanifold of $(L^2(\Omega))^3$, where the pressure has been removed from the governing equation using the Leray-Helmholtz formulation of the Navier-Stokes equation. This "abstract form" of the incompressible Navier-Stokes equation facilitates mathematical analysis. In the present paper, however, we will retain the pressure in our derivations; this more intuitive form both eases the treatment of inhomogeneous boundary conditions and facilitates the direct extension of the present analysis to compressible flows, as discussed in Appendix B.

For clarity, all differential equations are written in operator form in this discussion, with these operators defined when first introduced. The (nonlinear) Navier-Stokes operator for the present case, in which the flow is assumed to have uniform density and viscosity, is given by

$$\mathcal{N}(\mathbf{q}) = \begin{pmatrix} \dfrac{\partial u_j}{\partial x_j} \\ \dfrac{\partial u_i}{\partial t} + \dfrac{\partial u_j u_i}{\partial x_j} - \nu \dfrac{\partial^2 u_i}{\partial x_j^2} + \dfrac{\partial p}{\partial x_i} \end{pmatrix}. \tag{3.3}$$

Note that p is the pressure divided by the density and ν is the kinematic viscosity. Define also $\overline{\tau_w}/\rho \triangleq -\nu \, \partial\overline{u_1}/\partial n|_{\Gamma_2^\pm}$ as the mean skin friction on the wall for the uncontrolled turbulent channel flow divided by the density (averaged in space and time), $u_\tau \triangleq (\overline{\tau_w}/\rho)^{1/2}$ as the mean friction velocity, δ as the channel half-width, and $Re_\tau \triangleq u_\tau\delta/\nu$ as the Reynolds number based on the mean friction velocity and the channel half width. The flows considered in this work are constant mass

[1] By this, we mean that the mean pressure gradient is a quantity which is considered as constant when computing the adjoint field $\mathbf{q}^*$ and the gradient $\mathscr{D}\mathcal{J}/\mathscr{D}\phi$. The opposite viewpoint may also be taken in this framework; namely, the mean pressure gradient may be taken as a (scalar) variable and included together with the distributed field variable $\mathbf{q}$ in the optimization process. In this framework, an integral constant mass flux constraint is included together with the PDE governing the system (the Navier-Stokes equation) in the governing equation set. This formulation is a bit more cumbersome and leads to essentially the same results.

flux flows at $Re_\tau = 100$ and $Re_\tau = 180$. (This corresponds to Reynolds numbers based on the mean centreline velocity of the uncontrolled flow, $Re_c = u_c\,\delta/\nu$, of $Re_c = 1712$ and $Re_c = 3247$, and to Reynolds numbers based on the bulk velocity, $Re_B = u_B\,\delta/\nu$, of $Re_B = 1429$ and $Re_B = 2797$.) All velocities are normalized by the friction velocity u_τ, and therefore may also be marked with a $(^+)$ superscript. All lengths are normalized by δ unless marked with a $(^+)$ superscript, in which case they are normalized by the wall unit ν/u_τ. All times are normalized by δ/u_τ unless marked with a $(^+)$ superscript, in which case they are normalized by ν/u_τ^2. Note that, with this normalization, $\nu = 1/Re_\tau$ in the above equation for $\mathcal{N}(\mathbf{q})$.

Chapter 4

Numerical method

The control formulations discussed in §2 (and to be presented in greater detail in §6) were tested in direct numerical simulations of constant mass flux, fully-developed turbulent channel flows at both $Re_\tau = 100$ and $Re_\tau = 180$. The coarse-grid, inexpensive lower Reynolds number simulations were used to perform parametric studies to determine the appropriate range of parameters to test more accurately on a finer grid at the higher Reynolds number. In the present work, Fourier transform techniques are used to compute spatial derivatives in the homogeneous directions with 3/2 dealiasing of the nonlinear terms, and an exactly energy-conserving second-order finite difference scheme is used to compute spatial derivatives on the stretched grid in the wall-normal direction (see Appendix C). Very fine grid resolution is required near the wall to resolve the shear layer; the mesh is fairly fine even up to the centre of the domain because the second-order difference scheme used to compute the derivatives in this direction is numerically dispersive. The computational grid is staggered in the wall-normal direction to prevent decoupling of the even and odd modes of the pressure.

A substantially different numerical method was needed in the present computations than was used in, for example, the fully spectral code of Kim, Moin, & Moser (1987), in order to best facilitate implementation of the wall-normal velocity boundary conditions. The flow is advanced in time using an explicit low-storage third-order Runge-Kutta method for all terms involving x_1 and x_3 derivatives and an implicit Crank-Nicholson method at each Runge-Kutta substep for all terms involving x_2 derivatives, with a method based on that of Akselvoll and Moin (1995). A temporal discretization implicit in the x_2 derivatives is necessary to mitigate the CFL time step restriction when control is applied, as the control fluid at the wall is directed in the x_2 direction, which is precisely the region and direction in which the mesh must be refined most to resolve the shear layer. Unfortunately, this implicit time advancement necessitated the use of a finite-difference scheme in the wall-normal direction rather than the (more accurate) Chebyshev approach.

For the $Re_\tau = 180$ simulations, the number of Fourier modes used[1] is $170 \times 129 \times 170$ in the

[1]The number of modes used in the homogeneous directions for the fast Fourier transforms (FFTs), which is

x_1, x_2, and x_3 directions respectively (i.e. $256 \times 129 \times 256$ dealiased collocation points), and the size of the computational domain in wall units is $L_1^+ = 2260$, $L_2^+ = 360$, $L_3^+ = 1130$. The resulting effective grid resolution in the streamwise and spanwise directions (on collocation points determined without the extra $3/2$ padding) is $\Delta x_1^+ = 13$, $\Delta x_3^+ = 7$. Hyperbolic tangent stretching of the grid is used in the wall-normal direction, resulting in a grid spacing of $\Delta x_2^+ = 0.6$ adjacent to the wall and $\Delta x_2^+ = 5.2$ in the centre of the channel.

For the $Re_\tau = 100$ simulations, the number of Fourier modes used[1] is $42 \times 65 \times 42$ (i.e. $64 \times 65 \times 64$ dealiased collocation points), and the size of the computational domain is $L_1^+ = 1260$, $L_2^+ = 200$, $L_3^+ = 420$. The resulting effective grid resolution in the streamwise and spanwise directions is $\Delta x_1^+ = 30$, $\Delta x_3^+ = 10$. The wall-normal grid spacing is $\Delta x_2^+ = 0.7$ adjacent to the wall and $\Delta x_2^+ = 5.8$ in the centre of the channel.

expanded by a factor of $3/2$ to dealias the nonlinear terms, is an even power of two, which results in maximum efficiency of the FFT routines.

Chapter 5

Dynamics and statistics of uncontrolled system

The nature of a turbulent flow is well characterized by observing the fluid at various points throughout the channel in a reference frame which moves with the local velocity. In this reference frame, the point under consideration is a critical point, as the local streamline slope is indeterminate. Thus, a critical point analysis of the type discussed by Perry & Chong (1987), Chong, Perry, & Cantwell (1990), and Blackburn, Mansour, & Cantwell (1996) is appropriate. A single scalar quantity D, the discriminant of the velocity gradient tensor, provides a useful identification of regions in the flow which, in this context, are "focus" in nature. Such focus regions roughly correspond to "vortex-type" regions in a turbulent flowfield, though this description is only pointwise in nature.

The velocity gradient tensor discussed in this work is defined in wall units $A_{ij} \triangleq \partial u_i^+/\partial x_j^+$. The second and third invariants of A are $Q \triangleq \left\{[\mathrm{tr}(A)]^2 - \mathrm{tr}(A^2)\right\}/2$ and $R \triangleq -\det(A)$. The discriminant of the velocity gradient tensor is given by $D = (27/4)R^2 + Q^3$. Regions with $D > 0$ are characterized by a velocity gradient tensor with one real and two complex eigenvalues (and thus a swirling, vortex-type motion in the Lagrangian reference frame discussed above), whereas regions with $D \leq 0$ are characterized by three real eigenvalues. As illustrated in figure 4, visualizations of isosurfaces of the discriminant of the velocity gradient tensor provide a handy identification technique for the location of "vortex-type" motions in the turbulent flow. For clarity, the visualizations of the discriminant presented in this work identify only regions of positive discriminant greater than a small threshold value $D > D_{\mathrm{threshold}}$, where $D_{\mathrm{threshold}} = 10^{-5}$.

As direct numerical simulations produce a tremendous amount of data, it is important to analyze relevant statistics of the flowfields they generate, in addition to the instantaneous visualizations, in order to understand better the phenomena taking place in a quantitative sense and how these integral measures of the turbulence are modified by the application of control. Gross flowfield

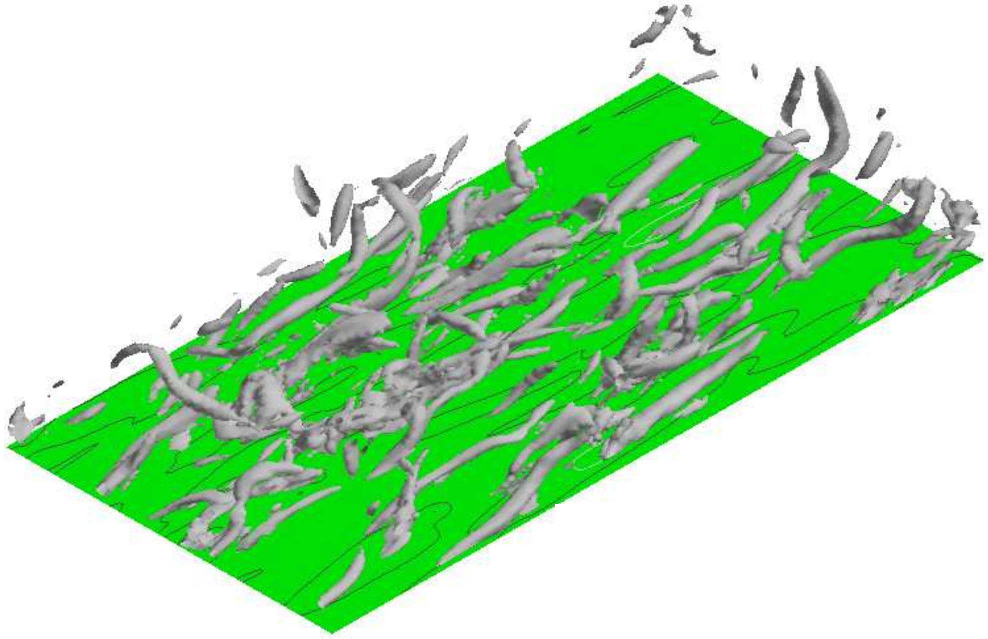

(a) Three-dimensional visualization.

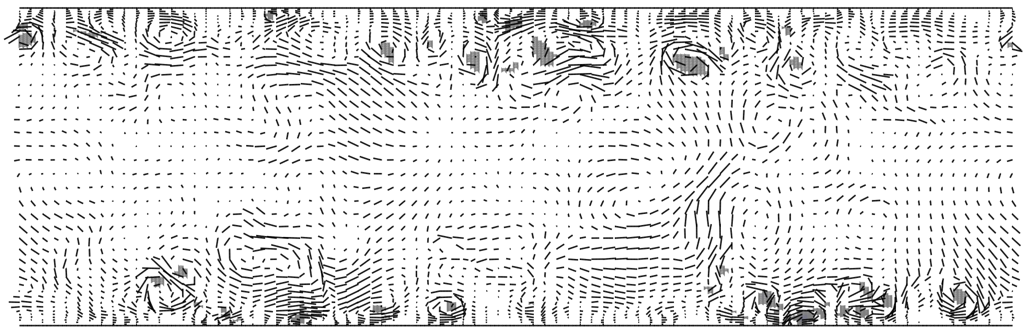

(b) Crossflow visualization.

Figure 4: Fully developed turbulent channel flow realization at $Re_\tau = 180$, no control. Regions of the flow with positive discriminant $D > D_{\text{threshold}}$ are shaded, indicating fluid motion which, in a pointwise sense, is vortical in nature. In the three-dimensional visualization, the flow is from lower left to upper right and, for clarity, only one quarter of the lower half of the domain Ω used in the computations (see figure 3) is shown. In the crossflow visualization, for clarity, the crossflow velocity vectors (indicated by the arrows) are marked on only one ninth of the gridpoints used in the computations in this crossflow plane.

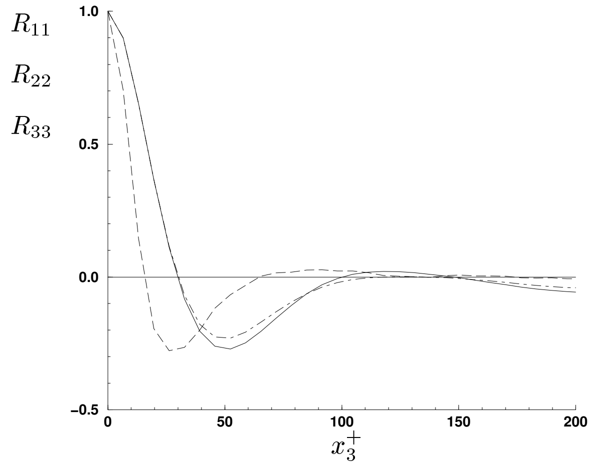

(a) Spanwise two-point correlations at $x_2^+ = 5.4$: ——, R_{11}; - - - -, R_{22}; —-—, R_{33}.

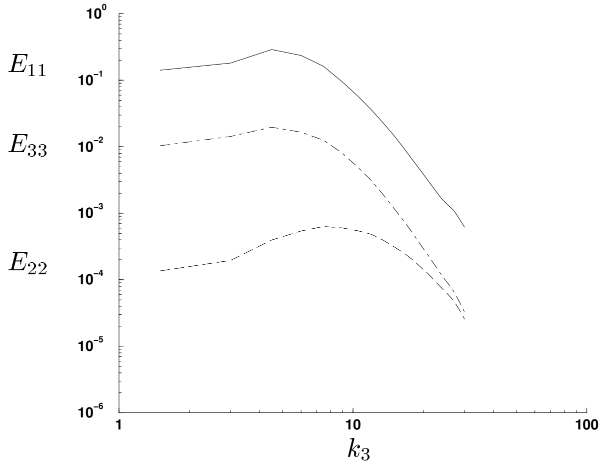

(b) Spanwise one-dimensional energy spectra at $x_2^+ = 5.4$: ——, E_{11}; - - - -, E_{22}; —-—, E_{33}.

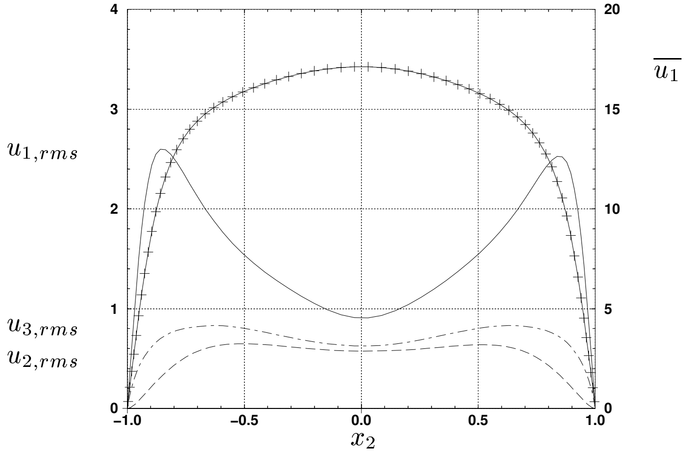

(c) Profiles of RMS velocity fluctuations (scale at left): ——, *$u_{1,rms}$*; - - - -, *$u_{2,rms}$*; —-—, *$u_{3,rms}$*, *and mean velocity (scale at right):* +, $\overline{u_1}$.

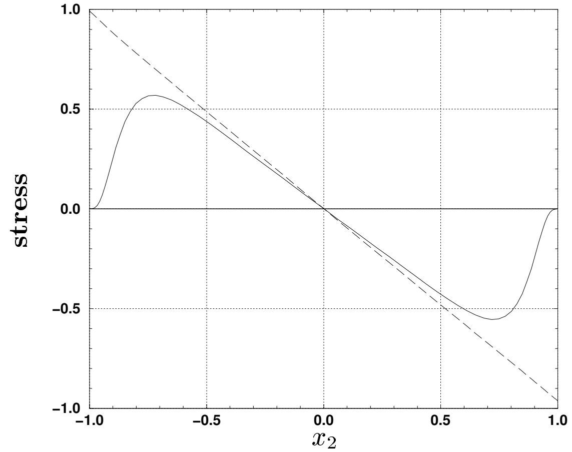

(d) Profiles of Reynolds stress and total stress: ——, *Reynolds stress* $-\overline{u_1 u_2}$; - - - -, *total stress* $-\overline{u_1 u_2} + \nu\, \partial \overline{u_1} / \partial x_2$.

Figure 5: Selected time-averaged statistics of the uncontrolled turbulent channel flow at $Re_\tau = 100$.

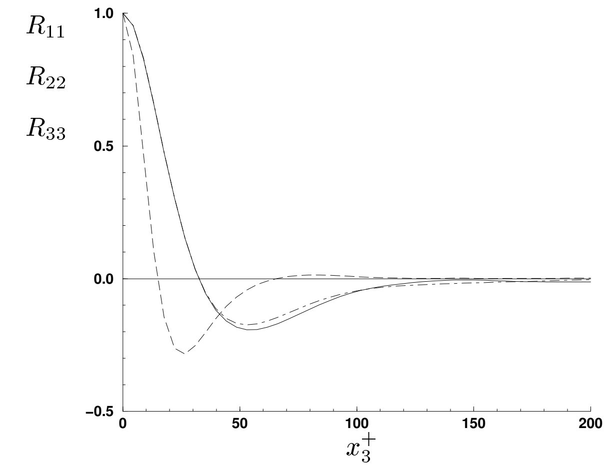

(a) Spanwise two-point correlations at $x_2^+ = 5.4$: ——, R_{11}; - - - -, R_{22}; —·—, R_{33}.

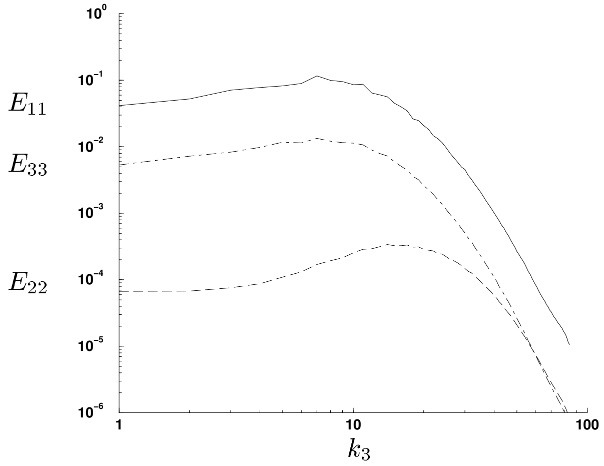

(b) Spanwise one-dimensional energy spectra at $x_2^+ = 5.4$: ——, E_{11}; - - - -, E_{22}; —·—, E_{33}.

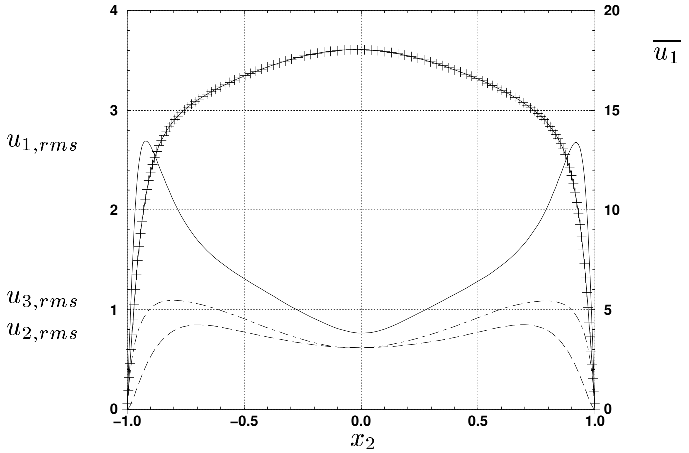

(c) Profiles of RMS velocity fluctuations (scale at left): ——, $u_{1,rms}$; - - - -, $u_{2,rms}$; —·—, $u_{3,rms}$, *and mean velocity (scale at right):* +, $\overline{u_1}$.

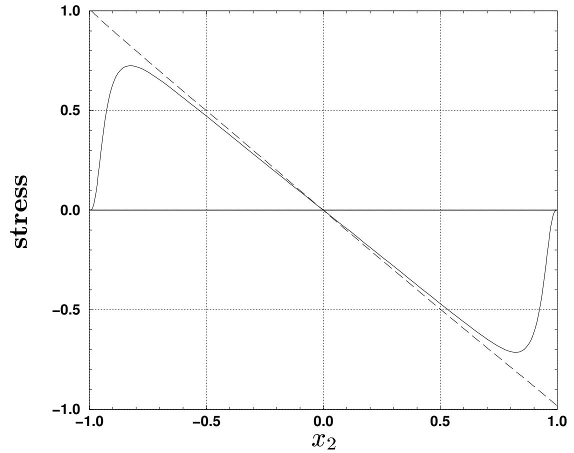

(d) Profiles of Reynolds stress and total stress: ——, *Reynolds stress* $-\overline{u_1 u_2}$; - - - -, *total stress* $-\overline{u_1 u_2} + \nu\, \partial \overline{u_1} / \partial x_2$.

Figure 6: Selected time-averaged statistics of the uncontrolled turbulent channel flow at $Re_\tau = 180$.

statistics useful for monitoring the time evolution of the flow include the total drag and the turbulent kinetic energy (TKE). The statistics used in the present work to examine the variation of the turbulence with distance from the wall x_2 are the mean velocity $\overline{u_1}$, the root-mean-square velocity fluctuations $u_{i,rms}$, the Reynolds stress $-\overline{u_1 u_2}$, the total stress $-\overline{u_1 u_2} + \nu\, \partial \overline{u_1} / \partial x_2$, and the two-point correlations $R_{ij}(\mathbf{r}) \triangleq \overline{u_i(\mathbf{x})\, u_j(\mathbf{x} + \mathbf{r})}$ and their Fourier transform, the spectra $E_{ij}(\mathbf{k})$. Note that the overbar $\overline{(\;)}$ implies averages in the homogeneous directions x_1 and x_3 and, when the flow is statistically stationary, in time. At times we will distinguish the fluctuating component of the flow $\mathbf{v}$ separately from the mean component $\overline{\mathbf{u}}$ such that $\mathbf{u} = \overline{\mathbf{u}} + \mathbf{v}$. Further discussion of these statistics and their behaviour in uncontrolled turbulent channel at $Re_\tau = 180$ may be found in Kim, Moin, & Moser (1987). Selected statistics from the present computations at $Re_\tau = 100$ and $Re_\tau = 180$ are shown in figures 5 and 6. Quantitative comparison of the $Re_\tau = 180$ statistics reported in figure 6 with the benchmark computations of Kim, Moin, & Moser (1987) indicate that the numerical method used in the present computations is sufficiently accurate.

Chapter 6

Application of optimal control theory to incompressible turbulence

The present chapter briefly derives the control approach used, without getting into the mathematics regarding the rigorous proofs of existence and uniqueness of the solution to the control problem or the convergence of the numerical algorithm. The notations are adapted from Abergel & Temam (1990) and Bewley, Temam, & Ziane (1999), to which readers are referred for discussions regarding these mathematical issues and the generalization to the robust control (i.e., noncooperative game) setting.

6.1 Statement of physical problem: definition of cost functional

The optimal control problem is essentially a problem of economics; the first step in solving it is to represent the problem of interest as a cost functional, $\mathcal{J}(\phi)$, to be minimized[1]. The performance of the control algorithm for this type of problem is quite sensitive to the cost functional definition, and thus this topic warrants a detailed analysis in the context of the flow physics under consideration. In the present problem, control ϕ is to be applied to minimize the drag averaged over a representative wall section and a long time horizon using the least amount of control effort possible. At present,

[1] In the approach taken here, the state equation is, effectively, taken into account in the cost functional $\mathcal{J}(\phi)$, and the minimization is performed with respect to the control variable ϕ alone. Another approach, sometimes referred to as the "all at once" approach, is to write the cost functional as $\mathcal{J}(\mathbf{u}, \phi)$ and to write the state equation separately, applying this equation as a feasibility constraint on the state $\mathbf{u}$ rather than incorporating it when computing the gradient of the cost functional (Heinkenschloss 1997). The former approach appears to be more easily managed numerically in systems with very large state dimension.

it appears as if optimization of the nonlinear Navier-Stokes control problem over an infinite time horizon, which would require the solution of a very difficult Hamilton-Jacobi-Bellman (HJB) problem in infinite dimension (Sritharan 1991), is computationally intractable. However, optimizations on intermediate time horizons (i.e., $T^+ \approx O(25)$) certainly are tractable. Thus, we must choose at the outset a "compromise" time horizon over which we will determine controls which optimize the given objective; without loss of generality, let us consider the optimization horizon $(0, T)$.

Case (a): minimization of drag

A relevant cost functional for the minimization of drag on the walls $\Gamma_2^{\pm}$ and over the horizon $(0, T)$ with finite control effort is

$$\mathcal{J}_{\text{DRAG}}(\phi) = -d_1 \int_0^T \int_{\Gamma_2^{\pm}} \nu \frac{\partial u_1(\phi)}{\partial n} \, d\mathbf{x} \, dt + \frac{\ell^2}{2} \int_0^T \int_{\Gamma_2^{\pm}} \phi^2 \, d\mathbf{x} \, dt.$$

The first term is a measure of exactly that quantity we would like to minimize[2]: in this case, the drag due to skin-friction (note that the negative sign is needed because $\partial/\partial n \triangleq \mathbf{n} \cdot \nabla$, where $\mathbf{n}$ is defined as an *outward* facing normal). The second term is a measure of the magnitude of the control. These quantities are integrated over the wall section and time period under consideration and weighted together with a factor ℓ^2, which represents the price of the control. This quantity is small if the control is "cheap" (which reduces the significance of the latter term and generally results in greater control effort), and large if applying control is "expensive".

Dimensional constants d_i, which are the appropriate functions of the kinematic viscosity ν, the channel half-width δ, and the friction velocity u_τ, are included in all cost functionals we will consider simply to make them dimensionally consistent.

Case (b): regulation of turbulent kinetic energy

As only an intermediate value of T can be afforded, minimization of a cost functional representing exactly the quantity of interest (drag) is not necessarily the most effective means of reducing the quantity of interest over the long term (as $t \to \infty$). As discussed earlier, turbulence causes wall-normal convective transport in the near-wall region which, in turn, increases the drag, heat transport, and scalar mixing in the flow. It is thus reasonable for the cost functional to target the turbulence (the "cause") over each finite optimization horizon rather than the drag increase due to the turbulence (the "effect"). More precisely, such a cost functional might target the time-averaged value of the

[2]Note that the drag reduction problem is a minimization problem, not a regulation problem: solutions in which the first term of $\mathcal{J}_{\text{DRAG}}$ are negative, if they exist, are preferred over those in which this term is zero. It is shown in Bewley, Temam, & Ziane (1999) that posing this type of cost functional (linear in the flow variable rather than quadratic in the flow variable) in no way hampers the proofs of existence and uniqueness of the solution of the control problem.

turbulent kinetic energy (TKE); a relevant cost functional for this formulation is[3]

$$\mathcal{J}_{\text{TKE(reg)}}(\phi) = \frac{d_2}{2}\int_0^T\int_\Omega |\mathbf{u}(\phi)|^2\,d\mathbf{x}\,dt + \frac{\ell^2}{2}\int_0^T\int_{\Gamma_2^\pm}\phi^2\,d\mathbf{x}\,dt.$$

Case (c): regulation of enstrophy

Among mathematical audiences, regulation of the square of the vorticity (i.e., the enstrophy) is sometimes preferred to the regulation of the turbulent kinetic energy. This preference is well-founded mathematically, as:

1. The Poincaré inequality implies that regulation of enstrophy (or the H^1-norm of the turbulent field) directly results in regulation of turbulent kinetic energy (the L^2-norm of the turbulent field). Mathematically speaking, in a continuous formulation, the converse is not necessarily true (though, once discretized, the two norms are "equivalent" up to a very large constant).
2. The Sobolev inequalities used for bounding the influence of the nonlinear term on a system governed by the Navier-Stokes equation are related to the H^1-norm of the turbulent field.

The cost functional appropriate for enstrophy regulation is

$$\mathcal{J}_{\text{ENS(reg)}}(\phi) = \frac{d_3}{2}\int_0^T\int_\Omega |\nabla\times\mathbf{u}(\phi)|^2\,d\mathbf{x}\,dt + \frac{\ell^2}{2}\int_0^T\int_{\Gamma_2^\pm}\phi^2\,d\mathbf{x}\,dt.$$

For the special case of locally-isotropic turbulence, there is a particularly simple relationship between the one-dimensional energy spectra and the one-dimensional enstrophy spectra, as shown in figure 7.

On physical grounds, it may be argued that controlling the turbulent kinetic energy is more effective than controlling the enstrophy. The explanation for this, at least in homogeneous isotropic turbulence, is classical (see figure 7): the low wavenumbers of turbulence generally feed the high wavenumbers, where the turbulent kinetic energy is effectively dissipated by viscosity. In this well-known "turbulent cascade", it is the low wave numbers that acquire the turbulent kinetic energy from the energy of the mean flow, and thus it is those which should be targeted by the cost functional. Using enstrophy in the cost functional, however, effectively weights the high wavenumbers of the turbulence spectrum by a factor of k^2. Further, the turbulent cascade of energy from the low wavenumbers to the high wavenumbers takes a finite amount of time which may not be small with respect to the optimization horizons T^+ which can be afforded in the simulations. Thus, for intermediate optimization horizons, $T^+ \approx O(25)$, perhaps one may identify the large spatial scales

[3]Note that, strictly speaking, $J_{\text{TKE(reg)}}(\phi)$ is influenced both by the turbulent kinetic energy $\int_0^T\int_\Omega |\mathbf{v}(\phi)|^2\,d\mathbf{x}\,dt$ and the effect of the mean field, $\int_0^T\int_\Omega |\bar{\mathbf{u}}(\phi)|^2\,d\mathbf{x}\,dt$. It was found in the present study (apparently due to the zero-mass-flux constraint (3.2)) that formulations based on $\int_0^T\int_\Omega |\mathbf{v}(\phi)|^2\,d\mathbf{x}\,dt$ and those based on $\int_0^T\int_\Omega |\mathbf{u}(\phi)|^2\,d\mathbf{x}\,dt$ give essentially identical results.

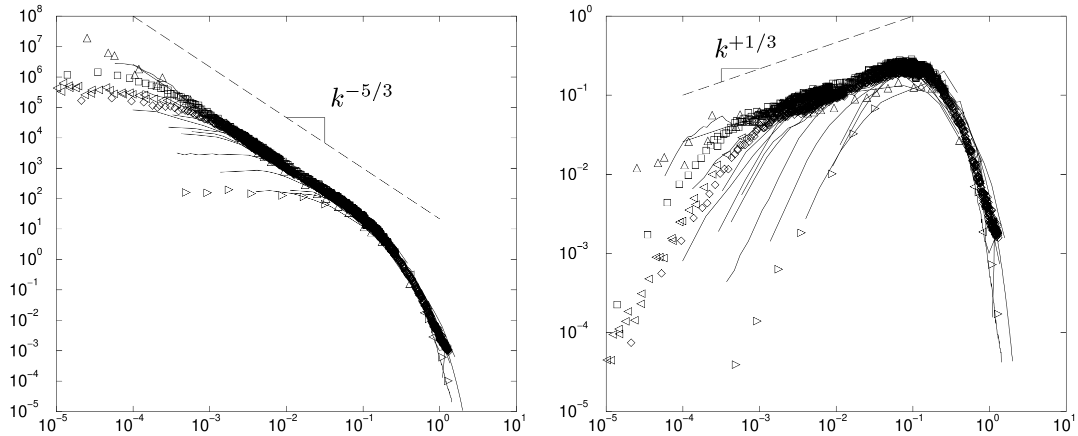

a) 1D energy spectra, $\frac{1}{2}E_{ii}(k)$ *vs. k.* *b) 1D enstrophy spectra,* $\frac{k^2}{2}E_{ii}(k)$ *vs. k.*

Figure 7: Kolmogorov's universal scaling for locally isotropic one-dimensional spectra, from Saddoughi & Veeravalli (1994), for a variety of different turbulent flows; see Saddoughi & Veeravalli (1994) for descriptions of the various different experiments reported in this figure and discussion of the important effects of nonisotropy. A common explanation of turbulence is that turbulent energy is extracted from the mean-flow kinetic energy or potential energy at the low wave numbers (large spatial scales), this energy cascades through the "inertial range" by a vortex stretching phenomenon which transfers energy to higher wavenumbers, and the energy is ultimately dissipated by viscosity at the high wave numbers (small spatial scales). The higher the Reynolds number, the longer this inertial range. As the energy cascade is largely unidirectional, the ultimate rate of turbulence dissipation at the small spatial scales is effectively set by the behavior of the turbulence at the large spatial scales. As indicated in this figure, consideration of the energy in the cost functional focuses control effort primarily on the low wave numbers of the turbulence spectrum, where the "driving mechanisms" for turbulence lie, whereas consideration of the enstrophy in the cost functional focuses control effort on the high wave numbers of the turbulence spectrum, where the turbulence is dissipated.

of the turbulence as the "cause" of the phenomena of interest and therefore favour cost functionals which emphasize those. In addition, formulations derived from enstrophy-based cost functionals, which focus on the turbulence at the dissipation scales, require much smaller actuators than formulations derived from TKE-based cost functionals, which focus on the largest coherent motions of the turbulence. Such actuators might be much more challenging to build. These arguments lend favour to TKE-based strategies over enstrophy-based strategies despite the mathematical preference (based on the Poincaré and Sobolev inequalities) to the contrary.

Case (d): regulation of large-scale and intermediate-scale structures

Due to considerations of both the physics of the phenomena at hand and its realization in hardware, we have argued that it might be better to control the large scales of turbulence rather than the small scales. We now show how this line of reasoning may be pursued even further. The idea is to select for the cost functional definition *lower* norms (e.g., H^{-1}, H^{-2}, etc.) on the flow term and *higher* norms (e.g., H^1, H^2, etc.) on the control term. This is now illustrated with a single example:

$$\mathcal{J}_{\text{LARGE(reg)}}(\phi) = -\frac{d_4}{2}\int_0^T\int_\Omega \mathbf{u}(\phi)\cdot\Delta^{-1}\mathbf{u}(\phi)\,d\mathbf{x}\,dt - \frac{\ell^2}{2}\int_0^T\int_{\Gamma_2^\pm}\phi\,\Delta\phi\,d\mathbf{x}\,dt.$$

Note that the term $\xi \triangleq \Delta^{-1}\mathbf{u}$ is easily found by solving a Poisson equation $\mathbf{u} = \Delta\xi$ with appropriate boundary conditions.

Effectively, such a cost functional targets a "smoothed" version of the velocity field $\mathbf{u}$, weighting most heavily the low spatial wavenumbers of the velocity field, while it penalizes the component of the control ϕ which is not smooth, weighting most heavily the high spatial wavenumbers of the control. Control formulations based on cost functionals with even greater emphasis on the large-scale structures follow in a natural manner from this example by taking higher powers of $(-\Delta)$, and are left as an exercise to the reader. Note that this smoothing can also be extended to the temporal fluctuations by replacing the spatial operators $(-\Delta)$ above with the operator $(\partial/\partial t - \nu\Delta)$; this particular type of smoothing is motivated by the linear terms of the Navier-Stokes equation itself.

In a turbulent channel flow at statistical equilibrium, the equation expressing the production, redistribution, and dissipation of the turbulent kinetic energy, referred to as the turbulent energy budget (Tennekes & Lumley 1972), is

$$\frac{\partial}{\partial x_2}\underbrace{\Big(\overline{v_2\,p} + \frac{1}{2}\overline{v_i\,v_i\,v_2} - 2\nu\,\overline{v_i\,s_{i2}}\Big)}_{\text{energy flux}} = \underbrace{-\overline{v_1\,v_2}\,\frac{\partial\overline{u_1}}{\partial x_2}}_{\mathscr{P}} \underbrace{-\,2\nu\,\overline{s_{ij}\,s_{ij}}}_{\epsilon},$$

where $s_{ij} \triangleq 1/2\,(\partial v_i/\partial x_j + \partial v_i/\partial x_j)$ and $v_i = u_i - \overline{u_i}$ denotes the fluctuating components of the velocity field. The energy flux terms serve to redistribute the turbulent energy from one point in the flow to another. The "production" term $\mathscr{P}$ normally extracts energy from the mean flow $\overline{u_1}$ to "feed" the turbulent energy cascade, whereas the viscous dissipation term ϵ dissipates energy from the turbulent cascade to the local environment by molecular (viscous) heating. The variation of the excess of production minus dissipation as a function of distance from the wall is shown in figure 8.

A substantial counter-argument to that for control of primarily the large scales of the turbulence may now be made for the case of wall-bounded turbulence treated in the present paper. The production of turbulence at the length scales of the coherent structures in the "inner layer" near the wall ($x_2^+ \lesssim 60$) is thought by some to have important communication with the larger scales in the outer layer via an "inverse cascade" of energy[4] (Jimenez 1999). As illustrated in figures 5a

[4] Note that a convincing argument can be made about the importance of the cascade of energy from small scales to large scales in turbulent flows in general. Gibson (1996) observes that in most flows of engineering interest (homogeneous isotropic turbulence being the notable exception), vorticity is introduced into irrotational regions in the flow at the small viscous scales through thin shear layers. If "turbulence" is defined as the region in the flow

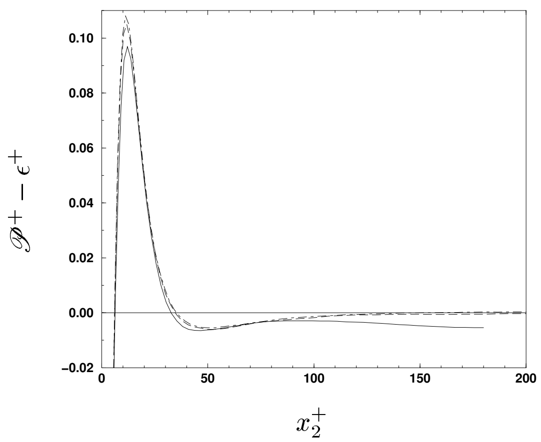

Figure 8: Excess energy production, $\mathscr{P} - \epsilon$, in wall units, as a function of distance from the wall. Data compiled by Jimenez (1999), for uncontrolled turbulent channel flows at: ——, $Re_\tau = 180$; - - - - , $Re_\tau = 395$; — - —, $Re_\tau = 590$; see Jimenez (1999) for descriptions of the various different computations reported in this figure.

and 6a, there is a clear "coherent-structure scale" to the turbulence near the wall of about 50 wall units which (at least, at the higher Reynolds numbers of engineering significance) certainly must be considered as intermediate between the large outer scales and the small dissipation scales. As shown in the $\mathscr{P} - \epsilon$ spike of figure 8 near $x_2^+ \approx 12$, it is this near-wall turbulence which dominates the turbulence production in the turbulent energy budget. This observation extends at least over the limited range of Reynolds numbers reported in the DNS results compiled in this figure. One may therefore hypothesize that the coherent structures themselves are a primary "cause" of the entire spectrum of wall-bounded turbulence, and target the flow perturbations at the specific length scale of these flow structures by employing a "bandpass filter" of sorts. A very simple and algebraically convenient form of such a bandpass filter may be defined such that

$$\mathscr{J}_{\text{INT(reg)}}(\phi) = -\frac{d_5}{2}\int_0^T\int_\Omega \mathbf{u}(\phi)\cdot\Delta_B^{-1}\mathbf{u}(\phi)\,d\mathbf{x}\,dt - \frac{\ell^2}{2}\int_0^T\int_{\Gamma_2^\pm}\phi\,\Delta_B\phi\,d\mathbf{x}\,dt.$$

where

$$\Delta_B = \Delta_S + \Delta_S^{-1} \qquad \text{with} \qquad \Delta_S = L_c^2\Delta \qquad \text{and} \qquad L_c^+ = 50.$$

To motivate the use of such a filter, note that, in a spectral direction, the influence of this filter on the Fourier transform of the velocity field is $\sim k^2/(k^4 + k_c^4)$, a function which is small for both large

where inertial forces ($\mathbf{v}\times\boldsymbol{\omega}$) dominate viscous forces, then the irrotational regions of the flow ($\boldsymbol{\omega} = \mathbf{0}$) must certainly be described as "non-turbulent", and the importance of the so-called "inverse cascade" (from small scales to large scales) in the overall energy budget is readily apparent.

k and small k and peaks at the wavenumber of interest, k_c, of the near-wall coherent structures. As for the large-scale filter, powers of $(-\Delta_B)$ may be used for faster roll-off away from the spatial wavenumber of interest.

For high Reynolds number flows, a counter-argument may be made to that for the control of the coherent-structure scale of the flow. The phenomena central to this argument, known as "shear sheltering", is perhaps best well known for the problem of plasma confinement in a tokamak fusion reactor, for which reversed magnetic shear greatly reduces the energy flux in the plasma (Kepner, Parker, & Decyk 1997). Though the problems of fluid turbulence and plasma turbulence are fundamentally different, Hunt & Durbin (1999) propose that the region of high shear might similarly insulate the near-wall region from the outer region of a high-Reynolds number turbulent boundary layer. Jacobs & Durbin (1998) provide some evidence for this by examination of linear fluctuations to a mean boundary-layer profile, observing that the shapes of the eigenmodes corresponding to the discrete and continuous spectra of the Orr-Sommerfeld equation are supported only in the near-wall and outer regions respectively. If, as this argument implies, the high shear of a high-Reynolds number turbulent flow successfully blocks the major fraction of the turbulent cascade of energy across the high shear region, it may indeed be better to target the large spatial scales (to affect the outer-layer structures) rather than the coherent-structure scales (to affect the near-wall structures).

As there are many fewer degrees of freedom in the large scales or intermediate scales of turbulence than there are in its complete spectrum, formulations which target either large-scale or coherent-structure-scale fluctuations in the flow might be expected to be better behaved numerically than TKE-based formulations, as the optimizations they entail are, effectively, lower dimensional and thus easier to perform. Though it is still the topic of some debate precisely which scales should be targeted by the control algorithm, the present method is sufficiently general to target whichever scales are of interest. Indeed, an interesting future use of the approach developed in this paper, once computers become fast enough to consider higher Reynolds numbers in this framework, is to shed light on this argument by comparing the effectiveness of controls targeting the large scales of turbulent boundary layers with that of controls targeting the coherent-structure scales of turbulent boundary layers.

Case (e): terminal control of turbulent kinetic energy

As described at the end of §2.1, it is appropriate to consider a cost functional which targets the *terminal value* (i.e., the value at the end of each optimization horizon) of the quantity of interest. We will illustrate with the example of the terminal control of turbulent kinetic energy. With the terminal control approach, the cost functional is not penalized for excursions of the turbulent kinetic energy during the middle of each optimization horizon, so long as these excursions lead to reduced values of the turbulent kinetic energy at the end of each optimization horizon. As referred to in the chess analogy, this is akin to "sacrificing" a piece in order to obtain long-term gain. A relevant cost functional for this approach is

$$\mathcal{J}_{\text{TKE(ter)}}(\phi) = \frac{d_6}{2}\int_\Omega |\mathbf{u}(\phi;T)|^2\,d\mathbf{x} + \frac{\ell^2}{2}\int_0^T\int_{\Gamma_2^\pm}\phi^2\,d\mathbf{x}\,dt.$$

6.2 Gradient of cost functional: general discussion

As suggested by Abergel and Temam (1990), a rigorous procedure may be developed to determine the sensitivity of a cost functional $\mathcal{J}$ to small modifications of the control ϕ for Navier-Stokes control problems of this sort. To do this, consider the linearized perturbation $\mathcal{J}'$ to the cost functional $\mathcal{J}$ resulting from an arbitrary perturbation ϕ' to the control ϕ. The quantity $\mathcal{J}'$ may be defined by a limiting process as the Fréchet differential (Vainberg 1964) of the cost functional $\mathcal{J}$ with respect to ϕ such that

$$\mathcal{J}'(\phi;\phi') \triangleq \lim_{\epsilon\to 0}\frac{\mathcal{J}(\phi+\epsilon\phi')-\mathcal{J}(\phi)}{\epsilon} \triangleq \int_0^T\int_{\Gamma_2^\pm}\frac{\mathscr{D}\mathcal{J}(\phi)}{\mathscr{D}\phi}\phi'\,d\mathbf{x}\,dt. \tag{6.1}$$

For the cases of interest here, the linearized cost functional perturbations $\mathcal{J}'$ resulting from a control perturbation ϕ' may be written as[5]

$$\begin{aligned}
\mathcal{J}'_{\text{DRAG}}(\phi;\phi') &= -d_1\int_0^T\int_{\Gamma_2^\pm}\nu\,\frac{\partial u_1'}{\partial n}\,d\mathbf{x}\,dt &&+\ell^2\int_0^T\int_{\Gamma_2^\pm}\phi\,\phi'\,d\mathbf{x}\,dt,\\
\mathcal{J}'_{\text{TKE(reg)}}(\phi;\phi') &= \ \ d_2\int_0^T\int_\Omega \mathbf{u}\cdot\mathbf{u}'\,d\mathbf{x}\,dt &&+\ell^2\int_0^T\int_{\Gamma_2^\pm}\phi\,\phi'\,d\mathbf{x}\,dt,\\
\mathcal{J}'_{\text{ENS(reg)}}(\phi;\phi') &= -d_3\int_0^T\int_\Omega \Delta\mathbf{u}\cdot\mathbf{u}'\,d\mathbf{x}\,dt &&+\ell^2\int_0^T\int_{\Gamma_2^\pm}\phi\,\phi'\,d\mathbf{x}\,dt,\\
\mathcal{J}'_{\text{LARGE(reg)}}(\phi;\phi') &= -d_4\int_0^T\int_\Omega \Delta^{-1}\mathbf{u}\cdot\mathbf{u}'\,d\mathbf{x}\,dt &&-\ell^2\int_0^T\int_{\Gamma_2^\pm}\Delta\phi\,\phi'\,d\mathbf{x}\,dt,\\
\mathcal{J}'_{\text{INT(reg)}}(\phi;\phi') &= -d_5\int_0^T\int_\Omega \Delta_B^{-1}\mathbf{u}\cdot\mathbf{u}'\,d\mathbf{x}\,dt &&-\ell^2\int_0^T\int_{\Gamma_2^\pm}\Delta_B\phi\,\phi'\,d\mathbf{x}\,dt,\\
\mathcal{J}'_{\text{TKE(ter)}}(\phi;\phi') &= \ \ d_6\int_\Omega \mathbf{u}(T)\cdot\mathbf{u}'(T)\,d\mathbf{x} &&+\ell^2\int_0^T\int_{\Gamma_2^\pm}\phi\,\phi'\,d\mathbf{x}\,dt,
\end{aligned}$$

where $\mathbf{u}'$ is the Fréchet differential of $\mathbf{u}$, as defined in the following subsection, and where we have made use of the identity $\Delta\mathbf{u} = -\nabla\times(\nabla\times\mathbf{u})$ (for $\nabla\cdot\mathbf{u}=0$) and the fact that the curl operator $(\nabla\times)$, the Laplacian (Δ), and the bandpass filter (Δ_B) are self-adjoint.

For each of the cost functionals under consideration, the linearized cost functional perturbation $\mathcal{J}'$ will be expressed as a simple linear convolution of some function of an appropriately defined adjoint

[5]Note that, for the remainder of this discussion, the functional dependence of $\mathbf{u}$ on ϕ is suppressed for notational clarity.

field $\mathbf{q}^*$ with the control perturbation ϕ', in a form identical to the right hand side of (6.1). As the resulting expression holds for arbitrary ϕ', the gradient $\mathscr{D}\mathcal{J}(\phi)/\mathscr{D}\phi$ may be identified immediately with this function of the solution to the adjoint problem. Mathematically, we say that $\mathscr{D}\mathcal{J}(\phi)/\mathscr{D}\phi$ is identified in a "weak" sense by such a procedure. Note that, in a finite-dimensional setting (i.e., when the problem is discretized in space and time), the gradient takes the form of a Jacobian of the scalar quantity $\mathcal{J}(\boldsymbol{\phi})$ with respect to the individual components of the (very high-dimensional) discretized vector $\boldsymbol{\phi}$.

With the gradient information so determined, any control ϕ on $(0, T)$ may be updated in the direction that, at least locally (i.e. for infinitesimal control updates), most effectively reduces the cost functional of interest. The finite distance the control is updated in this direction is determined with a line minimization algorithm. (This makes the iteration procedure very efficient and stable, even when considering inherently nonlinear phenomena, by guaranteeing that the cost functional of interest at least not increase from one iteration to the next.) The flow resulting from this updated control is then computed, the sensitivity of this new flow to further control modification is determined via the computation of a new adjoint field, and the process repeated. Upon convergence of this iteration, the flow is advanced with the optimized controls over the horizon $(0, T_a)$, where $T_a \leq T$, and an iteration for the optimal control over a new time horizon begins anew from time T_a, as discussed in the introduction to the receding horizon framework given in §2.1. Note that the controls computed near the end of each optimization horizon are determined without regard to the (inevitable) further development of the flow. Thus, the controls near the end of each optimization horizon (on (T_a, T)) may not be as effective in the long run as the controls near the beginning of each optimization horizon (on $(0, T_a)$) which are, in effect, optimized with greater foresight about the flow development. Thus, the controls on (T_a, T) are usually discarded and recalculated in the following optimization horizon in the receding horizon framework. This is analogous to the repeated re-evaluation of the game plan necessary after each move played during a game of chess.

6.2.1 Linearized perturbation field

Now consider the linearized perturbation $\mathbf{q}'$ to the flow $\mathbf{q}$ resulting from a perturbation ϕ' to the control ϕ. Again, the quantity $\mathbf{q}'$ may be defined by the limiting process of a Fréchet differential such that

$$\mathbf{q}' \triangleq \lim_{\epsilon \to 0} \frac{\mathbf{q}(\phi + \epsilon\phi') - \mathbf{q}(\phi)}{\epsilon}, \tag{6.2}$$

For the purpose of gaining physical intuition, it is useful to note that the quantity $\mathbf{q}'$, described above as a differential quantity, may instead be defined as the small perturbation to the state $\mathbf{q}$ arising from a small control perturbation ϕ' to the control ϕ. In such derivations, the notations $\delta\phi$ and $\delta\mathbf{q}$, denoting small perturbations to ϕ and $\mathbf{q}$, are used instead of the differential quantities ϕ'

and $\mathbf{q}'$. The two derivations are roughly equivalent, though the present derivation does not assume that primed quantities are small, rather, only that they are defined by a limiting process such as (6.2).

The equation governing the dependence of the linearized flow perturbation $\mathbf{q}'$ on the control perturbation ϕ' may be found by taking the Fréchet differential of the state equation (3.1). The result is

$$\mathcal{N}'(\mathbf{q})\,\mathbf{q}' = 0, \qquad \text{in } \Omega \tag{6.3a}$$

$$\mathbf{u}' = -\phi'\,\mathbf{n} \qquad \text{on } \Gamma_2^{\pm} \tag{6.3b}$$

$$\mathbf{u}' = 0 \qquad \text{at } t = 0, \tag{6.3c}$$

where the linearized Navier-Stokes operation $\mathcal{N}'(\mathbf{q})\,\mathbf{q}'$ is given by

$$\mathcal{N}'(\mathbf{q})\,\mathbf{q}' = \begin{pmatrix} \dfrac{\partial u_j'}{\partial x_j} \\ \dfrac{\partial u_i'}{\partial t} + \dfrac{\partial}{\partial x_j}\Big(u_j u_i' + u_j' u_i\Big) - \nu \dfrac{\partial^2 u_i'}{\partial x_j^2} + \dfrac{\partial p'}{\partial x_i} \end{pmatrix}. \tag{6.4}$$

The operation $\mathcal{N}'(\mathbf{q})\,\mathbf{q}'$ is a linear operation on the perturbation field $\mathbf{q}'$, though the operator $\mathcal{N}'(\mathbf{q})$ is itself a function of the solution $\mathbf{q}$ of the Navier-Stokes problem—note the presence of the velocity field $\mathbf{u}$ in (6.4). Equation (6.3) thus reflects the linear dependence of the perturbation field $\mathbf{q}'$ in the interior of the domain on the control perturbation ϕ' at the boundary. However, the implicit linear relationship $\mathbf{q}' = \mathbf{q}'(\phi')$ given by this equation is not yet tractable for expressing $\mathcal{J}'$ in a form similar to the r.h.s. of (6.1), from which $\mathscr{D}\mathcal{J}(\phi)/\mathscr{D}\phi$ may be deduced. For the purpose of determining a more useful relationship with which we may determine $\mathscr{D}\mathcal{J}(\phi)/\mathscr{D}\phi$, we now appeal to an adjoint identity.

6.2.2 Derivation of adjoint identity

This subsection derives the adjoint of the linear partial differential operator $\mathcal{N}'(\mathbf{q})$. For readers not familiar with this approach, a review of the derivation of an adjoint operator for a very simple case in the present notation is given in Appendix A. The adjoint derivation presented below extends in a straightforward manner to more complex equations, such as the compressible Euler equation, as shown in Appendix B (again, using the same notation). Such generality highlights the versatility of the present approach.

Define an inner product over the domain in space-time under consideration such that

$$\langle \mathbf{q}', \mathbf{q}^* \rangle = \int_0^T \int_\Omega \mathbf{q}' \cdot \mathbf{q}^* \, d\mathbf{x}\, dt,$$

and consider the identity

$$\boxed{\left\langle \mathcal{N}'(\mathbf{q})\,\mathbf{q}',\,\mathbf{q}^*\right\rangle \;=\; \left\langle \mathbf{q}',\,\mathcal{N}'(\mathbf{q})^*\,\mathbf{q}^*\right\rangle + \,b.} \tag{6.5}$$

Integration by parts may be used to move all differential operations from $\mathbf{q}'$ on the left hand side of (6.5) to $\mathbf{q}^*$ on the right hand side, resulting in the definition of the adjoint operator

$$\mathcal{N}'(\mathbf{q})^*\,\mathbf{q}^* = \begin{pmatrix} -\dfrac{\partial u_j^*}{\partial x_j} \\ -\dfrac{\partial u_i^*}{\partial t} - u_j\Big(\dfrac{\partial u_i^*}{\partial x_j} + \dfrac{\partial u_j^*}{\partial x_i}\Big) - \nu\dfrac{\partial^2 u_i^*}{\partial x_j^2} - \dfrac{\partial p^*}{\partial x_i} \end{pmatrix}, \tag{6.6}$$

where, again, the operation $\mathcal{N}'(\mathbf{q})^*\,\mathbf{q}^*$ is a linear operation on the adjoint field $\mathbf{q}^*$, and the operator $\mathcal{N}'(\mathbf{q})^*$ is itself a function of the solution $\mathbf{q}$ of the Navier-Stokes problem. From the integrations by parts, we also get several boundary terms:

$$\begin{aligned} b &= \int_\Omega \Big(u_j^*\,u_j'\Big)\Big|_{t=0}^{t=T}\,d\mathbf{x} \\ &\quad + \int_0^T \int_{\Gamma_2^\pm} n_j \Big[p^*\,u_j' + u_i^*\Big(u_j\,u_i' + u_j'\,u_i\Big) - \nu\Big(u_i^*\,\frac{\partial u_i'}{\partial x_j} - u_i'\,\frac{\partial u_i^*}{\partial x_j}\Big) + u_j^*\,p'\Big]\,d\mathbf{x}\,dt, \end{aligned}$$

where $\mathbf{n}$ denotes a unit outward normal to the surface. The quantity b is closely related to the bilinear concomitant discussed by Morse & Feshbach (1953), and the outline of the present derivation is related to the approach taken therein.

The identity (6.5) is the key to expressing $\mathcal{J}'$ in the desired form. An adjoint field $\mathbf{q}^*$ is first defined using the operator $\mathcal{N}'(\mathbf{q})^*$ together with appropriate forcing in an interior equation with appropriate boundary conditions and initial conditions. There is here some flexibility which we exploit to obtain a simple expression of $\mathcal{J}'$. Indeed, combining this definition of $\mathbf{q}^*$ with the definitions of $\mathbf{q}$ in (3.1) and $\mathbf{q}'$ in (6.3), the identity (6.5) reveals the desired expression, as will now be shown for the cases of interest in this paper.

6.2.3 Definition of adjoint field and identification of gradient

Case (a): minimization of drag

Consider an adjoint state defined (as yet, arbitrarily) by

$$\mathcal{N}'(\mathbf{q})^* \, \mathbf{q}^* = 0, \qquad \text{in } \Omega, \tag{6.7a}$$

$$\mathbf{u}^* = -d_1 \mathbf{r} \qquad \text{on } \Gamma_2^{\pm}, \tag{6.7b}$$

$$\mathbf{u}^* = 0 \qquad \text{at } t = T, \tag{6.7c}$$

where the adjoint operation $\mathcal{N}'(\mathbf{q})^* \, \mathbf{q}^*$ is given in (6.6) and $\mathbf{r}$ is a unit vector in the x_1 direction. Note that the adjoint problem (6.7), though linear, has complexity similar to that of the Navier-Stokes problem (3.1), and may be solved with similar numerical methods. Note also that the "initial" conditions in (6.7c) are defined at $t = T$, and are thus best referred to as "terminal" conditions. With this definition, the adjoint field must be marched *backward* in time over the optimization horizon—due to the sign of the time derivative and viscous terms in the adjoint operator $\mathcal{N}'(\mathbf{q})^*$ in (6.6), this is the natural direction for this time march. However, as the operator $\mathcal{N}'(\mathbf{q})^*$ is a function of $\mathbf{q}$, computation of the adjoint field $\mathbf{q}^*$ requires storage of the flow field $\mathbf{q}$ on $t \in [0, T]$, which itself must be computed with a *forward* march. This storage issue presents one of the numerical complications which preclude solution of the present optimization problem for large optimization intervals T. However, the problem is not insurmountable for intermediate values of $T^+ \lesssim O(100)$.

The identity (6.5) is now simplified using the equations defining the state field (3.1), the perturbation field (6.3), and the adjoint field (6.7). Due to the judicious choice of the RHS forcing to the adjoint problem in (6.7b), the identity (6.5) reduces (after some manipulation) to

$$-d_1 \int_0^T \int_{\Gamma_2^{\pm}} \nu \frac{\partial u_1'}{\partial n} \, d\mathbf{x} \, dt = \int_0^T \int_{\Gamma_2^{\pm}} p^* \, \phi' \, d\mathbf{x} \, dt.$$

Using this equation, the cost functional perturbation $\mathcal{J}'_{\text{DRAG}}$ may be rewritten as

$$\mathcal{J}'_{\text{DRAG}}(\phi; \phi') = \int_0^T \int_{\Gamma_2^{\pm}} \frac{\mathscr{D}\mathcal{J}_{\text{DRAG}}(\phi)}{\mathscr{D}\phi} \phi' \, d\mathbf{x} \, dt = \int_0^T \int_{\Gamma_2^{\pm}} \left(p^* + \ell^2 \, \phi\right) \phi' \, d\mathbf{x} \, dt.$$

As ϕ' is arbitrary, this implies that

$$g_{\text{DRAG}} \triangleq \frac{\mathscr{D}\mathcal{J}_{\text{DRAG}}(\phi)}{\mathscr{D}\phi} = p^* + \ell^2 \, \phi.$$

The desired gradient $\mathscr{D}\mathcal{J}_{\text{DRAG}}(\phi)/\mathscr{D}\phi$ is thus found to be a simple function of the solution of the adjoint problem proposed in (6.7).

Case (b): regulation of turbulent kinetic energy

Consider an adjoint state defined by

$$\mathscr{N}'(\mathbf{q})^* \,\mathbf{q}^* = d_2 \begin{pmatrix} 0 \\ \mathbf{u} \end{pmatrix}, \qquad \text{in } \Omega, \tag{6.8a}$$

$$\mathbf{u}^* = 0 \qquad \text{on } \Gamma_2^{\pm}, \tag{6.8b}$$

$$\mathbf{u}^* = 0 \qquad \text{at } t = T. \tag{6.8c}$$

The identity (6.5) is now simplified using the equations defining the state field (3.1), the perturbation field (6.3), and the adjoint field (6.8). Due to the judicious choice of the RHS forcing to the adjoint problem in (6.8a), the identity (6.5) reduces to

$$d_2 \int_0^T \int_\Omega \mathbf{u} \cdot \mathbf{u}' \, d\mathbf{x} \, dt = \int_0^T \int_{\Gamma_2^{\pm}} p^* \, \phi' \, d\mathbf{x} \, dt.$$

Using this equation, the cost functional perturbation $\mathscr{J}'_{\text{TKE(reg)}}$ may be rewritten in the desired form, as in case (a), and thus, as ϕ' is arbitrary, we find that

$$g_{\text{TKE(reg)}} \triangleq \frac{\mathscr{D}\mathscr{J}_{\text{TKE(reg)}}}{\mathscr{D}\phi} = p^* + \ell^2 \, \phi.$$

The desired gradient $\mathscr{D}\mathscr{J}_{\text{TKE(reg)}}(\phi)/\mathscr{D}\phi$ is thus found to be a simple function of the solution of the adjoint problem proposed in (6.8).

Case (c): regulation of enstrophy

Consider an adjoint state defined by

$$\mathscr{N}'(\mathbf{q})^* \,\mathbf{q}^* = d_3 \begin{pmatrix} 0 \\ -\Delta\mathbf{u} \end{pmatrix} \qquad \text{in } \Omega, \tag{6.9a}$$

$$\mathbf{u}^* = 0 \qquad \text{on } \Gamma_2^{\pm}, \tag{6.9b}$$

$$\mathbf{u}^* = 0 \qquad \text{at } t = T. \tag{6.9c}$$

The identity (6.5) is now simplified using the equations defining the state field (3.1), the perturbation field (6.3), and the adjoint field (6.9). Due to the judicious choice of the RHS forcing to the adjoint problem in (6.9a), the identity (6.5) reduces to

$$-d_3 \int_0^T \int_\Omega \Delta\mathbf{u} \cdot \mathbf{u}' \, d\mathbf{x} \, dt = \int_0^T \int_{\Gamma_2^{\pm}} p^* \, \phi' \, d\mathbf{x} \, dt.$$

Using this equation, the cost functional perturbation $\mathscr{J}'_{\text{ENS(reg)}}$ may be rewritten in the desired form, as in case (a), and thus, as ϕ' is arbitrary, we find that

$$g_{\text{ENS(reg)}} \triangleq \frac{\mathscr{D}\mathcal{J}_{\text{ENS(reg)}}}{\mathscr{D}\phi} = p^* + \ell^2\,\phi.$$

The desired gradient $\mathscr{D}\mathcal{J}_{\text{ENS(reg)}}(\phi)/\mathscr{D}\phi$ is thus found to be a simple function of the solution of the adjoint problem proposed in (6.9).

Case (d): regulation of large-scale and intermediate-scale structures

Consider an adjoint state defined by

$$\mathcal{N}'(\mathbf{q})^*\,\mathbf{q}^* = d_3\begin{pmatrix}0\\ -\Delta^{-1}\mathbf{u}\end{pmatrix} \qquad \text{in } \Omega, \tag{6.10a}$$

$$\mathbf{u}^* = 0 \qquad \text{on } \Gamma_2^{\pm}, \tag{6.10b}$$

$$\mathbf{u}^* = 0 \qquad \text{at } t = T. \tag{6.10c}$$

The identity (6.5) is now simplified using the equations defining the state field (3.1), the perturbation field (6.3), and the adjoint field (6.10). Due to the judicious choice of the RHS forcing to the adjoint problem in (6.10a), the identity (6.5) reduces to

$$-d_3\int_0^T\int_\Omega \Delta^{-1}\mathbf{u}\cdot\mathbf{u}'\,d\mathbf{x}\,dt = \int_0^T\int_{\Gamma_2^{\pm}} p^*\,\phi'\,d\mathbf{x}\,dt.$$

Using this equation, the cost functional perturbation $\mathcal{J}'_{\text{LARGE(reg)}}$ may be rewritten in the desired form, as in case (a), and thus, as ϕ' is arbitrary, we find that

$$g_{\text{LARGE(reg)}} \triangleq \frac{\mathscr{D}\mathcal{J}_{\text{LARGE(reg)}}}{\mathscr{D}\phi} = p^* - \ell^2\,\Delta\phi.$$

The desired gradient $\mathscr{D}\mathcal{J}_{\text{LARGE(reg)}}(\phi)/\mathscr{D}\phi$ is thus found to be a simple function of the solution of the adjoint problem proposed in (6.10).

The formulation following from $\mathcal{J}_{\text{INT(reg)}}$ is identical to that for $\mathcal{J}_{\text{LARGE(reg)}}$ with Δ replaced by Δ_B.

Case (e): terminal control of turbulent kinetic energy

Consider an adjoint state defined by

$$\mathcal{N}'(\mathbf{q})^* \, \mathbf{q}^* = 0, \qquad \text{in } \Omega, \tag{6.11a}$$

$$\mathbf{u}^* = 0 \qquad \text{on } \Gamma_2^{\pm}, \tag{6.11b}$$

$$\mathbf{u}^* = d_6 \, \mathbf{u}(T) \qquad \text{at } t = T. \tag{6.11c}$$

The identity (6.5) is now simplified using the equations defining the state field (3.1), the perturbation field (6.3), and the adjoint field (6.11). Due to the suitable choice of the RHS forcing to the adjoint problem in (6.11c), the identity (6.5) reduces to

$$d_6 \int_\Omega \mathbf{u}(T) \cdot \mathbf{u}'(T) \, d\mathbf{x} = \int_0^T \int_{\Gamma_2^{\pm}} p^* \, \phi' \, d\mathbf{x} \, dt.$$

Using this equation, the cost functional perturbation $\mathcal{J}'_{\text{TKE(ter)}}$ may be rewritten in the desired form, as in case (a), and thus, as ϕ' is arbitrary, we find that

$$g_{\text{TKE(ter)}} \triangleq \frac{\mathscr{D}\mathcal{J}_{\text{TKE(ter)}}}{\mathscr{D}\phi} = p^* + \ell^2 \, \phi.$$

The desired gradient $\mathscr{D}\mathcal{J}_{\text{TKE(ter)}}(\phi)/\mathscr{D}\phi$ is thus found to be a simple function of the solution of the adjoint problem proposed in (6.11).

6.2.4 The general framework

In the cases studied in the previous section, three possible locations of forcing for the adjoint problem were encountered: the interior equation, as in (6.8a), (6.9a) and (6.10a), the boundary conditions, as in (6.7b), and the terminal conditions, as in (6.11c). The domain of forcing appropriate for the adjoint problem is strictly a function of the domain in which cost functional to be minimized weights the flow quantities.

In this paper, we only consider control of the flow by modification of the boundary conditions (blowing/suction). In addition, however, the flow problem may also be forced by interior forcing (such as the Lorentz force exerted by electromagnetic fields on a conducting fluid) or optimized with respect to its initial conditions (a situation that arises in forecasting problems). Thus, there is a duality between the three possible sources of forcing in the flow problem and the three possible sources of forcing in the adjoint problem. This general mathematical framework is laid out in detail in Bewley, Temam, & Ziane (1999).

6.3 Gradient update to the control

6.3.1 Simple gradient

With the gradient information determined in the previous section, a strategy for optimization of the controls using a simple gradient algorithm may be proposed such that

$$\phi^{k+1} = \phi^k - \alpha^k\, g^k$$

over the entire optimization horizon $t \in (0, T)$, where k indicates the iteration number and α^k is a parameter of descent which governs how large an update is made. At each iteration, α^k is computed to be that value which locally minimizes the cost functional $\mathcal{J}(\phi)$ under consideration when the control ϕ^k is updated in the direction $-g^k$ of local maximum decrease of the cost functional $\mathcal{J}(\phi^k)$. This minimization is conducted with a numerically-stable line search algorithm. The iteration is initialized with $\phi^1 = 0$. As $k \to \infty$, such an algorithm will usually converge to some local minimum of $\mathcal{J}(\phi)$. Note that, due to the nonlinearity of the system, convergence to the global minimum will not in general be attained by such a scheme and that, as time proceeds, $\mathcal{J}$ will not necessarily decrease.

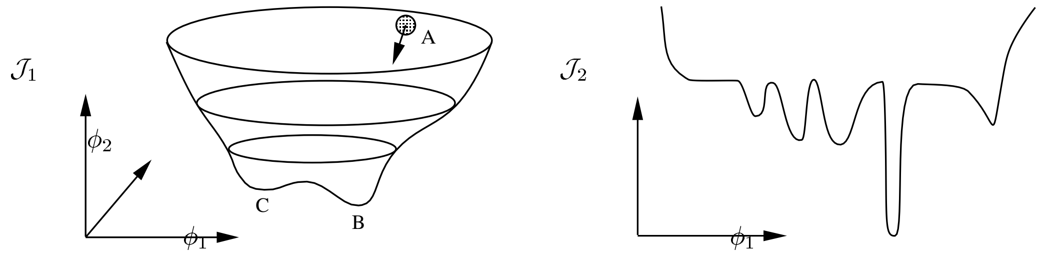

Figure 9: Possible shortcoming of gradient-based approaches: convergence to local minima.

To visualize the minimization problem in a low-dimensional setting, figure 9 illustrates the possible shape of a cost function $\mathcal{J}_1(\phi_1, \phi_2)$ in the space spanned by the setting of two control variables ϕ_1 and ϕ_2 in a discrete low-dimensional optimization problem. As shown in the figure, there will be some minimum point away from which the value of the cost function will be higher, and thus the shape of the cost function in this space might look something like a deformed bowl. Starting from point A in figure 9, computation of the appropriately-defined adjoint field provides information about the local shape of the bowl, as indicated by the shaded region: specifically, it identifies the direction of maximum decrease of the cost function, indicated by the arrow. By continually moving in the direction of steepest descent, the simple gradient algorithm eventually proceeds towards a minimum of the cost function. Note, however, that depending on where point A is relative to the minima, this algorithm may converge to the global minimum B or to some other local minimum

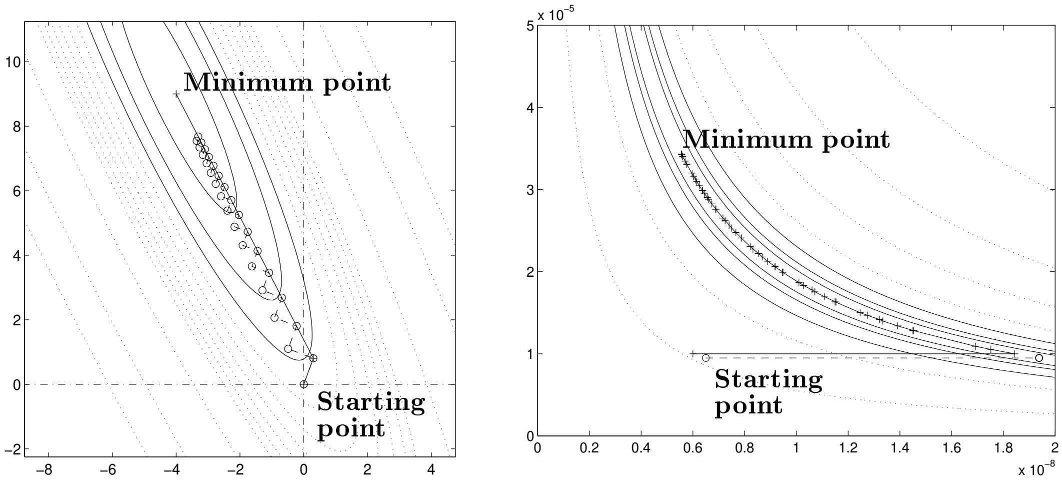

a) Quadratic $\mathcal{J}_3(\phi_1, \phi_2)$. b) Non-quadratic $\mathcal{J}_4(\phi_1, \phi_2)$.

Figure 10: Convergence of: ($\circ$) simple gradient, and ($+$) the Polak-Ribiere variant of the conjugate gradient algorithms when applied to find minima of two test functions of two scalar control variables ϕ_1 and ϕ_2 (horizontal and vertical axes). Contours illustrate the level surfaces of the test functions; contours corresponding to the smallest isovalues are solid, those corresponding to higher isovalues are dotted.

such as C; this is a drawback of searching with a gradient routine. To alleviate this difficulty, the gradient search routine may be initialized from several different starting points $\phi^{1,j}$ (chosen at random or from a regular array selected *a priori*), the optimization conducted from each starting point, and the performance of the different sets of optimized controls compared. Alternatively, a random disturbance can be added to the control update near the beginning of the optimization process (cooling this disturbance off near the end of the optimization) to "push" the algorithm out of shallow local minima. Both approaches effectively blend the "global" minimization capability of genetic algorithms with the fast convergence capability for very high-dimensional optimization problems of gradient-based algorithms, but neither approach was found to be necessary in the present work. Note that in pathological cases, such as the function $\mathcal{J}_2(\phi_1)$ illustrated in figure 9, gradient algorithms break down altogether, and strategies based on function evaluations alone are preferred (see §2.1).

6.3.2 Conjugate gradient

As shown in figure 10, the simple gradient approach described above is usually very inefficient. Even in quadratic minimization problems, for cases in which the function being minimized has a long, narrow "valley", the simple gradient algorithm often gets stuck "bouncing" from one side of the valley to the other without turning to proceed along the valley floor, as shown in figure 10a[6]. In such cases, the conjugate gradient algorithm has proven to be much more efficient, at the very modest cost of a slight increase in computational storage. This method proceeds in a direction which is a linear combination of the direction of maximum decrease of the cost function and the direction used in the previous descent step. Thus, like a skier negotiating a similar type of terrain, this scheme retains a momentum term that helps turn the descent path to proceed down narrow valleys. Further, the conjugate gradient approach may be adapted to be quite effective even for nonquadratic minimization problems, as demonstrated in figure 10b.

The model problem considered in figure 10a is the minimization of a simple function $\mathcal{J}_3(\phi_1, \phi_2)$ which is quadratic in the control variables; this problem illustrates an extremely low-order model of the cost function for the present flow problem if the state equation is assumed to be linear (e.g., for small perturbations of $\boldsymbol{\phi}$ from the minimum point of $\mathcal{J}(\boldsymbol{\phi})$). The model problem considered in figure 10b is a stiff chemical equilibrium problem to determine the equilibrium concentrations of the proton and carbonate species in a sodium bicarbonate solution; in this case, the function to be minimized, $\mathcal{J}_4(\phi_1, \phi_2)$, is a sixth order polynomial in the control variables. In both cases, the conjugate gradient algorithm converges to within machine zero of the absolute minimum of J. Convergence is attained in 2 iterations in the quadratic case and 60 iterations in the non-quadratic case.

In contrast, the simple gradient algorithm does not converge effectively to the minimum in either of these two simple test problems, even though 30 iterations are used in the fairly well-conditioned quadratic problem of figure 10a and 1000 iterations are used in the poorly-conditioned non-quadratic problem of figure 10b. In fact, in the non-quadratic case, the simple gradient algorithm makes no visible progress towards the minimum after the first iteration for the particular initial conditions shown, resulting in an error of over a factor of 3 in both of the concentrations. Based on the results of these tests, the conjugate gradient algorithm was selected for all control optimizations reported in the remainder of this work.

The particular variant of the conjugate gradient algorithm which appears to be best suited for most nonquadratic optimization problems, including the difficult case shown in figure 10b, is referred to as the *Polak-Ribiere* method (Polak 1971, Scales 1985, Press *et al.* 1986, Luenberger 1989). It is given by

$$\phi^{k+1} = \phi^k + \alpha^k\, h^k,$$

where the update direction h^k is initialized such that $h^1 = -g^1$ and defined thereafter by

$$h^k = -g^k + \beta^k\, h^{k-1},$$

[6]Note that, in the present approach, a line minimization is performed at each iteration in the descent direction. The "bouncing" behaviour shown in figure 10a may be alleviated somewhat by stopping short of a line minimization at each iteration, at the cost of slowing the convergence of the gradient algorithm significantly.

where the gradient g^k is determined by an adjoint formulation for the cost functional of interest $\mathcal{J}(\phi^k)$, as discussed in §6.2, and the coefficient β^k in the momentum term is given by

$$\beta^k = \frac{\left(g^k - g^{k-1}\right) \cdot g^k}{g^{k-1} \cdot g^{k-1}}.$$

Again, α^k is computed to be that value which minimizes the cost functional $\mathcal{J}(\phi)$ under consideration when the control ϕ^k is updated in the direction of descent h^k.

Applying this algorithm to minimize a quadratic function $J(\boldsymbol{\phi})$, the sequence of gradient vectors throughout the iteration are mutually orthogonal, so $g^{k-1} \cdot g^k = 0$. Neglecting numerical error, exact convergence is achieved in N iterations, where N is the dimension of the vector $\boldsymbol{\phi}$ being optimized, as shown in figure 10a for $N = 2$. For the minimization of nonquadratic functions, the term $g^{k-1} \cdot g^k$ tends to reset the conjugate gradient iteration towards a simple gradient behavior in nonquadratic regions, and thus, usually, speeds the convergence. However, such resetting behavior is not fully reliable, and thus it is generally useful to "bleed off" the excess momentum occasionally, taking $\beta^k = 0$ every 10 or 20 iterations and thereby resetting to a simple gradient step before continuing.

The dimension of the control in the present problem is quite large ($O(10^7)$ control variables per optimization horizon at $Re_\tau = 180$ and $T^+ = 40$), which precludes the use of second-order techniques which are based on the computation or approximation of the full Hessian matrix $\partial^2 \mathcal{J} / \partial \phi_i \, \partial \phi_j$ or its inverse during the control optimization. The number of elements in such a matrix scales with the square of the number of control variables, and is unmanageable in the present case. However, reduced-storage variants of variable metric methods (Vanderplaats 1984), such as the Davidon-Fletcher-Powell (DFP) method, the Broydon-Fletcher-Goldfarb-Shanno (BFGS) method, and the sequential quadratic programming (SQP) method, approximate the inverse Hessian information by outer products of various stored vectors, and thus achieve nearly second-order convergence without storage of the full Hessian matrix. Such techniques should be explored further for very large scale optimization problems such as the present in future work.

6.4 Numerical method for control computation

The adjoint problem is discretized and coded with a numerical method almost identical to that used to solve the flow problem on the same spatial grid (see §4). The velocity field is stored every 5 time steps on the forward sweep, with linear interpolation of these stored fields used on the backward sweep to determine the operator $\mathcal{N}'(\mathbf{q})^*$. The Polak-Ribiere variant of the conjugate gradient algorithm is used for the control update, with α computed at each iteration by Brent's method, a stable and numerically efficient line-minimization algorithm taken from Press *et al.* (1986) which begins the optimization with a "safe" golden section search and transfers to a "fast" inverse parabolic interpolation when the solution is approached.

Chapter 7

Performance of controlled systems

In order to validate the utility of the DNS-based predictive control approach, a series of simulations was performed using the code outlined in §4 and benchmarked in §5. These simulations bring to light several of the control issues discussed previously.

The horizon T over which the flow is optimized is a critical parameter which must be chosen carefully. The larger the optimization horizon, the more the cost functional represents the problem of interest, but the more the optimization problem increases in difficulty[1]. As shown in figure 11, it is worthwhile to consider as long a T as computationally affordable in order to maximize long-term performance. Returning to the chess analogy (see §2.1), this makes perfect sense: one can never win a game of chess looking forward in time just a single move. On the contrary, it is essential to estimate how the game will evolve. Note that relaminarization occurs in the present simulations for the $\mathcal{J}_{\text{TKE(ter)}}$ formulations when $T^+ \gtrsim 25$. Note also that, for simplicity, we have taken $T_a = T$ for all of the simulations reported here; variations of the ratio T_a/T will be explored in future work.

The lobed behaviour of figure 11 is expected, and is a consequence of the fact that we are using here a formulation based on the terminal control of TKE in the receding-horizon framework. As discussed at the end of §2.1, such a strategy allows excursions of the TKE over the short term to go unpenalized by the control algorithm so long as they lead to long term advantage (specifically, a reduced value of the TKE at the end of the optimization period). The idea is akin to allowing sacrifices during a game of chess.

In addition to the selection of T, the choice of the cost functional to be minimized, which mathematically defines the problem to be solved, is another critical decision which must be made. A discussion of the pros and cons of a variety of different cost functionals is presented in §6.1. Figure 12 shows the performance of the optimized controls for three of the most promising optimal control

[1] As mentioned previously, it appears as if optimization of the nonlinear Navier-Stokes control problem over an infinite time horizon, which would require the solution of a very difficult Hamilton-Jacobi-Bellman (HJB) problem in infinite dimension, is computationally intractable.

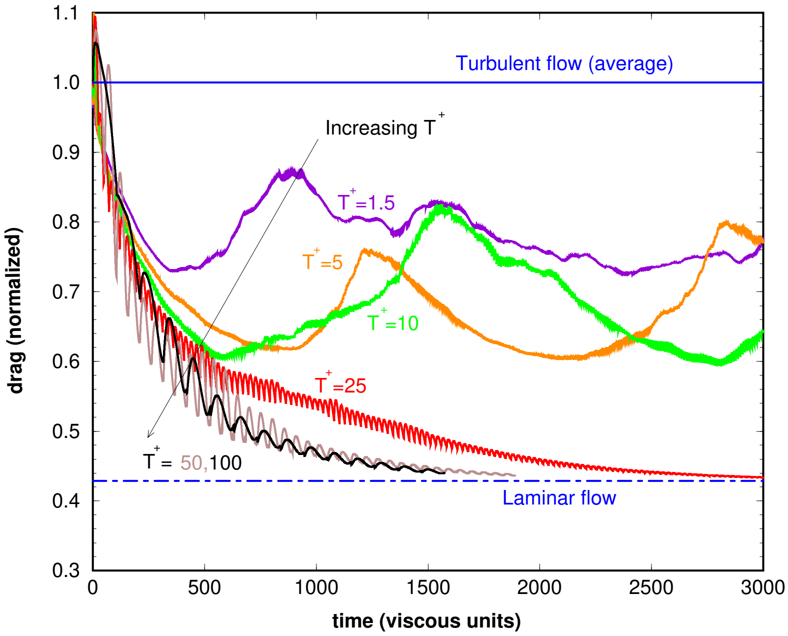

(a) History of drag.

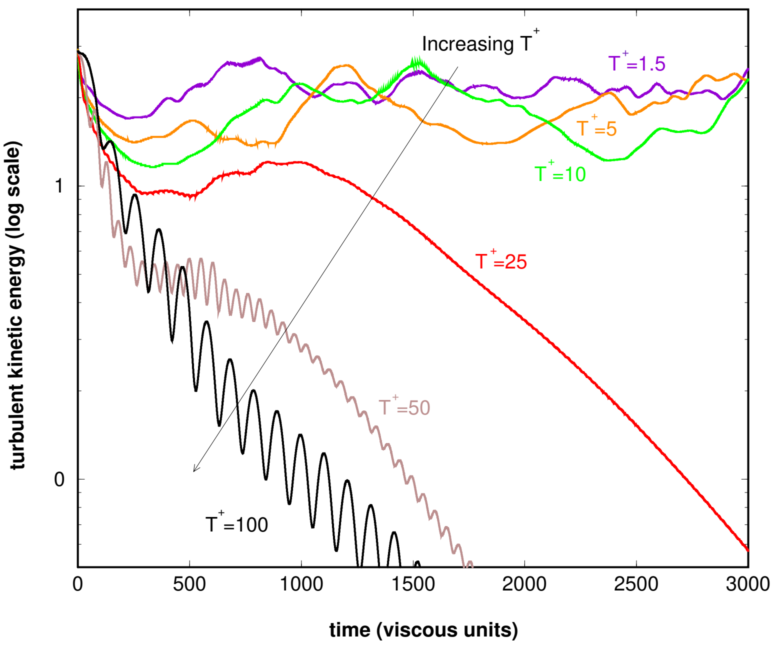

(b) History of turbulent kinetic energy.

Figure 11: Performance of optimized controls for formulations based on $\mathcal{J}_{\text{TKE(ter)}}$ as a function of the optimization horizon T^+ as computed in direct numerical simulations at $Re_\tau = 100$. For small optimization horizons ($T^+ = O(1)$), approximately 20% drag reduction is obtained, a result which can be obtained with a variety of other approaches. For sufficiently large optimization horizons ($T^+ \gtrsim 25$), the flow is returned to the region of stability of the laminar flow, and the flow relaminarizes.

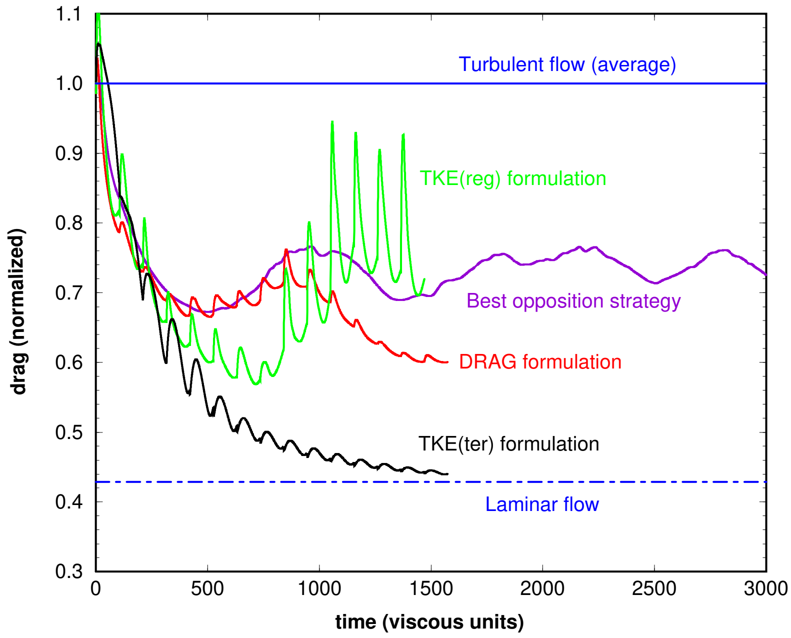

(a) History of drag.

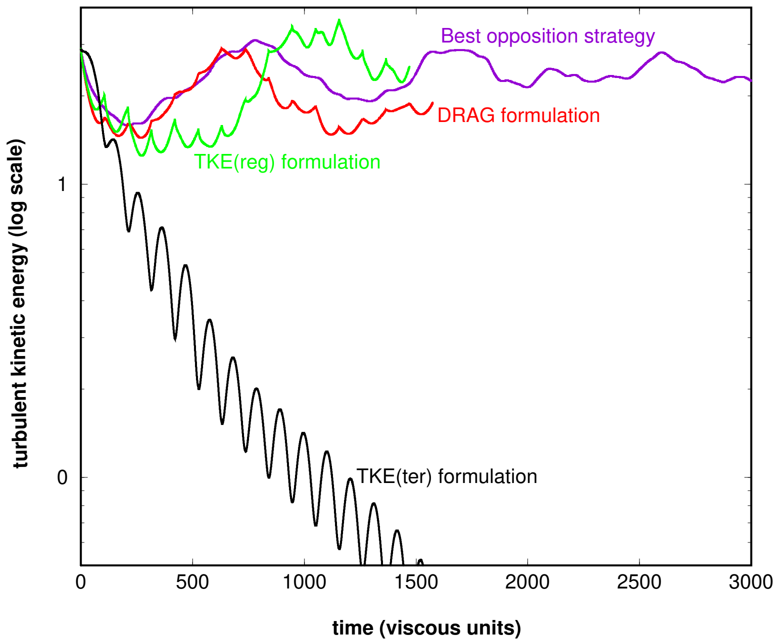

(b) History of turbulent kinetic energy.

Figure 12: Performance of optimized controls for three different optimal control formulations ($\mathcal{J}_{\text{DRAG}}$, $\mathcal{J}_{\text{TKE(reg)}}$, and $\mathcal{J}_{\text{TKE(ter)}}$ as labeled) as computed in direct numerical simulations at $Re_\tau = 100$. The optimization horizon was taken as $T^+ = 100$ for all three optimal control formulations shown here. The best opposition control strategy is shown for comparison.

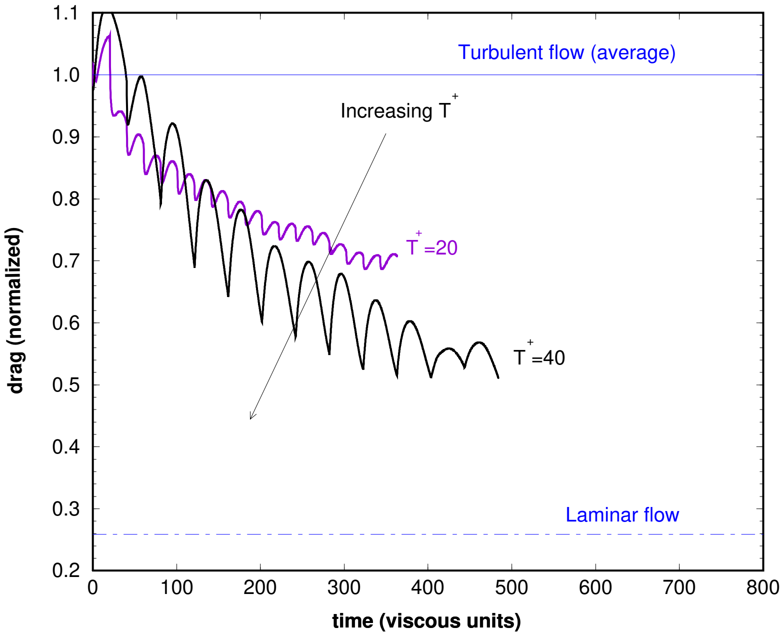

(a) History of drag.

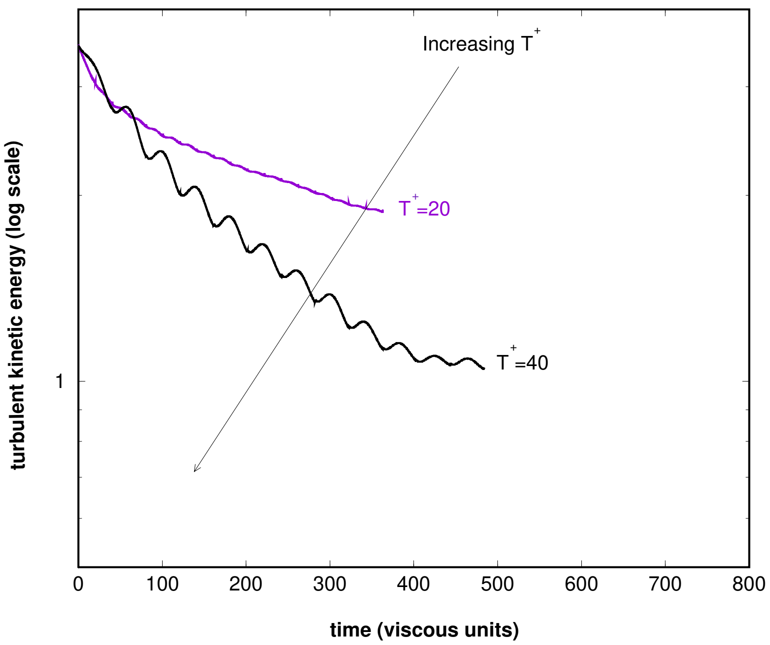

(b) History of turbulent kinetic energy.

Figure 13: Performance of optimized controls for formulations based on $\mathcal{J}_{\text{TKE(ter)}}$ as a function of the optimization horizon T^+ as computed in direct numerical simulations at $Re_\tau = 180$. Again, longer optimization horizons are seen to be superior. Unfortunately, due to the high number of iterations required, the present simulations are approximately 50 times more expensive than regular direct numerical simulations, and thus computations at this Reynolds number are prohibitively expensive.

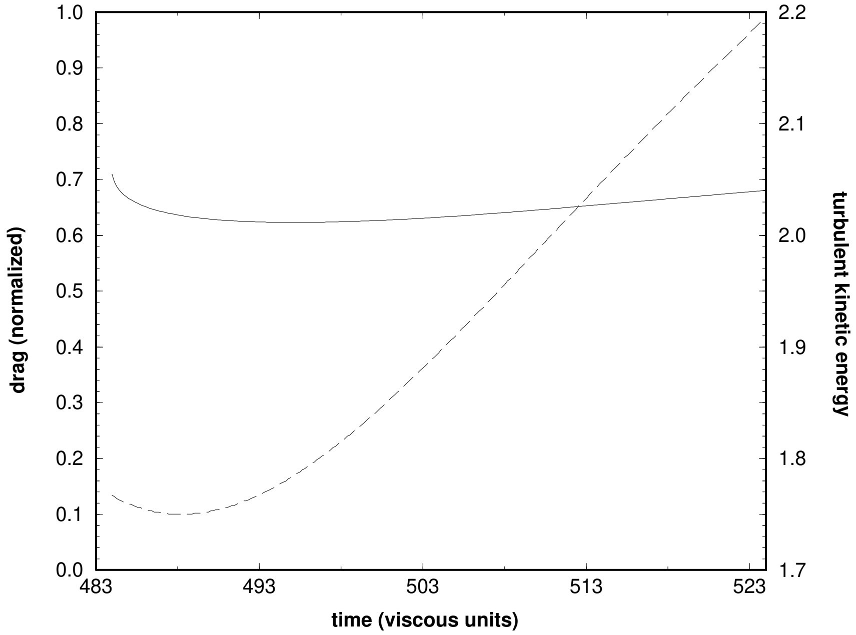

Figure 14: Response of system on $[t, t+T]$ in a controlled simulation ($\mathcal{J}_{\text{TKE(ter)}}$ formulation, $T^+ = 40$, and $Re_\tau = 180$) with control turned off at $t^+ = 483$: ———, drag (scale at left); - - - - , TKE (scale at right). The faster rise of the TKE indicates that it is a more sensitive indicator of turbulence regeneration in the flow.

formulations for $T^+ = 100$: specifically, those based on the minimization of $\mathcal{J}_{\text{DRAG}}$, $\mathcal{J}_{\text{TKE(reg)}}$, and $\mathcal{J}_{\text{TKE(ter)}}$. Over the long term, the $\mathcal{J}_{\text{TKE(ter)}}$ formulation is clearly superior, and is the only one of the three formulations which relaminarizes this particular flow in our present simulations.

Scaling the DNS-based predictive control approach to higher Reynolds numbers is extremely difficult due to its computational expense. In the present simulations for the larger values of T, the computational cost is approximately 50 times that of a regular DNS over the same time interval. This expense is due to iterative flow and adjoint computations and the extra flow computations required to optimize the descent parameter α at each iteration step (see figure 1 and §6.4 for further details). Many techniques have been proposed to streamline the computational algorithm, such as application of the reduced-storage BFGS approach (which would greatly reduce the need for extra flow computations to determine α), the solution of several suboptimal problems to precondition the optimal control problem over the full time interval (Heinkenschloss 1999), and the utilization of (cheaper) large eddy simulations (LES) during the iterative flow prediction and adjoint computation stages of the procedure (Chang & Collis 1999).

However, even with the above-mentioned computational expense of the present approach, figure 13 reveals that the approach can at least be extended to flows at $Re_\tau = 180$, leading (in the $T^+ = 40$ case) to about a 50% drag reduction and a factor of 3 in TKE reduction in 500 viscous time units. This is almost identical performance as that seen in figure 11 for the $T^+ = 50$ case at

$Re_\tau = 100$ over the same time period (500 viscous time units). Relaminarization of this flow should also therefore be possible with the present approach given a sufficient amount of computer time. As the simulation yielding the lower curves of figures 13a and 13b took approximately 1500 hours of single-processor Cray C90 time, extending these drag and TKE histories will be deferred until the improved optimization approaches discussed above have been developed. As both $Re_\tau = 100$ and $Re_\tau = 180$ should probably be considered as "low Reynolds number", the question of the ability to scale the present approach to "high Reynolds number" is left unanswered, though it is clear that more efficient numerical techniques should be explored before significantly higher Reynolds numbers are considered.

To address the question of why the formulation based on minimization of $\mathcal{J}_{\text{TKE(ter)}}$ worked better than the formulation based on minimization of $\mathcal{J}_{\text{DRAG}}$, the control was turned off at $t^+ = 483$ in one of the controlled simulations. With control off, the turbulence in the flow quickly regenerates and the flow eventually returns to the fully turbulent state[2]. The regeneration of turbulence over the time interval $[t, t+T]$ is shown in figure 14. As can be seen, the TKE (a measure of the fluctuations in the flow) responds much more quickly than does the drag (a measure of the mean flow profile) when characterizing the regeneration of turbulence in the flow. This provides numerical evidence for the statement made in §2.1 that turbulence is the "cause" and high drag is the "effect", and it is most effective to target the "cause" in the cost functional.

In the optimal calculations presented here, we chose $\ell = 10^{-2}$ (control effort is taken to be "cheap"), and the cost functional is dominated in all cases by the contribution of the term which is a function of u. Note that, for a linear system, small ℓ in the control formulation can result in a very large control magnitude. For the present nonlinear system, it was found that the small ℓ limit actually resulted in a finite control magnitude, with an rms magnitude of the control approximately equal to that used in the $y^+ = 15$ opposition control cases discussed in §1.2. Increased values of ℓ resulted in decreased control magnitude and reduced values of drag and TKE reduction.

The power utilized by the control algorithm is given by the rate of addition of kinetic energy to the flow plus the rate of work done against the (fluctuating) hydrodynamic pressure of the fluid. The straightforward expression for the power applied by the control algorithm on the horizon $[0, T]$ is

$$\mathcal{P}_\phi = \frac{1}{T} \int_0^T \int_{\Gamma_2^\pm} \phi \left(\frac{\phi^2}{2} + p \right) \, d\mathbf{x} \, dt,$$

whereas the power expense due to the drag of the flow (which is overcome by the mean pressure

[2]Note that this is a subcritical flow, but we are still well outside the domain of convergence of the laminar state at this point in the simulation.

gradient P_x) may be calculated as

$$\mathcal{P}_{DRAG} = \frac{P_x}{T} \int_0^T \int_\Omega u_1 \, d\mathbf{x} \, dt.$$

However, the expression for $\mathcal{P}_\phi$ accounts for both kinetic energy addition to the flow by blowing and also kinetic energy removal from the flow by suction, and the $p\,\phi$ work term is not necessarily positive[3]. In most physical implementations, however, it is unlikely that useful energy can be effectively extracted from the system by the actuators. Our idealization of blowing/suction applied as the actuation is too far removed from the actual application hardware to get a reliable estimate of the power requirements using the above expression for $\mathcal{P}_\phi$. Adding absolute value signs in a completely *ad hoc* manner and subtracting out the effect of the mean pressure $\bar{p}$, which is unspecified in the current system, a conservative estimate of the power used by an actual control algorithm might be concocted as

$$\frac{1}{T} \int_0^T \int_{\Gamma_2^\pm} \left(|\phi| \frac{\phi^2}{2} + |\phi(p - \bar{p})| \right) \, d\mathbf{x} \, dt.$$

Even with this conservative formula for estimating the power requirement of the actuators, the power required by the actuators in the present simulations is less than 1% of the power saved due to the drag reduction of the relaminarized flow. Thus we see that the control authority here is large: it is not by brute force, but rather by finesse, that relaminarization is attained.

[3]Note also that, due to the mass flux constraint on the control, (3.2), the mean value of pressure on the wall $\bar{p}$ does not affect $\mathcal{P}_\phi$.

Chapter 8

Conclusions

The purpose of this paper was to present the fundamental issues central to the application of optimal control theory in the predictive control framework to the problem of turbulence, and to illustrate the effectiveness of this approach in well-resolved direct numerical simulations of incompressible low-Reynolds number turbulent channel flows. Primary conclusions include:

1. There is sufficient control authority in small amounts of zero-net mass flux blowing and suction distributed intelligently over the walls to completely relaminarize a low Reynolds number turbulent channel flow.

2. The DNS-based receding-horizon predictive control framework, in which adjoint fields are used as the central component of a gradient-based optimization strategy, provides a numerically tractable algorithm for computing effective controls. The adjoint field computation is about as expensive as a flow field computation over the same time interval. The Polak-Ribiere variant of the conjugate gradient algorithm, with occasional resetting to a simple gradient step, is an effective minimization method utilizing this high-dimensional gradient information. The optimizations performed here are, to the best of our knowledge, the highest-dimensional control optimizations ever performed: on each optimization interval in the $Re_\tau = 180$, $T^+ = 40$ case (for which there were 280 time steps per optimization interval), there were $170 \times 170 \times 2 \times 280 \approx 10^7$ control variables and $170 \times 129 \times 170 \times 280 \approx 10^9$ state variables. The expense of the algorithm, of course, will be drastically reduced in the future—the purpose of the present simulations was to determine a best-case "benchmark".

3. There is sufficient flexibility in the present method that, with minor modification, it can be used to optimize controls for both regulation and terminal control problems targeting a wide variety of flow quantities of interest, with concentration on large, intermediate, or small length scales. One's *a priori* understanding of flow physics may therefore be blended with the mathematical optimization strategy by appropriate selection of the cost functional.

4. Formulations which optimize the controls over longer time horizons T have a significant advantage over formulations which optimize over shorter time horizons.

5. Formulations based on terminal control strategies, which allow excursions in the short term if they lead to long term advantage, are more effective than formulations based on regulation of the quantity of interest.

6. Formulations based on minimization of drag are less effective than formulations based on the terminal control of turbulent kinetic energy. Drag seems to be a less sensitive indicator of turbulence suppression or regeneration over the time interval than is the terminal value of turbulent kinetic energy.

Though not immediately implementable in hardware, the present work represents a significant step towards the determination of optimally effective yet implementable control strategies for the mitigation or enhancement of the consequential effects of turbulence in flows of real engineering interest. The simulation database resulting in the drag and TKE histories shown in §7 produced hundreds of gigabytes of data which will be combed in future work in an attempt to extract useful correlations which may be exploited by practical control algorithms. Further, based on the groundwork laid in the present paper, the seeds are now sown for the development of practical turbulence control algorithms via adjoint-based optimization of open-loop control parameters and/or the coefficients in implementable feedback control rules.

Appendix A

Review: derivation of a simple linear adjoint operator

Consider two scalars $q(t)$ and $q^*(t)$ on $t \in [0, T]$. Define an inner product such that

$$\langle q, q^* \rangle = \int_0^T q \cdot q^* \, dt. \tag{A.1}$$

Let $\mathcal{N} = \partial/\partial t$. The adjoint of $\mathcal{N}$ is found with

$$\boxed{\langle \mathcal{N} \, q, q^* \rangle \; = \; \langle q, \mathcal{N}^* q^* \rangle + \; b.} \tag{A.2}$$

Using integration by parts,

$$\int_0^T \left(\frac{\partial q}{\partial t} \right) q^* \, dt = \int_0^T q \left(-\frac{\partial q^*}{\partial t} \right) dt + q \, q^* \Big|_{t=T} - q \, q^* \Big|_{t=0} \tag{A.3}$$

Thus, $\mathcal{N}^* = -\partial/\partial t$ and $b = q \, q^* \Big|_{t=T} - q \, q^* \Big|_{t=0}$.

Appendix B

Derivation of adjoint compressible Euler equation

A convenient form of the compressible Euler equation for a perfect gas coupled with a passive scalar equation is

$$\begin{pmatrix} \dfrac{\partial \rho}{\partial t} + \nabla \cdot \mathbf{m} \\ \dfrac{\partial \mathbf{m}}{\partial t} + \nabla \cdot \dfrac{\mathbf{m} \otimes \mathbf{m}}{\rho} + \nabla p \\ \dfrac{\partial p}{\partial t} + \nabla \cdot \dfrac{p\,\mathbf{m}}{\rho} + (\gamma - 1)\, p \Big(\nabla \cdot \dfrac{\mathbf{m}}{\rho} \Big) \\ \dfrac{\partial \zeta}{\partial t} + \nabla \cdot \dfrac{\zeta\,\mathbf{m}}{\rho} \end{pmatrix} = 0. \tag{B.1}$$

where ρ is the density, $\mathbf{m} = \rho \mathbf{u}$ is the momentum vector, p is the pressure, $\zeta = \rho\,\xi$ is the density-weighted passive scalar concentration, γ is a constant, the dot $(\cdot)$ denotes the scalar product, and $\otimes$ denotes the tensor product. The quantities ρ, p, and ζ are scalar fields in the domain Ω and the quantity $\mathbf{m}$ is a vector field in the domain Ω. In a more compact notation, we will refer to this nonlinear equation simply as

$$\mathcal{N}(\mathbf{q}) = 0 \qquad \text{where} \qquad \mathbf{q} = \begin{pmatrix} p \\ \mathbf{m} \\ \rho \\ \zeta \end{pmatrix}.$$

Taking the Fréchet derivative of (B.1), it is seen that

$$\begin{pmatrix} \dfrac{\partial \rho'}{\partial t} + \nabla\cdot\mathbf{m}' \\ \dfrac{\partial \mathbf{m}'}{\partial t} + \nabla\cdot\Big(\dfrac{\mathbf{m}'\otimes\mathbf{m}}{\rho} + \dfrac{\mathbf{m}\otimes\mathbf{m}'}{\rho} - \dfrac{\rho'\,\mathbf{m}\otimes\mathbf{m}}{\rho^2}\Big) + \nabla p' \\ \dfrac{\partial p'}{\partial t} + \nabla\cdot\Big(\dfrac{p'\,\mathbf{m}}{\rho} + \dfrac{p\,\mathbf{m}'}{\rho} - \dfrac{\rho'\,p\,\mathbf{m}}{\rho^2}\Big) + (\gamma-1)\Big(p'\,\nabla\cdot\dfrac{\mathbf{m}}{\rho} + p\,\nabla\cdot\dfrac{\mathbf{m}'}{\rho} - p\,\nabla\cdot\dfrac{\rho'\,\mathbf{m}}{\rho^2}\Big) \\ \dfrac{\partial \zeta'}{\partial t} + \nabla\cdot\Big(\dfrac{\zeta'\,\mathbf{m}}{\rho} + \dfrac{\zeta\,\mathbf{m}'}{\rho} - \dfrac{\rho'\,\zeta\,\mathbf{m}}{\rho^2}\Big) \end{pmatrix} = 0.$$

Note that this equation is linear in the primed variables, and thus we may write it as

$$\mathcal{N}'(\mathbf{q})\,\mathbf{q}' = 0 \qquad \text{where} \qquad \mathbf{q}' = \begin{pmatrix} p' \\ \mathbf{m}' \\ \rho' \\ \zeta' \end{pmatrix}.$$

This notation indicates that the equation is linear in $\mathbf{q}'$, though the differential operator $\mathcal{N}'(\mathbf{q})$, which is found by Fréchet differentiation of the nonlinear operator $\mathcal{N}(\mathbf{q})$, is itself a (nonlinear) function of $\mathbf{q}$. In tensor form (where the adjoint calculus to be performed is easiest), the differential operation $\mathcal{N}'(\mathbf{q})\,\mathbf{q}'$ is written

$$\mathcal{N}'(\mathbf{q})\,\mathbf{q}' = \begin{pmatrix} \dfrac{\partial \rho'}{\partial t} + \dfrac{\partial m_j'}{\partial x_j} \\ \dfrac{\partial m_i'}{\partial t} + \dfrac{\partial}{\partial x_j}\Big(\dfrac{m_j'\,m_i}{\rho} + \dfrac{m_j\,m_i'}{\rho} - \dfrac{\rho'\,m_j\,m_i}{\rho^2}\Big) + \dfrac{\partial p'}{\partial x_i} \\ \dfrac{\partial p'}{\partial t} + \dfrac{\partial}{\partial x_j}\Big(\dfrac{p'\,m_j}{\rho} + \dfrac{p\,m_j'}{\rho} - \dfrac{\rho'\,p\,m_j}{\rho^2}\Big) + (\gamma-1)\Big(p'\,\dfrac{\partial}{\partial x_j}\dfrac{m_j}{\rho} + p\,\dfrac{\partial}{\partial x_j}\dfrac{m_j'}{\rho} - p\,\dfrac{\partial}{\partial x_j}\dfrac{\rho'\,m_j}{\rho^2}\Big) \\ \dfrac{\partial \zeta'}{\partial t} + \dfrac{\partial}{\partial x_j}\Big(\dfrac{\zeta'\,m_j}{\rho} + \dfrac{\zeta\,m_j'}{\rho} - \dfrac{\rho'\,\zeta\,m_j}{\rho^2}\Big) \end{pmatrix}.$$

We now determine an adjoint operator $\mathcal{N}'(\mathbf{q})^*$, which acts on an adjoint state $\mathbf{q}^*$, via the identity

$$\boxed{\big\langle \mathcal{N}'(\mathbf{q})\,\mathbf{q}',\,\mathbf{q}^*\big\rangle = \big\langle \mathbf{q}',\,\mathcal{N}'(\mathbf{q})^*\,\mathbf{q}^*\big\rangle + b,} \qquad \text{where} \qquad \mathbf{q}^* = \begin{pmatrix} p^* \\ \mathbf{m}^* \\ \rho^* \\ \zeta^* \end{pmatrix}, \tag{B.2}$$

and where the inner product is defined such that

$$\langle \mathbf{q}', \mathbf{q}^* \rangle = \int_0^T \int_\Omega \mathbf{q}' \cdot \mathbf{q}^* \, d\mathbf{x} \, dt.$$

Multiplying out $\mathcal{N}'(\mathbf{q})\,\mathbf{q}' \cdot \mathbf{q}^*$, rearranging, substituting in to the left-hand side of (B.2), and doing the appropriate integrations by parts to move all of the differential operations off of $\mathbf{q}'$ and onto $\mathbf{q}^*$, it is found that

$$\begin{aligned}
\mathbf{q}' \cdot N'(\mathbf{q})^* \, \mathbf{q}^* = {}& p' \left(-\frac{\partial \rho^*}{\partial t} - \frac{m_j}{\rho} \frac{\partial \rho^*}{\partial x_j} + (\gamma - 1)\rho^* \frac{\partial}{\partial x_j} \frac{m_j}{\rho} - \frac{\partial m_j^*}{\partial x_j} \right) \\
&+ m_i' \left(-\frac{\partial m_i^*}{\partial t} - \frac{p}{\rho} \frac{\partial \rho^*}{\partial x_i} - \frac{\gamma - 1}{\rho} \frac{\partial}{\partial x_i} \rho^* \, p - \frac{m_j}{\rho} \frac{\partial m_i^*}{\partial x_j} - \frac{m_j}{\rho} \frac{\partial m_j^*}{\partial x_i} - \frac{\partial p^*}{\partial x_i} - \frac{\zeta}{\rho} \frac{\partial \zeta^*}{\partial x_i} \right) \\
&+ \rho' \left(-\frac{\partial p^*}{\partial t} + \frac{p \, m_j}{\rho^2} \frac{\partial \rho^*}{\partial x_j} + \frac{(\gamma - 1)\, m_j}{\rho^2} \frac{\partial}{\partial x_j} \rho^* \, p + \frac{m_j \, m_k}{\rho^2} \frac{\partial m_k^*}{\partial x_j} + \frac{\zeta \, m_j}{\rho^2} \frac{\partial \zeta^*}{\partial x_j} \right) \\
&+ \zeta' \left(-\frac{\partial \zeta^*}{\partial t} - \frac{m_j}{\rho} \frac{\partial \zeta^*}{\partial x_j} \right),
\end{aligned}$$

which leads to the following expression for the adjoint operation

$$\mathcal{N}'(\mathbf{q})^* \, \mathbf{q}^* = \begin{pmatrix}
-\dfrac{\partial \rho^*}{\partial t} - \dfrac{m_j}{\rho} \dfrac{\partial \rho^*}{\partial x_j} + (\gamma - 1)\, \rho^* \dfrac{\partial}{\partial x_j} \dfrac{m_j}{\rho} - \dfrac{\partial m_j^*}{\partial x_j} \\
-\dfrac{\partial m_i^*}{\partial t} - \dfrac{p}{\rho} \dfrac{\partial \rho^*}{\partial x_i} - \dfrac{\gamma - 1}{\rho} \dfrac{\partial}{\partial x_i} \rho^* \, p - \dfrac{m_j}{\rho} \left(\dfrac{\partial m_i^*}{\partial x_j} + \dfrac{\partial m_j^*}{\partial x_i} \right) - \dfrac{\partial p^*}{\partial x_i} - \dfrac{\zeta}{\rho} \dfrac{\partial \zeta^*}{\partial x_i} \\
-\dfrac{\partial p^*}{\partial t} + \dfrac{p \, m_j}{\rho^2} \dfrac{\partial \rho^*}{\partial x_j} + \dfrac{(\gamma - 1)\, m_j}{\rho^2} \dfrac{\partial}{\partial x_j} \rho^* \, p + \dfrac{m_j \, m_k}{\rho^2} \dfrac{\partial m_k^*}{\partial x_j} + \dfrac{\zeta \, m_j}{\rho^2} \dfrac{\partial \zeta^*}{\partial x_j} \\
-\dfrac{\partial \zeta^*}{\partial t} - \dfrac{m_j}{\rho} \dfrac{\partial \zeta^*}{\partial x_j}
\end{pmatrix}.$$

Returning to the operator form, the adjoint operation $\mathcal{N}'(\mathbf{q})^* \, \mathbf{q}^*$ is written

$$\mathcal{N}'(\mathbf{q})^* \, \mathbf{q}^* = \begin{pmatrix}
-\dfrac{\partial \rho^*}{\partial t} - \dfrac{\mathbf{m}}{\rho} \cdot \nabla \rho^* + (\gamma - 1)\, \rho^* \nabla \cdot \dfrac{\mathbf{m}}{\rho} - \nabla \cdot \mathbf{m}^* \\
-\dfrac{\partial \mathbf{m}^*}{\partial t} - \dfrac{p}{\rho} \nabla \rho^* - \dfrac{\gamma - 1}{\rho} \nabla \rho^* \, p - \dfrac{\mathbf{m}}{\rho} \Big(\nabla \otimes \mathbf{m}^* + (\nabla \otimes \mathbf{m}^*)^T \Big) - \nabla p^* - \dfrac{\zeta}{\rho} \nabla \zeta^* \\
-\dfrac{\partial p^*}{\partial t} + \dfrac{p \, \mathbf{m}}{\rho^2} \cdot \nabla \rho^* + \dfrac{(\gamma - 1)\, \mathbf{m}}{\rho^2} \cdot \nabla \rho^* \, p + \dfrac{\mathbf{m}}{\rho} \cdot \Big(\dfrac{\mathbf{m}}{\rho} \cdot \nabla \Big) \mathbf{m}^* + \dfrac{\zeta \, \mathbf{m}}{\rho^2} \cdot \nabla \zeta^* \\
-\dfrac{\partial \zeta^*}{\partial t} - \dfrac{\mathbf{m}}{\rho} \cdot \nabla \zeta^*
\end{pmatrix}.$$

The boundary terms which result from the integrations by parts are

$$
\begin{aligned}
b = &\int_{\Omega} \Big(p^* \rho' + m_j^* m_j' + \rho^* p' + \zeta^* \zeta \Big)\Big|_0^T \, d\mathbf{x} \\
&+ \int_0^T \int_{\partial\Omega} n_j \Big[p^* m_j' + m_i^* \Big(\frac{m_j' m_i}{\rho} + \frac{m_j m_i'}{\rho} - \frac{\rho' m_j m_i}{\rho^2} \Big) + m_j^* p' \\
&\qquad + \rho^* \Big(\frac{p' m_j}{\rho} + \frac{p m_j'}{\rho} - \frac{\rho' p m_j}{\rho^2} + \frac{\gamma - 1}{\rho^2} \left(\rho p' m_j + \rho p m_j' - \rho' p m_j \right) \Big) \\
&\qquad + \zeta^* \Big(\frac{\zeta' m_j}{\rho} + \frac{\zeta m_j'}{\rho} - \frac{\rho' \zeta m_j}{\rho^2} \Big) \Big] \, d\mathbf{x} \, dt,
\end{aligned}
$$

where $\mathbf{n}$ denotes a unit outward normal to the surface $\partial\Omega$ of the domain Ω.

Appendix C

Details of numerical method for DNS of controlled turbulent channel flow

The equation governing the flow in the present case (with the forcing in a form slightly generalized from that in the text) is:

$$\mathcal{N}(\mathbf{q}) = \begin{pmatrix} \dfrac{\partial u_j}{\partial x_j} \\ \dfrac{\partial u_i}{\partial t} + \dfrac{\partial u_j u_i}{\partial x_j} - \nu \dfrac{\partial^2 u_i}{\partial x_j^2} + \dfrac{\partial p}{\partial x_i} \end{pmatrix} = \begin{pmatrix} 0 \\ -\delta_{1i}\, P_x(\mathbf{x}, t) + f_i(\phi) \end{pmatrix} \qquad \text{in } \Omega$$

with periodic boundary conditions on the velocity on $\Gamma_1^{\pm}$ and $\Gamma_3^{\pm}$ (the streamwise and spanwise directions) and a wall-normal control velocity distributed over the walls

$$\mathbf{u} = g_i(\phi) \qquad \text{on } \Gamma_2^{\pm},$$

where $\mathbf{n}$ is the unit outward normal to the boundary $\partial\Omega$, and prescribed initial conditions on the velocity

$$\mathbf{u} = \mathbf{u}_0 \qquad \text{at } t = 0.$$

To solve this problem computationally, the continuous flow field must be approximated on a discrete set of points in space. Further, the resulting approximate equation on this finite set of points must be advanced in time using discrete time steps. To minimize the expense of the computation, one desires to use as few spatial points as possible and as large time steps as possible while maintaining accuracy (in both space and time) and stability of the simulation. Since the flow is periodic in the streamwise direction, so that there is no inflow or outflow, it is critical that the numerical errors due to spatial and temporal discretization of the physical problem do not accumulate in a way which causes the simulation to be unstable. Subject this restriction, a scheme with high spatial accuracy is desired. Finally, with a particular spatial discretization, it is found that certain terms of the governing equation have more restrictive time step limitations than do others in the time-advancing algorithm. The most restrictive terms should be taken implicitly to allow for stability at "large" time steps (which, however, must be kept small enough to ensure accuracy of the computation), while other less restrictive terms may be taken explicitly. These issues guide the choice of spatial and temporal discretizations of the current problem, which are discussed in detail below.

C.1 Spatial discretization

A grid must be chosen to discretize the flow quantities in space. This grid is chosen to be equispaced and unstaggered in the streamwise (x_1) and spanwise (x_3) directions, allowing Fourier transforms to be used to accurately and efficiently compute all derivatives in these directions. A finite volume approach is used to determine discrete difference expressions for the derivatives in the wall normal direction, which is discretized with a hyperbolic tangent stretching function:

$$x_{2_n} = \frac{\tanh\left(C_s\left(\frac{2\,n}{NY}-1\right)\right)}{\tanh\left(C_s\right)}, \tag{C.1a}$$

with the integer n enumerating the grid in this direction. (A stretching parameter of $C_s = 1.75$ results in a fairly smooth grid, and is used in the present computations.) Note that $n = 0$ corresponds to the lower wall and $n = NY$ corresponds to the upper wall. With this as the base grid, we make the following definitions:

$$x_{2_{n-1/2}} = \frac{1}{2}\left(x_{2_n} + x_{2_{n-1}}\right) \tag{C.1b}$$

$$\Delta x_{2_{n-1/2}} = x_{2_n} - x_{2_{n-1}} \tag{C.1c}$$

$$\Delta x_{2_n} = x_{2_{n+1/2}} - x_{2_{n-1/2}} = \frac{1}{2}\left(\Delta x_{2_{n+1/2}} + \Delta x_{2_{n-1/2}}\right) \tag{C.1d}$$

In this discussion, the subscript n is used to indicate gridpoints at integer x_2 locations, and the subscript $n-1/2$ is used to indicate the gridpoints between these points. The wall-normal component of velocity u_2 is discretized on the n family of gridpoints and the streamwise and spanwise components of velocity u_1 and u_3 and the pressure p are discretized on the $n-1/2$ family of gridpoints. The motivation for staggering the wall-normal component of velocity from the pressure is to couple the pressure at the nodes with n even to the pressure at the nodes with n odd. This is a natural result of a staggered grid, but is not the case in non-staggered configurations. The streamwise and spanwise components of velocity must be discretized at the same x_2 locations as the pressure in order to solve the appropriate discretization of the continuity equation exactly in the fractional step algorithm, as will be shown later in this Appendix.

To interpolate these quantities to the adjacent gridpoints when necessary, the following interpolation formula is used for u_2:

$$\bar{u}_{2_{n-1/2}} = \frac{1}{2}\left(u_{2_n} + u_{2_{n-1}}\right) \qquad \text{(exactly second order)}$$

and the following interpolation formula are used for u_1 and u_3:

$$\begin{aligned}
\bar{u}_{1_n} &= \frac{1}{2}\left(u_{1_{n+1/2}} + u_{1_{n-1/2}}\right) && \text{(quasi-second order)}\\
\check{u}_{1_n} &= \frac{1}{2\,\Delta x_{2_n}}\left(\Delta x_{2_{n+1/2}} u_{1_{n+1/2}} + \Delta x_{2_{n-1/2}} u_{1_{n-1/2}}\right) && \text{(quasi-second order),}\\
\check{\check{u}}_{1_n} &= \frac{1}{2\,\Delta x_{2_n}}\left(\Delta x_{2_{n-1/2}} u_{1_{n+1/2}} + \Delta x_{2_{n+1/2}} u_{1_{n-1/2}}\right) && \text{(exactly second order).}
\end{aligned}$$

Interpolation for p is not required in the staggered grid formulation. As $x_{2_{n-1/2}}$ is midway between x_{2_n} and $x_{2_{n-1}}$, the interpolation formula for $\bar{u}_{2_{n-1/2}}$ is second-order accurate. As x_{2_n} is *not* midway between $x_{2_{n+1/2}}$ and $x_{2_{n-1/2}}$ on the stretched grid, only the interpolation formula for $\check{\check{u}}_{1_n}$ is truly second-order accurate. The formula for $\bar{u}_{1_n}$ and $\check{u}_{1_n}$ are only second-order accurate in the sense that, as NY is increased with the stretching function (C.1a) fixed, $\Delta x_{2_{n+1/2}}/\Delta x_{2_{n-1/2}} \to 1$, and all three forms approach a second order form.

The motivation for using interpolation forms which are only second order accurate in the sense described above stems from conservation issues, which are described in the following section. Though the "proper" second-order interpolation formula $\check{\check{u}}_{1_n}$ can be used everywhere, the discretization error of such an interpolation formula results in spurious sources and sinks of energy on a marginally-resolved stretched grid, which can lead to numerical instabilities. Proper use of the above interpolation formulae prevents discretization errors from contributing to the total energy of the flow. Note that a sufficiently smooth grid stretching function is used to minimize the inaccuracies caused by these interpolation formulae for reasonable values of NY.

For the notational convenience of extending difference formulae to the cells adjacent to the walls, we also make the following useful definitions:

$$\begin{aligned}
\Delta x_{2_{NY}} &= x_{2_{NY}} - x_{2_{NY-1/2}} & \qquad \Delta x_{2_0} &= x_{2_{1/2}} - x_{2_0}\\
u_{1_{NY+1/2}} &= \bar{u}_{1_{NY}} = g_{1_{NY}}(\phi) & \qquad u_{1_{-1/2}} &= \bar{u}_{1_0} = g_{1_0}(\phi)
\end{aligned}$$

$$u_{2_{NY+1}} = \bar{u}_{2_{NY+1/2}} = u_{2_{NY}} = g_{2_{NY}}(\phi) \qquad u_{2_{-1}} = \bar{u}_{2_{-1/2}} = u_{2_0} = g_{2_0}(\phi)$$
$$u_{3_{NY+1/2}} = \bar{u}_{3_{NY}} = g_{3_{NY}}(\phi) \qquad u_{3_{-1/2}} = \bar{u}_{3_0} = g_{3_0}(\phi).$$
$$p_{NY+1/2} = p_{NY} = p_{NY-1/2} \qquad p_{-1/2} = p_0 = p_{1/2}$$

With the spatial discretization of the flow quantities described above, the individual momentum equations are solved at the corresponding velocity points and the continuity equation is solved at the pressure points. The spatial discretization of the derivatives in the governing equation are now made precise:

$$\begin{pmatrix} \left.\dfrac{\delta u_j}{\delta x_j}\right|_{n-1/2} \\ \left[\dfrac{\partial u_1}{\partial t} + \dfrac{\delta\,(u_1 u_j)}{\delta x_j} - \nu \dfrac{\delta^2 u_1}{\delta x_j^2} + \dfrac{\delta p}{\delta x_1}\right]_{n-1/2} \\ \left[\dfrac{\partial u_2}{\partial t} + \dfrac{\delta\,(u_2 u_j)}{\delta x_j} - \nu \dfrac{\delta^2 u_2}{\delta x_j^2} + \dfrac{\delta p}{\delta x_2}\right]_{n} \\ \left[\dfrac{\partial u_3}{\partial t} + \dfrac{\delta\,(u_3 u_j)}{\delta x_j} - \nu \dfrac{\delta^2 u_3}{\delta x_j^2} + \dfrac{\delta p}{\delta x_3}\right]_{n-1/2} \end{pmatrix} = \begin{pmatrix} 0 \\ -P_x + f_{1_{n-1/2}}(\phi) \\ f_{2_n}(\phi) \\ f_{3_{n-1/2}}(\phi) \end{pmatrix} \tag{C.2}$$

All first and second derivatives in the x_1 and x_3 directions are computed in Fourier space according to:

$$\widehat{\frac{\delta_s q}{\delta x_1}} = i\,k_x\,\hat{q} \qquad \widehat{\frac{\delta_s q}{\delta x_3}} = i\,k_z\,\hat{q} \qquad \widehat{\frac{\delta_s^2 q}{\delta x_1}} = -k_x^2\,\hat{q} \qquad \widehat{\frac{\delta_s^2 q}{\delta x_3}} = -k_z^2\,\hat{q},$$

where the hat indicates the Fourier transform in the x_1 and x_3 directions with corresponding wavenumbers k_x and k_z, q is an arbitrary flow quantity, and the s subscript is used to emphasize that the derivative is evaluated spectrally. The convective terms involving derivatives in the x_2 direction are computed with quasi-second-order accurate formulae motivated by a finite volume analysis. Written out completely, the convective terms are:

$$\left.\frac{\delta\,(u_1 u_j)}{\delta x_j}\right|_{n-1/2} = \frac{\delta_s\,(u_1 u_1)_{n-1/2}}{\delta x_1} + \frac{(\bar{u}_1 u_2)_n - (\bar{u}_1 u_2)_{n-1}}{\Delta x_{2_{n-1/2}}} + \frac{\delta_s\,(u_1 u_3)_{n-1/2}}{\delta x_3}$$
$$\left.\frac{\delta\,(u_2 u_j)}{\delta x_j}\right|_{n} = \frac{\delta_s\,(u_2 \check{u}_1)_n}{\delta x_1} + \frac{(\bar{u}_2 \bar{u}_2)_{n+1/2} - (\bar{u}_2 \bar{u}_2)_{n-1/2}}{\Delta x_{2_n}} + \frac{\delta_s\,(u_2 \check{u}_3)_n}{\delta x_3}$$
$$\left.\frac{\delta\,(u_3 u_j)}{\delta x_j}\right|_{n-1/2} = \frac{\delta_s\,(u_3 u_1)_{n-1/2}}{\delta x_1} + \frac{(\bar{u}_3 u_2)_n - (\bar{u}_3 u_2)_{n-1}}{\Delta x_{2_{n-1/2}}} + \frac{\delta_s\,(u_3 u_3)_{n-1/2}}{\delta x_3}.$$

Note that the interpolation formulae chosen in the above expressions have been selected deliberately in order to achieve energy conservation, as discussed in the following section. The viscous terms involving derivatives in the x_2 direction are evaluated with a second-order accurate finite difference formula. Written out completely, the viscous terms are:

$$\begin{aligned}
\left.\frac{\delta^2 u_1}{\delta x_j^2}\right|_{n-1/2} &= \frac{\delta_s^2 u_{1_{n-1/2}}}{\delta x_1^2} + \left(\frac{u_{1_{n+1/2}} - u_{1_{n-1/2}}}{\Delta x_{2_n}} - \frac{u_{1_{n-1/2}} - u_{1_{n-3/2}}}{\Delta x_{2_{n-1}}}\right) / \Delta x_{2_{n-1/2}} + \frac{\delta_s^2 u_{1_{n-1/2}}}{\delta x_3^2} \\
\left.\frac{\delta^2 u_2}{\delta x_j^2}\right|_{n} &= \frac{\delta_s^2 u_{2_n}}{\delta x_1^2} + \left(\frac{u_{2_{n+1}} - u_{2_n}}{\Delta x_{2_{n+1/2}}} - \frac{u_{2_n} - u_{2_{n-1}}}{\Delta x_{2_{n-1/2}}}\right) / \Delta x_{2_n} + \frac{\delta_s^2 u_{2_n}}{\delta x_3^2} \\
\left.\frac{\delta^2 u_3}{\delta x_j^2}\right|_{n-1/2} &= \frac{\delta_s^2 u_{3_{n-1/2}}}{\delta x_1^2} + \left(\frac{u_{3_{n+1/2}} - u_{3_{n-1/2}}}{\Delta x_{2_n}} - \frac{u_{3_{n-1/2}} - u_{3_{n-3/2}}}{\Delta x_{2_{n-1}}}\right) / \Delta x_{2_{n-1/2}} + \frac{\delta_s^2 u_{3_{n-1/2}}}{\delta x_3^2}.
\end{aligned}$$

The required derivatives of p are given by

$$\left.\frac{\delta p}{\delta x_1}\right|_{n-1/2} = \frac{\delta_s p_{n-1/2}}{\delta x_1}, \qquad \left.\frac{\delta p}{\delta x_2}\right|_{n} = \frac{p_{n+1/2} - p_{n-1/2}}{\Delta x_{2_n}}, \qquad \left.\frac{\delta p}{\delta x_3}\right|_{n-1/2} = \frac{\delta_s p_{n-1/2}}{\delta x_3},$$

$$\left.\frac{\delta^2 p}{\delta x_j^2}\right|_{n-1/2} = \frac{\delta_s^2 p_{n-1/2}}{\delta x_1^2} + \left(\frac{p_{n+1/2} - p_{n-1/2}}{\Delta x_{2_n}} - \frac{p_{n-1/2} - p_{n-3/2}}{\Delta x_{2_{n-1}}}\right) / \Delta x_{2_{n-1/2}} + \frac{\delta_s^2 p_{n-1/2}}{\delta x_3^2}.$$

(The Laplacian of the pressure is required by the Poisson equation to update the pressure in the fractional step algorithm.) Finally, the discretization of the continuity equation is

$$\left.\frac{\delta u_j}{\delta x_j}\right|_{n-1/2} = \frac{\delta_s u_{1_{n-1/2}}}{\delta x_1} + \frac{u_{2_n} - u_{2_{n-1}}}{\Delta x_{2_{n-1/2}}} + \frac{\delta_s u_{3_{n-1/2}}}{\delta x_3}. \tag{C.3}$$

C.1.1 Conservation of mass, momentum, and energy

An important check on the stability of an incompressible channel flow code is that mass should be conserved to within machine round-off error, and spatial discretization errors should not contribute to the momentum and energy of the flow integrated over the channel volume.

To show that the total mass is conserved, the compressible continuity equation is integrated over the volume under consideration (with the integrals on the right hand side evaluated with a trapezoidal rule in the wall normal direction and spectral rules in the Fourier directions), verifying that numerical errors do not contribute to net sources of mass and thus the discretized system indeed conserves total mass exactly:

$$\begin{aligned}
\frac{\partial}{\partial t}\int_\Omega \rho\, dV &= -\int_\Omega \frac{\delta\, \rho u_j}{\delta x_j}\, dV \\
&= -\rho \int_x \int_z \sum_{n=1}^{NY} \Delta x_{2_{n-1/2}} \left(\frac{\delta_s u_{1_{n-1/2}}}{\delta x_1} + \frac{u_{2_n} - u_{2_{n-1}}}{\Delta x_{2_{n-1/2}}} + \frac{\delta_s u_{3_{n-1/2}}}{\delta x_3} \right) dx\, dz \\
&= -\rho \int_x \int_z \left(u_{2_{NY}} - u_{2_0} \right) dx\, dz = 0 \implies \text{Mass is conserved.}
\end{aligned}$$

To show that total momentum is conserved in each direction x_i for cases with $f_i(\phi) = 0$ and $g_i(\phi) = 0$, each component of the momentum equation in (C.2) is integrated over the volume under consideration:

$$\frac{\partial}{\partial t}\int_\Omega u_i\, dV = -\int_\Omega \left(\frac{\delta\,(u_i u_j)}{\delta x_j} + \frac{\delta p}{\delta x_i} + \delta_{1i}\, P_x - \nu \frac{\delta^2 u_i}{\delta x_j^2} \right) dV$$

$$= \begin{cases}
\begin{aligned}
-\int_x\int_z \sum_{n=1}^{NY} \Delta x_{2_{n-1/2}} \Big[&\frac{(\bar u_1 u_2)_n - (\bar u_1 u_2)_{n-1}}{\Delta x_{2_{n-1/2}}} + P_x \\
&- \nu \Big(\frac{u_{1_{n+1/2}} - u_{1_{n-1/2}}}{\Delta x_{2_n}} - \frac{u_{1_{n-1/2}} - u_{1_{n-3/2}}}{\Delta x_{2_{n-1}}} \Big) / \Delta x_{2_{n-1/2}} \Big]\, dx\, dz
\end{aligned} & \text{for } i = 1 \\[2ex]
\begin{aligned}
-\int_x\int_z \sum_{n=0}^{NY} \Delta x_{2_n} \Big[&\frac{(\bar u_2 \bar u_2)_{n+1/2} - (\bar u_2 \bar u_2)_{n-1/2}}{\Delta x_{2_n}} + \frac{p_{n+1/2} - p_{n-1/2}}{\Delta x_{2_n}} \\
&- \nu \Big(\frac{u_{2_{n+1}} - u_{2_n}}{\Delta x_{2_{n+1/2}}} - \frac{u_{2_n} - u_{2_{n-1}}}{\Delta x_{2_{n-1/2}}} \Big) / \Delta x_{2_n} \Big]\, dx\, dz
\end{aligned} & \text{for } i = 2 \\[2ex]
\begin{aligned}
-\int_x\int_z \sum_{n=1}^{NY} \Delta x_{2_{n-1/2}} \Big[&\frac{(\bar u_3 u_2)_n - (\bar u_3 u_2)_{n-1}}{\Delta x_{2_{n-1/2}}} \\
&- \nu \Big(\frac{u_{3_{n+1/2}} - u_{3_{n-1/2}}}{\Delta x_{2_n}} - \frac{u_{3_{n-1/2}} - u_{3_{n-3/2}}}{\Delta x_{2_{n-1}}} \Big) / \Delta x_{2_{n-1/2}} \Big]\, dx\, dz
\end{aligned} & \text{for } i = 3
\end{cases}$$

$$= \begin{cases}
-\int_x\int_z \left[2\,\delta\, P_x - \nu \left(\frac{u_{1_{NY}} - u_{1_{NY-1/2}}}{\Delta x_{2_{NY}}} - \frac{u_{1_{1/2}} - u_{1_0}}{\Delta x_{2_0}} \right) \right] dx\, dz & \text{for } i = 1 \\[2ex]
-\int_x\int_z \left[p_{NY} - p_0 \right] dx\, dz & \text{for } i = 2 \\[2ex]
-\int_x\int_z \left[-\nu \left(\frac{u_{3_{NY}} - u_{3_{NY-1/2}}}{\Delta x_{2_{NY}}} - \frac{u_{3_{1/2}} - u_{3_0}}{\Delta x_{2_0}} \right) \right] dx\, dz & \text{for } i = 3.
\end{cases}$$

In the limit that $\nu \to 0$ with $P_x = 0$, momentum is conserved in the x_1 and x_3 directions. Note that the wall pressure terms may result in small variations in the momentum in the x_2 direction, but non-physical spatial discretization errors do not contribute to this variation. For cases in which $\nu \neq 0$, it is seen that choosing

$$P_x = \frac{1}{V} \int_x \int_z \nu \left(\frac{u_{1_{NY}} - u_{1_{NY-1/2}}}{\Delta x_{2_{NY}}} - \frac{u_{1_{1/2}} - u_{1_0}}{\Delta x_{2_0}} \right) dx\, dz, \tag{C.4}$$

where $V = 2\delta\, L_x\, L_z$ is the volume of the domain under consideration, maintains the x_1 component of momentum (i.e. mass flux) constant by exactly balancing the skin friction integrated over the walls with the force applied by the mean pressure gradient.

The viscous terms of the Navier-Stokes equation result in energy dissipation at the small scales, which, in channel flow, is replenished by the action of the pressure gradient P_x on the flow at the large scale. To show that energy is conserved in cases with $\nu = P_x = f_i(\phi) = g_i(\phi) = 0$, the momentum equation in (C.2) is multiplied by u_i and integrated over the volume under consideration (underbraced sums "telescope" and therefore cancel):

$$
\begin{aligned}
&\frac{\partial}{\partial t}\int_\Omega \frac{u_i^2}{2}\, dV = -\int_\Omega u_i \left(\frac{\delta\,(u_i u_j)}{\delta x_j} + \frac{\delta p}{\delta x_i}\right) dV \\
&= -\int_x\int_z \Bigg[\sum_{n=1}^{NY} \Delta x_{2_{n-1/2}}\, u_{1_{n-1/2}} \left(\frac{\delta_s\,(u_1 u_1)_{n-1/2}}{\delta x_1} + \frac{(\bar{u}_1 u_2)_n - (\bar{u}_1 u_2)_{n-1}}{\Delta x_{2_{n-1/2}}} + \frac{\delta_s\,(u_1 u_3)_{n-1/2}}{\delta x_3} + \frac{\delta_s p_{n-1/2}}{\delta x_1}\right) \\
&\quad + \sum_{n=0}^{NY} \Delta x_{2_n}\, u_{2_n} \left(\frac{\delta_s\,(u_2 \check{u}_1)_n}{\delta x_1} + \frac{(\bar{u}_2 \bar{u}_2)_{n+1/2} - (\bar{u}_2 \bar{u}_2)_{n-1/2}}{\Delta x_{2_n}} + \frac{\delta_s\,(u_2 \check{u}_3)_n}{\delta x_3} + \frac{p_{n+1/2} - p_{n-1/2}}{\Delta x_{2_n}}\right) \\
&\quad + \sum_{n=1}^{NY} \Delta x_{2_{n-1/2}}\, u_{3_{n-1/2}} \left(\frac{\delta_s\,(u_3 u_1)_{n-1/2}}{\delta x_1} + \frac{(\bar{u}_3 u_2)_n - (\bar{u}_3 u_2)_{n-1}}{\Delta x_{2_{n-1/2}}} + \frac{\delta_s\,(u_3 u_3)_{n-1/2}}{\delta x_3} + \frac{\delta_s p_{n-1/2}}{\delta x_3}\right) \Bigg] dx\, dz \\
&= -\int_x\int_z \Bigg[\sum_{n=1}^{NY} \Delta x_{2_{n-1/2}}\, p_{n-1/2} \left(-\frac{\delta_s u_{1_{n-1/2}}}{\delta x_1} - \frac{u_{2_n} - u_{2_{n-1}}}{\Delta x_{2_{n-1/2}}} - \frac{\delta_s u_{3_{n-1/2}}}{\delta x_3}\right) \\
&\quad + \sum_{n=1}^{NY} \Delta x_{2_{n-1/2}} \left(\frac{u_{1_{n-1/2}}^2 + \left(u_{1_n}^2 + u_{1_n}^2\right)/2 + u_{1_{n-1/2}}^2}{2} - p_{n-1/2}\right) \left(\frac{\delta_s u_{1_{n-1/2}}}{\delta x_1} + \frac{\delta_s u_{3_{n-1/2}}}{\delta x_3}\right) dx\, dz \\
&\quad + \sum_{n=1}^{NY} \frac{1}{2} \left(\underbrace{u_{1_{n-1/2}} u_{1_{n+1/2}} u_{2_n} - u_{1_{n-1/2}} u_{1_{n-3/2}} u_{2_{n-1}}} + u_{1_{n-1/2}} u_{1_{n-1/2}} u_{2_n} - u_{1_{n-1/2}} u_{1_{n-1/2}} u_{2_{n-1}}\right) \\
&\quad + \sum_{n=1}^{NY-1} \frac{1}{4} \left(\underbrace{u_{2_n} u_{2_{n+1}} u_{2_{n+1}} - u_{2_n} u_{2_{n-1}} u_{2_n}} + \underbrace{u_{2_n} u_{2_{n+1}} u_{2_n} - u_{2_n} u_{2_{n-1}} u_{2_{n-1}}} + u_{2_n} u_{2_n} u_{2_{n+1}} - u_{2_n} u_{2_n} u_{2_{n-1}}\right) \\
&\quad + \sum_{n=1}^{NY} \frac{1}{2} \left(\underbrace{u_{3_{n-1/2}} u_{3_{n+1/2}} u_{2_n} - u_{3_{n-1/2}} u_{3_{n-3/2}} u_{2_{n-1}}} + u_{3_{n-1/2}} u_{3_{n-1/2}} u_{2_n} - u_{3_{n-1/2}} u_{3_{n-1/2}} u_{2_{n-1}}\right) \Bigg] dx\, dz \\
&= \int_x\int_z \sum_{n=1}^{NY} \Delta x_{2_{n-1/2}} \left(p_{n-1/2} - \frac{u_{1_{n-1/2}}^2 + \dfrac{u_{2_n}^2 + u_{2_{n-1}}^2}{2} + u_{3_{n-1/2}}^2}{2}\right) \left(\frac{\delta_s u_{1_{n-1/2}}}{\delta x_1} + \frac{u_{2_n} - u_{2_{n-1}}}{\Delta x_{2_{n-1/2}}} + \frac{\delta_s u_{3_{n-1/2}}}{\delta x_3}\right) dx\, dz \\
&= 0 \qquad \Longrightarrow \text{energy is conserved.}
\end{aligned}
$$

In the above derivation, it was assumed that integration by parts is valid in the spectral directions. Strictly speaking, this is only true if these directions are fully resolved, so that there is no possibility of aliasing. However, no calculation of a turbulent flow is ever "fully resolved". To make them affordable, direct numerical simulations are inevitably conducted with as few modes as possible which still give accurate results. There are two ways of handling the necessary truncation of the

Fourier series representation of the flow field under consideration: A) to allow the cascade of energy to higher wavenumbers (due to the nonlinear products) to alias back to lower wavenumbers, hoping that the effect of this aliasing will be minimal, or B) to zero out all higher-order variations resulting from nonlinear products, using the 3/2 dealiasing rule. Method A creates spurious energy sources, as the above derivation does *not* hold when the Fourier series are truncated (due to the fact that integration by parts in the spectral directions is invalid), and thus can lead to an unstable code. Method B constantly drains off the energy of all unresolved modes, and thus energy is not conserved in this case either. However, method B guarantees that no spurious numerical energy *sources* ever appear in the flow due to the Fourier series truncation, and thus can not destabilize the code. Thus, all calculations presented in this report are dealiased in the spectral directions.

Some additional algebra used in the energy conservation proof outlined above now follows (no summation is implied on the subscripts α and β). The step involving the integration by parts in a spectral direction β (neglecting the effects of truncation of the Fourier series) is:

$$\begin{aligned}
\int u_\alpha \frac{\delta_s u_\alpha u_\beta}{\delta x_\beta}\, dx_\beta &= \int \left(u_\alpha^2 \frac{\delta_s u_\beta}{\delta x_\beta} + u_\alpha u_\beta \frac{\delta_s u_\alpha}{\delta x_\beta} \right) dx_\beta \\
&= \int \left(u_\alpha^2 \frac{\delta_s u_\beta}{\delta x_\beta} - u_\alpha \frac{\delta_s u_\alpha u_\beta}{\delta x_\beta} \right) dx_\beta \\
\Rightarrow \int u_\alpha \frac{\delta_s u_\alpha u_\beta}{\delta x_\beta}\, dx_\beta &= \frac{1}{2} \int u_\alpha^2 \frac{\delta_s u_\beta}{\delta x_\beta}\, dx_\beta .
\end{aligned}$$

The x_2 derivatives in the convective terms of the x_2 momentum equation are written:

$$\begin{aligned}
\frac{1}{4} \sum_{n=1}^{NY-1} u_{2_n}^2 \left(u_{2_{n+1}} - u_{2_{n-1}} \right) &= \frac{1}{4} \sum_{n=1}^{NY-1} u_{2_n}^2 \left[\left(u_{2_{n+1}} - u_{2_n} \right) + \left(u_{2_n} - u_{2_{n-1}} \right) \right] \\
&= \frac{1}{2} \sum_{n=1}^{NY} \frac{u_{2_n}^2 + u_{2_{n-1}}^2}{2} \left(u_{2_n} - u_{2_{n-1}} \right).
\end{aligned}$$

Finally, the terms involving $\check{u}_\alpha$ are written:

$$\begin{aligned}
\sum_{n=1}^{NY-1} \Delta x_{2_n}\, u_{2_n} \frac{\delta_s \left(u_2 \check{u}_\alpha \right)_n}{\delta x_\alpha} &= \frac{1}{2} \sum_{n=1}^{NY-1} \left(\Delta x_{2_{n+1/2}}\, u_{2_n} \frac{\delta_s u_{2_n} u_{\alpha_{n+1/2}}}{\delta x_\alpha} + \Delta x_{2_{n-1/2}}\, u_{2_n} \frac{\delta_s u_{2_n} u_{\alpha_{n-1/2}}}{\delta x_\alpha} \right) \\
&= \frac{1}{4} \sum_{n=1}^{NY-1} \left(\Delta x_{2_{n+1/2}}\, u_{2_n}^2 \frac{\delta_s u_{\alpha_{n+1/2}}}{\delta x_\alpha} + \Delta x_{2_{n-1/2}}\, u_{2_n}^2 \frac{\delta_s u_{\alpha_{n-1/2}}}{\delta x_\alpha} \right) \\
&= \frac{1}{2} \sum_{n=1}^{NY-1} \Delta x_{2_{n-1/2}} \frac{u_{2_n}^2 + u_{2_{n-1}}^2}{2} \frac{\delta_s u_{\alpha_{n-1/2}}}{\delta x_\alpha}.
\end{aligned}$$

C.2 Temporal discretization of flow problem

The temporal discretization used in the present work is identical to that used by Akselvoll & Moin (1995), and therefore will be written here with minimal explanation. The reader is referred to Akselvoll & Moin (1995) for a clear description of the details of the derivation of this temporal discretization.

Let the operator A_i represent the terms treated explicitly (third order Runge-Kutta) and B_i represent the terms treated implicitly in the Navier Stokes equation (C.2):

$$\begin{aligned}
\frac{u_i^k - u_i^{k-1}}{\Delta t} &= \beta_k \left(B_i(u_j^k) + B_i(u_j^{k-1})\right) + \gamma_k A_i(u_j^{k-1}) + \zeta_k A_i(u_j^{k-2}) \\
&\quad + 2\beta_k \left(-\frac{\delta p^k}{\delta x_i} - \delta_{1i} P_x + f_i(\phi^{k-1})\right) \\
\frac{\delta u_i^k}{\delta x_i} &= 0,
\end{aligned}$$

where the explicit and implicit operators are given, as in Akselvoll & Moin (1995), by:

$$\begin{aligned}
A_1(u_j) =& \frac{\delta}{\delta x_1}\left[\nu \frac{\delta u_1}{\delta x_1}\right] + \frac{\delta}{\delta x_3}\left[\nu \frac{\delta u_1}{\delta x_3}\right] - \frac{\delta u_1 u_1}{\delta x_1} - \frac{\delta u_3 u_1}{\delta x_3} \\
A_2(u_j) =& \frac{\delta}{\delta x_1}\left[\nu \frac{\delta u_2}{\delta x_1}\right] + \frac{\delta}{\delta x_3}\left[\nu \frac{\delta u_2}{\delta x_3}\right] - \frac{\delta u_1 u_2}{\delta x_1} - \frac{\delta u_3 u_2}{\delta x_3} \\
A_3(u_j) =& \frac{\delta}{\delta x_1}\left[\nu \frac{\delta u_3}{\delta x_1}\right] + \frac{\delta}{\delta x_3}\left[\nu \frac{\delta u_3}{\delta x_3}\right] - \frac{\delta u_1 u_3}{\delta x_1} - \frac{\delta u_3 u_3}{\delta x_3} \\
B_1(u_j) =& \frac{\delta}{\delta x_2}\left[\nu \frac{\delta u_1}{\delta x_2}\right] - \frac{\delta u_2 u_1}{\delta x_2} \\
B_2(u_j) =& \frac{\delta}{\delta x_2}\left[\nu \frac{\delta u_2}{\delta x_2}\right] - \frac{\delta u_2 u_2}{\delta x_2} \\
B_3(u_j) =& \frac{\delta}{\delta x_2}\left[\nu \frac{\delta u_3}{\delta x_2}\right] - \frac{\delta u_2 u_3}{\delta x_2}.
\end{aligned}$$

The Runge-Kutta coefficients used in the present computations are:

$$\begin{aligned}
\beta_1 &= \frac{4}{15}, & \beta_2 &= \frac{1}{15}, & \beta_3 &= \frac{1}{6}, \\
\gamma_1 &= \frac{8}{15}, & \gamma_2 &= \frac{5}{12}, & \gamma_3 &= \frac{3}{4}, \\
\zeta_1 &= 0, & \zeta_2 &= -\frac{17}{60}, & \zeta_3 &= -\frac{5}{12}.
\end{aligned}$$

An important key to the success of the present approach is that wall-normal derivatives may be linearized (without loss of overall accuracy of the method) according to

$$\overline{B}_2(u_j^k) = \frac{\delta}{\delta x_2}\left[\nu \frac{\delta u_2^k}{\delta x_2}\right] - 2\frac{\delta u_2^{k-1} u_2^k}{\delta x_2} + \frac{\delta u_2^{k-1} u_2^{k-1}}{\delta x_2}. \tag{C.5}$$

The fractional step method for the flow problem may now be written out (in order of computation in the actual code) as follows. The right hand sides, containing all terms computed explicitly, are first computed:

$$\begin{aligned}
R_1 =& u_1^{k-1} + \beta_k \Delta t \left(\frac{\delta}{\delta x_2}\left[\nu \frac{\delta u_1^{k-1}}{\delta x_2}\right] - \frac{\delta u_2^{k-1} u_1^{k-1}}{\delta x_2} \right) \\
&+ \gamma_k \Delta t A_1(u_j^{k-1}) + \zeta_k \Delta t A_1(u_j^{k-2}) + 2\beta_k \Delta t \left(-\frac{\delta p^{k-1}}{\delta x_1} - P_x + f_1(\phi^{k-1}) \right) \\
R_2 =& u_2^{k-1} + \beta_k \Delta t \left(\frac{\delta}{\delta x_2}\left[\nu \frac{\delta u_2^{k-1}}{\delta x_2}\right] \right) \\
&+ \gamma_k \Delta t A_2(u_j^{k-1}) + \zeta_k \Delta t A_2(u_j^{k-2}) + 2\beta_k \Delta t \left(-\frac{\delta p^{k-1}}{\delta x_2} + f_2(\phi^{k-1}) \right) \\
R_3 =& u_3^{k-1} + \beta_k \Delta t \left(\frac{\delta}{\delta x_2}\left[\nu \frac{\delta u_3^{k-1}}{\delta x_2}\right] - \frac{\delta u_2^{k-1} u_3^{k-1}}{\delta x_2} \right) \\
&+ \gamma_k \Delta t A_3(u_j^{k-1}) + \zeta_k \Delta t A_3(u_j^{k-2}) + 2\beta_k \Delta t \left(-\frac{\delta p^{k-1}}{\delta x_3} + f_3(\phi^{k-1}) \right).
\end{aligned}$$

Note that the pressure is accounted for explicitly in the above expressions. With the right hand sides computed, the implicit (tridiagonal) problem for the x_2 component of a (non-divergence-free) intermediate field $\hat{\mathbf{u}}$ may be solved based on the linearized treatment of the implicit wall-normal derivatives:

$$\left\{ 1 - \beta_k \Delta t \frac{\delta}{\delta x_2}\left[\nu \frac{\delta \cdot}{\delta x_2}\right] + 2\beta_k \Delta t \frac{\delta u_2^{k-1} \cdot}{\delta x_2} \right\} \hat{u}_2 = R_2.$$

With $\hat{u}_2$ computed, the implicit problems for the x_1 and x_3 components of $\hat{\mathbf{u}}$ may be solved:

$$\left\{ 1 - \beta_k \Delta t \frac{\delta}{\delta x_2}\left[\nu \frac{\delta \cdot}{\delta x_2}\right] + \beta_k \Delta t \frac{\delta \hat{u}_2 \cdot}{\delta x_2} \right\} \hat{u}_1 = R_1$$

$$\left\{ 1 - \beta_k \Delta t \frac{\delta}{\delta x_2}\left[\nu \frac{\delta \cdot}{\delta x_2}\right] + \beta_k \Delta t \frac{\delta \hat{u}_2 \cdot}{\delta x_2} \right\} \hat{u}_3 = R_3.$$

Finally, a Poisson equation for the pressure update $\varphi = p^k - p^{k-1}$ is computed based on the divergence of this intermediate field:

$$\frac{\delta \varphi}{\delta x_i \delta x_i} = \frac{1}{2\beta_k \Delta t} \frac{\delta \hat{u}_i}{\delta x_i}.$$

The pressure update term φ is then used both to project the intermediate velocity field $\hat{\mathbf{u}}$ onto a divergence free field $\mathbf{u}^k$

$$u_i^k = \hat{u}_i - 2\beta_k \Delta t \frac{\delta \varphi}{\delta x_i},$$

and, of course, to update the pressure p^k itself

$$p^k = p^{k-1} + \varphi.$$

C.3 Temporal discretization of adjoint problem

The temporal discretization for the adjoint problem follows closely that of the flow problem developed in the previous section. The equation governing the adjoint is

$$\mathcal{N}'(\mathbf{q})^* \, \mathbf{q}^* = \begin{pmatrix} -\dfrac{\partial u_j^*}{\partial x_j} \\ -\dfrac{\partial u_i^*}{\partial t} - u_j \Big(\dfrac{\partial u_i^*}{\partial x_j} + \dfrac{\partial u_j^*}{\partial x_i} \Big) - \nu \dfrac{\partial^2 u_i^*}{\partial x_j^2} - \dfrac{\partial p^*}{\partial x_i} \end{pmatrix} = \begin{pmatrix} 0 \\ f_i^* \end{pmatrix} \qquad \text{in } \Omega$$

with boundary conditions, initial conditions, and interior forcing terms f_i^* which vary from case to case, as outlined in the main text. In order to simplify the notation for the remainder of this appendix, in which superscripts indicate the Runge-Kutta substep, the tilde notation ($\tilde{}$) will be adopted for the adjoint field rather than the asterisk notation (*).

Let the operator A_i represent the terms treated explicitly (third order Runge-Kutta) and B_i represent the terms treated implicitly in the adjoint equation (above):

$$\begin{aligned} \frac{\tilde{u}_i^k - \tilde{u}_i^{k-1}}{-\Delta t} &= \beta_k \left(B_i(\tilde{u}_j^k) + B_i(\tilde{u}_j^{k-1}) \right) + \gamma_k A_i(\tilde{u}_j^{k-1}) + \zeta_k A_i(\tilde{u}_j^{k-2}) \\ &\quad + 2\beta_k \left(\frac{\delta \tilde{p}^k}{\delta x_i} + \tilde{f}_i \right) \\ \frac{\delta \tilde{u}_i^k}{\delta x_i} &= 0 \end{aligned}$$

where the explicit and implicit operators are given by :

$$
\begin{aligned}
A_1(\tilde{u}_j) =& \frac{\delta}{\delta x_1}\left[\nu\frac{\delta \tilde{u}_1}{\delta x_1}\right] + \frac{\delta}{\delta x_3}\left[\nu\frac{\delta \tilde{u}_1}{\delta x_3}\right] + 2u_1\frac{\delta \tilde{u}_1}{\delta x_1} + u_2\frac{\delta \tilde{u}_2}{\delta x_1} + u_3\Big(\frac{\delta \tilde{u}_1}{\delta x_3} + \frac{\delta \tilde{u}_3}{\delta x_1}\Big)\\
A_2(\tilde{u}_j) =& \frac{\delta}{\delta x_1}\left[\nu\frac{\delta \tilde{u}_2}{\delta x_1}\right] + \frac{\delta}{\delta x_3}\left[\nu\frac{\delta \tilde{u}_2}{\delta x_3}\right] + u_1\frac{\delta \tilde{u}_2}{\delta x_1} - 2u_2\Big(\frac{\delta \tilde{u}_1}{\delta x_1} + \frac{\delta \tilde{u}_3}{\delta x_3}\Big) + u_3\frac{\delta \tilde{u}_2}{\delta x_3}\\
A_3(\tilde{u}_j) =& \frac{\delta}{\delta x_1}\left[\nu\frac{\delta \tilde{u}_3}{\delta x_1}\right] + \frac{\delta}{\delta x_3}\left[\nu\frac{\delta \tilde{u}_3}{\delta x_3}\right] + u_1\Big(\frac{\delta \tilde{u}_3}{\delta x_1} + \frac{\delta \tilde{u}_1}{\delta x_3}\Big) + u_2\frac{\delta \tilde{u}_2}{\delta x_3} + 2u_3\frac{\delta \tilde{u}_3}{\delta x_3}
\end{aligned}
$$

$$
\begin{aligned}
B_1(\tilde{u}_j) =& \frac{\delta}{\delta x_2}\left[\nu\frac{\delta \tilde{u}_1}{\delta x_2}\right] + u_2\frac{\delta \tilde{u}_1}{\delta x_2}\\
B_2(\tilde{u}_j) =& \frac{\delta}{\delta x_2}\left[\nu\frac{\delta \tilde{u}_2}{\delta x_2}\right] + u_1\frac{\delta \tilde{u}_1}{\delta x_2} + u_3\frac{\delta \tilde{u}_3}{\delta x_2}\\
B_3(\tilde{u}_j) =& \frac{\delta}{\delta x_2}\left[\nu\frac{\delta \tilde{u}_3}{\delta x_2}\right] + u_2\frac{\delta \tilde{u}_3}{\delta x_2}
\end{aligned}
$$

The fractional step method for adjoint problem may now be written out (in order of computation in the actual code) as follows. The right hand sides, containing all terms computed explicitly, are first computed:

$$
\begin{aligned}
\tilde{R}_1 =& \tilde{u}_1^{k-1} - \beta_k\Delta t\left(\frac{\delta}{\delta x_2}\left[\nu\frac{\delta \tilde{u}_1^{k-1}}{\delta x_2}\right] + u_2^{k-1}\frac{\delta \tilde{u}_1^{k-1}}{\delta x_2}\right)\\
&- \gamma_k\Delta t A_1(\tilde{u}_j^{k-1}) - \zeta_k\Delta t A_1(\tilde{u}_j^{k-2}) - 2\beta_k\Delta t\left(\frac{\delta \tilde{p}^{k-1}}{\delta x_1} + \tilde{f}_1\right)\\
\tilde{R}_2 =& \tilde{u}_2^{k-1} - \beta_k\Delta t\left(\frac{\delta}{\delta x_2}\left[\nu\frac{\delta \tilde{u}_2^{k-1}}{\delta x_2}\right] + u_1^{k-1}\frac{\delta \tilde{u}_1^{k-1}}{\delta x_2} + u_3^{k-1}\frac{\delta \tilde{u}_3^{k-1}}{\delta x_2}\right)\\
&- \gamma_k\Delta t A_2(\tilde{u}_j^{k-1}) - \zeta_k\Delta t A_2(\tilde{u}_j^{k-2}) - 2\beta_k\Delta t\left(\frac{\delta \tilde{p}^{k-1}}{\delta x_2} + \tilde{f}_2\right)\\
\tilde{R}_3 =& \tilde{u}_3^{k-1} - \beta_k\Delta t\left(\frac{\delta}{\delta x_2}\left[\nu\frac{\delta \tilde{u}_3^{k-1}}{\delta x_2}\right] + u_2^{k-1}\frac{\delta \tilde{u}_3^{k-1}}{\delta x_2}\right)\\
&- \gamma_k\Delta t A_3(\tilde{u}_j^{k-1}) - \zeta_k\Delta t A_3(\tilde{u}_j^{k-2}) - 2\beta_k\Delta t\left(\frac{\delta \tilde{p}^{k-1}}{\delta x_3} + \tilde{f}_3\right).
\end{aligned}
$$

With the right hand sides computed, the implicit (tridiagonal) problems for a (non-divergence-free) intermediate field $\hat{\mathbf{u}}$ may be solved:

$$
\left\{1 + \beta_k\Delta t\frac{\delta}{\delta x_2}\left[\nu\frac{\delta\cdot}{\delta x_2}\right] + \beta_k\Delta t\, u_2^k\frac{\delta\cdot}{\delta x_2}\right\}\hat{u}_1 = \tilde{R}_1
$$

$$\left\{1 + \beta_k \Delta t \frac{\delta}{\delta x_2}\left[\nu \frac{\delta\cdot}{\delta x_2}\right] + \beta_k \Delta t\, u_2^k \frac{\delta\cdot}{\delta x_2}\right\} \hat{u}_3 = \tilde{R}_3$$

$$\left\{1 + \beta_k \Delta t \frac{\delta}{\delta x_2}\left[\nu \frac{\delta\cdot}{\delta x_2}\right]\right\} \hat{u}_2 = \tilde{R}_2 - \beta_k \Delta t \left(u_1 \frac{\delta \hat{u}_1^k}{\delta x_2} + u_3 \frac{\delta \hat{u}_3^k}{\delta x_2}\right).$$

Finally, a Poisson equation for the adjoint pressure update $\tilde{\varphi} = \tilde{p}^k - \tilde{p}^{k-1}$ is computed based on the divergence of this intermediate field:

$$\frac{\delta \tilde{\varphi}}{\delta x_i \delta x_i} = \frac{1}{2\beta_k \Delta t} \frac{\delta \hat{u}_i}{\delta x_i}.$$

The adjoint pressure update term $(\tilde{p}^k - \tilde{p}^{k-1})$ is then used both to project the intermediate velocity field $\hat{\mathbf{u}}$ onto a divergence free field $\tilde{\mathbf{u}}^k$

$$\tilde{u}_i^k = \hat{u}_i - 2\beta_k \Delta t \frac{\delta \tilde{\varphi}}{\delta x_i},$$

and, of course, to update the adjoint pressure $\tilde{p}^k$ itself

$$\tilde{p}^k = \tilde{p}^{k-1} + \tilde{\varphi}.$$

REFERENCES

Abergel, F. & Temam, R. 1990 On some control problems in fluid mechanics. *Theor. and Comp. Fluid Dyn.* **1**, 303-325.

Akselvoll, K. & Moin, P. 1995 Large eddy simulation of turbulent confined coannular jets and turbulent flow over a backward facing step. *Report TF-63*, Thermosciences Division, Dept. of Mech. Eng., Stanford University.

Atkinson, G.W. 1993 *Chess and machine intuition.* Ablex.

Aubry, N., Holmes, P., Lumley, J.L., & Stone, E. 1988 The dynamics of coherent structures in the wall region of a turulent boundary layer. *J. Fluid Mech.* **192**, 115-173.

Bamieh, B. 1997 The structure of optimal controllers of spatially-invariant distributed parameter systems. *Proceedings of the 36th IEEE Conference on Decision and Control*, Dec 8-12, San Diego.

Barbu, V., & Sritharan, S.S. 1998 $\mathcal{H}_\infty$ control theory of fluid dynamics. *Proc. R. Soc. Lond. A* **454**, 3009-3033.

Bechert, D.W., Bruse, M., Hage, W. & Meyer R. 1997 Biological surfaces and their technological application - laboratory and flight experiments on drag reduction and separation control. *AIAA Paper No.* 97-1960.

BERKOOZ, G., HOLMES, P., & LUMLEY, J.L. 1993 The proper orthogonal decomposition in the analysis of turbulent flows. *Ann. Rev. Fluid Mech.* **25**, 539-575.

BEWLEY, T.R. 1999 Linear control and estimation of nonlinear chaotic convection: harnessing the butterfly effect. *Phys. Fluids*, **11**, (5), 1169-1186.

BEWLEY, T.R., CHOI, H., TEMAM, R., & MOIN, P. 1993 Optimal feedback control of turbulent channel flow. *1993 Annual Research Briefs*, Center for Turbulence Research, Stanford University/NASA Ames.

BEWLEY, T.R., FREUND, J.B., MOIN, P., CAIN, A., & PAREKH, D.E. 1998 Optimization of forcing profiles for turbulent jets. *Bulletin of The American Physical Society*, **43** (9), 2075.

BEWLEY, T.R., & LIU, S. 1998 Optimal and robust control and estimation of linear paths to transition. *J. Fluid Mech.* **365**, 305-349.

BEWLEY, T.R., MOIN, P., & TEMAM, R. 1996 A method for optimizing feedback control rules for wall-bounded turbulent flows based on control theory. *Proceedings of the ASME Fluids Engineering Summer Meeting*, ASME FED **237**, p. 279-285.

BEWLEY, T.R., MOIN, P., & TEMAM, R. 1997 Optimal and robust approaches for linear and nonlinear regulation problems in fluid mechanics. *AIAA Paper No.* 97-1872.

BEWLEY, T.R., TEMAM, R., & ZIANE, M. 1999 A general framework for robust control in fluid mechanics. To appear in *Physica D*.

BLACKBURN, H.M., MANSOUR, N.N., & CANTWELL, B.J. 1996 Topology of fine-scale motions in turbulent channel flow. *J. Fluid Mech.* **310**, 269-292.

BRYSON, A.E., & HO, Y.-C. 1975 *Applied optimal control.* Hemisphere.

CHANG, Y., & COLLIS, S.S. 1999 Active control of turbulent channel flows based on large-eddy simulation. Proceedings of the 3rd ASME/JSME Joint Fluids Engineering Conference, FEDSM99-6929. July 18-23, San Francisco.

CHOI, H., MOIN, P., & KIM, J. 1993 Direct numerical simulation of turbulent flow over riblets. *J. Fluid Mech.* **255**, 503-539.

CHOI, H., MOIN, P., & KIM, J. 1994 Active turbulence control for drag reduction in wall-bounded flows. *J. Fluid Mech.* **262**, 75-110.

CHONG, M.S., PERRY, A.E., & CANTWELL B.J. 1990 A general classification of three-dimensional flow fields. *Phys Fluids* A **2**, 765-777.

CLARKE, D. 1994 *Advances in model-based predictive control.* Oxford University Press.

COLLER, B.D., HOLMES, P., & LUMLEY, J.L. 1994 Control of bursting in boundary layer models. *Appl. Mech. Rev.* **47** (6), part 2, S139-S143.

COLLER, B.D., HOLMES, P., & LUMLEY, J.L. 1994 Control of noisy heteroclinic cycles. *Physica* D **72**, 135-160.

CORTELEZZI, L., LEE, K.H., KIM, J., & SPEYER, J.L. 1999 Skin-friction drag reduction via robust reduced-order linear feedback control. *Int. J. Comp. Fluid Dyn.*, submitted.

DOYLE, J.C., GLOVER, K., KHARGONEKAR, P.P., & FRANCIS, B.A. 1989 State-space solutions to standard $\mathcal{H}_2$ and $\mathcal{H}_\infty$ control problems. *IEEE Trans. Auto. Control* **34**, 831-847.

FARRELL, B.F., & IOANNOU, P.J. 1993 Stochastic forcing of the linearized Navier-Stokes equation. *Phys.*

Fluids A **5**, 2600-2609.

FEYNMAN, R.P. 1959 There's plenty of room at the bottom. Presented at the *Annual meeting of the American Physical Society* on December 29, 1959. First published in *Engineering and Science*, Caltech, February 1960.

FINLAYSON, B.A. 1972 *The Method of Weighted Residuals and Variational Principles.* Academic.

FURSIKOV, A.V., GUNZBURGER, M.D., & HOU, L.S. 1998 Boundary value problems and optimal boundary control for the Navier-Stokes system: the two-dimensional case. *SIAM J. Control Optim.* **36**, 852-894.

GAD EL HAK, M. 1996 Modern developments in flow control. *Appl. Mech. Rev.* **49** (7), 365-379.

GARCI, C.E., PRETT, D.M., & MORARI, M. 1990 Model predictive control: theory and practice–a survey. *Automatica* **3**, 335.

GIBSON, C.H. 1996 Turbulence in the ocean, atmosphere, galaxy, and universe. *Appl. Mech. Rev.* **49** (5), 299-315.

GREEN, M., & LIMEBEER, D.J.N. 1995 *Linear robust control.* Prentice-Hall.

GUNZBURGER, M.D., HOU, L., & SVOBODNY, T.P. 1990 A numerical method for drag minimization via the suction and injection of mass through the boundary. In *Stabilization of Flexible Structures* (ed. J.P. Zolesio). Springer.

GUNZBURGER, M.D. (Editor) 1995 *Flow Control.* Springer.

HAMMOND, E.P., BEWLEY, T.R., & MOIN, P. 1998 Observed mechanisms for turbulence attenuation and enhancement in opposition-controlled wall-bounded flows. *Physics of Fluids*, **10**, 2421-2423.

HEINKENSCHLOSS, M. 1997 Optimization Methods for Optimal Control Problems. In *Lecture Notes, Summer School on Continuous Optimization*, Hamburg-Harburg, Germany, September 22-26.

HEINKENSCHLOSS, M. 1999 From suboptimal to optimal control. *Proceedings of the NSF Workshop on Control of Flows*, UC San Diego, May 31 - June 1.

HERTZ, J., KROGH, A., & PALMER, R.G. 1991 *Introduction to the Theory of Neural Computation.* Addison-Wesley.

HILL, D.C. 1993 Drag reduction at a plane wall. *1993 Annual Research Briefs*, Center for Turbulence Research, Stanford University/NASA Ames.

HO, C.-M., & TAI, Y.-C. 1996 Review: MEMS and its applications for flow control. *ASME Journal of Fluid Engineering*, **118**, 437-447.

HO, C.-M., & TAI, Y.-C. 1998 Micro-electro-mechanical systems (MEMS) and fluid flows. *Ann. Rev. Fluid Mech.* **30**, 579-612.

HOLMES, P., LUMLEY, J.L., & BERKOOZ, G. 1996 *Turbulence, Coherent Structures, Dynamical Systems and Symmetry.* Cambridge.

HUNT, J.C.R., & DURBIN, P.A. 1999 Perturbed vortical layers and shear sheltering. *Fluid Dynamics Research* **24**, 375-404.

IOANNOU, P.A., & SUN, J. 1996 *Robust adaptive control.* Prentice-Hall.

JACOBS, C.R., SIMO, J.C., BEAUPRÉ, G.S., & CARTER, D.R. 1997 Adaptive bone remodelling incorporating simultaneous density and anisotropy considerations. *J. Biomechanics*, **30**, 603-613.

JACOBS, R.G., & DURBIN, P.A. 1998 Shear sheltering and the continuous spectrum of the Orr-Sommerfeld equation. *Phys. Fluids*, **10**, 2006-2011.

Jimenez, J. 1999 The physics of wall turbulence. *Physica A* **263**, 252-262.

Joshi, S.S., Speyer, J.L., & Kim, J. 1997 A systems theory approach to the feedback stabilization of infinitesimal and finite-amplitude disturbances in plane Poiseuille flow. *J. Fluid Mech.* **332**, 157-184.

Keefe, L.R. 1993 Drag reduction in channel flow using nonlinear control. *AIAA Paper* 93-3279.

Keefe, L.R. 1995 Drag reduction by nonlinear flow control. *NASA CR*-195058.

Keefe, L.R. 1997 A normal vorticity actuator for near-wall modification of turbulent shear flows. *AIAA Paper* 97-0547.

Keefe, L.R., Moin, P., & Kim, J. 1992 The dimension of attractors underlying periodic turbulent Poiseuille flow. *J. Fluid Mech.* **242**, 1-29.

Kepner, J., Parker, S., & Decyk, V. 1997 Simulating plasma turbulence in tokamaks. *SIAM News*, **30** (4), 1-7.

Kim, J., Moin, P., & Moser, R. 1987 Turbulence statistics in fully developed channel flow at low Reynolds number. *J. Fluid Mech.* **177**, 133-166.

Koumoutsakos, P. 1997 Active control of vortex-wall interactions. *Phys. Fluids*, **9**, 3808-3816.

Koumoutsakos, P. 1999 Vorticity flux control for a turbulent channel flow. *Phys. Fluids*, **11**, 248-250.

Koumoutsakos, P., Freund, J., & Parekh 1998 Evolution strategies for parameter optimization in controlled jet flows. *Proceedings of the 1998 CTR Summer Program*, Center for Turbulence Research, Stanford University/NASA Ames.

Lagnese, J.E., Russell, D.L., & White, L. (Editors) 1995 *Control and optimal design of distributed parameter systems.* Springer.

Lee, C., Kim, J., Babcock, D., & Goodman, R. 1997 Application of neural network to turbulence control for drag reduction. *Phys. Fluids*, **9**, 1740-7.

Lee, C., Kim, J., & Choi, H. 1998 Suboptimal control of turbulent channel flow for drag reduction. *J. Fluid Mech.* **358**, 245-258.

Lions, J.L. 1968 *Controle Optimal des Systèmes Gouvernés par des Equations aux Dérivées Partielles.* Dunod. (English translation, Springer.)

Luenberger, D.G. 1969 *Optimization by Vector Space Methods.* Wiley.

Lumley, J.L., & Blossey, P.N. 1998 Control of turbulence. *Ann. Rev. Fluid Mech.* **30**, 311-327.

Mayne, D.Q., & Michalska, H. 1990 Receding horizon control of nonlinear systems. *IEEE Trans. Auto. Control* **35**, 814-824.

McMichael, J.M. 1996 Progress and prospects for active flow control using Microfabricated Electro-Mechanical Systems (MEMS). *AIAA Paper No.* 96-0306.

Michalewicz, Z. 1996 *Genetic algorithms + data structures = evolution programs.* Springer.

Moin, P., & Bewley, T. 1994 Feedback control of turbulence. *Appl. Mech. Rev.* **47** (6), part 2, S3-S13.

Morse, P.M. & Feshbach, H. 1953 *Methods of Theoretical Physics.* McGraw-Hill.

Muske, K.R., & Edgar, T.F. 1997 Nonlinear state estimation. In *Nonlinear Process Control* (ed. M.A. Henson & D.E. Seborg). Prentice Hall.

Newborn, M. 1997 *Kasparov versus Deep Blue: computer chess comes of age.* Springer.

OTT, E.A., GREBOGI, C., & YORKE, J.A. 1990 Controlling chaos. *Phys. Rev. Lett.* **64**, 1196.

PADMANABHAN, K.T., BOWMAN, C.T., & POWELL, J.D. 1993 Development of an adaptive optimal combustion control strategy. *The Combustion Institute Paper No.* 93-092.

PERRY, A.E. & CHONG, M.S. 1987 A description of eddying motions and flow patterns using critical-point concepts. *Ann. Rev. Fluid Mech.* **19**, 125-55.

PETZOLD, L.R., ROSEN, J.B., GILL, P.E., JAY, L.O., & PARK K. 1997 Numerical optimal control of parabolic PDEs using DASOPT. In *Large Scale Optimization with Applications. Part II: Optimal Design and Control* (ed. L. Biegler, T. Coleman, A. Conn & F. Santosa). Springer.

POLAK, E 1971 *Computational methods in optimization.* Academic.

PRESS, W.H., FLANNERY, B.P., TEUKOLSKY, S.A., & VETTERLING, W.T. 1986 *Numerical Recipes.* Cambridge.

REUTHER, J., JAMESON, A., FARMER, J., MARTINELLI, L., & SAUNDERS, D. 1996 Aerodynamic shape optimization of complex aircraft configurations via an adjoint formulation. *AIAA Paper No.* 96-0094.

SADDOUGHI, S.G., & VEERAVALLI, S.V. 1994 Local isotropy in turbulent boundary layers. *J. Fluid Mech.* **268**, 333-372.

SCALES, L.E. 1985 *Introduction to non-linear optimization.* Springer-Verlag.

SEBORG, D.E., EDGAR, T.F., & MELLICHAMP, D.A. 1989 *Process dynamics and control.* Wiley.

SOETERBOEK, R. 1992 *Predictive control: a unified approach.* Prentice Hall.

SRITHARAN, S.S. 1991 Dynamic programming of the Navier-Stokes equations. *Systems and Control Letters* **16**, 299-307.

SRITHARAN, S.S. 1998 *Optimal control of viscous flows.* SIAM.

SUTTON, G.J., & BITMEAD, R.R. 1999 Performance and computational implementation of nonlinear model predictive control. In *Nonlinear model predictive control: assessment and future directions* (ed. F. Allöwer & A. Zheng). Birkhäuser.

TEMAM, R. 1984 *Navier-Stokes equations*, Studies in mathematics and its applications 2. North-Holland.

VAINBERG, M. 1964 *Variational methods for the study of nonlinear operators.* Holden-Day.

VANDERPLAATS, G.N. 1984 *Numerical optimization techniques for engineering design.* McGraw-Hill.

VILLEMAGNE, C. & SKELTON, R. 1988 Model reductions using a projection formulation. *Int. J. Contr.* **46**, 2141-2169.

VOGEL & WADE 1995 Analysis of costate discretizations in parameter estimation for linear evolution equations. *SIAM J. Control and Optimization* **33**, 227-254.

YANG, T.H., & POLAK, E. 1997 Moving horizon control of nonlinear systems with input saturation, disturbances, and plant uncertainty. *Inter. Journal of Contr.* **58**, 875-903.

ZHOU, K., DOYLE, J.C., & GLOVER, K. 1996 *Robust and Optimal Control.* Prentice-Hall.

Part IV

A general framework for robust control in fluid mechanics

Part IV has been submitted for publication as

Bewley, T.R., Temam, R., & Ziane, M. 1999 A general framework for robust control in fluid mechanics. Submitted to *Physica D*.

Abstract

The application of *optimal* control theory to complex problems in fluid mechanics has proven to be quite effective when complete state information from high-resolution numerical simulations is available (Moin & Bewley 1994; Bewley, Moin, & Temam 1999). In this approach, an iterative optimization algorithm based on the repeated computation of an adjoint field is used to optimize the controls for finite-horizon nonlinear flow problems (Abergel & Temam 1990). In order to extend this infinite-dimensional optimization approach to control externally-disturbed flows in which the controls must be determined based on limited noisy flow measurements alone, it is necessary that the controls computed be insensitive to both state disturbances and measurement noise. For this reason, *robust* control theory, a generalization of optimal control theory, has been examined as a technique by which effective control algorithms which are insensitive to a broad class of external disturbances may be developed for a wide variety of infinite-dimensional linear and nonlinear problems in fluid mechanics. An aim of the present paper is to put such algorithms into a rigorous mathematical framework, for it cannot be assumed at the outset that a solution to the infinite-dimensional robust control problem even exists. In this paper, conditions on the initial data, the parameters in the cost functional, and the regularity of the problem are established such that existence and uniqueness of the solution to the robust control problem can be proven. Both linear and nonlinear problems are treated, and the 2D and 3D nonlinear cases are treated separately in order to get the best possible estimates. Several generalizations are discussed and an appropriate numerical method is proposed.

Chapter 1

Introduction

In its essence, robust control theory (Doyle *et al.* 1989, Green & Limebeer 1995) may be summarized as Murphy's law (Bewley, Moin, & Temam 1997) taken seriously:

If a worst-case system disturbance <u>can</u> disrupt
a controlled closed-loop system, it <u>will</u>.

When designing a robust controller, therefore, one should *plan* on a finite component of the worst-case disturbance aggravating the system, and design a controller which is suited to handle even this extreme situation. A controller which is designed to work even in the presence of a finite component of the worst-case disturbance will also be robust to a wide class of other possible disturbances which, by definition, are not as detrimental to the control objective as the worst-case disturbance. Thus, the problem of finding a robust control is intimately coupled with the problem of finding the worst-case disturbance, in the spirit of a non-cooperative game.

To summarize briefly the robust control approach in the time domain, a cost functional $\mathcal{J}$ describing the control problem at hand is defined that weighs together the (distributed) disturbance ψ, the (distributed) control ϕ, and the flow perturbation $u(\psi,\phi)$ in the domain Ω over the time period of consideration $[0,T]$. The cost functional considered in the present work is of the form

$$\begin{aligned}\mathcal{J}(\psi,\phi) = \frac{1}{2}\int_0^T\int_\Omega |\mathcal{C}_1 u|^2\,dx\,dt + \frac{1}{2}\int_\Omega |\mathcal{C}_2 u(x,T)|^2\,dx - \int_0^T\int_{\partial\Omega} \mathcal{C}_3 \nu \frac{\partial u}{\partial n}\cdot \vec{r}\,d\Gamma\,dt \\ + \frac{1}{2}\int_0^T\int_\Omega \left[\ell^2|\phi|^2 - \gamma^2|\psi|^2\right]dx\,dt.\end{aligned}$$

This cost functional is simultaneously maximized with respect to the disturbance ψ and minimized with respect to the control ϕ, as illustrated in figure 1. The robust control problem is considered to be solved when a saddle point $(\bar\psi,\bar\phi)$ is reached; note that such a solution, if it exists, is not necessarily unique. The dependence of the cost functional $\mathcal{J}$ on the flow perturbation $u = u(\psi,\phi)$ itself is treated in a fairly general form; four cases of particular interest are:

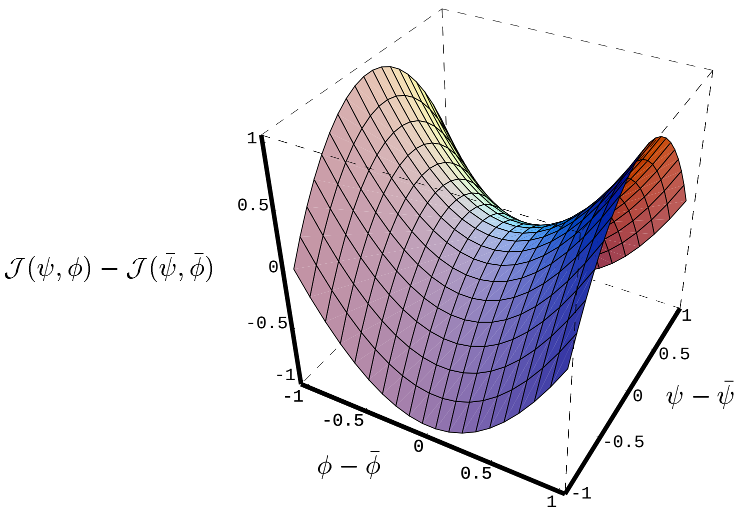

Figure 1: Schematic of a saddle point representing the neighborhood of a solution to a robust control problem with one scalar disturbance variable ψ and one scalar control variable ϕ. When the robust control problem is solved, the cost function $\mathcal{J}$ is simultaneously maximized with respect to ψ and minimized with respect to ϕ, and a saddle point such as $(\bar\psi, \bar\phi)$ is reached. The present article formulates an infinite-dimensional extension of this concept, where the cost $\mathcal{J}$ is related to a distributed disturbance ψ and a distributed control ϕ through the solution of the Navier-Stokes equation.

a. $\mathcal{C}_1 = d_1\, I$ and $\mathcal{C}_2 = \mathcal{C}_3 = 0 \Rightarrow$ regulation of turbulent kinetic energy;

b. $\mathcal{C}_1 = d_2\, \nabla\times$ and $\mathcal{C}_2 = \mathcal{C}_3 = 0 \Rightarrow$ regulation of the square of the vorticity;

c. $\mathcal{C}_2 = d_3\, I$ and $\mathcal{C}_1 = \mathcal{C}_3 = 0 \Rightarrow$ terminal control of turbulent kinetic energy;

d. $\mathcal{C}_3 = d_4\, I$ and $\mathcal{C}_1 = \mathcal{C}_2 = 0 \Rightarrow$ minimization of the time-average skin-friction in the direction $\vec{r}$ integrated over the boundary of the domain. Note that $\vec{n}$ is the unit outward normal vector to $\partial\Omega$.

All four of these cases, and many others, may be considered in the present framework, and the extension to other cost functionals is straightforward. The dimensional constants d_i (which are the appropriate functions of the kinematic viscosity ν, a characteristic length L_0, and a characteristic velocity U_0), as well as ℓ and γ, are included to make the cost functional dimensionally consistent and to account for the relative weight of each individual term.

It can not be assumed at the outset that a solution to the infinite-dimensional min/max problem described above even exists. However, it is established in the present article that, for a sufficiently large γ and reasonable requirements on the regularity of the problem (described later in this introduction), a solution to this min/max problem indeed does exist, with the (finite) magnitudes of the disturbance and the control governed by the scalar parameters γ and ℓ. To accomplish this, we will extend the optimal control setting of Abergel & Temam (1990) to analyze the non-cooperative differential game of the robust control setting in which a saddle point $(\bar{\psi}, \bar{\phi})$ is sought. Our approach is based on the saddle-point existence and characterization results given in, *e.g.*, Ekeland & Temam (1974).

The optimization of interior forcing profiles (ψ, ϕ) will be examined in detail, first for the linearized Navier-Stokes equation (§2), then for the full nonlinear Navier-Stokes equation (§3). We will then generalize to the problems of boundary control (§4.1), with the possibility of corners in the boundary of the domain Ω, and data assimilation (§4.2), in which the initial conditions are optimized to solve an estimation/forecasting problem based on flow measurements on $[0, T]$. Finally, a tractable numerical algorithm for solving all of the robust control problems discussed herein is presented (§5).

The numerical approach proposed to solve the robust control problem is based on computations of an $O(N)$ adjoint field, where N is the number of grid points used to resolve the continuous flow problem. Note that $N \gtrsim O(10^5)$ for problems of engineering interest today, and this number may be expected only to increase in the future. Computation of the adjoint field is only as difficult as the computation of the flow itself, and thus is a numerically tractable approach to the control problem whenever the computation of the flow itself is numerically tractable. In contrast, control approaches based on the solution of $O(N^2)$ Riccati equations or Hamilton-Jacobi-Bellman formulations have not been shown to be numerically tractable for discretizations with $N > O(100)$, and thus are, so far, inadequate to treat many of the problems of interest in fluid mechanics with a sufficient degree of resolution.

1.1 An intuitive introduction to robust control theory

Consider the present problem as a differential game between an engineer seeking the "best" control ϕ which stabilizes the flow perturbation with limited control effort and, simultaneously, nature seeking the "maximally malevolent" disturbance ψ which destabilizes the flow perturbation with limited disturbance magnitude (Green & Limebeer 1995). The parameter γ^2 factors into such a competition as a weighting on the magnitude of the disturbance which nature can afford to offer, in a manner analogous to the parameter ℓ^2, which is a weighting on the magnitude of the control which the engineer can afford to offer.

The parameter ℓ^2 may be interpreted as the "price" of the control to the engineer. The $\ell \to \infty$ limit corresponds to prohibitively "expensive" control, and results in $\phi \to 0$ in the minimization with respect to ϕ for the present problem. Reduced values of ℓ increase the cost functional less upon the application of a control ϕ. A nonzero control results whenever the control ϕ can affect the flow perturbation u in such a way that the net cost functional $\mathcal{J}$ is reduced.

The parameter γ^2 may be interpreted as the "price" of the disturbance to nature. The $\gamma \to \infty$ limit results in $\psi \to 0$ in the maximization with respect to ψ, leading to the optimal control formulation of Abergel & Temam (1990) for ϕ alone. Reduced values of γ decrease the cost functional less upon the application of a disturbance ψ. A nonzero disturbance results whenever the disturbance ψ can affect the flow perturbation u in such a way that the net cost functional $\mathcal{J}$ is increased.

Solving for the control ϕ which is effective even in the presence of a disturbance ψ which maximally spoils the control objective is a way of achieving system robustness. A control which works even in the presence of the malevolent disturbance ψ will also be robust to a wide class of other possible disturbances. Put another way, the introduction of the worst-case disturbance in the robust approach is a means of "detuning" the optimal controls. It results in a set of controls which may have somewhat degraded performance when no disturbances are present. However, much greater system robustness (*i.e.*, better performance) is attained in cases for which unknown disturbances are present in the system, and thus the approach is relevant for applications in physical systems, in which unpredictable disturbances are ubiquitous.

In the present systems, for $\gamma < \gamma_0$ for some critical value γ_0 (an upper bound of which is established in this article), the non-cooperative game is not known to have a finite solution; essentially, the malevolent disturbance wins. The control ϕ corresponding to $\gamma = \gamma_0$ results in a stable system even when nature is on the brink of making the system unstable. However, the control determined with $\gamma = \gamma_0$ is not always the most suitable, as it may result in a very large control magnitude and degraded performance in response to disturbances with structure more benign than the worst-case scenario. In the implementation, variation of ℓ and γ provides the flexibility in the control design which is necessary to achieve the desired trade-offs between Gaussian and worst-case disturbance response and the control magnitude required (Bewley & Liu 1998).

1.1.1 The general framework

In figures 2 and 3, we identify all possible sources of forcing in the present control problem, which is shown in §2.2 and §3.3 to boil down to a two-point boundary-value problem for a coupled set of PDEs: one for the flow perturbation u and one for an adjoint[1] field $\tilde{u}$. All three possible locations of forcing of the flow problem and all three possible locations of forcing of the adjoint problem are considered in the present framework. By so doing, we establish a general framework in which the robust control approach, discussed herein, can be applied to a wide variety of problems in fluid mechanics.

1.1.2 Related literature

Robust control of infinite-dimensional linear systems is discussed in a fairly general operator-Riccati setting in Foias, Özbay, & Tannenbaum (1996), Barbu (1995), and van Keulen (1993). Though the systems considered in these references are linear (*e.g.*, wave equations) and the issues raised are

[1]Note that the adjoint field used in this work represents the sensitivity of the portion of the cost functional $\mathcal{J}$ which depends on u to modification of the forcing (ψ, ϕ) of the flow problem.

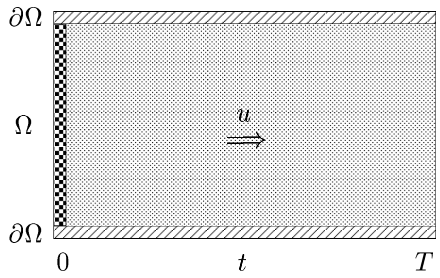

Figure 2: Schematic representation of the space-time domain over which the flow field u is defined. The arrow indicates the direction in time that the p.d.e. is marched. The possible regions of forcing in the system defining u are:

(1) the right-hand side of the p.d.e., indicated with shading, representing flow control by interior volume forcing, as discussed in §2 and §3 (*e.g.*, externally-applied electromagnetic forcing by wall-mounted magnets and electrodes);

(2) the boundary conditions, indicated with diagonal stripes, representing flow control by boundary forcing, as discussed in §4.1 (*e.g.*, wall transpiration);

(3) the initial conditions, indicated with checkerboard, representing optimization of the initial state in a data assimilation framework, as discussed in §4.2 (*e.g.*, the weather forecasting problem).

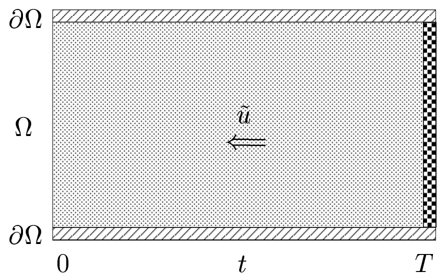

Figure 3: Schematic representation of the space-time domain over which the adjoint field $\tilde{u}$ is defined. The arrow indicates the direction in time that the p.d.e. is marched. The possible regions of forcing in the system defining $\tilde{u}$, corresponding exactly to the possible domains in which the cost functional $\mathcal{J}$ can depend on u, are:

(1) the right-hand side of the p.d.e., indicated with shading, representing regulation of an interior quantity (*e.g.*, turbulent kinetic energy, cases a and b of introduction);

(2) the boundary conditions, indicated with diagonal stripes, representing regulation of a boundary quantity (*e.g.*, wall skin-friction, case d of introduction);

(3) the terminal conditions, indicated with checkerboard, representing terminal control of an interior quantity (*e.g.*, turbulent kinetic energy, case c of introduction).

An interesting singularity arises when considering the terminal control of a boundary quantity such as wall skin-friction. The (inhomogeneous) boundary conditions on the adjoint field for such a case are the same as in the corresponding regulation problem with a delta function applied at time $t = T$.

primarily related to linear operators in infinite dimension, these references provide useful background material for the present discussion; see also Weiss & Weiss (1997) for related work in the context of optimal control problems. Most of these references consider the linear case and optimizations over the infinite time horizon, a setting that is effectively analyzed in the frequency domain and referred to as $\mathcal{H}_\infty$ control (with reference to the Hardy spaces on which they are developed and the L^∞-norms of the input-output transfer functions that they bound). The reader is referred to Zhou, Doyle, & Glover (1996) for details from this perspective in the finite-dimensional setting, and the above mentioned references for details in the infinite-dimensional setting. Of course, there is a wide body of literature concerning generally the theory of control of systems governed by PDEs, including the equations of fluid mechanics: for highlights, the reader is referred for instance to the recent volumes compiled by Banks (1992), Banks, Fabiano, & Ito (1993), Gunzburger (1995), Lagnese, Russell, & White (1995), and Sritharan (1998).

Robust control of the Navier-Stokes equation in the operator-Riccati ($\mathcal{H}_\infty$) setting is discussed in detail by Barbu & Sritharan (1998). In this work, a robust control problem (on the infinite time horizon) which is γ-suboptimal for the linearized Navier-Stokes equation is stated as the solution of an algebraic Riccati equation, assuming appropriate detectability and stabilizability constraints on the system; then it is shown that this solution is also γ-suboptimal for the full (nonlinear) Navier-Stokes equation in a sufficiently small neighborhood of the origin.

The present analysis differs in several respects. One major difference is that, here, it is not assumed that the system is stabilizable or detectable, a spectral hypothesis difficult to verify in practice. In fact, effective controls may be found by the present noncooperative optimization approach even if the turbulence may not be subdued entirely in the flow of interest.

As mentioned previously, the robust control problem is solved in the present work by an iterative optimization involving adjoint fields, a numerically-tractable approach whenever the computation of the flow itself is numerically tractable (see, e.g., Bewley, Moin, & Temam 1999, handling 33×10^6 modes in the optimal control framework). In contrast, the largest control Riccati equations solved to date for flow control problems involved Schur decompositions of 280×280 matrices at very high numerical precision (corresponding to a control problem with 140 modes) and relied on the special structure of the problem formulation (stabilization of laminar flow in a plane channel) in order to decouple the control problem at different spatial wavenumbers in the two homogeneous directions in the flow (Bewley & Liu 1998); see also an 18×18 Riccati system (corresponding to a control problem with 9 modes) in a closely related problem by Joshi, Speyer, & Kim (1995). Furthermore, Riccati-based approaches do not extend readily to other geometries (where such decoupling is not present) or to higher-dimensional optimization problems due to their very poor numerical conditioning for large systems. Thus, in the more general setting, iterative adjoint-based control optimizations are preferred over Riccati-based approaches. When optimized over a sufficiently long time horizon T in a receding-horizon predictive control framework, the performance of such schemes (in the optimal control case) has proven to be excellent even in fully turbulent flows (see Bewley, Moin, & Temam 1999, where the drag of a 3D channel flow is reduced to that of the laminar state from an initial state of fully-developed turbulence).

Finally, the present work treats a number of special cases separately (the linear case, the nonlinear 3D case, and the nonlinear 2D case, with interior forcing, boundary forcing, or initial condition optimization) to get sharp estimates on the regularity of the system required in order to be able to prove existence and uniqueness of the solution to an appropriately-stated robust control problem.

One of the several applications of the present work is the development of estimator-based feedback control algorithms for flow systems. In order to make such algorithms implementable in hardware in real time, reduced-order models of the flow system which are accurate in the controlled framework (*i.e.*, not just for the uncontrolled system) are a high priority. Much of the pioneering work in the development of reduced-basis representations of nonlinear infinite-dimensional fluid systems is reviewed in the book by Holmes, Lumley, & Berkooz (1996); a review in the context of application to turbulence control is given by Lumley & Blossey (1998). Reduced-basis approaches for related problems are also discussed by Burns & King (1998), Cortelezzi & Speyer (1998), and Cortelezzi, Lee, Kim, & Speyer (1999). The latter reference obtains a linear model reduction by truncating those linear eigenmodes with low observability or controllability from the model and report, in their case, a drag reduction to 50% below the laminar level by application of a zero-net mass flux linear controller to a 2D unsteady channel flow. An alternative model reduction strategy was proposed in Bewley (1999), where it was observed that, in the highly nonorthogonal (*i.e.*, nearly defective) situation often encountered in fluid mechanics, model reduction schemes mindful of the transfer function of interest, such as the p, q Markov covariance equivalent realization (Villemagne & Skelton 1988) or optimal Hankel norm approximation (Zhou, Doyle, & Glover 1996), are well suited.

1.2 Governing equations

We begin with the Navier-Stokes equation for a flow U in an open domain $\Omega \subset \mathbb{R}^3$ such that, in $\Omega \times (0, \infty)$, we have

$$\begin{cases} \dfrac{\partial U}{\partial t} - \nu \Delta U + (U \cdot \nabla) U + \nabla P = F, \\ \operatorname{div} U = 0, \\ U = 0 \qquad \text{on } \partial\Omega, \\ U = U_0 \qquad \text{at } t = 0. \end{cases} \tag{1.1}$$

In the bulk of this article, we focus our attention on the case in which the forcing is applied by way of an interior volume force on the right-hand side of the momentum equation. A stationary or non-stationary solution $U(x,t)$ to this equation with a corresponding forcing $F(x,t)$ will be referred to as the "target" flow for the control problem. (If no target flow is known or given, U and F are taken as zero.)

We are interested in the robust regulation of the deviation of the flow from the desired target (U, F). In §2, we consider the control of the linearized equation which models small perturbations (u, f) to the target flow (U, F) with Dirichlet boundary conditions and known initial conditions such that, in $\Omega \times (0, \infty)$, we have

$$\begin{cases} \dfrac{\partial u}{\partial t} - \nu \Delta u + (u \cdot \nabla) U + (U \cdot \nabla) u + \nabla p = f, \\ \text{div } u = 0, \\ u = 0 \qquad \text{on } \partial\Omega, \\ u = u_0 \qquad \text{at } t = 0. \end{cases} \tag{1.2}$$

In §3, we consider the control of the full nonlinear equation which models large perturbations (u, f) to the target flow (U, F) such that, in $\Omega \times (0, \infty)$, we have

$$\begin{cases} \dfrac{\partial u}{\partial t} - \nu \Delta u + (u \cdot \nabla) U + (U \cdot \nabla) u + (u \cdot \nabla) u + \nabla p = f, \\ \text{div } u = 0, \\ u = 0 \qquad \text{on } \partial\Omega, \\ u = u_0 \qquad \text{at } t = 0. \end{cases} \tag{1.3}$$

In §4, we will generalize this setting to examine the optimization of boundary controls and the optimization of initial conditions.

1.3 Mathematical setting

Let Ω be a bounded open set of $\mathbb{R}^3$ with boundary $\partial\Omega$, and let $\vec{n}$ be the unit outward normal vector to $\partial\Omega$. We denote by $H^s(\Omega)$, for $s \in \mathbb{R}$, the Sobolev spaces constructed on $L^2(\Omega)$, and by $H_0^s(\Omega)$, for $s > 1/2$, the closure of $C_0^\infty(\Omega)$ in $H^s(\Omega)$. Following Temam (1984), we set $X = \left\{u \in ((C_0^\infty(\Omega))^3;\ \text{div } u = 0\right\}$, and denote by H (resp. V) the closure of X in $(L^2(\Omega))^3$ (resp. $(H^1(\Omega))^3$); we have

$$H = \left\{u \in (L^2(\Omega))^3;\ \text{div } u = 0 \text{ in } \Omega, \quad u \cdot \vec{n} = 0 \text{ on } \partial\Omega\right\}$$

and

$$V = \left\{u \in (H_0^1(\Omega))^3;\ \text{div } u = 0 \text{ in } \Omega\right\}.$$

The scalar product on H is denoted by $(u,v) = \int_\Omega u \cdot v\, dx$, that on V is denoted by $((u,v)) = \int_\Omega \nabla u \cdot \nabla v\, dx$, and the associated norms are denoted by $|\cdot|_{L^2(\Omega)}$ and $\|\cdot\|$ respectively. We denote by A the Stokes operator, defined as an isomorphism from V onto the dual V' of V such that, for $u \in V$, Au is defined by

$$\langle Au, v\rangle_{V',V} = ((u,v)), \quad \forall\, v \in V,$$

where $\langle \cdot,\cdot\rangle_{V',V}$ is the duality bracket between V' and V. The operator A is extended to H as a linear unbounded operator with domain $D(A) = (H^2(\Omega))^3 \cap V$ when $\partial\Omega$ is a C^2 surface; the case of boundary forcing in a domain Ω with corners is treated in §4.1. We also recall the Leray-Hopf projector $\mathcal{P}$, which is the orthogonal projector of the non-divergence-free space $(L^2(\Omega))^3$ onto the divergence-free space H. The Stokes operator is defined with this projector such that

$$Au = -\mathcal{P}\big(\Delta u\big), \quad \forall\, u \in D(A). \tag{1.4}$$

We shall denote by $0 < \lambda_1 \leq \lambda_2 \leq \ldots$ the increasing sequence of the eigenvalues of A. Define the bilinear mapping B by

$$B(u,v) = \mathcal{P}\big((u\cdot\nabla)v\big), \quad \forall\, u,v \in V. \tag{1.5}$$

Note that B is a bilinear mapping from V into V'. Define a continuous trilinear form b on V such that, with $u,v,w \in (H^1(\Omega))^3$, we have

$$\begin{aligned} b(u,v,w) &= \langle B(u,v), w\rangle_{V',V} \\ &= \int_\Omega (u\cdot\nabla)v \cdot w\, dx = \int_\Omega u_i \frac{\partial v_j}{\partial x_i} w_j\, dx, \end{aligned}$$

where Einstein's summation is assumed.

1.4 Abstract form of governing equations

The operators A and B may be used to write the Navier-Stokes equation in the "abstract form" useful for mathematical analysis. By application of the Leray projector to (1.2), noting (1.4), (1.5), and that $\mathcal{P}u = u$ and $\mathcal{P}(\nabla p) = 0$, the linearized Navier-Stokes equation may be written in the form

$$\begin{cases} \dfrac{du}{dt} + \nu A u + B(u,U) + B(U,u) = \mathcal{P}f, \\ u \in V, \\ u = u_0 \qquad \text{at } t = 0, \end{cases} \tag{1.6}$$

where the regularity required on f, u_0, and U are

$$\begin{cases} f \in L^2(0,T;L^2), \quad \forall\, T > 0; \\ u_0 \in V; \quad U \in L^\infty(0,T;V) \cap L^2(0,T;D(A)). \end{cases} \tag{1.7}$$

Similarly, application of the Leray projector to the nonlinear form (1.3) gives

$$\begin{cases} \dfrac{du}{dt} + \nu A u + B(u,U) + B(U,u) + B(u,u) = \mathcal{P} f, \\ u \in V, \\ u = u_0 \qquad\qquad \text{at } t = 0. \end{cases} \tag{1.8}$$

1.5 Control framework

In the control framework, the interior forcing f is decomposed into a disturbance $\psi \in L^2(0,T;L^2)$ and a control $\phi \in L^2(0,T;L^2)$, with $T > 0$, in the spirit of the non-cooperative game discussed in §1.1. Thus, we write f as

$$f = B_1 \psi + B_2 \phi, \tag{1.9}$$

where B_1 and B_2 are taken here as given bounded operators[2] on $(L^2(\Omega))^3$. Only the divergence-free part of the forcing f will affect the evolution of the velocity field u, as seen on the right-hand side of the governing equations (1.6) and (1.8). Thus, in the remainder of this article, we consider only the divergence-free part of the forcing by writing

$$\begin{aligned} \mathcal{P} f &= \mathcal{P}(B_1 \psi + B_2 \phi) \\ &= \mathcal{B}_1 \psi + \mathcal{B}_2 \phi, \end{aligned} \tag{1.10}$$

where $\mathcal{B}_1 = \mathcal{P} B_1$ and $\mathcal{B}_2 = \mathcal{P} B_2$ are mappings from $(L^2(\Omega))^3$ to H.

The difference $f - \mathcal{P} f$ may be written as the gradient of a scalar and thus will only modify the pressure p in (1.2) and (1.3). As the Navier-Stokes equation in the abstract form is implicitly confined to a divergence-free submanifold of $(L^2(\Omega))^3$, the pressure p may be neglected in the mathematical analysis.

[2]Note that B_1 and B_2 quantify the profile of the forcing inside the domain Ω which results from modification of the disturbance and control variables ψ and ϕ. Generally speaking, ψ and ϕ might be defined on a subdomain of Ω.

1.6 Important identities and inequalities

We now recall some important properties of the nonlinear operator b, which can be found, for instance, in Ladyzhenskaya (1969), Lions (1969), and Temam (1984). First, we have the orthogonality identity

$$b(u,v,v) = 0, \quad \forall\, u,v \in V, \tag{1.11}$$

as a consequence of div $u = 0$, as shown by integration by parts. Moreover, the continuity of the nonlinear mapping in various functional spaces is expressed by the following classical inequalities: there exists a numerical coefficient $C_0 = C_0(\Omega)$ such that

$$\begin{cases} |b(u,v,w)| \leq C_0 \|u\| \|v\|^{1/2} |Av|_{L^2}^{1/2} |w|_{L^2}, & \forall\, u \in V,\ v \in D(A),\ w \in H, \\ |b(u,v,w)| \leq C_0 |u|_{L^2}^{1/4} |Au|_{L^2}^{3/4} \|v\| |w|_{L^2}, & \forall\, u \in D(A),\ v \in V,\ w \in H, \\ |b(u,v,w)| \leq C_0 |u|_{L^2}^{1/4} \|u\|^{3/4} \|v\| |w|_{L^2}^{1/4} \|w\|^{3/4}, & \forall\, u \in V,\ v \in V,\ w \in V. \end{cases} \tag{1.12}$$

where C_0 as well as the C_i hereafter denote positive numerical coefficients whose values may be different in each inequality.

Note that the mapping $u \mapsto B(u) = B(u,u)$ is differentiable from V into V'. Its differential is defined by

$$\begin{aligned} B'(u)v &= B(u,v) + B(v,u) \qquad \forall\, v \in V \\ &= \mathcal{P}\big((u \cdot \nabla)v + (v \cdot \nabla)u\big). \end{aligned} \tag{1.13}$$

Let $B'(u)^*$ denote the adjoint of $B'(u)$ for the duality between V and V'. (Note that, since V is a Hilbert space and therefore reflexive, the dual of V' can be identified with V.) The adjoint operator $B'(u)^*$ is thus defined by

$$\langle v, B'(u)w \rangle_{V,V'} = \langle B'(u)^* v, w \rangle_{V',V} \,. \tag{1.14}$$

It follows from integration by parts (Abergel & Temam 1990) that

$$\begin{aligned} \langle B'(u)^* v, w \rangle_{V',V} &= \int_\Omega \left(\frac{\partial u_i}{\partial x_j} v_i - \frac{\partial v_j}{\partial x_i} u_i \right) w_j \, dx \\ &= \int_\Omega \big((\nabla u)^T \cdot v - (\nabla v) \cdot u \big) \cdot w \, dx, \end{aligned} \tag{1.15}$$

where, again, Einstein's summation is assumed.

The use of adjoint operators to define an appropriate $O(N)$ adjoint field is central to the development of an efficient numerical algorithm to solve the robust control problem. An iterative approach to the solution of a two-point boundary value problem is presented in §5 such that, at each iteration k (on the entire time interval $[0,T]$), a flow field and a corresponding adjoint field are computed to determine the gradients $\mathcal{DJ}/\mathcal{D}\psi$ and $\mathcal{DJ}/\mathcal{D}\phi$ in the vicinity of (ψ^k, ϕ^k). The disturbance ψ^k and the control ϕ^k (again, on the entire time interval $[0,T]$) are then updated, based on this gradient information, and new flow and adjoint fields are computed until the iteration in k converges and a saddle point for the linear or the full nonlinear problem is reached.

The estimates developed in this work in order to prove the existence of a solution to the robust control problem involve integration by parts and the following five fundamental inequalities, which are repeated here for review: the Cauchy-Schwarz inequality $|(u,v)| \le |u|_{L^2}\,|v|_{L^2}$, Hölder's inequality

$$\int f_1 \cdots f_n \, dx \le \big|f_1\big|_{L^{p_1}} \cdots \big|f_n\big|_{L^{p_n}}, \quad \big|f\big|_{L^p} = \Big(\int \big|f\big|^p dx \Big)^{\frac{1}{p}}, \quad \frac{1}{p_1} + \cdots \frac{1}{p_n} = 1,$$

the Poincaré inequalities $|u|_{L^2} \le \lambda_1^{-1/2} \|u\|$ and $\|u\| \le \lambda_1^{-1/2} |Au|_{L^2}$, Young's inequality in the form

$$a\,b \le \frac{\epsilon}{p}\, a^p + \frac{\epsilon^{-q/p}}{q}\, b^q, \qquad \forall\, a, b, \epsilon > 0, \quad \forall\, p \;\text{ s.t. }\; 1 < p < \infty, \quad \frac{1}{p} + \frac{1}{q} = 1,$$

and Gronwall's lemma

$$\frac{dy}{dt} \le g y + h, \quad \forall\, t \ge 0 \quad \Longrightarrow$$
$$y(t) \le y(0) \exp\left(\int_0^t g(\tau)\, d\tau \right) + \int_0^t h(s) \exp\left(\int_s^t g(\tau)\, d\tau \right) ds, \quad \forall\, t \ge 0.$$

Chapter 2

The linear problem

As discussed in the introduction, the objective in the robust control problem is to find the best control ϕ in the presence of the disturbance ψ which maximally spoils the control objective. The cost functional considered in the present work, in the mathematical setting described in §1.4, is given by

$$\begin{aligned}\mathcal{J}(\psi,\phi) = \frac{1}{2}\int_0^T \left|\mathcal{C}_1 u\right|^2_{L^2(\Omega)} dt + \frac{1}{2}\left|\mathcal{C}_2 u(T)\right|^2_{L^2(\Omega)} - \int_0^T \big(\mathcal{C}_3 \nu \frac{\partial u}{\partial n}, \vec{r}\big)_{L^2(\partial\Omega)} dt \\ + \frac{1}{2}\int_0^T \Big[\ell^2 \left|\phi\right|^2_{L^2(\Omega)} - \gamma^2 \left|\psi\right|^2_{L^2(\Omega)}\Big] dt,\end{aligned} \tag{2.1}$$

where the scalar control parameters γ and ℓ are given, $\vec{r}$ is a known vector field on $\partial\Omega$, $\vec{n}$ is the unit outward normal vector to $\partial\Omega$, and $\mathcal{C}_3^* \vec{r}\cdot\vec{n} = 0$. The operators $\mathcal{C}_1$ and $\mathcal{C}_2$ are unbounded operators on $(L^2(\Omega))^3$ satisfying

$$\left|\mathcal{C}_i v\right|^2_{L^2(\Omega)} \le \alpha \left|v\right|^2_{L^2(\Omega)} + \beta \left\|v\right\|^2 \quad \text{for} \quad i = 1, 2, \quad \forall\, v \in V, \tag{2.2}$$

with $\alpha \ge 0,\ \beta \ge 0$, and $\alpha + \beta > 0$, and $\mathcal{C}_3$ is a bounded operator of $(L^2(\partial\Omega))^3$ so that, by the trace theorem (Lions & Magenes 1972), we have

$$\left|\big(\mathcal{C}_3 \nu \frac{\partial v}{\partial n}, \vec{r}\big)_{L^2(\partial\Omega)}\right| \le \kappa\nu \left\|v\right\|_{H^{3/2}(\Omega)} \le \kappa'\nu \left\|v\right\|^{1/2} \left|Av\right|^{1/2}_{L^2(\Omega)} \quad \forall\, v \in D(A), \tag{2.3}$$

where κ and κ' depend upon $\vec{r}$ and Ω. Note that $(\partial/\partial n) : u \mapsto (\partial u/\partial n)|_{\partial\Omega}$ is a mapping from $\mathcal{C}^\infty(\bar{\Omega})$ to $\mathcal{C}^\infty(\partial\Omega)$ (where $\bar{\Omega}$ is the closure of Ω), which extends by continuity to a mapping from $H^s(\Omega)$ to $H^{s-3/2}(\partial\Omega)$ for $s > 3/2$ (Lions & Magenes 1972).

In this chapter, the flow u is assumed to be related to the disturbance ψ and the control ϕ

through the linearized Navier-Stokes equation

$$\begin{cases} \dfrac{du}{dt} + \nu A u + B(u,U) + B(U,u) = \mathcal{B}_1\psi + \mathcal{B}_2\phi, \\ u \in V, \\ u = u_0 \qquad\qquad \text{at } t = 0, \end{cases} \tag{2.4}$$

which models small deviations of the flow perturbation u from the desired target flow U. The regularity required is given by

$$\begin{cases} (\psi,\phi) \in L^2(0,T;L^2) \times L^2(0,T;L^2); \quad \mathcal{B}_1, \mathcal{B}_2 \in \mathcal{L}(L^2,H); \\ u_0 \in V; \quad U \in L^\infty(0,T;V) \cap L^2(0,T;D(A)), \end{cases} \tag{2.5}$$

where the Stokes operator A, the bilinear mapping B, and other notations are described in §1.4. The robust control problem to be solved is:

Definition 4 *The disturbance $\bar{\psi} \in L^2(0,T;L^2)$ and control $\bar{\phi} \in L^2(0,T;L^2)$, and the solution $\bar{u} = u(\bar{\psi},\bar{\phi})$ to* (2.4) *associated with $(\bar{\psi},\bar{\phi})$, are said to solve the robust control problem when a saddle point $(\bar{\psi},\bar{\phi})$ of the cost functional $\mathcal{J}$ defined in* (2.1) *is reached such that*

$$\mathcal{J}(\psi,\bar{\phi}) \leq \mathcal{J}(\bar{\psi},\bar{\phi}) \leq \mathcal{J}(\bar{\psi},\phi) \qquad \forall\ (\psi,\phi) \in L^2(0,T;L^2) \times L^2(0,T;L^2). \tag{2.6}$$

In this chapter, we will establish both existence and uniqueness of the solution to the robust control problem stated in Definition 2.1, and identify this solution as a function of the unique solution of a two-point boundary value problem for a linear flow/adjoint system on $[0,T]$.

2.1 Existence of a solution to the robust control problem

The proof of the existence of a solution $(\bar{\psi},\bar{\phi})$ to the robust control problem for the linear case is based on the following existence result:

Proposition 5 *Let $\mathcal{J}$ be a functional defined on $X \times Y$, where X and Y are non-empty, closed, unbounded, convex sets. If $\mathcal{J}$ satisfies*

(a) $\forall\ \psi \in X, \quad \phi \mapsto \mathcal{J}(\psi,\phi)$ is convex lower semicontinuous,

(b) $\forall\ \phi \in Y, \quad \psi \mapsto \mathcal{J}(\psi,\phi)$ is concave upper semicontinuous,

(c) $\exists\ \psi_0 \in X$ such that $\displaystyle\lim_{\|\phi\|_Y \to +\infty} \mathcal{J}(\psi_0,\phi) = +\infty$,

(d) $\exists\ \phi_0 \in Y$ such that $\displaystyle\lim_{\|\psi\|_X \to +\infty} \mathcal{J}(\psi,\phi_0) = -\infty$, *then the functional* $\mathcal{J}$ *has at least one saddle point* $(\bar{\psi}, \bar{\phi})$ *and*

$$\mathcal{J}(\bar{\psi}, \bar{\phi}) = \underset{\phi \in Y}{\text{Min}} \ \underset{\psi \in X}{\text{Sup}} \, \mathcal{J}(\psi, \phi) = \underset{\psi \in X}{\text{Max}} \ \underset{\phi \in Y}{\text{Inf}} \ \mathcal{J}(\psi, \phi).$$

Proof. The proof is given in Ekeland & Temam (1974). □

In order to establish conditions (a) through (d) of Proposition 2.2 for the present problem, we need to analyze the evolution equation (2.4).

It can be proven rigorously (Ladyzhenskaya 1969, Lions 1969, and Temam 1984) that, given $u_0 \in V$, $U \in L^\infty(0,T;V) \cap L^2(0,T;D(A))$, and $(\psi, \phi) \in L^2(0,T;L^2) \times L^2(0,T;L^2)$, there exists a unique solution u of (2.4) such that

$$u \in L^\infty(0,T;V) \cap L^2(0,T;D(A)) \quad \forall\, T > 0.$$

The proof is based on the following *a priori* estimates. Multiplying (2.4) with u, noting the definition $\mathcal{P}f = \mathcal{B}_1\psi + \mathcal{B}_2\phi$ in (1.10) and the orthogonality of (1.11), and applying the Cauchy-Schwarz, Poincaré, and Young's inequalities to the $(\mathcal{P}f, u)$ term and (1.12) to the $b(u, U, u)$ term, we can write

$$\begin{aligned}\frac{1}{2}\frac{d}{dt}|u|_{L^2}^2 + \nu\|u\|^2 &= (\mathcal{P}f, u) - b(u, U, u) \\ &\le \frac{1}{2\nu\lambda_1}|\mathcal{P}f|_{L^2}^2 + \frac{\nu}{2}\|u\|^2 + C_0\|U\||u|_{L^2}^{1/2}\|u\|^{3/2}\end{aligned}$$

and thus, again noting that C_0 absorbs numerical constants,

$$\frac{d}{dt}|u|_{L^2}^2 + \nu\|u\|^2 \le \frac{1}{\nu\lambda_1}\,|\mathcal{P}f|_{L^2}^2 + C_0\|U\||u|_{L^2}^{1/2}\|u\|^{3/2}.$$

An additional application of Young's inequality leads to

$$\frac{d}{dt}|u|_{L^2}^2 + \frac{\nu}{2}\|u\|^2 \le \frac{1}{\nu\lambda_1}\,|\mathcal{P}f|_{L^2}^2 + \frac{C_0}{\nu^3}\|U\|^4|u|_{L^2}^2. \tag{2.7}$$

Let $M_0(t) = C_0\nu^{-3}\int_0^t \|U\|^4\, d\tau$ and thus $M_0'(t) = C_0\nu^{-3}\|U(t)\|^4$. Applying Gronwall's lemma to (2.7), we have

$$|u(t)|_{L^2}^2 \le e^{M_0(t)}\,|u_0|_{L^2}^2 + \frac{e^{M_0(t)}}{\nu\lambda_1}\int_0^t |\mathcal{P}f|_{L^2}^2\, ds. \tag{2.8}$$

Also, by integrating (2.7) from 0 to t, multiplying vy $2/(\nu t)$, and then substituting with the integral of $M_0'(s)$ times (2.8) from 0 to t, we have

$$\begin{aligned}\frac{1}{t}\int_0^t \|u\|^2 ds &\le \frac{2}{\nu^2\lambda_1 t}\int_0^t |\mathcal{P}f|_{L^2}^2\, ds + \frac{2}{\nu t}\int_0^t M_0'(s)\,|u(s)|_{L^2}^2\, ds + \frac{2}{\nu t}\,|u_0|_{L^2}^2 \\ &\le \frac{2e^{M_0(t)}}{\nu t}\,|u_0|_{L^2}^2 + \frac{2e^{M_0(t)}}{\nu^2\lambda_1 t}\int_0^t |\mathcal{P}f|_{L^2}^2\, ds.\end{aligned} \tag{2.9}$$

Similarly, multiplying (2.4) with Au and applying the Cauchy-Schwarz and Young's inequalities to the $(\mathcal{P}f, Au)$ term, we can write

$$\begin{aligned}\frac{1}{2}\frac{d}{dt}\|u\|^2 + \nu|Au|_{L^2}^2 &= (\mathcal{P}f, Au) - b(u,U,Au) - b(U,u,Au) \\ &\le \frac{1}{2\nu}\,|\mathcal{P}f|_{L^2}^2 + \frac{\nu}{2}|Au|_{L^2}^2 + |b(u,U,Au)| + |b(U,u,Au)|\end{aligned}$$

and thus, applying (1.12),

$$\begin{aligned}\frac{d}{dt}\|u\|^2 + \nu|Au|_{L^2}^2 \le \frac{1}{\nu}\,|\mathcal{P}f|_{L^2}^2 &+ C_0\|U\|^{1/2}|AU|_{L^2}^{1/2}\|u\||Au|_{L^2} \\ &+ C_0|U|_{L^2}^{1/4}|AU|_{L^2}^{3/4}\|u\||Au|_{L^2}.\end{aligned}$$

Additional application of Young's inequality leads to

$$\frac{d}{dt}\|u\|^2 + \frac{\nu}{2}|Au|_{L^2}^2 \le \frac{1}{\nu}\,|\mathcal{P}f|_{L^2}^2 + \frac{C_0}{\nu}\left(\|U\||AU|_{L^2} + |U|_{L^2}^{1/2}|AU|_{L^2}^{3/2}\right)\|u\|^2.$$

Let $M_1(t) = C_0\nu^{-1}\int_0^t (\|U\||AU|_{L^2} + |U|_{L^2}^{1/2}|AU|_{L^2}^{3/2})\, d\tau$. Applying Gronwall's lemma as done in (2.8), we have

$$\|u(t)\|^2 \le e^{M_1(t)}\,\|u_0\|^2 + \frac{e^{M_1(t)}}{\nu}\int_0^t |\mathcal{P}f|_{L^2}^2\, ds, \tag{2.10}$$

and, with a derivation analogous to that leading to (2.9), we have

$$\frac{1}{t}\int_0^t |Au|_{L^2}^2\, ds \le \frac{2e^{M_1(t)}}{\nu t}\,\|u_0\|^2 + \frac{2e^{M_1(t)}}{\nu^2 t}\int_0^t |\mathcal{P}f|_{L^2}^2\, ds. \tag{2.11}$$

The *a priori* estimates (2.8), (2.9), (2.10), and (2.11) allow us to characterize the mapping $(\psi,\phi) \mapsto u(\psi,\phi)$. Specifically, we have:

Lemma 6 *Take $U \in L^\infty(0,T;V) \cap L^2(0,T;D(A))$ and let u be the solution of (2.4). The mappings $(\psi,\phi) \mapsto u(\psi,\phi)$ from $L^2(0,T;L^2) \times L^2(0,T;L^2)$ into $L^2(0,T;V)$ and $(\psi,\phi) \mapsto u(\psi,\phi)|_T$ from $L^2(0,T;L^2) \times L^2(0,T;L^2)$ into V are affine and continuous. For $u_0 \in V$ and $(\psi,\phi) \in L^2(0,T;L^2) \times L^2(0,T;L^2)$, the mappings $(\psi,\phi) \mapsto u(\psi,\phi)$ and $(\psi,\phi) \mapsto u(\psi,\phi)|_T$ have Gâteau* *derivatives* $u'(\psi',\phi')$ *and* $u'(\psi',\phi')|_T$ *in every direction* $(\psi',\phi') \in L^2(0,T;L^2) \times L^2(0,T;L^2)$. *Finally, the Gâteau derivative* $u'(\psi',\phi')$ *solves the linear evolution equation*

$$\begin{cases} \dfrac{du'}{dt} + \nu A u' + B'(U)u' = \mathcal{B}_1\psi' + \mathcal{B}_2\phi', \\ u' \in V, \\ u' = 0 \qquad \text{at } t = 0, \end{cases} \tag{2.12}$$

and it follows that $u'(\psi',\phi') \in L^\infty(0,T;V) \cap L^2(0,T;D(A))$.

Proof. The fact that $(\psi,\phi) \mapsto u(\psi,\phi)$ and $(\psi,\phi) \mapsto u(\psi,\phi)|_T$ are affine and continuous follows from the linearity of (2.4) and the *a priori* estimates (2.8), (2.9), (2.10), and (2.11). The existence of the Gâteau derivatives as well as their characterization by (2.12) is proved in Abergel & Temam (1990), to which we refer the reader for more details. $\square$

Remark 7 *The solution* $u'(\psi',\phi')$ *of* (2.12) *can be expressed as a function of* ψ' *and* ϕ' *in terms of the Green-Oseen's kernels* $G_\psi(x,t,x',t')$ *and* $G_\phi(x,t,x',t')$ *(see Ladyzhenskaya 1969); formally, we write*

$$\begin{aligned} u'(x,t;\psi',\phi') &= \int_0^T \int_\Omega \Big(G_\psi(x,t,x',t')\,\psi'(x',t') + G_\phi(x,t,x',t')\,\phi'(x',t')\Big)dx'\,dt' \\ &\triangleq G_\psi \cdot \psi' + G_\phi \cdot \phi'. \end{aligned}$$

Notationally, we will denote G_ψ *by* $\mathcal{D}u/\mathcal{D}\psi$ *and* G_ϕ *by* $\mathcal{D}u/\mathcal{D}\phi$, *and thus* $u'(\psi',\phi') = (\mathcal{D}u/\mathcal{D}\psi)\cdot\psi' + (\mathcal{D}u/\mathcal{D}\phi)\cdot\phi'$. *Physically,* $u'(\psi',\phi')$ *may be thought of as the linear approximation to the perturbation to* u *when a perturbation* ψ' *is added to the disturbance* ψ *and a perturbation* ϕ' *is added to the control* ϕ. *A finite dimensional discretization of the Green-Oseen's kernel* $G_\psi = \mathcal{D}u/\mathcal{D}\psi$ *may be taken as the Jacobian of the discretization of* u *with respect to the discretization of* ψ, *as suggested by this notation; an analogous interpretation may be attributed to* $G_\phi = \mathcal{D}u/\mathcal{D}\phi$. *By causality,* $G_\psi(x,t,x',t') = G_\phi(x,t,x',t') = 0$ *for* $t - t' < 0$.

With Lemma 2.3 established, we are ready to prove that conditions (a)-(d) of Proposition 2.2 are satisfied for the present robust control problem:

Lemma 8 *Let $u_0 \in V$. There exists γ_1 such that, for $\gamma \geq \gamma_1$, we have*

$$\begin{array}{ll}
\text{(A)} & \forall\, \psi \in L^2(0,T;L^2), \quad \phi \mapsto \mathcal{J}(\psi,\phi) \text{ is convex lower semicontinuous,} \\
\text{(B)} & \forall\, \phi \in L^2(0,T;L^2), \quad \psi \mapsto \mathcal{J}(\psi,\phi) \text{ is concave upper semicontinuous,} \\
\text{(C)} & \displaystyle\lim_{|\phi|_{L^2(0,T;L^2)} \to +\infty} \mathcal{J}(0,\phi) = +\infty, \\
\text{(D)} & \displaystyle\lim_{|\psi|_{L^2(0,T;L^2)} \to +\infty} \mathcal{J}(\psi,0) = -\infty.
\end{array}$$

Proof. Condition (A): by Lemma 2.3, the map $\phi \mapsto \mathcal{J}(\psi,\phi)$ is lower semicontinuous. As $\phi \mapsto u(\psi,\phi)$ is affine, the convexity of $\phi \mapsto \mathcal{J}(\psi,\phi)$ follows promptly.

Condition (B): by Lemma 2.3, the map $\psi \mapsto \mathcal{J}(\psi,\phi)$ is upper semicontinuous. In order to prove concavity, it is sufficient to show that

$$h(\rho) = \mathcal{J}(\psi + \rho\psi', \phi)$$

is concave w.r.t. ρ, *i.e.*, $h''(\rho) < 0$. Taking $u'(\psi',0) = (\mathcal{D}u/\mathcal{D}\psi)\cdot\psi'$, we compute

$$\begin{aligned}
h'(\rho) = &\int_0^T \left(\mathcal{C}_1 u, \mathcal{C}_1 u'\right)_{L^2(\Omega)} dt + \left(\mathcal{C}_2 u(T), \mathcal{C}_2 u'(T)\right)_{L^2(\Omega)} \\
&- \int_0^T \left(\mathcal{C}_3 \nu \frac{\partial u'}{\partial n}, \vec{r}\right)_{L^2(\partial\Omega)} dt - \gamma^2 \int_0^T \left(\psi + \rho\psi', \psi'\right)_{L^2(\Omega)} dt.
\end{aligned}$$

It is clear that u' is independent of ρ. Therefore,

$$h''(\rho) = \int_0^T \left|\mathcal{C}_1 u'\right|^2_{L^2(\Omega)} dt + \left|\mathcal{C}_2 u'(T)\right|^2_{L^2(\Omega)} - \gamma^2 \int_0^T \left|\psi'\right|^2_{L^2(\Omega)} dt.$$

Note that $u' = (\mathcal{D}u/\mathcal{D}\psi)\cdot\psi'$ satisfies (2.12) by Lemma 2.3, and thus the *a priori* estimates (2.8), (2.9), (2.10), and (2.11) also follow upon substitution of $u'(\psi',0)$ for $u(\psi,\phi)$, mutatis mutandis. Upon making such a substitution to (2.2) and applying (2.9) and the Poincaré and Cauchy-Schwarz inequalities, noting that $u' = 0$ at $t = 0$, we find that

$$\begin{aligned}
\int_0^T \left|\mathcal{C}_1 u'\right|^2_{L^2(\Omega)} dt &\leq \alpha \int_0^T \left|u'\right|^2_{L^2(\Omega)} dt + \beta \int_0^T \left\|u'\right\|^2 dt \\
&\leq \left(\frac{\alpha}{\lambda_1} + \beta\right) \frac{2e^{M_0(T)}}{\nu^2 \lambda_1} \int_0^T \left|\mathcal{B}_1 \psi'\right|^2_{L^2(\Omega)} dt \\
&\leq \left(\frac{\alpha}{\lambda_1} + \beta\right) \frac{2e^{M_0(T)}}{\nu^2 \lambda_1} \left|\mathcal{B}_1\right|^2_{\mathcal{L}(L^2,H)} \int_0^T \left|\psi'\right|^2_{L^2(\Omega)} dt,
\end{aligned}$$

and similarly, by applying (2.2), (2.8), and (2.10) to $u'(\psi', 0)$,

$$|\mathcal{C}_2 u'(T)|^2_{L^2(\Omega)} \leq \Big(\frac{\alpha}{\nu\lambda_1}\, e^{M_0(T)} + \frac{\beta}{\nu}\, e^{M_1(T)}\Big) |\mathcal{B}_1|^2_{\mathcal{L}(L^2,H)} \int_0^T |\psi'|^2_{L^2(\Omega)}\, dt.$$

Now under the assumption that

$$\gamma^2 \geq \gamma_1^2 = 2\Big[\Big(\frac{\alpha}{\lambda_1} + \beta\Big)\frac{2e^{M_0(T)}}{\nu^2\lambda_1} + \frac{\alpha}{\nu\lambda_1}\, e^{M_0(T)} + \frac{\beta}{\nu}\, e^{M_1(T)}\Big] |\mathcal{B}_1|^2_{\mathcal{L}(L^2,H)}, \tag{2.13}$$

we have $h''(\rho) < 0$ for $\rho \in \mathbb{R}$. Thus the function h is concave, and the concavity of $\psi \mapsto \mathcal{J}(\psi, \phi)$ follows immediately.

Condition (C): Applying (2.3) to (2.1) and taking $\psi = 0$, we can write

$$\mathcal{J}(0, \phi) \geq \frac{\ell^2}{2} \int_0^T |\phi|^2_{L^2(\Omega)}\, dt - \kappa'\nu \int_0^T \|u\|^{1/2} |Au|^{1/2}_{L^2(\Omega)}\, dt.$$

By the *a priori* estimates (2.8), (2.9), (2.10), and (2.11), it is straightforward to show that there exist constants $C_0 = C_0(T, \Omega, \|u_0\|)$ and $C_1 = C_1(T, \Omega, \|u_0\|)$ such that the latter term is bounded by an expression which is affine in ϕ, *i.e.*,

$$\kappa'\nu \int_0^T \|u\|^{1/2} |Au|^{1/2}_{L^2}\, dt \leq C_0 |\phi|_{L^2(0,T;L^2)} + C_1,$$

and thus

$$\mathcal{J}(0, \phi) \geq \frac{\ell^2}{2} |\phi|^2_{L^2(0,T;L^2)} - C_0 |\phi|_{L^2(0,T;L^2)} - C_1,$$

and condition (C) follows promptly.

Condition (D): Upon substituting (2.9) into (2.2), as done for condition B, and considering $u(\psi, 0)$, it follows that

$$\int_0^T |\mathcal{C}_1 u|^2_{L^2(\Omega)}\, dt \leq \Big(\frac{\alpha}{\lambda_1} + \beta\Big)\frac{2e^{M_0(T)}}{\nu^2\lambda_1} |\mathcal{B}_1|^2_{\mathcal{L}(L^2,H)} \int_0^T |\psi|^2_{L^2(\Omega)}\, dt + C_1,$$

where $C_1 = C_1(T, \Omega, \|u_0\|)$. Similarly, by (2.2), (2.8), and (2.10), we have

$$|\mathcal{C}_2 u(T)|^2_{L^2(\Omega)} \leq \Big(\frac{\alpha}{\nu\lambda_1}\, e^{M_0(T)} + \frac{\beta}{\nu}\, e^{M_1(T)}\Big) |\mathcal{B}_1|^2_{\mathcal{L}(L^2,H)} \int_0^T |\psi|^2_{L^2(\Omega)}\, dt + C_1.$$

Finally, we may bound the linear term in $\mathcal{J}(\psi,0)$ by an expression which is affine in ψ with a procedure analogous to that used for condition (C) above. Thus, if $\gamma^2 \geq \gamma_1^2$, we have

$$\begin{aligned}\mathcal{J}(\psi,0) &= \frac{1}{2}\int_0^T \big|\mathcal{C}_1 u\big|^2_{L^2(\Omega)}\,dt + \frac{1}{2}\big|\mathcal{C}_2 u(T)\big|^2_{L^2(\Omega)} - \int_0^T \big(\mathcal{C}_3 \nu \frac{\partial u}{\partial n}, \vec{r}\big)_{L^2(\partial\Omega)}\,dt \\ &\quad - \frac{\gamma^2}{2}\int_0^T \big|\psi\big|^2_{L^2(\Omega)}\,dt \\ &\leq -\frac{\gamma^2}{4}\big|\psi\big|^2_{L^2(0,T;L^2)} + C_0\big|\psi\big|_{L^2(0,T;L^2)} + C_1,\end{aligned}$$

which implies (D). $\square$

Putting the statements of this section together, we have established existence of a solution $(\bar{\psi},\bar{\phi})$ to the robust control problem of Definition 2.1 for the linear case with $\gamma > \gamma_1$:

Theorem 9 *(Existence of a solution to the robust control problem, linear case.) Assume that $\gamma > \gamma_1$, where*

$$\gamma_1^2 = 2\Big[\Big(\frac{\alpha}{\lambda_1} + \beta\Big)\frac{2e^{M_0(T)}}{\nu^2\lambda_1} + \frac{\alpha}{\nu\lambda_1}\,e^{M_0(T)} + \frac{\beta}{\nu}\,e^{M_1(T)}\Big]\big|\mathcal{B}_1\big|^2_{\mathcal{L}(L^2,H)}.$$

Then there exists a saddle point $(\bar{\psi},\bar{\phi})$ and $u(\bar{\psi},\bar{\phi})$ such that

$$\mathcal{J}(\psi,\bar{\phi}) \leq \mathcal{J}(\bar{\psi},\bar{\phi}) \leq \mathcal{J}(\bar{\psi},\phi) \qquad \forall\ (\psi,\phi) \in L^2(0,T;L^2) \times L^2(0,T;L^2).$$

It follows that γ_1 is an upper bound on the critical value γ_0 discussed in §1.1.

Proof. The proof follows directly from Lemmas 2.3 and 2.5 and Proposition 2.2. $\square$

2.2 Identification of the unique solution to the robust control problem

The existence of a saddle point $(\bar{\psi},\bar{\phi})$ of the functional $\mathcal{J}$, established in the previous section, implies that

$$\frac{\mathcal{D}\mathcal{J}}{\mathcal{D}\psi}(\bar{\psi},\bar{\phi}) = 0 \quad \text{and} \quad \frac{\mathcal{D}\mathcal{J}}{\mathcal{D}\phi}(\bar{\psi},\bar{\phi}) = 0. \tag{2.14}$$

Differentiation of (2.1) leads to expressions for these gradients in weak form:

$$\begin{aligned}\frac{\mathcal{D}\mathcal{J}}{\mathcal{D}\psi}(\psi,\phi)\cdot\psi' &= \int_0^T \big(\mathcal{C}_1 u, \mathcal{C}_1\frac{\mathcal{D}u}{\mathcal{D}\psi}\cdot\psi'\big)_{L^2(\Omega)}\,dt + \big(\mathcal{C}_2 u(T), \mathcal{C}_2\frac{\mathcal{D}u(T)}{\mathcal{D}\psi}\cdot\psi'\big)_{L^2(\Omega)}\\ &\quad -\int_0^T \big(\mathcal{C}_3\nu\frac{\partial}{\partial n}\frac{\mathcal{D}u}{\mathcal{D}\psi}\cdot\psi', \vec{r}\big)_{L^2(\partial\Omega)}\,dt - \gamma^2\int_0^T \big(\psi,\psi'\big)_{L^2(\Omega)}\,dt,\end{aligned} \tag{2.15}$$

$$\begin{aligned}\frac{\mathcal{D}\mathcal{J}}{\mathcal{D}\phi}(\psi,\phi)\cdot\phi' &= \int_0^T \big(\mathcal{C}_1 u, \mathcal{C}_1\frac{\mathcal{D}u}{\mathcal{D}\phi}\cdot\phi'\big)_{L^2(\Omega)}\,dt + \big(\mathcal{C}_2 u(T), \mathcal{C}_2\frac{\mathcal{D}u(T)}{\mathcal{D}\phi}\cdot\phi'\big)_{L^2(\Omega)}\\ &\quad -\int_0^T \big(\mathcal{C}_3\nu\frac{\partial}{\partial n}\frac{\mathcal{D}u}{\mathcal{D}\phi}\cdot\phi', \vec{r}\big)_{L^2(\partial\Omega)}\,dt + \ell^2\int_0^T \big(\phi,\phi'\big)_{L^2(\Omega)}\,dt.\end{aligned} \tag{2.16}$$

In order to determine the solution to the robust control problem, we define an adjoint state by the equation

$$\begin{cases} -\dfrac{d\tilde{u}}{dt} + \nu\mathcal{A}^*\tilde{u} + B'(U)^*\tilde{u} = \mathcal{C}_1^*\mathcal{C}_1\, u,\\ \tilde{u}(t)\in V_r = \left\{v\in (H^1(\Omega))^3;\ \mathrm{div}\ v = 0 \text{ in } \Omega,\quad v = \mathcal{C}_3^*\vec{r} \text{ on } \partial\Omega\right\},\quad t<T,\\ \tilde{u} = \mathcal{C}_2^*\mathcal{C}_2\, u\in H \qquad\quad \text{at } t = T,\end{cases} \tag{2.17}$$

where $\mathcal{A}^*$ is the unbounded operator on $H\cap H^1$ uniquely defined by

$$\big(u',\mathcal{A}^*\tilde{u}\big)_{L^2(\Omega)} = \big(Au',\tilde{u}\big)_{L^2(\Omega)} + \big(\frac{\partial u'}{\partial n},\tilde{u}\big)_{L^2(\partial\Omega)} \quad \text{for } u'\in D(A),\ \tilde{u}\in H\cap H^1.$$

We have the following:

Lemma 10 *Let $u(\psi,\phi)$ be the solution of (2.4) with the regularity on ψ, ϕ, u_0, and U given in (2.5), let $u'(\psi',\phi')$ be the solution of (2.12) with $(\psi',\phi')\in L^2(0,T;L^2)\times L^2(0,T;L^2)$, and let $\tilde{u}$ be the solution of (2.17). Then*

$$\begin{aligned}\int_0^T \big(\mathcal{C}_1^*\mathcal{C}_1 u, u'\big)_{L^2(\Omega)}\,dt + \big(\mathcal{C}_2^*\mathcal{C}_2 u(T), u'(T)\big)_{L^2(\Omega)} - \int_0^T \big(\mathcal{C}_3\nu\frac{\partial u'}{\partial n},\vec{r}\big)_{L^2(\partial\Omega)}\,dt\\ = \int_0^T \Big[\big(\mathcal{B}_1^*\tilde{u},\psi'\big)_{L^2(\Omega)} + \big(\mathcal{B}_2^*\tilde{u},\phi'\big)_{L^2(\Omega)}\Big]\,dt\end{aligned} \tag{2.18}$$

where $\mathcal{B}_1^*$ and $\mathcal{B}_2^*$ are the adjoints in $L^2(\Omega)$ of the operators $\mathcal{B}_1$ and $\mathcal{B}_2$.

Proof. The proof follows from integration by parts and the regularity of u, u' and $\tilde{u}$:

$$\begin{aligned}
&\int_0^T \big(\mathcal{C}_1^*\mathcal{C}_1 u, u'\big)_{L^2(\Omega)}\, dt + \big(\mathcal{C}_2^*\mathcal{C}_2 u(T), u'(T)\big)_{L^2(\Omega)} - \int_0^T \big(\mathcal{C}_3 \nu \frac{\partial u'}{\partial n}, \vec{r}\big)_{L^2(\partial\Omega)}\, dt \\
&\quad = \int_0^T \big([-\frac{d\tilde{u}}{dt} + \nu \mathcal{A}^*\tilde{u} + B'(U)^*\tilde{u}], u'\big)_{L^2(\Omega)}\, dt \\
&\qquad + \big(\tilde{u}(T), u'(T)\big)_{L^2(\Omega)} - \int_0^T \big(\nu \frac{\partial u'}{\partial n}, \tilde{u}\big)_{L^2(\partial\Omega)}\, dt \\
&\quad = \int_0^T \big(\tilde{u}, [\frac{du'}{dt} + \nu A u' + B'(U)u']\big)_{L^2(\Omega)}\, dt \\
&\quad = \int_0^T \big(\tilde{u}, [\mathcal{B}_1\psi' + \mathcal{B}_2\phi']\big)_{L^2(\Omega)}\, dt \\
&\quad = \int_0^T \Big[\big(\mathcal{B}_1^*\tilde{u}, \psi'\big)_{L^2(\Omega)} + \big(\mathcal{B}_2^*\tilde{u}, \phi'\big)_{L^2(\Omega)}\Big]\, dt. \qquad \square
\end{aligned}$$

Application of (2.18) to (2.15), with $\phi' = 0$ and taking $\psi' \in L^2(0,T;L^2)$ as arbitrary, leads to an expression for the gradient $\mathcal{DJ}/\mathcal{D}\psi$:

$$\frac{\mathcal{DJ}}{\mathcal{D}\psi}(\psi, \phi) = \mathcal{B}_1^*\, \tilde{u} - \gamma^2 \psi. \tag{2.19}$$

Similarly, application of (2.18) to (2.16), with $\psi' = 0$ and taking $\phi' \in L^2(0,T;L^2)$ as arbitrary, leads to an expression for the gradient $\mathcal{DJ}/\mathcal{D}\phi$:

$$\frac{\mathcal{DJ}}{\mathcal{D}\phi}(\psi, \phi) = \mathcal{B}_2^*\, \tilde{u} + \ell^2 \phi. \tag{2.20}$$

Now we prove the main result of this chapter:

Theorem 11 *Let $(\bar{\psi}, \bar{\phi})$ be a solution to the robust control problem stated in Definition 2.1. Then*

$$\bar{\psi} = \frac{1}{\gamma^2}\, \mathcal{B}_1^*\, \tilde{u} \quad \text{and} \quad \bar{\phi} = -\frac{1}{\ell^2}\, \mathcal{B}_2^*\, \tilde{u}, \tag{2.21}$$

where $\tilde{u}$ is found from the solution $(u, \tilde{u})$ of the following coupled system:

$$
\begin{cases}
\dfrac{du}{dt} + \nu A u + B(u,U) + B(U,u) = \left(\dfrac{1}{\gamma^2}\,\mathcal{B}_1\mathcal{B}_1^* - \dfrac{1}{\ell^2}\,\mathcal{B}_2\mathcal{B}_2^*\right)\tilde{u}, \\
-\dfrac{d\tilde{u}}{dt} + \nu\mathcal{A}^*\tilde{u} + B'(U)^*\tilde{u} = \mathcal{C}_1^*\mathcal{C}_1 u, \\
u \in V, \\
\tilde{u}(t) \in V_r = \left\{v \in (H^1(\Omega))^3;\ \text{div } v = 0 \text{ in } \Omega,\quad v = \mathcal{C}_3^*\vec{r} \text{ on } \partial\Omega\right\}, \quad t < T, \\
u(0) = u_0 \quad \text{and } \tilde{u}(T) = \mathcal{C}_2^*\mathcal{C}_2\, u(T),
\end{cases}
\tag{2.22}
$$

which admits a unique solution for sufficiently large γ.

Proof. The existence of a solution to the robust control problem is established by Theorem 2.6 for $\gamma > \gamma_1$.

A necessary condition for $(\bar{\psi}, \bar{\phi})$ to be a saddle point of the functional $\mathcal{J}$ is given by (2.14). Thus, (2.19) and (2.20) imply that (2.21) follows from the definition of the coupled system developed in this section and summarized in (2.22).

The uniqueness of the solution of the coupled system (2.22) is classical. For

$$\gamma > \gamma_2(|\mathcal{B}_1|_{\mathcal{L}(L^2,H)}, |\mathcal{B}_2|_{\mathcal{L}(L^2,H)}, \ell),$$

it is clear that $\mathcal{D} = -\left(\gamma^{-2}\,\mathcal{B}_1\mathcal{B}_1^* - \ell^{-2}\,\mathcal{B}_2\mathcal{B}_2^*\right)$ is positive definite. The proof of uniqueness then follows by taking the difference $(u_3, \tilde{u}_3)$ of two solutions $(u_1, \tilde{u}_1)$ and $(u_2, \tilde{u}_2)$, multiplying the u_3 equation by $\tilde{u}_3$ and the $\tilde{u}_3$ equation by u_3, integrating between 0 and T, and then subtracting the two resulting equations. This results in

$$
\begin{aligned}
(u_3(T), \tilde{u}_3(T)) - (u_3(0), \tilde{u}_3(0)) &+ \\
&\int_0^T \left[\left(\mathcal{D}\tilde{u}_3(t), \tilde{u}_3(t)\right) + \left(\mathcal{C}_1^*\mathcal{C}_1 u_3(t), u_3(t)\right)\right] dt = 0,
\end{aligned}
$$

with $u_3(0) = 0$ and $\tilde{u}_3(T) = \mathcal{C}_2^*\mathcal{C}_2\, u_3(T)$, from which we conclude that $u_3 = \tilde{u}_3 = 0$, and thus the solution is unique. $\square$

To summarize §2, for $\gamma > \max(\gamma_1, \gamma_2)$, a solution to the robust control problem stated in Definition 2.1 exists, is unique, and is given by (2.21).

Chapter 3

The nonlinear problem

In this chapter, we apply the analysis of the previous chapter to the 2D and 3D nonlinear problems. We consider the same cost functional as in the previous chapter,

$$\begin{aligned}\mathcal{J}(\psi,\phi) = \frac{1}{2}\int_0^T \Big|\mathcal{C}_1 u\Big|^2_{L^2(\Omega)} dt + \frac{1}{2}\Big|\mathcal{C}_2 u(T)\Big|^2_{L^2(\Omega)} - \int_0^T \Big(\mathcal{C}_3 \nu \frac{\partial u}{\partial n}, \vec{r}\Big)_{L^2(\partial\Omega)} dt \\ + \frac{1}{2}\int_0^T \Big[\ell^2 \Big|\phi\Big|^2_{L^2(\Omega)} - \gamma^2 \Big|\psi\Big|^2_{L^2(\Omega)}\Big] dt.\end{aligned} \tag{3.1}$$

Recall that the operators $\mathcal{C}_1$, $\mathcal{C}_2$, and $\mathcal{C}_3$ satisfy (2.2), (2.3), and $\mathcal{C}_3^* \vec{r} \cdot \vec{n} = 0$. Assume now that u satisfies the nonlinear Navier-Stokes equation

$$\begin{cases} \dfrac{du}{dt} + \nu A u + B(u,U) + B(U,u) + B(u,u) = \mathcal{B}_1 \psi + \mathcal{B}_2 \phi, \\ u \in V, \\ u = u_0 \qquad \text{at } t = 0, \end{cases} \tag{3.2}$$

which models large deviations of the flow perturbation u from the desired target flow U. The regularity required on ψ, ϕ, $\mathcal{B}_1$, $\mathcal{B}_2$, u_0, and U are the same as in (2.5).

The robust control problem to be solved in the nonlinear case is:

Definition 12 *Let $\mathcal{X}$ and $\mathcal{Y}$ be bounded subsets of $L^2(0,T;L^2)$. The disturbance $\bar{\psi} \in \mathcal{X}$ and control $\bar{\phi} \in \mathcal{Y}$, and the solution $\bar{u} = u(\bar{\psi},\bar{\phi})$ to (3.2) associated with $(\bar{\psi},\bar{\phi})$, are said to solve the robust control problem when a saddle point $(\bar{\psi},\bar{\phi})$ of the cost functional $\mathcal{J}$ defined in (3.1) is reached such that*

$$\mathcal{J}(\psi,\bar{\phi}) \le \mathcal{J}(\bar{\psi},\bar{\phi}) \le \mathcal{J}(\bar{\psi},\phi) \qquad \forall\ (\psi,\phi) \in \mathcal{X} \times \mathcal{Y}. \tag{3.3}$$

In this chapter, we will establish existence of a solution to the robust control problem for the case in which the flow perturbation u is related to the disturbance ψ and the control ϕ through the nonlinear Navier-Stokes equation (3.2). The analysis is similar to that for the linear problem in the previous chapter. Note that §3.1 will consider the 3D case, and §3.2 will focus specifically on the 2D case, for which stronger results may be established.

3.1 Existence of a solution to the robust control problem, 3D case

The proof of existence in this section is similar to that for the linear problem, but is restricted to cases of either "small data" or "small T". The former assumption is valid when attempting to delay transition to turbulence (*i.e.*, keeping a laminar flow laminar) in an externally-disturbed flow that is linearly stable but nonlinearly unstable, and is of important engineering significance (Bewley & Liu 1998). The latter assumption has been termed the "suboptimal" approximation in earlier work, and has been shown to deliver simple control strategies with reduced long-term performance (Bewley *et al.* 1993; Hill 1993; Lee, Kim & Choi 1998). The restrictions used to prove existence of a solution to the robust control problem in the present case are due simply to the current lack of regularity results for the 3D Navier-Stokes equation, not to a shortcoming of the present analysis of the robust control framework.

To proceed under the constraint of a small data condition, we restrict the bounded set $\mathcal{X} \times \mathcal{Y}$ of $L^2(0,T;L^2) \times L^2(0,T;L^2)$ by the condition that, for any (ψ, ϕ) in $\mathcal{X} \times \mathcal{Y}$, we have

$$|\mathcal{B}_1\psi|^2_{L^2(0,T;H)} + |\mathcal{B}_2\phi|^2_{L^2(0,T;H)} \leq C_1 \lambda_1^{1/2} \nu^3.$$

We will mention by way of two remarks that this restriction on $\mathcal{X} \times \mathcal{Y}$ may be lifted in the existence proof if T is sufficiently small. The proof of the existence of a solution $(\bar{\psi}, \bar{\phi})$ on $\mathcal{X} \times \mathcal{Y}$ for the nonlinear, 3D case is based on the following existence result:

Proposition 13 *Let $\mathcal{J}$ be a functional defined on $\mathcal{X} \times \mathcal{Y}$, where $\mathcal{X}$ and $\mathcal{Y}$ are non-empty, closed, bounded, convex sets. If $\mathcal{J}$ satisfies*

$$\begin{array}{lll} \text{(a)} & \forall\, \phi \in \mathcal{Y}, \quad \psi \mapsto \mathcal{J}(\psi,\phi) & \text{is concave upper semicontinuous,} \\ \text{(b)} & \forall\, \psi \in \mathcal{X}, \quad \phi \mapsto \mathcal{J}(\psi,\phi) & \text{is convex lower semicontinuous.} \end{array}$$

then the functional $\mathcal{J}$ has at least one saddle point $(\bar{\psi}, \bar{\phi})$ on $\mathcal{X} \times \mathcal{Y}$, which is defined by

$$\mathcal{J}(\bar{\psi},\bar{\phi}) = \operatorname*{Min}_{\phi\in\mathcal{Y}} \operatorname*{Max}_{\psi\in\mathcal{X}} \mathcal{J}(\psi,\phi) = \operatorname*{Max}_{\psi\in\mathcal{X}} \operatorname*{Min}_{\phi\in\mathcal{Y}} \mathcal{J}(\psi,\phi).$$

Proof. The proof is given in Ekeland & Temam (1974). □

In order to establish conditions (a) and (b) of Proposition 3.2 for the present problem, we need to analyze the evolution equation (3.2). It can be proven rigorously (following the framework of Ladyzhenskaya 1969, Lions 1969, and Temam 1984) that there exists an $R > 0$ such that, given $u_0 \in V$, $U \in L^\infty(0,T;V) \cap L^2(0,T;D(A))$, and the small data constraints

$$\|u_0\| \leq R \quad \text{and} \quad (\psi, \phi) \in \mathcal{X} \times \mathcal{Y},$$

there exists a unique solution u of (3.2) such that

$$u \in L^2(0,T;D(A)) \cap L^\infty(0,T;V) \quad \forall\, T > 0.$$

The proof is based on the following *a priori* estimates. Multiplying (3.2) with u and noting by (1.11) that $b(u,u,u) = 0$, the estimates (2.8) and (2.9) follow as in the linear case; specifically,

$$|u(t)|_{L^2}^2 \leq e^{M_0(t)}\, |u_0|_{L^2}^2 + \frac{e^{M_0(t)}}{\nu\lambda_1} \int_0^t |\mathcal{P}f|_{L^2}^2\, ds \tag{3.4}$$

and

$$\frac{1}{t}\int_0^t \|u\|^2 ds \leq \frac{2e^{M_0(t)}}{\nu t}\, |u_0|_{L^2}^2 + \frac{2e^{M_0(t)}}{\nu^2\lambda_1 t} \int_0^t |\mathcal{P}f|_{L^2}^2\, ds, \tag{3.5}$$

where $M_0(t) = C_0 \nu^{-3} \int_0^t \|U\|^4\, d\tau$.

Also, multiplying (3.2) with Au and following a line of reasoning similar to the linear case, we can write

$$\begin{aligned} \frac{d}{dt}\|u\|^2 + \nu |Au|_{L^2}^2 \leq \frac{1}{\nu}\, |\mathcal{P}f|_{L^2}^2 + C_0 \left(\|U\|^{1/2} |AU|_{L^2}^{1/2} + |U|_{L^2}^{1/4} |AU|_{L^2}^{3/4} \right) \|u\| |Au|_{L^2} \\ + C_1 \|u\|^{3/2} |Au|_{L^2}^{3/2}. \end{aligned}$$

Application of Young's inequality to the first line and the Poincaré inequality to the second line leads to

$$\begin{aligned} \frac{d}{dt}\|u\|^2 + \frac{\nu}{2}|Au|_{L^2}^2 \leq \frac{1}{\nu}\, |\mathcal{P}f|_{L^2}^2 + \frac{C_2}{\nu} \left(\|U\| |AU|_{L^2} + |U|_{L^2}^{1/2} |AU|_{L^2}^{3/2} \right) \|u\|^2 \\ + C_3 \lambda^{-1/4} \|u\| |Au|_{L^2}^2. \end{aligned} \tag{3.6}$$

For the remainder of this derivation, we will fix the coefficients C_2 and C_3 in (3.6), not allowing them to further absorb numerical constants.

Now prescribe that the initial conditions u_0, the target flow U, and the forcing $\mathcal{P}f = \mathcal{B}_1\psi + \mathcal{B}_2\phi$

be small, specifically:

$$\|u_0\| \leq \frac{\nu\lambda_1^{1/4}}{16\,C_3}, \qquad \left(\|U(t)\||AU(t)|_{L^2} + |U(t)|_{L^2}^{1/2}|AU(t)|_{L^2}^{3/2}\right) \leq \frac{\nu^2\lambda_1}{8\,C_2} \quad \forall\, t,$$
$$\text{and} \qquad \int_0^t |\mathcal{P}f|_{L^2}^2\,ds \leq 2\nu\,\|u_0\|^2 \quad \forall\, t. \tag{3.7}$$

Assume t^* is the maximal time such that

$$\|u(t)\| \leq 2\,\|u_0\| \quad \text{for } 0 \leq t \leq t^*; \tag{3.8}$$

by continuity, this implies that equality is achieved at $t = t^*$ such that

$$\|u(t^*)\|^2 = 4\,\|u_0\|^2\,. \tag{3.9}$$

We shall show that this assumption leads to a contradiction, which implies that t^* is instead unbounded, and thus that (3.8) is valid for all t when the conditions of (3.7) are met. Applying the conditions (3.8) and (3.7) to (3.6) and noting the Poincaré inequality, it follows that

$$\frac{d}{dt}\|u\|^2 + \frac{\nu}{4}\,|Au|_{L^2}^2 \leq \frac{1}{\nu}\,|\mathcal{P}f|_{L^2}^2 \quad \text{for } 0 \leq t \leq t^*. \tag{3.10}$$

Hence, by the Poincaré inequality and Gronwall's lemma,

$$\|u(t)\|^2 \leq e^{-\nu\lambda_1 t/4}\,\|u_0\|^2 + \frac{1}{\nu}\int_0^t |\mathcal{P}f|_{L^2}^2\,ds \quad \text{for } 0 \leq t \leq t^*$$

and thus

$$\|u(t)\|^2 \leq 3\|u_0\|^2 \quad \text{for } 0 \leq t \leq t^*.$$

We have arrived at a contradiction with (3.9), and therefore our assumption that t^* is bounded must be false. Thus, given the small data conditions of (3.7), it follows that t^* is unbounded and thus

$$\|u(t)\|^2 \leq e^{-\nu\lambda_1 t/4}\,\|u_0\|^2 + \frac{1}{\nu}\int_0^t |\mathcal{P}f|_{L^2}^2\,ds \quad \forall\, t \tag{3.11}$$

and, from integration of (3.10),

$$\frac{1}{t}\int_0^t |Au|_{L^2}^2\,ds \leq \frac{4}{\nu t}\,\|u_0\|^2 + \frac{4}{\nu^2 t}\int_0^t |\mathcal{P}f|_{L^2}^2\,ds \quad \forall\, t. \tag{3.12}$$

Remark 14 *The estimates* (3.11) *and* (3.12) *also follow without prescribing constraints on* u_0*,* U*,* *or $\mathcal{P}f$ but instead prescribing small time, specifically:*

$$t^* < t_0^* = \left(\frac{1}{\nu}\int_0^T |\mathcal{P}f|_{L^2}^2 ds + M_1' + \frac{C_0}{\nu^3}(1+\|u_0\|^2)^2\right)^{-1}. \tag{3.13}$$

As opposed to the linearized problem studied in §2, the mappings $(\psi,\phi) \mapsto u(\psi,\phi)$ and $(\psi,\phi) \mapsto u(\psi,\phi)|_T$ here are not affine. We have only the following:

Lemma 15 *Let u be the solution of (3.2) with $u_0 \in V$, $T > 0$, $U \in L^\infty(0,T;V) \cap L^2(0,T;D(A))$, and $(\psi,\phi) \in \mathcal{X} \times \mathcal{Y}$ such that the small data conditions of (3.7) are satisfied. The mappings $(\psi,\phi) \mapsto u(\psi,\phi)$ and $(\psi,\phi) \mapsto u(\psi,\phi)|_T$ have Gâteau derivatives $u'(\psi',\phi')$ and $u'(\psi',\phi')|_T$ in every direction $(\psi',\phi') \in L^2(0,T;L^2) \times L^2(0,T;L^2)$. Further, the Gâteau derivative $u'(\psi',\phi')$ solves the linear evolution equation*

$$\begin{cases} \dfrac{du'}{dt} + \nu A u' + B'(U+u)u' = \mathcal{B}_1\psi' + \mathcal{B}_2\phi', \\ u' \in V, \\ u' = 0 \qquad\qquad \text{at } t = 0, \end{cases} \tag{3.14}$$

and it follows that $u'(\psi',\phi') \in L^\infty(0,T;V) \cap L^2(0,T;D(A))$.

Proof. The existence of the Gâteau derivatives as well as their characterization by (2.12) follows as in Abergel & Temam (1990), to which we refer the reader for more details. □

Remark 16 *By Remark 3.3, Lemma 3.4 also holds when a condition of small time is satisfied (i.e., $T < t_0^*$) in lieu of the small data condition of (3.7).*

Lemma 17 *Let $u_0 \in V$ satisfying (3.7). There exists $\gamma_0 = \gamma_0(\|u_0\|, \nu, T)$ such that, for $\gamma \geq \gamma_0$, we have*

$$\begin{aligned} &\text{(A)} \qquad \forall\, \phi \in \mathcal{Y}, \quad \psi \mapsto \mathcal{J}(\psi,\phi) \;\; \text{is concave upper semicontinuous,} \\ &\text{(B)} \qquad \forall\, \psi \in \mathcal{X}, \quad \phi \mapsto \mathcal{J}(\psi,\phi) \;\; \text{is convex lower semicontinuous.} \end{aligned}$$

Proof. First, we note that by Lemma 3.4, and since the norm is lower semi-continuous, the map $\psi \mapsto \mathcal{J}(\psi,\phi)$ is upper semicontinuous while the map $\phi \mapsto \mathcal{J}(\psi,\phi)$ is lower semi-continuous.

Condition (A): by Lemma 3.4, and since the norm is lower semicontinuous, the map $\psi \mapsto \mathcal{J}(\psi,\phi)$ is upper semicontinuous. In order to prove concavity, it is sufficient to show that

$$h(\rho) = \mathcal{J}(\psi + \rho\psi', \phi)$$

is concave w.r.t. ρ near $\rho = 0$, *i.e.*, $h''(0) < 0$. Taking $u'(\psi', 0) = (\mathcal{D}u/\mathcal{D}\psi) \cdot \psi'$, we compute

$$\begin{aligned} h'(\rho) = &\int_0^T \big(\mathcal{C}_1 u, \mathcal{C}_1 u'\big)_{L^2(\Omega)}\, dt + \big(\mathcal{C}_2 u(T), \mathcal{C}_2 u'(T)\big)_{L^2(\Omega)} \\ &- \int_0^T \big(\mathcal{C}_3 \nu \frac{\partial u'}{\partial n}, \vec{r}\big)_{L^2(\partial\Omega)}\, dt - \gamma^2 \int_0^T \big(\psi + \rho\psi', \psi'\big)_{L^2(\Omega)}\, dt. \end{aligned}$$

Note by (3.14) that u' is a solution of

$$\begin{cases} \dfrac{du'}{dt} + \nu A u' + B(U+u, u') + B(u', U+u) = \mathcal{B}_1 \psi', \\ u' \in V, \\ u' = 0 \qquad \text{at } t = 0. \end{cases}$$

Noting the similarity to the linear equation (2.4), and following the derivations leading to (2.8)-(2.11), we have the following *a priori* estimates on u':

$$\begin{aligned} &|u'(t)|_{L^2}^2 \le \frac{e^{M_2(t)}}{\nu\lambda_1} \int_0^t |\mathcal{B}_1\psi'|_{L^2}^2\, ds, \qquad &&\int_0^t \|u'\|^2 ds \le \frac{2e^{M_2(t)}}{\nu^2\lambda_1} \int_0^t |\mathcal{B}_1\psi'|_{L^2}^2\, ds, \\ &\|u'(t)\|^2 \le \frac{e^{M_3(t)}}{\nu} \int_0^t |\mathcal{B}_1\psi'|_{L^2}^2\, ds, &&\int_0^t |Au'|_{L^2}^2\, ds \le \frac{2e^{M_3(t)}}{\nu^2} \int_0^t |\mathcal{B}_1\psi'|_{L^2}^2\, ds, \end{aligned}$$

with

$$\begin{aligned} M_2(t) &= C_0 \nu^{-3} \int_0^t \|U+u\|^4\, d\tau \qquad \text{and} \\ M_3(t) &= C_0 \nu^{-1} \int_0^t (\|U+u\| |A(U+u)|_{L^2} + |U+u|_{L^2}^{1/2} |A(U+u)|_{L^2}^{3/2})\, d\tau. \end{aligned}$$

Similarly, $u'' = (\mathcal{D}^2 u/\mathcal{D}\psi^2) \cdot \psi' \cdot \hat{\psi}'$ is a solution of

$$\begin{cases} \dfrac{du''}{dt} + \nu A u'' + B(U+u, u'') + B(u'', U+u) = \mathcal{F}, \\ u'' \in V, \\ u'' = 0 \qquad \text{at } t = 0. \end{cases}$$

where, taking $u' = (\mathcal{D}u/\mathcal{D}\psi) \cdot \psi'$ and $\hat{u}' = (\mathcal{D}u/\mathcal{D}\psi) \cdot \hat{\psi}'$,

$$\mathcal{F} = -B\big(\hat{u}', u'\big) - B\big(u', \hat{u}'\big).$$

The *a priori* estimates for u'' follow as for u' by replacing $\mathcal{B}_1\psi$ with $\mathcal{F}$.

Taking $\hat{\psi}' = \psi'$, and thus $\hat{u}' = u'$, we now write

$$\begin{aligned} h''(\rho) = &\int_0^T \left|\mathcal{C}_1 u'\right|^2_{L^2(\Omega)} dt + \int_0^T \left(\mathcal{C}_1 u, \mathcal{C}_1 u''\right)_{L^2(\Omega)} dt + \left|\mathcal{C}_2 u'(T)\right|^2_{L^2(\Omega)} \\ &+ \left(\mathcal{C}_2 u(T), \mathcal{C}_2 u''(T)\right)_{L^2(\Omega)} - \int_0^T \left(\mathcal{C}_3 \nu \frac{\partial u''}{\partial n}, \vec{r}\right)_{L^2(\partial\Omega)} dt - \gamma^2 \int_0^T \left|\psi'\right|^2_{L^2(\Omega)} dt. \end{aligned}$$

We will show that, for sufficiently large γ, the last term dominates in this expression and thus $h''(0) < 0$ when $(\psi, \phi) \in \mathcal{X} \times \mathcal{Y}$. First notice by (1.12) that $|\mathcal{F}|_{L^2} \leq C_0 \|u'\|^{3/2} |Au'|^{1/2}$, and thus that

$$\begin{aligned} \left|\mathcal{F}\right|^2_{L^2(0,t,L^2(\Omega))} &\leq \frac{C_0 e^{[3M_3(t)+M_2(t)]/2}}{\nu^3 \lambda_1^{1/2}} \left(\left|\mathcal{B}_1\right|^2_{\mathcal{L}(L^2,H)}\right)^2 \left(\left|\psi'\right|^2_{L^2(0,t;L^2(\Omega))}\right)^2 \\ &= M_4(t) \left(\left|\psi'\right|^2_{L^2(0,t;L^2(\Omega))}\right)^2. \end{aligned}$$

Then, given (2.2), (2.3), and our *a priori* estimates for u, u', and u'', we have

$$\begin{aligned} \left|\mathcal{C}_1 u'\right|^2_{L^2(0,T;L^2(\Omega))} &\leq \left(\frac{\alpha}{\lambda_1} + \beta\right) \frac{2e^{M_2(T)}}{\nu^2 \lambda_1} \left|\mathcal{B}_1\right|^2_{\mathcal{L}(L^2,H)} \left|\psi'\right|^2_{L^2(0,T;L^2(\Omega))} \\ &= D_1 \left|\psi'\right|^2_{L^2(0,T;L^2(\Omega))}, \\ \left|\left(\mathcal{C}_1 u, \mathcal{C}_1 u''\right)_{L^2(0,T;L^2(\Omega))}\right| &\leq \left(\left|\mathcal{C}_1 u\right|^2_{L^2(0,T;L^2(\Omega))}\right)^{1/2} \left(\left|\mathcal{C}_1 u''\right|^2_{L^2(0,T;L^2(\Omega))}\right)^{1/2} \\ &\leq \left(\frac{\alpha}{\lambda_1} + \beta\right) \left(3T\|u_0\|^2\right)^{1/2} \left(\frac{2e^{M_2(T)}}{\nu^2 \lambda_1} M_4(T)\right)^{1/2} \left|\psi'\right|^2_{L^2(0,T;L^2(\Omega))} \\ &= D_2 \left|\psi'\right|^2_{L^2(0,T;L^2(\Omega))}, \\ \left|\mathcal{C}_2 u'(T)\right|^2_{L^2(\Omega)} &\leq \left(\frac{\alpha}{\lambda_1} + \beta\right) \frac{e^{M_3(T)}}{\nu} \left|\mathcal{B}_1\right|^2_{\mathcal{L}(L^2,H)} \left|\psi'\right|^2_{L^2(0,T;L^2(\Omega))} \\ &= D_3 \left|\psi'\right|^2_{L^2(0,T;L^2(\Omega))}, \\ \left|\left(\mathcal{C}_2 u(T), \mathcal{C}_2 u''(T)\right)_{L^2(\Omega)}\right| &\leq \left(\left|\mathcal{C}_2 u\right|^2_{L^2(\Omega)}\right)^{1/2} \left(\left|\mathcal{C}_2 u''\right|^2_{L^2(\Omega)}\right)^{1/2} \\ &\leq \left(\frac{\alpha}{\lambda_1} + \beta\right) \left(3\|u_0\|^2\right)^{1/2} \left(\frac{e^{M_3(T)}}{\nu} M_4(T)\right)^{1/2} \left|\psi'\right|^2_{L^2(0,T;L^2(\Omega))} \\ &= D_4 \left|\psi'\right|^2_{L^2(0,T;L^2(\Omega))}, \\ \left|\left(\mathcal{C}_3 \nu \frac{\partial u''}{\partial n}, \vec{r}\right)_{L^2(0,T;L^2(\partial\Omega))}\right| &\leq \kappa' \nu T^{1/2} \left|u''\right|^{1/2}_{L^2(0,T;V)} \left|u''\right|^{1/2}_{L^2(0,T;D(A))} \\ &\leq \frac{\kappa'(2T)^{1/2} e^{[M_2(T)+M_3(T)]/4}}{\lambda_1^{1/4}} M_4^{1/2}(T) \left|\psi'\right|^2_{L^2(0,T;L^2(\Omega))} \\ &= D_5 \left|\psi'\right|^2_{L^2(0,T;L^2(\Omega))}. \end{aligned}$$

Thus, under the assumption that

$$\gamma^2 > \gamma_3^2 = D_1 + D_2 + D_3 + D_4 + D_5, \tag{3.15}$$

we have

$$h''(0) \leq (\gamma_3^2 - \gamma^2) \left|\psi'\right|^2_{L^2(0,T;L^2(\Omega))} < 0 \qquad \forall\, \psi' \neq 0. \tag{3.16}$$

The concavity of $\psi \mapsto \mathcal{J}(\psi,\phi)$ follows immediately.

Condition (B): by Lemma 3.4, and since the norm is lower semicontinuous, the map $\phi \mapsto \mathcal{J}(\psi,\phi)$ is upper semicontinuous. In order to prove convexity, it is sufficient to show that

$$g(\rho) = \mathcal{J}(\psi, \phi + \rho\phi')$$

is convex w.r.t. ρ near $\rho = 0$, *i.e.*, $g''(0) > 0$. Note that

$$\begin{aligned} g''(\rho) = &\int_0^T \left|\mathcal{C}_1 u'\right|^2_{L^2(\Omega)} dt + \int_0^T \left(\mathcal{C}_1 u, \mathcal{C}_1 u''\right)_{L^2(\Omega)} dt + \left|\mathcal{C}_2 u'(T)\right|^2_{L^2(\Omega)} \\ &+ \left(\mathcal{C}_2 u(T), \mathcal{C}_2 u''(T)\right)_{L^2(\Omega)} - \int_0^T \left(\mathcal{C}_3 \nu \frac{\partial u''}{\partial n}, \vec{r}\right)_{L^2(\partial\Omega)} dt + \ell^2 \int_0^T \left|\phi'\right|^2_{L^2(\Omega)} dt. \end{aligned}$$

Also note that the *a priori* estimates on $u' = (\mathcal{D}u/\mathcal{D}\phi) \cdot \phi'$ and $u'' = (\mathcal{D}^2 u/\mathcal{D}\phi^2) \cdot \phi' \cdot \hat{\phi}'$ and the bounds on the various terms of $g''(\rho)$ follow immediately as in the proof of condition (A) with $\mathcal{B}_2\phi'$ replacing $\mathcal{B}_1\psi'$ everywhere. Thus, under the assumption that

$$\ell^2 > \ell_1^2 = D_2 + D_4 + D_5, \tag{3.17}$$

we have

$$g''(0) \geq (\ell^2 - \ell_1^2) \left|\phi'\right|^2_{L^2(0,T;L^2(\Omega))} > 0 \qquad \forall\, \phi' \neq 0. \tag{3.18}$$

The convexity of $\phi \mapsto \mathcal{J}(\psi,\phi)$ follows immediately. $\square$

Putting the statements of this section together, we have established existence of a solution $(\bar{\psi}, \bar{\phi})$ to the robust control problem of Definition 3.1 for the 3D nonlinear case with sufficiently large γ and ℓ and sufficiently small data or sufficiently small T:

Theorem 18 *(Existence of a solution to the robust control problem, nonlinear 3D case.) Assume that $\gamma > \gamma_3$ and $\ell > \ell_1$, where γ_3 is defined as in* (3.15) *and ℓ_1 is defined as in* (3.17)*, and that either the small T constraint is satisfied, $T < t_0^*$, or that u_0, U, and $\mathcal{P}f$ are sufficiently small such that the small data constraints in* (3.7) *are satisfied. Then there exists a saddle point $(\bar{\psi}, \bar{\phi})$ on $\mathcal{X} \times \mathcal{Y}$*

and an associated $\bar{u} = u(\bar{\psi}, \bar{\phi})$ *such that*

$$\mathcal{J}(\psi, \bar{\phi}) \leq \mathcal{J}(\bar{\psi}, \bar{\phi}) \leq \mathcal{J}(\bar{\psi}, \phi) \qquad \forall\ (\psi, \phi) \in \mathcal{X} \times \mathcal{Y}.$$

Proof. The proof follows promptly from Lemmas 3.4 and 3.6 and Proposition 3.2. □

3.2 Existence of a solution to the robust control problem, 2D case

The proof of the existence of a robust control solution $(\bar{\psi}, \bar{\phi})$ for the nonlinear problem in the 2D case is similar to that for the 3D case in the previous section, with no small data or small T restriction. The improvement is due to the existence of improved versions of the inequalities (1.12) in the 2D case; specifically, we have

$$\begin{cases} |b(u,v,w)| \leq C_0 |u|^{1/2} \|u\|^{1/2} \|v\|^{1/2} |Av|_{L^2}^{1/2} |w|_{L^2}, & \forall\ u \in V,\ v \in D(A),\ w \in H, \\ |b(u,v,w)| \leq C_0 |u|_{L^2}^{1/2} |Au|_{L^2}^{1/2} \|v\| |w|_{L^2}, & \forall\ u \in D(A),\ v \in V,\ w \in H, \\ |b(u,v,w)| \leq C_0 |u|_{L^2}^{1/2} \|u\|^{1/2} \|v\| |w|_{L^2}^{1/2} \|w\|^{1/2}, & \forall\ u \in V,\ v \in V,\ w \in V. \end{cases}$$

We have, as in the 3D case (without any small data restriction)

$$|u(t)|_{L^2}^2 \leq e^{M_0(t)}\, |u_0|_{L^2}^2 + \frac{e^{M_0(t)}}{\nu \lambda_1} \int_0^t |\mathcal{P}f|_{L^2}^2\, ds.$$

and

$$\frac{1}{t} \int_0^t \|u\|^2 ds \leq \frac{2e^{M_0(t)}}{\nu t}\, |u_0|_{L^2}^2 + \frac{2e^{M_0(t)}}{\nu^2 \lambda_1 t} \int_0^t |\mathcal{P}f|_{L^2}^2\, ds,$$

where $M_0(t) = C_0 \nu^{-3} \int_0^t \|U\|^4\, d\tau$. Multiplying (3.2) with Au, we now have

$$\frac{d}{dt}\|u\|^2 + \nu |Au|_{L^2}^2 \leq \frac{1}{\nu}\, |\mathcal{P}f|_{L^2}^2 + C_0 \left(|U|^{1/2} |AU|_{L^2}^{1/2} + |U|_{L^2}^{1/2} |AU|_{L^2}^{1/2} \right) \|u\| |Au|_{L^2} + C_1 |u|^{1/2} \|u\| |Au|_{L^2}^{3/2}.$$

Applying Young's inequality,

$$\frac{d}{dt}\|u\|^2 + \nu |Au|_{L^2}^2 \leq \frac{1}{\nu}\, |\mathcal{P}f|_{L^2}^2 + \frac{C_0}{\nu} \left(|U| |AU|_{L^2} + |U|_{L^2} |AU|_{L^2} \right) \|u\|^2 + \frac{C_1}{\nu^3} |u|^2 \|u\|^4.$$

Set $g(t) = \frac{C_0}{\nu}\left(|U||AU|_{L^2} + |U|_{L^2}|AU|_{L^2}\right) + \frac{C_1}{\nu^3}|u|^2\|u\|^2$ and note that

$$\begin{aligned}\int_0^t g(\tau)\,d\tau &\leq M_6(t) + \sup_{0\leq\tau<t}|u(\tau)|_{L^2}^2\int_0^t \|u\|^2 ds \\ &\leq M_6(t) + \frac{2}{\nu}\left(e^{M_0(t)}\,|u_0|_{L^2}^2 + \frac{e^{M_0(t)}}{\nu\lambda_1}\int_0^t |\mathcal{P}f|_{L^2}^2\,ds\right)^2 = M_5(t),\end{aligned}$$

where $M_6(t) = C_0/\nu\int_0^t \left(|U||AU|_{L^2} + |U|_{L^2}|AU|_{L^2}\right)ds$. It follows by Gronwall's lemma that

$$\|u(t)\|^2 \leq e^{M_5(t)}\,\|u_0\|^2 + \frac{e^{M_5(t)}}{\nu}\int_0^t |\mathcal{P}f|_{L^2}^2\,ds.$$

Using this estimate of $\|u(t)\|^2$, which has been established with no small data or small T constraint, sufficient conditions on γ and ℓ for the existence of a solution to the robust control problem follow immediately as in the 3D case:

Theorem 19 *(Existence of a solution to the robust control problem, nonlinear 2D case.) Assume that $\mathcal{X}$ and $\mathcal{Y}$ are non-empty, closed, bounded, convex subsets of $L^2(0,T;L^2)$ and that $\gamma > \gamma_4$ and $\ell > \ell_2$, where $\gamma_4 = \gamma_4(\mathcal{X},\mathcal{Y})$ and $\ell_2 = \ell_2(\mathcal{X},\mathcal{Y})$ are defined with a procedure identical to that in the 3D case but with the modified estimates given above. Then there exists a saddle point $(\bar\psi,\bar\phi)$ on $\mathcal{X}\times\mathcal{Y}$ and an associated $\bar u = u(\bar\psi,\bar\phi)$ such that*

$$\mathcal{J}(\psi,\bar\phi) \leq \mathcal{J}(\bar\psi,\bar\phi) \leq \mathcal{J}(\bar\psi,\phi) \qquad \forall\ (\psi,\phi)\in\mathcal{X}\times\mathcal{Y}.$$

Proof. Follows promptly as in the 3D case with the modified estimates given above. □

3.3 Identification of the gradients to determine the unique solution

Now we prove the main result of this chapter:

Theorem 20 *For sufficiently large γ and ℓ, the solution to the robust control problem stated in Definition 3.1 exists and is unique. Further, the gradients of the cost functional $\mathcal{J}$ in* (3.1) *are given by*

$$\frac{\mathcal{D}\mathcal{J}}{\mathcal{D}\psi}(\psi,\phi) = \mathcal{B}_1^*\,\tilde u - \gamma^2\psi \quad\text{ and }\quad \frac{\mathcal{D}\mathcal{J}}{\mathcal{D}\phi}(\psi,\phi) = \mathcal{B}_2^*\,\tilde u + \ell^2\phi, \tag{3.19}$$

where $\tilde{u}$ is found from the solution $(u, \tilde{u})$ of the following coupled system:

$$\begin{cases} \dfrac{du}{dt} + \nu A u + B(u,U) + B(U,u) + B(u,u) = \mathcal{B}_1\psi + \mathcal{B}_2\phi, \\ -\dfrac{d\tilde{u}}{dt} + \nu \mathcal{A}^*\tilde{u} + B'(U+u)^*\tilde{u} = \mathcal{C}_1^*\mathcal{C}_1 u, \\ u \in V, \\ \tilde{u}(t) \in V_r = \left\{ v \in (H^1(\Omega))^3;\ \text{div } v = 0 \text{ in } \Omega, \quad v = \mathcal{C}_3^*\vec{r} \text{ on } \partial\Omega \right\}, \quad t < T, \\ u(0) = u_0 \quad \text{and } \tilde{u}(T) = \mathcal{C}_2^*\mathcal{C}_2\, u(T). \end{cases} \tag{3.20}$$

Proof. The existence of a robust control solution to the nonlinear problem was proved in §3.1 for the 3D case, subject to a small data constraint or a small T constraint, and in §3.2 for the 2D case, with no such constraint.

As in the linear case, the gradients $\mathcal{DJ}/\mathcal{D}\psi$ and $\mathcal{DJ}/\mathcal{D}\phi$ may be determined by computation of the coupled system (3.20), from whence (3.19) follows. Note that, for the 3D robust control problem stated in Definition 3.1, solutions $(\bar{\psi}, \bar{\phi})$ to the robust control problem may not satisfy $\mathcal{DJ}/\mathcal{D}\psi = \mathcal{DJ}/\mathcal{D}\phi = 0$, as they may be located on the boundary of the domain $\mathcal{X} \times \mathcal{Y}$.

Uniqueness in the nonlinear case is proved by contradiction as follows: assume that $(\bar{\psi}, \bar{\phi})$ and $(\tilde{\psi}, \tilde{\phi})$ are two distinct saddle points in $\mathcal{X} \times \mathcal{Y}$. It follows from the statements of strict concavity (3.16) and strict convexity (3.18) that

$$\mathcal{J}(\tilde{\psi}, \tilde{\phi}) < \mathcal{J}(\tilde{\psi}, \bar{\phi}) < \mathcal{J}(\bar{\psi}, \bar{\phi}) \qquad \text{and} \qquad \mathcal{J}(\bar{\psi}, \bar{\phi}) < \mathcal{J}(\bar{\psi}, \tilde{\phi}) < \mathcal{J}(\tilde{\psi}, \tilde{\phi}).$$

This is a contradiction, and thus the saddle point $(\bar{\psi}, \bar{\phi})$ is unique. $\square$

To summarize §3, for sufficiently large γ and ℓ in both the 2D case and the 3D case (the latter of which is confined in the analysis either by a small data or a small T constraint), a solution to the robust control problem stated in Definition 3.1 exists and is unique. Further, the gradients $\mathcal{DJ}/\mathcal{D}\psi$ and $\mathcal{DJ}/\mathcal{D}\phi$, which may be used to determine this solution with a numerical algorithm such as that proposed in §5, may be identified as a simple function of an appropriately-defined adjoint field.

Chapter 4

Generalizations

We now consider two straightforward generalizations of the robust control framework laid out in §2 and §3, first for the problem of boundary control (§4.1), then for the problem of data assimilation (§4.2).

4.1 The boundary control problem in a domain with corners

In this section, we will discuss the robust control problem assuming that the control ϕ now acts upon the flow by modification of the boundary conditions on the velocity u. It will be shown that the effect of boundary forcing on the flow velocity inside the domain Ω may be accounted for by a "lifting" procedure which constructs an equivalent interior forcing profile to account for the boundary forcing (Hopf 1955). With such a construction, the proofs of existence and uniqueness of the robust control problem follow as in the previous sections with slight modifications. Further, the identification of the gradients $\mathcal{DJ}/\mathcal{D}\psi$ and $\mathcal{DJ}/\mathcal{D}\phi$ is, again, straightforward. In the present work we treat domains with corners, avoiding the smoothing of the boundary used in Abergel & Temam (1990).

The cost functional considered in this section is analogous to that used in previous sections

$$\begin{aligned} \mathcal{J}(\psi,\phi) = \frac{1}{2}\int_0^T \big|\mathcal{C}_1 u\big|^2_{L^2(\Omega)}\,dt + \frac{1}{2}\big|\mathcal{C}_2 u(T)\big|^2_{L^2(\Omega)} - \int_0^T \big(\mathcal{C}_3 \nu \frac{\partial u}{\partial n}, \vec{r}\big)_{L^2(\partial\Omega)}\,dt \\ + \frac{1}{2}\int_0^T \Big[\ell^2 \big|\phi\big|^2_{L^2(\partial\Omega)} - \gamma^2\big|\psi\big|^2_{L^2(\Omega)}\Big]\,dt, \end{aligned} \tag{4.1}$$

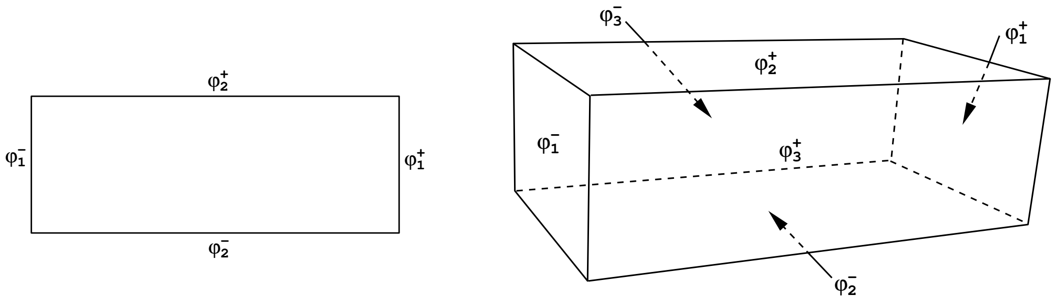

Figure 4: Cornered domains considered for the problem of boundary forcing in §4.1.1. The analysis of the flow control problem in these 2D and 3D "driven cavities" is easily generalized to account for periodicity in one or two directions (*i.e.*, channel flow and duct flow) and, more generally, for domains of any convex shape.

where the flow is governed by

$$\begin{cases} \dfrac{\partial u}{\partial t} - \nu \Delta u + (u \cdot \nabla) U + (U \cdot \nabla) u + (u \cdot \nabla) u + \nabla p = B_1 \psi, \\ \text{div } u = 0, \\ u = \mathcal{B}_2 \phi & \text{on } \partial\Omega, \\ u = u_0 & \text{at } t = 0, \end{cases} \tag{4.2}$$

where we restrict $\phi \in H^1(0,T;L^2(\partial\Omega))^3)$, $\mathcal{C}_3^* \vec{r} \cdot \vec{n} = 0$, and $\mathcal{B}_2$ to be a mapping from $(L^2(\partial\Omega))^3$ to $(H^{3/2+\epsilon}(\partial\Omega))^3$, $\epsilon > 0$, such that $\big(\mathcal{B}_2 \phi, \vec{n}\big)_{L^2(\partial\Omega)} = \int_{\partial\Omega} \mathcal{B}_2 \phi \cdot \vec{n} \, d\Gamma = 0$, where $\vec{n}$ is the unit outward normal vector to $\partial\Omega$. Note the control forcing $\varphi = \mathcal{B}_2 \phi$, which is allowed on all three velocity components, is confined to the boundary $\partial\Omega$ of the domain in the present section.

4.1.1 Transformation of problem to the interior forcing framework

For simplicity, let us assume a rectangular two or three dimensional domain $\Omega = \prod_{i=1}^m (-L_i, L_i)$, where $m = 2$ or 3, as depicted in figure 4. Suppose that the boundary forcing belongs to the closure, in an appropriate Sobolev space, of infinitely differentiable functions with compact support on each smooth component of $\partial\Omega$. Specifically, the boundary of Ω is given by

$$\partial\Omega = \bigcup_{i=1}^{n} \big(\Gamma_i^+ \bigcup \Gamma_i^-\big) \qquad \text{and} \qquad \Gamma_i^\pm = \big\{(x_1, \ldots x_n) \in \partial\Omega; x_i = \pm L_i\big\},$$

and the boundary controls $\varphi_i^\pm$ on each face $\Gamma_i^\pm$ of Ω satisfy

$$\varphi_i^\pm \in H^1\big(0,T; H_0^{3/2+\epsilon}(\Gamma_i^\pm)\big), \qquad \text{where} \qquad \epsilon > 0.$$

Using Ziane (1995), $\exists \Phi \in H^1(0,T;H^2(\Omega))$ such that

$$\begin{cases} \dfrac{\partial \Phi}{\partial t} - \nu \Delta \Phi + \nabla \pi = 0, \\ \text{div } \Phi = 0, \\ \Phi = \varphi_i^{\pm} & \text{on } \Gamma_i^{\pm}, \\ \Phi = u_0 & \text{at } t = 0. \end{cases}$$

Furthermore, making use of Φ as an intermediate lifting, Hopf's technique[1] (Hopf 1955, Lions 1969, Temam 1984) may be used to determine a $\Theta \in H^1(0,T;H^2(\Omega))$ such that

$$\begin{cases} \text{div } \Theta = 0, \\ \Theta = \varphi_i^{\pm} & \text{on } \Gamma_i^{\pm}, \end{cases}$$

where Θ is constructed such that

$$b(u,\Theta,u) \le \frac{\nu}{4}\|u\|^2. \tag{4.3}$$

Now set $v = u - \Theta$. As v, by construction, has homogeneous boundary conditions, we may return to the familiar abstract form

$$\begin{cases} \dfrac{dv}{dt} + \nu A v + B(v, U+\Theta) + B(U+\Theta, v) + B(v,v) = \mathcal{F}, \\ v \in V, \\ v = u_0 - \Theta(0) & \text{at } t = 0, \end{cases} \tag{4.4}$$

where

$$\mathcal{F} = \mathcal{B}_1 \psi - \frac{d\Theta}{dt} - \nu A \Theta - B(\Theta,\Theta) - B(U,\Theta) - B(\Theta,U).$$

Note that $\mathcal{F} \in L^2(0,T;H)$ and that

$$\|\mathcal{F}\|_{L^2(0,T;H)} \le C_0 \sum_{i=1}^{n} \|\varphi_i^{\pm}\|_{H^1(0,T;H_0^{3/2+\epsilon}(\Gamma_i^{\pm}))} + \|\mathcal{B}_1\psi\|_{L^2(0,T;H)}. \tag{4.5}$$

Theorem 21 *Existence and uniqueness of the solution to the robust control problems posed in §2 and §3 extend directly to the case of boundary forcing.*

[1] Note that the support of the lifting Θ of the boundary forcing φ determined by Hopf's approach is included in a neighborhood of the boundary. Note also that Hopf's technique can be easily generalized to work for the rectangular domains Ω of figure 4 and, in fact, for any convex domain.

Proof. Noting the estimates (4.3) and (4.5), the existence and uniqueness of v follow promptly from the developments in §2 and §3 applied to (4.4), with $U+\Theta$ replacing U and $\mathcal{F}$ replacing $\mathcal{P}f$, mutatis mutandis. The existence and uniqueness of $u = v + \Theta$ follow directly. □

4.1.2 Identification of gradients

The existence and uniqueness of a robust control solution for the problem with boundary control were proved in §4.1.1 by reducing it to the interior forcing problem, which has already been considered thoroughly in §2 and §3. We now identify the gradients $\mathcal{DJ}/\mathcal{D}\psi$ and $\mathcal{DJ}/\mathcal{D}\phi$ necessary to find a solution to the robust data assimilation problem with the algorithm of §5 by coupling the flow system (4.2) with an adjoint system defined by

$$\begin{cases} -\dfrac{\partial \tilde{u}}{\partial t} - \nu\Delta\tilde{u} + (\nabla[U+u])^T\cdot\tilde{u} - (\nabla\tilde{u})\cdot[U+u] + \nabla\tilde{p} = \mathcal{C}_1^*\mathcal{C}_1 u, \\ \text{div } \tilde{u} = 0, \\ \tilde{u} = \mathcal{C}_3^*\vec{r} \qquad \text{on } \partial\Omega, \\ \tilde{u} = \mathcal{C}_2^*\mathcal{C}_2\, u \qquad \text{at } t = T. \end{cases} \tag{4.6}$$

Since

$$\begin{aligned}
&\int_0^T \big(\mathcal{C}_1^*\mathcal{C}_1 u, u'\big)_{L^2(\Omega)}\,dt + \big(\mathcal{C}_2^*\mathcal{C}_2 u(T), u'(T)\big)_{L^2(\Omega)} - \int_0^T \big(\mathcal{C}_3\nu\frac{\partial u'}{\partial n}, \vec{r}\big)_{L^2(\partial\Omega)}\,dt \\
&\quad= \int_0^T \big(\big[-\frac{\partial\tilde{u}}{\partial t} - \nu\Delta\tilde{u} + (\nabla[U+u])^T\cdot\tilde{u} - (\nabla\tilde{u})\cdot[U+u] + \nabla\tilde{p}\big], u'\big)_{L^2(\Omega)}\,dt \\
&\qquad + \big(\tilde{u}(T), u'(T)\big)_{L^2(\Omega)} - \int_0^T \big(\nu\frac{\partial u'}{\partial n}, \tilde{u}\big)_{L^2(\partial\Omega)}\,dt \\
&\quad= \int_0^T \big(\tilde{u}, \big[\frac{\partial u'}{\partial t} - \nu\Delta u' + ([U+u]\cdot\nabla)u' + (u'\cdot\nabla)[U+u] + \nabla p'\big]\big)_{L^2(\Omega)}\,dt \\
&\qquad + \int_0^T \Big[\big(\tilde{p}, u'\cdot\vec{n}\big)_{L^2(\partial\Omega)} - \big(\tilde{p}, \nabla\cdot u'\big)_{L^2(\Omega)} + \big(p', \nabla\cdot\tilde{u}\big)_{L^2(\Omega)} - \big(p', \tilde{u}\cdot\vec{n}\big)_{L^2(\partial\Omega)} \\
&\qquad\qquad - \big(\nu\frac{\partial\tilde{u}}{\partial n}, u'\big)_{L^2(\partial\Omega)} - \big((\tilde{u}\cdot\vec{n})[U+u], u'\big)_{L^2(\partial\Omega)}\Big]\,dt \\
&\quad= \int_0^T \big(\tilde{u}, \mathcal{B}_1\psi'\big)_{L^2(\Omega)}\,dt + \int_0^T \big(\big[-\nu\frac{\partial\tilde{u}}{\partial n} + \tilde{p}\vec{n}\big], \mathcal{B}_2\phi'\big)_{L^2(\partial\Omega)}\,dt \\
&\quad= \int_0^T \big(\mathcal{B}_1^*\tilde{u}, \psi'\big)_{L^2(\Omega)}\,dt + \int_0^T \big(\mathcal{B}_2^*\big[-\nu\frac{\partial\tilde{u}}{\partial n} + \tilde{p}\vec{n}\big], \phi'\big)_{L^2(\partial\Omega)}\,dt,
\end{aligned}$$

it follows that

$$\frac{\mathcal{D}\mathcal{J}}{\mathcal{D}\psi}(\psi,\phi) = \mathcal{B}_1^*\,\tilde{u} - \gamma^2\psi \quad \text{and} \quad \frac{\mathcal{D}\mathcal{J}}{\mathcal{D}\phi}(\psi,\phi) = \mathcal{B}_2^*\,\big[-\nu\frac{\partial\tilde{u}}{\partial n} + \tilde{p}\,\vec{n}\big] + \ell^2\phi.$$

The appearance of $\tilde{p}$ in this derivation is due to the fact that we have allowed $\mathcal{B}_2\phi\cdot\vec{n}\neq 0$, *i.e.*, we have allowed the case of boundary forcing by wall transpiration (blowing/suction). If we restrict the problem to wall-tangential control velocities only (*i.e.*, $\mathcal{B}_2\phi\cdot\vec{n}=0$), then the $\tilde{p}$ term will disappear from the expression for the gradient. Conversely, if we restrict the problem to wall-normal control velocities only, with $\mathcal{C}_3^*\vec{r}$ constant over the walls, then the $\partial\tilde{u}/\partial n$ term will disappear from the expression for the gradient.

To summarize §4.1, for sufficiently large γ, a solution to the robust control problem for the case of boundary forcing exists and is unique. Further, the gradients $\mathcal{D}\mathcal{J}/\mathcal{D}\psi$ and $\mathcal{D}\mathcal{J}/\mathcal{D}\phi$, which may be used to determine this solution with a numerical algorithm such as that proposed in §5, may be identified as a simple function of an appropriately-defined adjoint field.

4.2 The data assimilation problem

In this section, we will discuss a robust estimation problem wherein the "control" to be determined is, in fact, the initial condition on the velocity field, *i.e.*, $u_0=\mathcal{B}_2\phi$. This framework is useful in data assimilation problems: given a set of measurements of some actual flow v on $[0,T]$, determine a "best" estimate as to the initial state u_0 in the model u that leads to the observed system behavior, while simultaneously forcing the model system with a small component of the worst-case disturbance ψ which perturbs u away from the observed system behavior. Chaotic problems, such as weather systems, are highly susceptible to the small disturbances present in all physical systems. Thus, this robust estimation framework should help to reduce the component of the initial state most susceptible to external disturbances and thereby prove to be a valuable tool for improving the fidelity of such estimates.

Define $w=u-v$ as the amount the estimated flow u differs from the actual flow v. A cost functional may be defined as in the previous problems, but now forced by the measurement errors $\mathcal{C}_1 w$, $\mathcal{C}_2 w(T)$, and $\mathcal{C}_3\nu(\partial w/\partial n)|_{\partial\Omega}$ on the interior, at the final time, and at the boundaries, respectively, such that

$$\begin{aligned}\mathcal{J}(\psi,\phi) = \frac{1}{2}\int_0^T \big|\mathcal{C}_1 w\big|^2_{L^2(\Omega)}\,dt + \frac{1}{2}\big|\mathcal{C}_2 w(T)\big|^2_{L^2(\Omega)} + \frac{1}{2}\int_0^T \big|\mathcal{C}_3\nu\frac{\partial w}{\partial n}\big|^2_{L^2(\partial\Omega)}\,dt \\ + \frac{\ell^2}{2}\big|\phi\big|^2_{L^2(\Omega)} - \frac{\gamma^2}{2}\int_0^T \big|\psi\big|^2_{L^2(\Omega)}\,dt,\end{aligned} \tag{4.7}$$

where $\mathcal{C}_3^*\mathcal{C}_3\,\nu(\partial w/\partial n)\cdot\vec{n}=0$. The measurements of the actual flow $\mathcal{C}_1 v$, $\mathcal{C}_2 v(T)$, and $\mathcal{C}_3\nu(\partial v/\partial n)|_{\partial\Omega}$ are assumed to be given. In order to find the best estimate u of the actual flow v, we seek the best initial conditions ϕ, subject to the worst disturbance forcing ψ, such that $\mathcal{J}$ is minimized, where the estimate u is governed by

$$\begin{cases} \dfrac{du}{dt} + \nu A u + B(u,U) + B(U,u) + B(u,u) = \mathcal{B}_1\psi, \\ u \in V, \\ u = \mathcal{B}_2\phi \qquad \text{at } t = 0, \end{cases} \tag{4.8}$$

where $\phi \in (L^2(\Omega))^3$ and $\mathcal{B}_2$ is a mapping from $(L^2(\Omega))^3$ to V.

Theorem 22 *Existence and uniqueness of the solution to the robust control problems posed in §2 and §3 extend directly to the data assimilation framework.*

Proof. The developments of §2 and §3 extend directly to the present case with no further estimates required. □

4.2.1 Identification of gradients

The existence and uniqueness of a robust solution for the data assimilation problem were found by appealing directly to the interior forcing problem, which has already been considered thoroughly in §2 and §3. We now identify the gradients $\mathcal{D}\mathcal{J}/\mathcal{D}\psi$ and $\mathcal{D}\mathcal{J}/\mathcal{D}\phi$ necessary to find a solution to the robust data assimilation problem with the algorithm of §5. The derivation is very similar to those encountered earlier.

Differentiation of (4.7) leads to expressions for the gradients in weak form:

$$\begin{aligned} \frac{\mathcal{D}\mathcal{J}}{\mathcal{D}\psi}(\bar\psi,\bar\phi)\cdot\psi' &= \int_0^T \big(\mathcal{C}_1 w, \mathcal{C}_1 \frac{\mathcal{D}u}{\mathcal{D}\psi}\cdot\psi'\big)_{L^2(\Omega)}\,dt + \big(\mathcal{C}_2 w(T), \mathcal{C}_2\frac{\mathcal{D}u(T)}{\mathcal{D}\psi}\cdot\psi'\big)_{L^2(\Omega)} \\ &\quad + \int_0^T \big(\mathcal{C}_3\nu\frac{\partial w}{\partial n}, \mathcal{C}_3\nu\frac{\partial}{\partial n}\frac{\mathcal{D}u}{\mathcal{D}\psi}\cdot\psi'\big)_{L^2(\partial\Omega)}\,dt - \gamma^2\int_0^T \big(\bar\psi,\psi'\big)_{L^2(\Omega)}\,dt, \\ \frac{\mathcal{D}\mathcal{J}}{\mathcal{D}\phi}(\bar\psi,\bar\phi)\cdot\phi' &= \int_0^T \big(\mathcal{C}_1 w, \mathcal{C}_1 \frac{\mathcal{D}u}{\mathcal{D}\phi}\cdot\phi'\big)_{L^2(\Omega)}\,dt + \big(\mathcal{C}_2 w(T), \mathcal{C}_2\frac{\mathcal{D}u(T)}{\mathcal{D}\phi}\cdot\phi'\big)_{L^2(\Omega)} \\ &\quad + \int_0^T \big(\mathcal{C}_3\nu\frac{\partial w}{\partial n}, \mathcal{C}_3\nu\frac{\partial}{\partial n}\frac{\mathcal{D}u}{\mathcal{D}\phi}\cdot\phi'\big)_{L^2(\partial\Omega)}\,dt + \ell^2\big(\bar\phi,\phi'\big)_{L^2(\Omega)}. \end{aligned} \tag{4.9}$$

In order to determine a solution to the robust data assimilation problem, we define an adjoint state by the equation

$$\begin{cases} -\dfrac{d\tilde u}{dt} + \nu\mathcal{A}^*\tilde u + B'(U+u)^*\tilde u = \mathcal{C}_1^*\mathcal{C}_1\, w, \\ \tilde u(t) \in V_w = \left\{ v \in (H^1(\Omega))^3;\ \operatorname{div} v = 0 \text{ in } \Omega,\quad v = -\mathcal{C}_3^*\mathcal{C}_3\,\nu\dfrac{\partial w}{\partial n} \text{ on } \partial\Omega \right\},\quad t<T, \\ \tilde u = \mathcal{C}_2^*\mathcal{C}_2\, w \in H \qquad \text{at } t=T, \end{cases}$$

where $\mathcal{A}^*$ is defined by

$$\big(u', \mathcal{A}^*\tilde u\big)_{L^2(\Omega)} = \big(Au', \tilde u\big)_{L^2(\Omega)} + \big(\frac{\partial u'}{\partial n}, \tilde u\big)_{L^2(\partial\Omega)} \ \text{ for } u' \in D(A), \text{ and } \tilde u \in V_w.$$

Note again that $\mathcal{C}_3^*\mathcal{C}_3\,\nu(\partial w/\partial n)\cdot\vec n = 0$. Note that the adjoint state is forced by the measurement errors $\mathcal{C}_1 w$, $\mathcal{C}_2 w(T)$, and $\mathcal{C}_3\nu(\partial w/\partial n)|_{\partial\Omega}$. From integration by parts and the regularity of u, u' and $\tilde u$, which follows as in the previous chapters, we have

$$\begin{aligned} &\int_0^T \big(\mathcal{C}_1^*\mathcal{C}_1 w, u'\big)_{L^2(\Omega)}\,dt + \big(\mathcal{C}_2^*\mathcal{C}_2 w(T), u'(T)\big)_{L^2(\Omega)} + \int_0^T \big(\mathcal{C}_3^*\mathcal{C}_3\nu\frac{\partial w}{\partial n}, \nu\frac{\partial u'}{\partial n}\big)_{L^2(\partial\Omega)}\,dt \\ &\quad = \int_0^T \big(\big[-\frac{d\tilde u}{dt} + \nu\mathcal{A}^*\tilde u + B'(U+u)^*\tilde u\big], u'\big)_{L^2(\Omega)}\,dt \\ &\qquad + \big(\tilde u(T), u'(T)\big)_{L^2(\Omega)} - \int_0^T \big(\tilde u, \nu\frac{\partial u'}{\partial n}\big)_{L^2(\partial\Omega)}\,dt \\ &\quad = \int_0^T \big(\tilde u, \big[\frac{du'}{dt} + \nu A u' + B'(U+u)u'\big]\big)_{L^2(\Omega)}\,dt + \big(\tilde u(0), u'(0)\big)_{L^2(\Omega)} \\ &\quad = \int_0^T \big(\tilde u, \mathcal{B}_1\psi'\big)_{L^2(\Omega)}\,dt + \big(\tilde u(0), \mathcal{B}_2\phi'\big)_{L^2(\Omega)} \\ &\quad = \int_0^T \big(\mathcal{B}_1^*\tilde u, \psi'\big)_{L^2(\Omega)}\,dt + \big(\mathcal{B}_2^*\tilde u(0), \phi'\big)_{L^2(\Omega)}. \end{aligned}$$

Thus, (4.9), with $\phi' = 0$ and taking $\psi' \in L^2(0,T;L^2)$ as arbitrary, leads to an expression for the gradient $\mathcal{DJ}/\mathcal{D}\psi$:

$$\frac{\mathcal{DJ}}{\mathcal{D}\psi}(\bar\psi, \bar\phi) = \mathcal{B}_1^*\,\tilde u - \gamma^2\psi.$$

Similarly, with $\psi' = 0$ and taking $\phi' \in L^2$ as arbitrary,

$$\frac{\mathcal{DJ}}{\mathcal{D}\phi}(\bar\psi, \bar\phi) = \mathcal{B}_2^*\,\tilde u(0) + \ell^2\phi.$$

To summarize §4.2, for sufficiently large γ and ℓ, a solution to the robust setting of the data assimilation problem exists and is unique. Further, the gradients $\mathcal{DJ}/\mathcal{D}\psi$ and $\mathcal{DJ}/\mathcal{D}\phi$, which may be used to determine this solution with a numerical algorithm such as that proposed in §5, may be identified as a simple function of an appropriately-defined adjoint field.

Chapter 5

Numerical algorithm for determination of robust control solution

A select number of important linear robust control problems may be derived from the Navier-Stokes equation and discretized accurately with a system of small state dimension [$N \lesssim O(100)$]. For such problems, the two-point boundary-value problem of (2.22) may be stated and solved as a Riccati problem, as demonstrated by Bewley & Liu (1998) for the problem of stabilization of plane channel flow. For nonlinear robust control problems of fairly low state dimension, the two-point boundary-valued problem may be stated as the Hamilton-Jacobi-Bellman inequality and solved via the notions of L^2 gain, passivity, and control Lyapunov functions, as described by Van der Schaft (1996), Isidori (1995), and Freeman & Kokotovic (1996).

The majority of linear and nonlinear problems in fluid mechanics, however, require quite a large state dimension for adequate resolution [$N \gtrsim O(10^5)$]. For such problems, a computational approach which does not rely on the computation and storage of $O(N^2)$ fields is an absolute necessity. As suggested for the optimal case by Abergel & Temam (1990), an iterative numerical algorithm is now proposed to find a saddle-point solution to the two-point boundary value problem of both linear and nonlinear robust control problems based on the repeated computation of an $O(N)$ adjoint field.

Algorithm 1

1. *Initialize* $k = 0$ *and* $(\psi^0, \phi^0) = 0$ *on* $t \in [0, T]$, *where* k *is the iteration index and* (ψ^k, ϕ^k) *is the numerical approximation of the disturbance and the control during the* k*'th iteration of the algorithm.*

2. *Determine the state* u^k *on* $[0, T]$ *from the state equation (Navier-Stokes) based on the initial conditions* u_0 *and with the forcing* (ψ^k, ϕ^k).

3. *Determine the adjoint* $\tilde{u}^k$ *on* $[0, T]$ *from the adjoint equation based on the state* u^k.

4. *Determine local expressions for the gradients*

$$\frac{\mathcal{DJ}}{\mathcal{D}\psi}(\psi^k, \phi^k) \quad \text{and} \quad \frac{\mathcal{DJ}}{\mathcal{D}\phi}(\psi^k, \phi^k)$$

based on the adjoint $\tilde{u}^k$.

5. *Determine the updated disturbance* ψ^{k+1} *with*

$$\psi^{k+1} = \psi^k + \alpha^k \frac{\mathcal{DJ}}{\mathcal{D}\psi}(\psi^k, \phi^k)$$

where $0 < C_1 \leq \alpha^k \leq C_2 < 1$, *where* C_1 *and* C_2 *depend on the second derivative of* $\mathcal{J}$.

6. *Determine the updated control* ϕ^{k+1} *with*

$$\phi^{k+1} = \phi^k - \beta^k \frac{\mathcal{DJ}}{\mathcal{D}\phi}(\psi^k, \phi^k)$$

where $0 < C_1 \leq \beta^k \leq C_2 < 1$.

7. *Increment index:* $k = k + 1$. *Repeat from step 2 until converged.*

The proof of the convergence of Algorithm 1 is currently under development and will appear elsewhere.

In order to arrive at an algorithm which is numerically efficient, but for which a proof of convergence is not available, α^k and β^k themselves may be determined by an iterative procedure, specifically:

Algorithm 2 *Follow the same procedure as in Algorithm 1, but now:*

- *let α^k be selected by a numerically robust line maximization algorithm, based on repeated "trial" computations of ψ^{k+1} for various different choices of α^k and computing the resulting effect on the cost functional $\mathcal{J}(\psi^{k+1}, \phi^k)$. Such an approach guarantees local line maximization of $\mathcal{J}$ in the direction of the gradient $[\mathcal{D}\mathcal{J}/\mathcal{D}\psi](\psi^k, \phi^k)$ from the point (ψ^k, ϕ^k) even for nonlinear problems. Efficient numerical algorithms for such a line maximization (i.e., optimization of the single scalar parameter α^k) are well established. Note that α^k is chosen while holding the control ϕ^k fixed.*

- *let β^k be selected by a line minimization algorithm, based on repeated "trial" computations of ϕ^{k+1} for various different choices of β^k and computing the resulting effect on the cost functional $\mathcal{J}(\psi^k, \phi^{k+1})$, in a manner analogous to that for α^k. Note that β^k is chosen while holding the disturbance ψ^k fixed.*

Note that Algorithm 2 may be modified by setting $\alpha^k = 0$ (*i.e.*, $\psi^{k+1} = \psi^k$) for k odd and setting $\beta^k = 0$ (*i.e.*, $\phi^{k+1} = \phi^k$) for k even. Note also that, for the purpose of numerical computation, it is often most efficient to compute the line minimizations only approximately, in order to reduce the number of computations required to select α^k and β^k.

Chapter 6

Conclusions

A framework for robust control has been developed for problems governed by the Navier-Stokes equation. Existence and uniqueness of the solution to the robust control problem have been proven, and upper bounds on the minimum value of γ_0 for which a solution exists have been established. Cost functionals which account for both the regulation and the terminal control of both interior quantities and boundary quantities have been accounted for. Interior forcing, boundary forcing, and the optimization of the initial state (*i.e.*, data assimilation) have been considered. Together, this set of problems constitutes a complete family of problems governed by the flow/adjoint two-point boundary value problem. Finally, a tractable numerical algorithm (based on repeated computations of an adjoint field) to solve the robust control problem has been proposed.

The first author would like to acknowledge financial support of the the Franklin P. and Caroline M. Johnson Graduate Fellowship at Stanford University and the support of AFOSR contract number F49620-97-Z-0021 (to The Boeing Company) through Boeing Purchase order Z70742 to Stanford University. The second author would like to acknowledge financial support of the National Science Foundation under grant NSF-DMS-9705229 and the support of the Research Fund of Indiana University. The third author would like to acknowledge the financial support of a CTR fellowship.

REFERENCES

ABERGEL, F., & TEMAM, R. 1990 On some control problems in fluid mechanics. *Theor. and Comp. Fluid Dyn.* **1**, 303-325.

BEWLEY, T.R., CHOI, H., TEMAM, R., & MOIN, P. 1993 Optimal feedback control of turbulent channel flow. *1993 Annual Research Briefs*, Center for Turbulence Research, Stanford University/NASA Ames.

BEWLEY, T.R. & LIU, S. 1998 Optimal and robust control and estimation of linear paths to transition. Accepted for publication in *J. Fluid Mech.*

BEWLEY, T.R., MOIN, P., & TEMAM, R. 1997 Optimal and robust approaches for linear and nonlinear regulation problems in fluid mechanics. *AIAA Paper No.* 97-1872.

BEWLEY, T.R., MOIN, P., & TEMAM, R. 1998 Optimal control of turbulence. To be submitted to *J. Fluid Mech.*

DOYLE, J.C., GLOVER, K., KHARGONEKAR, P.P., & FRANCIS, B.A. 1989 State-space solutions to standard $\mathcal{H}_2$ and $\mathcal{H}_\infty$ control problems. *IEEE Trans. Auto. Control* **34**, 8, 831-847.

EKELAND, I., & TEMAM, R. 1974 *Convex analysis and variational problems.* Dunod, 1974 (in French). English translation: North Holland, 1976.

FREEMAN, R., & KOKOTOVIC, P. 1996 *Robust nonlinear control design: state-space and Lyapunov techniques.* Birkhauser.

GREEN, M., & LIMEBEER, D.J.N. 1995 *Linear robust control.* Prentice-Hall.

HILL, D.C. 1993 Drag reduction at a plane wall. *1993 Annual Research Briefs*, Center for Turbulence Research, Stanford University/NASA Ames.

HOPF, E. 1955 *On nonlinear partial differential equations*, Lecture series of the symposium on partial differential equations. Berkeley.

ISIDORI, A. 1995 *Nonlinear control systems.* Springer.

LADYZHENSKAYA, O.A. 1969 *The mathematical theory of viscous incompressible flow.* Gordon & Breach.

LEE, C., KIM, J., & CHOI, H. 1998 Suboptimal control of turbulent channel flow for drag reduction. *J. Fluid Mech.* **358**, 245-258.

LIONS, J.L. 1969 *Quelques méthodes de résolution des problèmes nonlinéaires.* Gauthier Villars.

LIONS, J.L. & MAGENES, E. 1972 *Nonhomogeneous boundary value problems and applications.* Springer.

MOIN, P, & BEWLEY, T.R. 1994 Feedback control of turbulence. *Appl. Mech. Rev.* **47** (6), part 2, S3-S13.

TEMAM, R. 1984 *Navier-Stokes equations*, Studies in mathematics and its applications 2. North-Holland.

VAN DER SCHAFT, A. 1996 *L_2-gain and passivity techniques in nonlinear control*, Lecture notes in control and information sciences 218. Springer.

ZIANE, M. 1995 Regularity results for Stokes type systems. *Applicable Analysis* **58**, 263-292.

APPENDIX

Feedback control of turbulence: a survey of approaches

The appendix has been published, in a slightly modified form, as

Moin, P., & Bewley, T.R. 1994 Feedback control of turbulence. *Appl. Mech. Rev.* **47** (6), part 2, S3-S13.

Abstract

A brief review of current approaches to active feedback control of the fluctuations arising in turbulent flows is presented in this appendix, emphasizing the mathematical techniques involved. Active feedback control schemes are categorized and compared by examining the extent to which they are based on the governing flow equations. These schemes are broken down into the following categories: adaptive schemes, schemes based on heuristic physical arguments, schemes based on a dynamical systems approach, and schemes based on optimal control theory applied directly to the Navier-Stokes equations. Recent advances in methods of implementing small scale flow control ideas are also reviewed.

Postscript

The review contained in this appendix was published in June of 1994, near the inception of the research which lead to the present report, and is reprinted here with only minor editorial changes. It thus describes the frame of mind which lead to the present research, and not the conclusions to be drawn from it. Flow control literature which appeared between 1994 and 1998 which relates to the present work is reviewed in the appropriate sections in the main body of this report.

Chapter 1

Background

Many important advances have been made in the past decade in the field of turbulence control; recent reviews include: Bandyopadhyay (1986), Bushnell and McGinley (1989), Blackwelder (1989), Fiedler and Fernholz (1990), and Gad-el-Hak (1989, 1993). This chapter will review one aspect of this subject: active feedback control of turbulence.

Active control schemes refer to methods which add energy to a flow, such as unsteady wall transpiration or the prescribed motion of an actuator. These are in contrast to passive techniques, which modify a flow without unsteady external input. Passive techniques include the placement of longitudinal grooves (riblets) on a surface to reduce the drag caused by turbulence (Choi *et al.* 1993b, Walsh 1990) and the use of compliant walls which deform in response to the overlying flow to stabilize a laminar boundary layer (Riley *et al.* 1988).

The external energy added in an active control scheme may be determined in advance (in which case the control scheme is termed open-loop or feedforward) or coordinated with real-time measurements of the flow itself (termed closed-loop or feedback control). The periodic forcing of a round jet (Lee and Reynolds 1985) to produce bifurcation (splitting into two jets) or blooming (expansion to a wide spray of vortex rings) and the hydrodynamic Lorenz forcing of an electrolytic fluid (Nosenchuck and Brown 1993) to restructure flow perturbations in the near wall region are excellent examples of effective open-loop control configurations in turbulent flows. However, in cases in which the control must interact with a specific set of turbulent fluctuations already present in the flow, such as the coherent structures, the random aspect of these structures reduces the effectiveness of an open-loop configuration. In these cases, we seek a "feedback control law" to relate measurements of the state of the turbulence in the flow to the resulting distribution in space and time of the control energy. It is this mathematical relation between what is sensed and what control is applied which is systematically discussed in this report. The feedback referred to in this context should not be confused with the feedback of information caused by the upstream influence of events which take place downstream through the flow itself, as discussed by Ho and Huerre (1984).

Adam Smith, in *The Division of Labour* (1776), recalls:

> *"In the first fire-engines, a boy was constantly employed to open and shut alternately the communication between the boiler and the cylinder, according as the piston either ascended or descended. One of those boys, who loved to play with his companions, observed that, by tying a string from the handle of the valve which opened this communication to another part of the machine, the valve would open and shut without his assistance, and leave him at liberty to divert himself with his play fellows."*

In the present study, our valves are the actuators, the points on the "machine" to which we have access to tie are the sensors, and our string is the feedback control law. As the resourceful boy, we seek the best arrangement of this string.

The importance of coherent motions in turbulent flows (Robinson 1991) provides a physical target for active turbulence control schemes. Through feedback, control effort may be coordinated to manipulate these structures. This can have a profound overall effect on the turbulence. Herein lies the mathematical challenge of feedback turbulence control: in the midst of the vast range of spatial and temporal fluctuations of turbulence, identify those unstable coherent structures responsible for the regeneration of the turbulence and the most efficient distribution of control energy to achieve a desired effect.

Large-scale flow management schemes, which sense the gross flow features and then alter fixed or slowly-varying set points of the flow (e.g. the air-fuel ratio in a combustor) in order to optimize some combination of parameters, are well developed. One application is IC engine control (Amstutz *et al.* 1993), where the quantity of fuel injected may be actively updated using a linear quadratic regulator to maintain stoichiometry and thereby reduce pollutants and improve efficiency. Another example is combustion optimization (Padmanabhan *et al.* 1993), where the parameters for various open-loop actuators (e.g. speakers and vortex generating jets) are slowly altered using an optimization algorithm to simultaneously minimize r.m.s. pressure fluctuations and maximize volumetric heat release. It is the subject of the present work to attack a technologically more challenging problem: small scale manipulation of the turbulent fluctuations themselves.

Feedback control of turbulence has been incorporated for millennia by birds and fishes. Adaptations range from structural modifications, such as bird feathers and shark denticles which protrude under certain flow conditions to become drag-reducing vortex generators (Bushnell and Moore 1991), to behavioral modifications, such as the active turning of the head of a schooling fish into the direction of cross-flow created by the tail of the fish ahead to align the boundary layer flow with its body and thereby reduce drag (Lighthill 1993). Man has only recently gained enough understanding of turbulence to effectively alter it through such an active fashion.

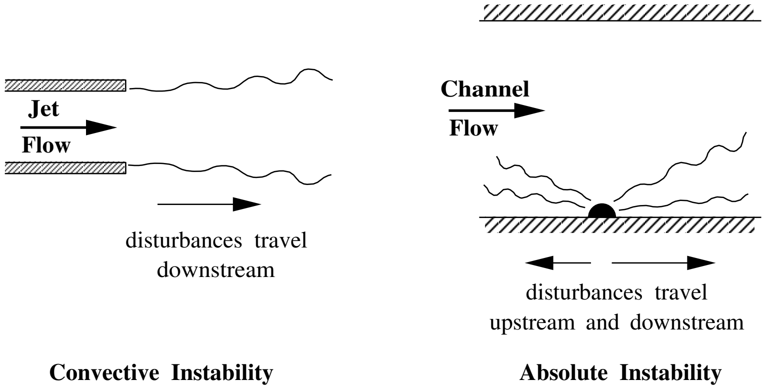

Figure 5: Two types of flow instability.

In §2, current methods of feedback control are categorized by examining their mathematical dependence on the equations governing the flow phenomenon to be controlled. This development provides the reader with the phylogeny of and, ultimately, an introduction to optimal control as a means to determine effective control rules for fluid-mechanical problems.

Several devices have recently been developed which may be used to detect and force turbulent flows; a cursory review of these is given in §3.

Linear stability theory (Drazin and Reid 1981) can be quite useful when considering flow control problems. For example, in some flow configurations, all growing disturbances convect downstream from their source, in which case the flow is said to be convectively unstable. This is in contrast to the case in which some of the growing disturbances can travel back upstream and continually disrupt the flow even after the initial disturbance is neutralized, which is referred to as absolute instability (see figure 1). In configurations which are convectively unstable, active control schemes applied near the point where perturbations originate can be especially effective.

Receptivity issues (Goldstein and Hultgren 1989 and Hill 1993a), which are closely related to the stability problem, can also provide some guidance for the design of control laws by identifying where stable and unstable modes are most easily modified in a particular flow (Hill 1992). Though related to the control problem, space does not permit review of stability and receptivity issues in this manuscript.

Chapter 2

Feedback control schemes

In this section, current methods of feedback control are categorized by examining their mathematical dependence on the equations governing the flow phenomenon to be controlled. The first category reviewed is adaptive schemes, which attempt to develop models and controllers for turbulent fluctuations via some learning algorithm without regard for the detailed flow physics. We then touch upon schemes based on heuristic physical arguments, which have found some success in flows in which the coherent motions are qualitatively understood. The dynamical systems approach is also described. In this approach, turbulence is decomposed into a small number of representative modes and the dynamics of these modes examined to determine appropriate control schemes. Finally, schemes based on optimal control theory applied directly to the Navier-Stokes equations are motivated and introduced. In these schemes, the desired quantity to be minimized is written mathematically as a cost functional, and then this cost functional is minimized in the space of the control by appealing directly to the equations governing the flow itself.

2.1 Adaptive schemes

Schemes belonging to this class perform system identification and controller determination without regard for the dynamics known to take place in the flow or the Navier-Stokes equations known to govern these dynamics. These schemes all use some adaptive method which, through adjustment of parameters by the engineer or via optimization by the scheme itself, tune the parameters of the feedback control law to achieve satisfactory results. The control algorithm may be based on feedback control theory for linear dynamic systems, linear or non-linear adaptive networks, or other standard techniques which have been developed and used in a wide variety of disciplines. These schemes are effective for simple control configurations. However, for configurations with multiple noisy sensors and complex flow dynamics, the ability of adaptive schemes to converge to efficient control algorithms is reduced.

If a system may be modeled accurately as responding linearly to control input, a very wide range of techniques may be used to build a controller with no knowledge of the equations governing the system. Possible techniques include root locus analyses, Bode design techniques, and linear quadratic regulators (Franklin *et al.* 1991). Kwong and Dowling (1993) provide a good example of the effective use of such techniques to design a feedback controller to reduce the unsteadiness and improve the pressure recovery in a diffuser. By performing a frequency sweep with an actuator and plotting the resulting response at a sensor downstream, the effective (linear) transfer function of the flow configuration was deduced; this process is termed system identification. With this system model, a controller was designed using Bode analysis techniques. Note that systems which are dominated by non-linear effects can not be analyzed or effectively controlled using these linear transfer function techniques (Choi *et al.* 1993a). Modified techniques, though cumbersome, can be used to account for system nonlinearities in this framework (Graham and McRuer 1961, Gelb and Vander Velde 1968).

Candel (1992) investigated the use of a linear adaptive algorithm called the Least Mean Squares (LMS) method (Isermann *et al.* 1992) to optimize the parameters of a feedback control arrangement in a combustor. The control arrangement was rather simple: one sensor was connected through a simple transfer function to one actuator, and a second sensor was used to monitor the performance of this feedback system. The parameters of the transfer function were then varied according to the LMS algorithm to maximize some performance measure based on the output of the monitoring sensor. Note that this type of system is only capable of representing linear relationships. To control flow effects which themselves develop (approximately) linearly, however, such as the early stages of development of Tollmien-Schlichting waves in a boundary layer (and a wide range of other phenomena), this is the most appropriate adaptive scheme to use, as it's convergence properties are better than those of non-linear adaptive algorithms.

Jacobson and Reynolds (1993a) and Fan *et al.* (1993) have investigated the use of non-linear adaptive algorithms called neural networks for the purpose of flow control. These schemes relate the outputs of the sensors to the inputs of the actuators through a non-linear function with variable coefficients and sigmoid saturation functions. An update scheme called the back-propagation algorithm has been developed which allows update of these coefficients based on error measures in a manner similar to the LMS algorithm for the linear configuration above. With a sufficient number of terms, this non-linear configuration can represent complex control laws; however, hand tuning of adaptation parameters is needed to achieve good convergence properties. Many improvements on the standard neural network configuration are possible to achieve better convergence properties (Hertz *et al.* 1991); these techniques should be exploited as much as possible when implementing non-linear adaptive algorithms for best results.

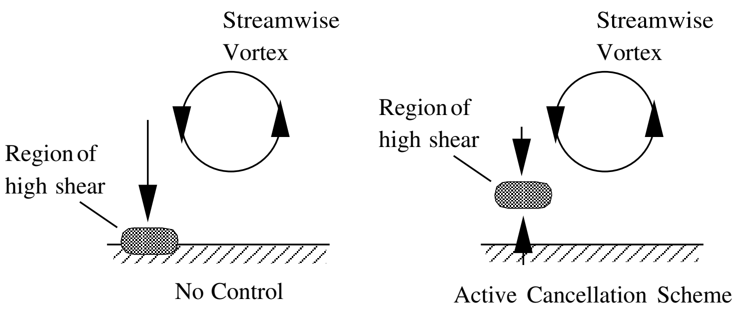

Figure 6: An active cancellation scheme applied to turbulent flow, from Choi *et al.* (1994).

2.2 Schemes based on physical arguments

In situations in which the dominant physics is well understood, judgment can guide an engineer to design effective control schemes. Success is limited, however, by the engineer's understanding of the physical processes involved; in the case of turbulence, our understanding is still limited despite several decades of intense research.

A good example of the use of physical understanding in the design of flow control schemes is the active cancellation of disturbances. Thomas (1990) reviews several independent investigations of active cancellation schemes applied to delay the onset of transition in boundary layers. Most of these experiments investigated the production of disturbances designed to counter the effects of artificially produced wave-like disturbances introduced further upstream; this is a considerably easier problem than dealing with the fleeting disturbances which appear naturally. Through the tuning of the amplitude and phase of a feedback control law, several of the schemes successfully delayed the transition that was caused by the upstream disturbances.

An active cancellation scheme was used by Choi *et al.* (1994), to reduce the drag in a fully-developed turbulent flow by mitigating the effect of the near-wall vortices. By opposing the near-wall motions of the fluid, which are caused by the near-wall vortices, with an opposing wall control as shown in figure 2, the high shear region was lifted away from the wall. A direct numerical simulation of this scheme applied to turbulent channel flow demonstrated about 20 percent drag reduction when the control was chosen to oppose the vertical motion at $y^+ = 10$. The $y^+ = 10$ sensing location achieved the best results. When this sensing location was moved above $y^+ = 25$ and the same control scheme was used, the flow response to the control became unbounded. Sensing the instantaneous normal velocity at $y^+ = 10$ is, of course, very impractical.

It is highly desirable to confine both sensing and actuation to the wall, as discussed in §3. Thus, Choi *et al.* computed the correlation of quantities measurable at the wall with the normal velocity above the wall. Surprisingly, the wall pressure did not exhibit a high correlation with the normal velocity. Using a Taylor series expansion and the equation of continuity, they obtained an expression relating the normal velocity at a point near the wall to the instantaneous wall shear. However, using this expression to estimate the normal velocity away from the wall resulted in only a 6 percent drag reduction. This is comparable to the drag reduction that can be achieved with simpler, passive means such as riblets.

2.3 Schemes based on dynamical systems

The tools of dynamical systems theory have proven useful in analyzing and interpreting turbulence dynamics (Aubry *et al.* 1988). Due to their large range of spatial and temporal scales, turbulent flows are known to have relatively high dimensions in this framework even at fairly low Reynolds numbers, which makes analysis of these systems quite difficult (Keefe *et al.* 1992). However, there has been some instructive work in representing the dynamics of coherent structures in boundary layers with systems of much lower dimension using the proper orthogonal decomposition (POD) method (Aubry *et al.* 1988, Berkooz *et al.* 1992, 1993). This method provides a set of eigenfunctions which are particularly efficient in representing second order turbulence statistics with a small number of modes. The algebraic complexity of the equations governing the turbulence is increased when expressed in this modal form.

As an example of how a low-order decomposition of a turbulent flow can be used for control, let us reconsider the reduction of drag in a wall-bounded flow. In the dynamical systems framework, the movement of the coherent structures may be represented locally as the orbiting of a low dimensional state (perhaps 10 to 20 modes) around several unstable fixed points; the passage of one set of coherent structures leads to a jump in the state to a different unstable orbit, or to a different distribution of coherent structures (Bloch and Marsden 1989a,b). Through the action of control, the unstable orbits around some of these fixed points may be stabilized. When this is achieved, some of these stabilized orbits will have more desirable qualities than others. The goal is then to converge to the nearest stabilized orbit with desirable qualities, in this case, to an orbit with low drag.

Research in the development of control schemes based on this method of stabilizing the attractors of a low-dimensional approximation of a turbulent chaotic system is still in progress. Keefe (1993a,b) has investigated the use of the OGY method (of Ott, Grebogi, and Yorke 1990) for feedback control of turbulence with limited control energy.

The OGY method is illustrated in figure 3. The state of the turbulence is represented schematically as the intersection of a stable manifold and an unstable manifold. The desired trajectory moves along the path shown. If control could be applied to put the state of the flow onto the stable manifold exactly and there were no noise in the system, the state would converge toward the desired trajectory and no further control would be needed. However, noise in the system caused by the unmodeled dynamics of the flow prohibits this, and thus the state always has a tendency to wander off in the unstable directions. Thus, control effort must be applied to move the state towards the stable

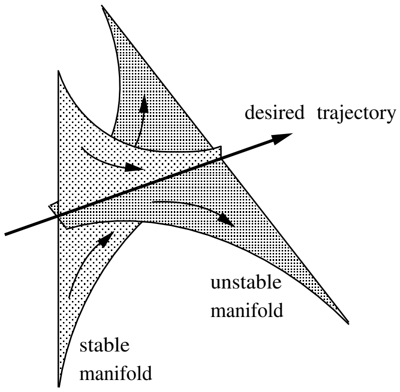

Figure 7: The OGY method, from Keefe *et al.* (1993b).

manifold to stabilize the system to the desired orbit. Note that this is more efficient than applying control to move the state towards the desired trajectory itself, as no control forcing is needed in the stable directions. Keefe (1993b) suggests applying an intermittent control forcing, shutting off the control when it is within a prescribed tolerance from the stable manifold. Though attempting to make a certain orbit completely stable would require excessive amounts of control energy, partial stabilization of orbits with desirable qualities could reap some benefits.

As a simple example illustrating this technique, consider balancing a baseball in the center of a saddle on the back of a standing horse. No matter how calm the horse, there will always be some motion which will tend to perturb the baseball. According to the OGY method, control need only be applied to get the baseball back up on the centerline of the horse (in the most direct manner possible) because the shape of the saddle itself will tend to keep the ball centered between the horse's head and his tail. This example just has one mode (the location of the baseball), one stable direction (front/back), and one unstable direction (left/right), with perturbations caused by unanticipated motions of the horse. A dynamical system modeling a turbulent flow, in comparison, will have several interdependent modes and several stable and unstable "directions" (referred to collectively as manifolds), with perturbations, perhaps quite large, caused by the unmodeled dynamics of the flow. Further complicating the flow control problem, the desired flow dynamics are not stationary, and the shape of the saddle which describes the dynamics of the modes is quite complex.

2.4 Optimal control schemes

The above schemes, though exhibiting varying degrees of success for the purposes for which they were designed, fail to provide us with a rigorous theory to determine the most efficient feedback control law for a given flow control problem. Application of optimal control theory directly to the equations of motion governing the flow itself, the Navier-Stokes equations, provides this rigorous framework for flow control (Abergel and Temam 1990). With optimal control schemes, we have a systematic method with which we may derive feedback control laws for the most efficient distribution of control effort to achieve various desired effects. A full derivation of the optimal control method for general flow control problems is given in the body of this report; however, an brief introduction to optimal control is in order here to motivate this work.

The seminal idea of the optimal control method is the minimization of a cost functional which is written to represent the physical problem of interest. Minimization of this functional is achieved by computing the gradient of the cost functional in the space of the control through an adjoint formulation, then updating the control with a gradient algorithm. For an unsteady problem such as turbulence, the cost functional is usually a time-averaged quantity; an unsteady control is found which minimizes this functional over some finite interval of time. This control, over the entire time interval under consideration, is iteratively updated using a gradient scheme until the best solution is reached.

A very brief outline of an optimal control example

Consider the problem of the reduction of the x_1-component of skin friction in a turbulent flow via small amounts of wall transpiration (blowing and suction) on the walls $\Gamma_2^{\pm}$. The control applied to the wall normal velocity is represented by ϕ such that the boundary conditions on flow velocities on the walls are: $u_i = \phi n_i$, where n_i is a wall-normal unit vector directed *out* of the flow domain. The integral of ϕ over the walls is taken to be zero so that there is no net mass flux through the walls at any instant.

As mentioned above, the first step in solving an optimal control problem is to represent the control problem of interest as a cost functional, $\mathcal{J}(\phi)$, to be minimized. In the present work, this is taken to be a weighted sum of the flow quantity to be altered and a measure of the net control effort. For the present example, the cost functional takes the form

$$\mathcal{J}_{\text{DRAG}}(\phi) = -d_1 \int_0^T \int_{\Gamma_2^{\pm}} \nu \, \frac{\partial u_1}{\partial n} \, d\mathbf{x} \, dt + \frac{\ell^2}{2} \int_0^T \int_{\Gamma_2^{\pm}} \phi^2 \, d\mathbf{x} \, dt.$$

The first term on the right-hand side is a measure of exactly that quantity we would like to reduce—in this case, the x_1 component of skin friction. Note that the factor d_1 is included simply to make the cost functional dimensionally consistent. The second term is a measure of the magnitude of the control. These quantities are integrated over the section of wall under consideration and over the time period under consideration, beginning at $t = 0$ (without loss of generality) and of duration T. Finally, they are weighted together with a factor ℓ^2, which represents the price of the control.

To compute the gradient of the cost functional in the space of the control, we begin by writing the Fréchet differential of the cost functional $\mathcal{J}_{\text{DRAG}}(\phi)$ as

$$\mathcal{J}'_{\text{DRAG}}(\phi,\phi') \triangleq \lim_{\epsilon\to 0} \frac{\mathcal{J}_{\text{DRAG}}(\phi+\epsilon\phi') - \mathcal{J}_{\text{DRAG}}(\phi)}{\epsilon} \triangleq \int_0^T \int_{\Gamma_2^\pm} \frac{\mathscr{D}\mathcal{J}_{\text{DRAG}}(\phi)}{\mathscr{D}\phi}\phi'\,d\mathbf{x}\,dt$$
$$= -d_1 \int_0^T \int_{\Gamma_2^\pm} \nu\,\frac{\partial u_1'}{\partial n}\,d\mathbf{x}\,dt + \ell^2 \int_0^T \int_{\Gamma_2^\pm} \phi\,\phi'\,d\mathbf{x}\,dt.$$

The differential is the derivative of the cost $\mathcal{J}_{\text{DRAG}}(\phi)$ in the space of the control ϕ taken in some arbitrary control update direction ϕ'. Through adjoint calculus, it is a straightforward process to re-express the integrand in the second term on the RHS as a term which multiplies ϕ', which results in

$$\int_0^T \int_{\Gamma_2^\pm} \left(\frac{\mathscr{D}\mathcal{J}_{\text{DRAG}}(\phi)}{\mathscr{D}\phi} - p^* - \ell^2\,\phi \right) \phi'\,d\mathbf{x}\,dt = 0,$$

where p^* is the adjoint pressure on the wall, which comes out of the solution of an adjoint differential equation, which itself depends on the state of the flow and thus must be solved at every time step. (A full description of how to calculate the appropriate adjoint variables for a wide variety of flow control problems, including the present problem, is given in parts III and IV of this report.) As the control distribution ϕ' is arbitrary, we may now extract the desired expression for the gradient:

$$\frac{\mathscr{D}\mathcal{J}_{\text{DRAG}}(\phi)}{\mathscr{D}\phi} = p^* + \ell^2\,\phi.$$

With this information, the control may be updated according to a gradient algorithm such as

$$\phi^{k+1} = \phi^k - \alpha\,\frac{\mathscr{D}\mathcal{J}_{\text{DRAG}}(\phi^k)}{\mathscr{D}\phi},$$

where k is the iteration index and α is a (sufficiently small) descent parameter. The control is iterated until convergence using this procedure for the time interval under consideration.

To make the optimal method practical for implementation, certain approximations are commonly made, the most significant of which is that the optimization is often performed considering only very short-time developments of the flow—we shall call this the "suboptimal approximation". The implications of this approximation are severe, and are discussed in detail in Part III of this report.

Using direct numerical simulation, a suboptimal approximation of the method in the above example has been proven effective in turbulent channel flow, giving a 17% drag reduction via small amounts of wall-normal blowing and suction (Bewley *et al.* 1993). This computation used the idealization that all the turbulent fluctuations above the wall were known and could be accounted for when computing the adjoint pressure p^*. By approximating the velocities near the wall with a Taylor series expansion from the wall, the adjoint problem may be cast in a form which, with further approximations, may be solved analytically (Hill 1993b); preliminary computations of this type of scheme result in a 15% drag reduction, showing that performance is not significantly degraded by making these approximations (Bewley *et al.* 1993). Further, these approximate schemes are algebraically much simpler to implement, as they do not require the on-line solution of an adjoint differential equation at each time step.

2.5 Discussion

For very simple feedback configurations with just a handful of sensors and actuators, adaptive schemes have been shown to perform well. However, as the configurations get more complex, allowing the possibility of more effective manipulation of the flow, the most effective feedback control law also becomes more complex. In such cases, the performance of adaptive schemes degrade and become highly dependent upon the method of training; we are thus motivated to base the control law on the flow physics.

This physical basis of a feedback control law may be made intuitively or mathematically. An intuitive control law has the attractive property that it is usually quite simple (i.e. countering the near wall vertical motion of the fluid with an opposite wall control). However, its performance is limited by the engineer's understanding of the flow phenomenon to be controlled.

For the purpose of designing a mathematical control law, it is logical to make a low order model of the turbulent structures and then to design a control scheme based on an examination of the dynamics of this model. The theoretical development of the best model to use for this is currently under investigation. Low order models of the flow have been used to analyze the dynamics of the coherent structures present in the flow. This interpretation of the turbulent structures allows identification and possible stabilization of orbits with desirable properties in this low dimensional model. Thus, control may be applied to encourage the desired dynamics of the coherent structures.

At the opposite end of the scale from adaptive schemes, optimal control schemes explore various possible developments of the flow over some time interval (using the Navier-Stokes equations and assumed complete information of the initial flow state) and then mathematically arrive at the optimum set of control velocities over this interval to minimize a given time-averaged cost functional. However, such schemes require a) very large computer resources, and b) full information about the exact state of the flow at the initial time. Various methods to reduce these schemes to practical feedback control laws are discussed in the body of this report.

Chapter 3

Implementation Issues

As illustrated in our introductory metaphor, any feedback control system consists of three components: the valve, the tie down points, and the string—in the language of control theory: actuators, sensors, and the control law. After the above discussion of various ideas, ranging from simple to quite elaborate, on how to arrange the string, we will now review recent developments of the devices to which the ends of this string may be tied.

The most notable advance in the past few years in the area of implementing turbulence control ideas has been the emergence of Micro Electro Mechanical Systems (MEMS) technology, which employs the methods developed for the fabrication of silicon chips to construct very small mechanical devices (Wise 1991). Miniaturization of this scale for both sensors and actuators is necessary for feedback control of turbulence due to the very small scales of the coherent structures in high Reynolds numbers flows of engineering interest. New questions arise in the fabrication of flow devices in silicon, which makes this an active area of current research (see recent Proceedings of the IEEE MEMS Workshops for several examples). Researchers are currently attempting to miniaturize several of the devices reviewed herein using MEMS technology.

3.1 Methods of sensing

Two desirable attributes of flow sensors are that they be robust and that they don't significantly disrupt the flow. For these reasons, most practical sensors for active flow control are flush mounted on a wall. At a wall, we may measure both skin friction and wall pressure.

For situations in which the wall pressure is important (for instance, in control schemes designed to reduce flow-induced noise), there are a plethora of devices, essentially small microphones, which have been developed for measuring pressure fluctuations. One example by Cho *et al.* (1989) is a capacitive pressure sensor built with a small flexible membrane. Note, however, that it has been found (Choi *et al.* 1994) that pressure is not a good indicator for detecting and controlling the sweep and ejection events which accompany near-wall coherent structures in wall-bounded flows.

Using a Taylor series extrapolation, the near wall flow may be estimated directly from shear stress measurements on the wall, though these estimates are only valid fairly near the wall (Choi *et al.* 1994). For the purpose of shear stress measurement at a wall, several types of sensors have been investigated recently; we will review four of the most popular: floating element sensors, piezo-electric foils, hot films, and surface acoustic wave (SAW) sensors.

A floating element sensor consists of a small rectangular patch of silicon supported by thin beams (Haritonidis 1988). The flow over the device exerts shear forces on the patch and the resulting stresses in the supporting beams may be measured by various methods, including the differential measure of capacitance (Schmidt *et al.* 1988) and an active electrostatic re-balancing technique with a comb actuator (Jaecklin *et al.* 1992). This device is quite attractive because it directly measures shear stress in a way that doesn't interfere with the flow. However, the yield in the fabrication of these devices is still quite low (about 10 percent) due to the intricacies in their design. Further perfection of design and manufacturing techniques may make this device quite promising.

Piezoelectric foils consist of thin films of polyvinylidene-fluoride (PVDF) coated with a very thin layer of aluminum (Nitsche *et al.* 1989). Portions of the PVDF films are crystallized, and the resulting artificial polarization exhibits a piezoelectric effect when subjected to normal and shear stresses. Detectors placed below the films then sense the field created by the piezo effect of the sheared crystal. The manufacture of these devices is simple and robust, but their sensitivity to both normal and shear stresses poses difficulties. To measure shear stress, Nitsche *et al.* propose placing two detectors side by side in opposite configurations so that, by combining the signals from the two sensors, the effects of the normal stress cancel and the resulting signal is proportional to the shear stress. However, the small magnitude of the signals being measured results in the familiar problem of losing the signal in the noise created by imperfect cancellation of the contributions due to the normal stress fluctuations.

A hot film sensor may be used as an indirect measure of skin friction by calibrating the heat transfer of the film as a function of the applied shear; however, care must be taken in this calibration, as the static and dynamic responses differ (Alfredsson *et al.* 1988) and the response is nonlinear. Such a sensor is easy to manufacture but difficult to use as it doesn't measure skin friction directly; if used underwater, a hot film sensor must be thermally coupled but electrically isolated from the flow, and the thermal cross talk from other sensors and/or actuators must be minimized—this would be difficult in a control configuration where sensors and actuators must be placed in close proximity.

Devices may also be built to measure the propagation speed of surface acoustic waves (Varadan *et al.* 1989, 1990). The surface wave propagation speed is a function of the stresses caused by the overlying flow; by building devices which measure the wave speed in alternate directions, one may estimate the instantaneous shear stress. These devices are quite sensitive and respond linearly to the shear stress; however, they are also sensitive to the normal stress, temperature fluctuations, electric

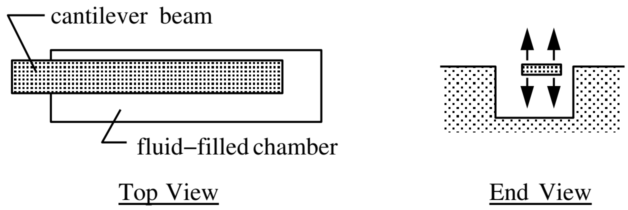

Figure 8: Beam-chamber configuration, from Jacobson and Reynolds (1993b).

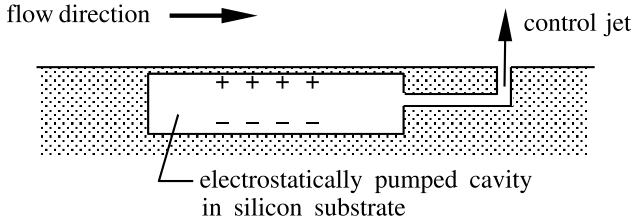

Figure 9: Electrostatically pumped cavity (side view), from Breuer (1993).

noise, and drift of the resonant frequency of the oscillator circuit—any system using SAW devices must be able to account for these dependencies in a way that doesn't lose the signal in the noise created by imperfect cancellation in the differencing process.

3.2 Methods of actuation

Several ideas for the active manipulation of small scale turbulent structures near a wall are currently under investigation; below is a description of a few of the more popular configurations (Wilkinson 1990 discusses others).

Figure 4 illustrates a beam situated over a cavity which is allowed to passively fill with fluid from all sides. By vibrating the beam at its resonant frequency, it can be made to force the fluid out of the cavity. The vibration can be created by a piezoelectric effect (Wiltse and Glezer 1993 and Jacobson and Reynolds 1993b) or by periodic optical heating of one side of the beam (Lammerink *et al.* 1991). The output through the narrow gap is concentrated and directed primarily in the vertical direction. By taking advantage of the different flow patterns caused by upward and downward motions of the beam, a strong flow pattern may be established. It has been observed that the flow field created by such a device is a set of counter-rotating vortices centered over the narrow gap with common flow up; by modulating the vibration amplitude, the magnitude of this disturbance may be controlled. An advantage of this method is the strong flow field it can create; disadvantages are that this flow field is necessarily quite complicated and the beam itself is difficult to manufacture and rather fragile.

Electrostatic forces or conventional speakers may be used to pump the fluid inside a cavity (Breuer

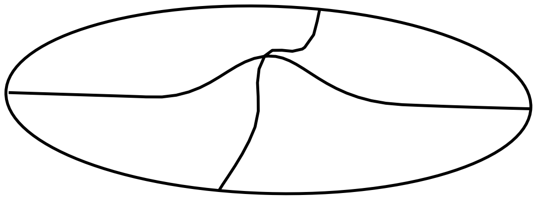

Figure 10: Variable bump, from Lumley (1989).

1993, Meier and Zhou 1991, Weinstein and Balasubramanian 1977). In Breuer's configuration (figure 5), the cavity leads to a small hole through which the excess volume of fluid must travel. This results in very precise blowing and suction applied through the actuation hole. Difficulties include the fragility of the membrane and the tendency of the membrane to short out by touching the lower wall of the cavity.

Figure 6 shows a bump on a surface which may be regulated by a piezoelectric material underneath a membrane (Lumley 1989). In Lumley's configuration, the bump is approximately Gaussian in shape; the flow field caused by the bump may be visualized as a horseshoe vortex with a common flow towards the wall immediately downstream of the device. One problem with this device is that getting sufficient displacement with piezo material is difficult. A different mechanism which alleviates this problem (but has a significant activation time) is a solenoid-activated valve leading to a high pressure source below the membrane (Breuer *et al.* 1989). A variant on this idea is to create the pressure below the membrane by the controlled phase transition boiling of a liquid—this avenue has yet to be thoroughly explored (Wise 1991). Bumps may also be activated by attaching magnets to the membrane and situating electromagnets below (Wilkinson and Balasubramanian 1985) or electrostatically forcing the membrane itself (Weinstein and Balasubramanian 1977). Variable bump devices have the potential of being more robust than cantilevered beams and pumped cavities; however, the perturbation to the flow field caused by the bump is complicated.

Differential wall heating is another possible method of control (Liepmann *et al.* 1982, Nosenchuck *et al.* 1987). Using wall heating to create the velocity fluctuations actually has several simultaneous effects, including the alteration of the specific volume of the heated fluid, associated buoyancy effects, and changes in viscosity, all of which should be accounted for by the control scheme. The idea is attractive from the robustness standpoint because it has no moving parts. However, for control of turbulence in practical applications, very high power heaters and very low thermal capacitance of the wall would be required to achieve the necessary frequency response. This might be most easily realized using a laser with optical fiber access to small metal patches on the surface. For a discussion of optical heating issues, see Lammerink *et al.* (1991).

Finally, if the fluid is electrolytic or can easily be made that way by addition of salts, hydrodynamic Lorenz forcing is another control option (Nosenchuck and Brown 1993, Tsinober 1990). The work of Nosenchuck and Brown, though open loop, is an excellent example of the effectiveness of this forcing technique. In their configuration, electric and magnetic fields are applied in the streamwise and spanwise directions with the use of well-positioned magnets and electrodes. By varying the electric field with an active control circuit, this configuration could be used in a feedback configuration. However, manufacturing such units on a scale small enough to interact actively with turbulent coherent structures might prove to be difficult.

3.3 Other considerations

Flow control is most effective when applied to critical flow regimes. As mentioned in the abstract, one method of finding these critical regimes is by a receptivity analysis of the flow under consideration. For example, the effects of a control scheme can be quite dramatic when applied near the transition point of a boundary layer flow, the separation point on an airfoil, or the nozzle of a jet, where flow instabilities magnify quickly. However, skin friction reduction by active control in a fully turbulent regime would be approximately proportional to the surface area covered by the actuators. For the reduction of skin friction drag over large surface areas, inexpensive, modular systems that are both robust and simple to diagnose and replace are the only alternative.

A modular configuration which has been proposed by Gad-el-Hak (1993) and Reynolds (1993) is to tile a portion of the surface of an airplane with sensor-actuator-controller units fabricated in silicon which can be mass-produced using MEMS technology. The layout of the sensors and the actuators in the tiles must be designed carefully, as the direction of the flow may not be known a priori and would change with flight conditions. Estimates on the requirements for control units under flight conditions have been computed by Wilkinson (1990) and Gad-el-Hak (1993). At the typical aircraft cruise conditions quoted by Gad-el-Hak ($u_\infty = 300$ m/s, $u_\tau = 10$ m/s, $\nu = 3 \cdot 10^{-5}$ m^2/s), the wall unit scale is $\nu/u_\tau = 3$ μm and the non-dimensional time unit is $\nu/u_\tau^2 = 0.3$ μsec. The average spanwise spacing of the streaky structures is about 100 wall units; a few sensors and actuators must span this gap in order to effectively counter the turbulent motion, implying actuators and sensors with widths on the order of 50 μm. The passage of coherent structures at these flight conditions (estimated by the time it takes a coherent structure to convect at $0.8 \cdot u_\infty$ a distance of 400 wall units) would be approximately once every 5 μsec. Power requirements are considered by Muntz *et al.* (1993). These guidelines give very rough estimates on the spatial density of sensors and actuators and the response time required in this implementation—production of control units on this scale with today's technology would be difficult.

Chapter 4

Concluding remarks

Current investigations down several different avenues of possible feedback control schemes provide the theoretical groundwork for future applications. More immediately, and of equal significance, current investigations of the feedback control of turbulence are enhancing our fundamental understanding of the mechanisms responsible for the maintenance and regeneration of turbulence itself.

The advent of micro Electro Mechanical Systems technology for both sensors and actuators allows us to begin to consider practical implementations. Even with these advances, schemes which require the coverage of large surface areas with thousands of sensors and actuators are at present out of reach. The applications which are currently most promising for the implementation of feedback control schemes have critical areas where the flow is quite sensitive to modification, such as areas of separation or transition.

Returning to the metaphorical steam engine, simultaneous development of the string, the valve, and the tie-down points leave us optimistic about future developments in this field.

REFERENCES

ABERGEL, F. & TEMAM, R. 1990 On some control problems in fluid mechanics. *Theor. and Comp. Fluid Dyn.* **1**, 303-325.

ALFREDSSON, P.H., JOHANSSON, A.V., HARITONIDIS, J.H., & ECKELMANN, H. 1988 The fluctuating wall-shear stress and the velocity field in the viscous sublayer. *Phys. Fluids* **31**, 5, 1026-1033.

AMSTUTZ, A., FEKETE, N.P., & POWELL, J.D. 1993 Model-based air-fuel ratio control in SI engines with a switch-type EGO sensor. *SAE Paper* 940972.

ANDERSON, S.R., & D'SOUZA, A.F. 1994 Feedback control of separation and transition to turbulence in unsteady flow. Submitted for publication to *J Fluid Mech.*

AUBRY, N., HOLMES, P., LUMLEY, J.L., & STONE, E. 1988 The dynamics of coherent structuresin the wall region of a turulent boundary layer. *J. Fluid Mech.* **192**, 115-173.

BANDYOPADHYAY, P.R. 1986 Review-Mean flow in turbulent boundary layers disturbed to alter skin friction. *J. of Fluids Eng.* **108**, 127-140.

BERKOOZ, G., HOLMES, P., & LUMLEY, J.L. 1992 Low dimensional models of the wall region in a turbulent boundary layer: new results. *Physica* D **58**, 402-406.

BERKOOZ, G., HOLMES, P., & LUMLEY, J.L. 1993 The proper orthogonal decomposition in the analysis of turbulent flows. *Ann. Rev. Fluid Mech.* **25**, 539-575.

BEWLEY, T.R., CHOI, H., TEMAM, R., & MOIN, P. 1993 Optimal feedback control of turbulent channel flow. *Annual Research Briefs* – 1993, Center for Turbulence Research, Stanford U./NASA Ames.

BEWLEY, T.R., & MOIN, P. 1994 Optimal control of turbulent channel flows. *Active control of vibration and noise*, ASME DE **75**, 221.

BLACKWELDER, R.F. 1989 Some ideas on the control of near-wall eddies. *AIAA Paper* 89-1009.

BLOCH, A.M. & MARSDEN, J.E. 1989a Control and stabilization of systems with homoclinic orbits. *Proc. of the IEEE Conference on Decision and Control including The Symposium on Adaptive Processes* **3**, 2238-2242.

BLOCH, A.M. & MARSDEN, J.E. 1989b Controlling Homoclinic Orbits. *Theoret. Comput. Fluid Dyn.* **1**, 179-190.

BREUER, K.S. 1993 Micromachined sensors and actuators for the measurement and control of complex flows. *Proc. of the 1993 AFOSR Contractors Meeting.*

BREUER, K.S., HARITONIDIS, J.H., & LANDAHL, M.T. 1989 The control of transient disturbances in a flat plate boundary layer through active wall motion. *Phys Fluids* A **1**, 3, 574-582.

BUSHNELL, D.M. & MCGINLEY, C.B. 1989 Turbulence control in wall flows. *Ann. Rev. Fluid Mech.* **21**, 1-20.

BUSHNELL, D.M. & MOORE, K.J. 1991 Drag reduction in nature. *Ann. Rev. Fluid Mech.* **23**, 65-79.

CANDEL, S.M. 1992 Combustion instabilities coupled by pressure waves and their active control. *Proc. of the 24th Symposium on Combustion*, The Combustion Institute, 1277-1296.

CHO, S.T., NAJAFI, K., LOWMAN, C.L., & WISE, K.D. 1989 An ultrasensitive silicon pressure-based flowmeter. *IEDM Technical Digest*, Dec 89, 499-502.

CHOI, H., TEMAM, R., MOIN, P., & KIM, J. 1993a Feedback control for unsteady flow and its application to the stochastic Burgers equation. *J. Fluid Mech.* **253**, 509-543.

CHOI, H., MOIN, P., & KIM, J. 1993b Direct numerical simulation of turbulent flow over riblets. *J. Fluid Mech.* **255**, 503-539.

CHOI, H., MOIN, P., & KIM, J. 1994 Active turbulence control for drag reduction in wall-bounded flows. *J. Fluid Mech.* **262**, 75-110.

DRAZIN, P.G., & REID, W.H. 1981 *Hydrodynamic Stability.* Cambridge University Press.

FAN, X., HOFMANN, L., & HERBERT, T. 1993 Active flow control with neural networks. *AIAA Paper* 93-3273.

FATTORINI, H.O. & SRITHARAN, S.S. 1992 Existance of optimal controls for viscous flow problems. *Proc. Roy. Soc. Lond.* A **439**, 81-102.

FIEDLER, H.E. & FERNHOLZ, H.H. 1990 On management and control of turbulent shear flows. *Prog. Aerospace Sci.* **27**, 305-387.

FRANKLIN, G.F., POWELL, J.D., & EMAMI-NAEINI, A. 1991 *Feedback Control of Dynamical Systems.* Addison-Wesley.

GAD-EL-HAK, M. 1989 *Frontiers in experimental fluid mechanics.* Lecture Notes in Engineering **46**.

GAD-EL-HAK, M. 1993 Innovative control of turbulent flows. *AIAA Paper* 93-3268.

GELB, A., & VANDER VELDE, W.E. 1968 *Multiple-input Describing Functions and Nonlinear System Design.* McGraw-Hill.

GOLDSTEIN, M.E., & HULTGREN, L.S. 1989 Boundary-layer receptivity to long-wave free-stream disturbances. *Ann. Rev. Fluid Mech.* **21**, 137-166.

GRAHAM, D., & MCRUER, D. 1961 *Analysis of Nonlinear Control Systems.* Wiley.

GREENBERG, M.D. 1971 *Applications of Green's Functions in Science and Engineering.* Prentice Hall.

HARITONIDIS, J.H. 1988 *The measurement of wall shear stress.* In *Advances in Fluid Mechanics Measurements*, ed. Gad-el-Hak, Springer Verlag.

HERTZ, J., KROGH, A., & PALMER, R.G. 1991 *Introduction to the Theory of Neural Computation.* Addison-Wesley.

HILL, D.C. 1992 A theoretical approach for analyzing the restabilization of wakes. *AIAA Paper* 92-0067.

HILL, D.C. 1993a Adjoint systems and their role in the receptivity problem for boundary layers. *CTR Manuscript* 146, Stanford U.

HILL, D.C. 1993b Drag reduction at a plane wall. *Annual Research Briefs* – 1993, Center for Turbulence Research, Stanford U./NASA Ames.

HO, C.M. & HUERRE, P. 1984 Perturbed free shear layers. *Ann. Rev. Fluid Mech.* **16**, 365-424.

HOU, L.S. & RAVINDRAN, S.S. 1993 Computation of boundary optimal control problems for an electrically conducting fluid. Submitted to *J. Comput. Phys.*

ISERMANN, R., LACHMANN, K.H., & MATKO, D. 1992 *Adaptive Control Systems.* Prentice Hall.

JACOBSON, S.A. & REYNOLDS, W.C. 1993a Active control of boundary layer wall shear stress using self-learning neural networks. *AIAA Paper* 93-3272.

JACOBSON, S.A. & REYNOLDS, W.C. 1993b Active boundary layer control using flush mounted surface actuators. *Bull. Am. Phys. Soc.* **38**, 12, 2197.

JAECKLIN, V.P., LINDER, C., DE ROOIJ, N.F., MORET, J.M., BISCHOF, R., & RUDOLF, F. 1992 Novel Polysilicon comb actuators for xy-stages. *Proc. 1992 IEEE MEMS Workshop.*

KEEFE, L.R. 1993a Drag reduction in channel flow using nonlinear control. *AIAA Paper* 93-3279.

KEEFE, L.R. 1993b Two nonlinear control schemes contrasted on a hydrodynamiclike model. *Phys. Fluids* A **5**, 4, 931-947.

KEEFE, L.R., MOIN, P., & KIM, J. 1992 The dimension of attractors underlying periodic turbulent Poiseuille flow. *J. Fluid Mech.* **242**, 1-29.

KWONG, A.H.M. & DOWLING, A.P. 1993 Active boundary layer control in diffusers. *AIAA Paper* 93-3255.

LAMMERINK, T.S.J., ELWENSPOEK, M., & FLUITMAN, J.H.J. 1991 Optical excitation of micro-mechanical resonators. *Proc. 1991 IEEE MEMS Workshop.*

LEE, M., & REYNOLDS, W.C. 1985 Bifurcating and blooming jets. *Rept TF-22*, Thermosciences Division, Dept. of Mech. Eng., Stanford U.

LIEPMANN, H.W., BROWN, G.L., & NOSENCHUCK, D.M. 1982 Control of laminar instability waves using a new technique. *J. Fluid Mech.* **118**, 187-204.

LIGHTHILL, J. 1993 An active mechanism of drag reduction in herring. Seminar presented at Stanford U. on August 3, 1993.

LUMLEY, J.L. 1989 Low dimensional models of the wall region of a turbulent boundary layer, and the possibility of control. *Proc. of the Tenth Australasian Fluid Mechanics Conference.*

MEIER, H.U. & ZHOU, M.D. 1991 The development of acoustic generators and their application as a boundary layer transition control device. *Experiments in Fluids* **11**, 93-104.

MUNTZ, E.P., SHIFLETT, G.R., WADSWORTH, D., & BLACKWELDER, R.F. 1993 Transient energy release pressure driven microactuators for flow control. *AIAA Paper* 93-3271.

NITSCHE, W., MIROW, P., & SZODRUCH, J. 1989 Piezo-electric foils as a means of sensing unsteady surface forces. *Experiments in Fluids*, **7**, 2, 111-118.

NOSENCHUCK, D.M., & BROWN, G.L. 1993 Control of turbulent wall shear stress using arrays of TFM tiles. *Bull. Am. Phys. Soc.* **38**, 12, 2197.

NOSENCHUCK, D.M., LYNCH, M.K., & STRATTON, J.P. 1987 Active control of sublayer disturbances using an array of heating-elements. *Proc. of the ASME/JSME Thermal Engineering Joint Conference*, **2**, 619-627.

OTT, E.A., GREBOGI, C., & YORKE, J.A. 1990 Controlling chaos. *Phys. Rev. Lett.* **64**, 11, 1196.

PADMANABHAN, K.T., BOWMAN, C.T., & POWELL, J.D. 1993 Development of an adaptive optimal combustion control strategy. *The Combustion Institute Paper* 93-092.

REYNOLDS, WC 1993 Private communication.

RILEY, J.J., GAD-EL-HAK, M., & METCALFE, R.W. 1988 Compliant Coatings. *Ann. Rev. Fluid Mech.* **20**, 393-420.

ROBINSON, S.K. 1991 Coherent motions in the turbulent boundary layer. *Ann. Rev. Fluid Mech.* **23**, 601-639.

SCHMIDT, M.A., HOWE, R.T., SENTURIA, S.D., & HARITONIDIS, J.H. 1988 Design and calibration of a microfabricated floating element shear stress sensor. *IEEE Trans. Electron. Devices* **35**, 6, 750-757.

SMITH, A. 1776 *The division of labor.* In *Of men and machines*, by Lewis, A.O. (1963) Dutton & Co.

SRITHARAN, S.S. 1993 Stochastic optimal control and nonlinear filtering of turbulence. *Bull. Am. Phys. Soc.* **38**, 12, 2276.

THOMAS, A.S.W. 1990 Active wave control of boundary-layer transition. In *Viscous drag reduction in boundary layers*, eds. Bushnell, D.M. & Hefner, J.N., *Progress in Astro. and Aeronautics* **123**, 179-199, AIAA, Washington, D.C.

TSINOBER, A. 1990 MHD flow drag reduction. In *Viscous drag reduction in boundary layers*, eds. Bushnell, D.M. & Hefner, J.N., *Progress in Astro. and Aeronautics* **123**, 179-199, AIAA, Washington, D.C.

VAINBERG, M. 1964 *Variational Methods for the Study of Nonlinear Operators.* Holden-Day.

VARADAN, V.V., ROH, Y.R., & VARADAN, V.K. 1989 Local/global SAW sensors for turbulence. *Proc. 1989 IEEE Ultrasonics Symposium*, Montreal.

VARADAN, V.V., ROH, Y.R., SHANKAR, B., & VARADAN, V.K. 1990 Measurement of the skin friction associated with turbulent flows in air and water using SAW devices. *Proc. 1990 IEEE Ultrasonics Symposium*, Montreal.

WALSH, M.J. 1990 Riblets. In *Viscous drag reduction in boundary layers*, eds. Bushnell, D.M. & Hefner, J.N., *Progress in Astro. and Aeronautics* **123**, 203-261, AIAA, Washington, D.C.

WEINSTEIN, L.M., & BALASUBRAMANIAN, R. 1977 An electrostatically driven surface for flexible wall drag reduction studies. *Second International Conference on Drag Reduction*, Cambridge, England.

WILKINSON, S.P. 1990 Interactive wall turbulence control. In *Viscous drag reduction in boundary layers*, eds. Bushnell, D.M. & Hefner, J.N., *Progress in Astro. and Aeronautics* **123**, 479-509, AIAA, Washington, D.C.

WILKINSON, S.P. & BALASUBRAMANIAN, R. 1985 Turbulent burst control through phase-locked traveling surface depressions. *AIAA Paper* 85-0536.

WILTSE, J.M. & GLEZER, A. 1993 Manipulation of free shear flows using piezoelectric actuators. *J. Fluid Mech.* **249**, 261-285.

WISE, K.D. 1991 Integrated microelectromechanical systems: a perspective on MEMS in the 90s. *Proc. 1991 IEEE MEMS Workshop*, 33-38.